



# **Asphalt Research Consortium**

## **Quarterly Technical Progress Report January 1-March 31, 2010**

April 2010

Prepared for  
Federal Highway Administration  
Contract No. DTFH61-07-H-00009

By  
Western Research Institute  
Texas A&M University  
University of Wisconsin-Madison  
University of Nevada-Reno  
Advanced Asphalt Technologies

[www.westernresearch.org](http://www.westernresearch.org)  
[www.ARC.unr.edu](http://www.ARC.unr.edu)

# TABLE OF CONTENTS

INTRODUCTION .....	1
GENERAL CONSORTIUM ACTIVITIES .....	3
PROGRAM AREA: MOISTURE DAMAGE.....	5
Category M1: Adhesion.....	5
Category M2: Cohesion .....	14
Category M3: Aggregate Surface .....	19
Category M4: Modeling.....	28
Category M5: Moisture Damage Prediction System .....	29
PROGRAM AREA: FATIGUE.....	33
Category F1: Material and Mixture Properties .....	33
Category F2: Test Method Development.....	62
Category F3: Modeling .....	76
PROGRAM AREA: ENGINEERED MATERIALS.....	117
Category E1: Modeling.....	117
Category E2: Design Guidance.....	139
PROGRAM AREA: VEHICLE-PAVEMENT INTERACTION.....	183
Category VP1: Workshop .....	183
Category VP2: Design Guidance .....	183
Category VP3: Modeling .....	189
PROGRAM AREA: VALIDATION.....	197
Category V1: Field Validation.....	196
Category V2: Accelerated Pavement Testing .....	198
Category V3: R&D Validation .....	199
PROGRAM AREA: TECHNOLOGY DEVELOPMENT.....	207
PROGRAM AREA: TECHNOLOGY TRANSFER.....	209
Category TT1: Outreach and Databases .....	209



## **INTRODUCTION**

This document is the Quarterly Report for the period of January 1 to March 31, 2010 for the Federal Highway Administration (FHWA) Contract DTFH61-07-H-00009, the Asphalt Research Consortium (ARC). The Consortium is coordinated by Western Research Institute with partners Texas A&M University, the University of Wisconsin-Madison, the University of Nevada Reno, and Advanced Asphalt Technologies.

The Quarterly Report is grouped into seven areas, Moisture Damage, Fatigue, Engineered Paving Materials, Vehicle-Pavement Interaction, Validation, Technology Development, and Technology Transfer. The format of the report is based upon the Research Work Plan that is grouped by Work Element and Subtask.

This Quarterly Report summarizes the work accomplishments, data, and analysis for the various Work Elements and Subtasks. This report is being presented in a summary form. The Quarter of January 1 to March 31, 2010 is fourth quarter of the Year 3 contract year. Reviewers may want to reference the Year 3 Work Plan and perhaps the Year 4 Work Plan. There is also background information regarding the research plan contained in the Revised Year 2 Work Plan. The more detailed information about the research such as approaches to test method development, data collection, and analyses will be reported in research publications as part of the deliverables. All of the Work Plans, as well as many other documents, including quarterly reports, are posted on the ARC website, [www.ARC.unr.edu](http://www.ARC.unr.edu).

## **SUPPORT OF FHWA AND DOT STRATEGIC GOALS**

The Asphalt Research Consortium research is responsive to the needs of asphalt engineers and technologists, state DOT's, and supports the FHWA Strategic Goals and the Asphalt Pavement Road Map. More specifically, the research reported here supports the Strategic Goals of safety, mobility, and environmental stewardship. By addressing the causes of pavement failure and thus determining methods to improve asphalt pavement durability and longevity, this research will provide the motoring public with increased safety and mobility. The research directed at improved use of recycled asphalt pavement (RAP), warm mix asphalt, and cold mix asphalt supports the Strategic Goal of environmental stewardship.



## **GENERAL CONSORTIUM ACTIVITIES**

### **PROGRESS THIS QUARTER**

Many ARC members attended the TRB Annual Meeting in Washington DC during the week of January 13, 2010. Several presentations were made by ARC members on results of the research in both podium and poster sessions. Also during TRB week, presentations were made at the “DAWG” forum on Pavement Performance Data Analysis and the International Society of Asphalt Pavements (ISAP) Technical Committee on Constitutive Modeling of Asphaltic Materials meeting. ARC members also participate on TRB committees.

A brief ARC advisory board meeting was conducted during TRB week to keep all members up to date. The ARC Asphalt Microstructural Modeling team members Mr. Troy Pauli, Dr. Michael Greenfield, Dr. Linbing Wang, and Dr. Jeffrey Bullard met during TRB week to discuss project progress, coordination, and work plans.

Several ARC members attended and made presentations at the Binder, Mix & Construction, and Fundamental Properties & Advanced Models ETG meetings in Irvine, California on February 22–26, 2010. A considerable portion of the ETG meetings was related to review of the ARC Year 4 Work Plan.

Manitoba Infrastructure and Transportation hosted a one-day seminar on March 3 where ARC members presented results from the Manitoba RAP and WMA field sites.

ARC members attended and presentations were made at the Association of Asphalt Paving Technologists meeting in Sacramento, California

Dr. Hussain Bahia made presentations to the Rocky Mountain User-Producer group on March 24.

### **WORK PLANNED FOR NEXT QUARTER**

ARC members are planning on attending and making presentations at the European Asphalt Technology Association (EATA) meeting in Parma, Italy in June.

ARC members, Dr. Hussain Bahia, Dr. Elie Hajj, and Dr. Eric Kalberer, are planning on attending the RAP Expert Task Group meeting in Auburn, Alabama on May 19 & 20, 2010 that is being hosted by the Auburn University and the National Center for Asphalt Technology. An update on the RAP research being conducted by the ARC will be presented.



## PROGRAM AREA: MOISTURE DAMAGE

### CATEGORY M1: ADHESION

#### Work Element M1a: Affinity of Asphalt to Aggregate (UWM)

##### Work Done This Quarter

In this quarter, the newly developed Bitumen Bond Strength (BBS) test was used to evaluate the effect of moisture conditioning time on the bond strength of asphalt-aggregate systems. An experimental matrix, which included different binders, modifications and aggregate types to account for different chemical and physical conditions in the aggregate-asphalt interface, was completed in this quarter. The materials used are listed in table M1a.1.

Table M1a.1. Materials used to evaluate moisture damage in aggregate-binder interface using the BBS test.

<b>Solution</b>	Tap Water
<b>Mineral Surfaces</b>	Granite
	Limestone
<b>Asphalt Binders</b>	CRM 58-28
	FH 64-22
<b>Modified Asphalt Binders</b>	CRM 58-28 + 2% SBS
	CRM 58-28 + 1% PPA
	FH 64-22 + Elvaloy
	FH 64-22 + 1% PPA

SBS = styrene-butadiene-styrene. PPA = polyphosphoric acid.

For this set of experiments, samples were conditioned in tap water for 0, 6, 24, 48 and 96 hours. The type of failure (adhesive or cohesive) observed after BBS experiments is shown in table M1a.2. Note that all unconditioned (i.e., dry) samples showed cohesive failure (i.e., failure within asphalt). On the other hand, adhesive failure (i.e., between aggregate and binder) was observed in the conditioned specimens.

On both limestone and granite surfaces the failure mode changed after moisture exposure, showing that the nature of the aggregate greatly affects adhesion. From the analysis of the results, limestone aggregate is shown to have higher adhesive bond to asphalt binder than granite, and thus more resistance to adhesive failure.

Table M1a.2. Influence of conditioning time and aggregate type in the failure mode.

Asphalt Binder Type	CT (hr)	Sol	Failure Type	
			Granite	Limestone
FH 64-22 neat	Dry	Tap Water	Cohesion	Cohesion
	6		Adhesion	Cohesion
	24		Adhesion	Cohesion
	48		50%A -50%C	50%A -50%C
	96		Cohesion	Cohesion
FH 64-22+Elvaloy	Dry	Tap Water	Cohesion	Cohesion
	6		Cohesion	Cohesion
	24		Adhesion	Cohesion
	48		Cohesion	50%A -50%C
	96		Cohesion	Cohesion
FH 64-22+1%PPA	Dry	Tap Water	Cohesion	Cohesion
	6		Cohesion	Cohesion
	24		Cohesion	Cohesion
	48		Cohesion	Cohesion
	96		Cohesion	Cohesion
CRM 58-28 neat	Dry	Tap Water	Cohesion	Cohesion
	6		Cohesion	Cohesion
	24		Cohesion	Cohesion
	48		Adhesion	Cohesion
	96		Adhesion	Adhesion
CRM 58-28+2%SBS	Dry	Tap Water	Cohesion	Cohesion
	6		Adhesion	Cohesion
	24		Adhesion	Cohesion
	48		50%A -50%C	Adhesion
	96		Adhesion	Adhesion
CRM 58-28+1%PPA	Dry	Tap Water	Cohesion	Cohesion
	6		Cohesion	Cohesion
	24		Cohesion	Cohesion
	48		Cohesion	Cohesion
	96		Cohesion	Cohesion

CT = conditioning time. Sol = solution.

The effect of conditioning time on the pull-off strength of the asphalt-aggregate systems tested can be observed in figure M1a.1. Note that the average pull-off strength was calculated from four replicates. The conditioning of specimens in water has caused a significant reduction in the pull-off strength and has also changed the failure mode (cohesive to adhesive), regardless of the selected asphalt binder or aggregate type. These results are expected since the water is believed to be able to penetrate through the aggregate, which is a porous material, and hence weaken the

bond at the asphalt-aggregate interface (Kanitpong and Bahia 2003). The longer the conditioning time in water, the weaker the interface bond and the lower the pull-off strength value.

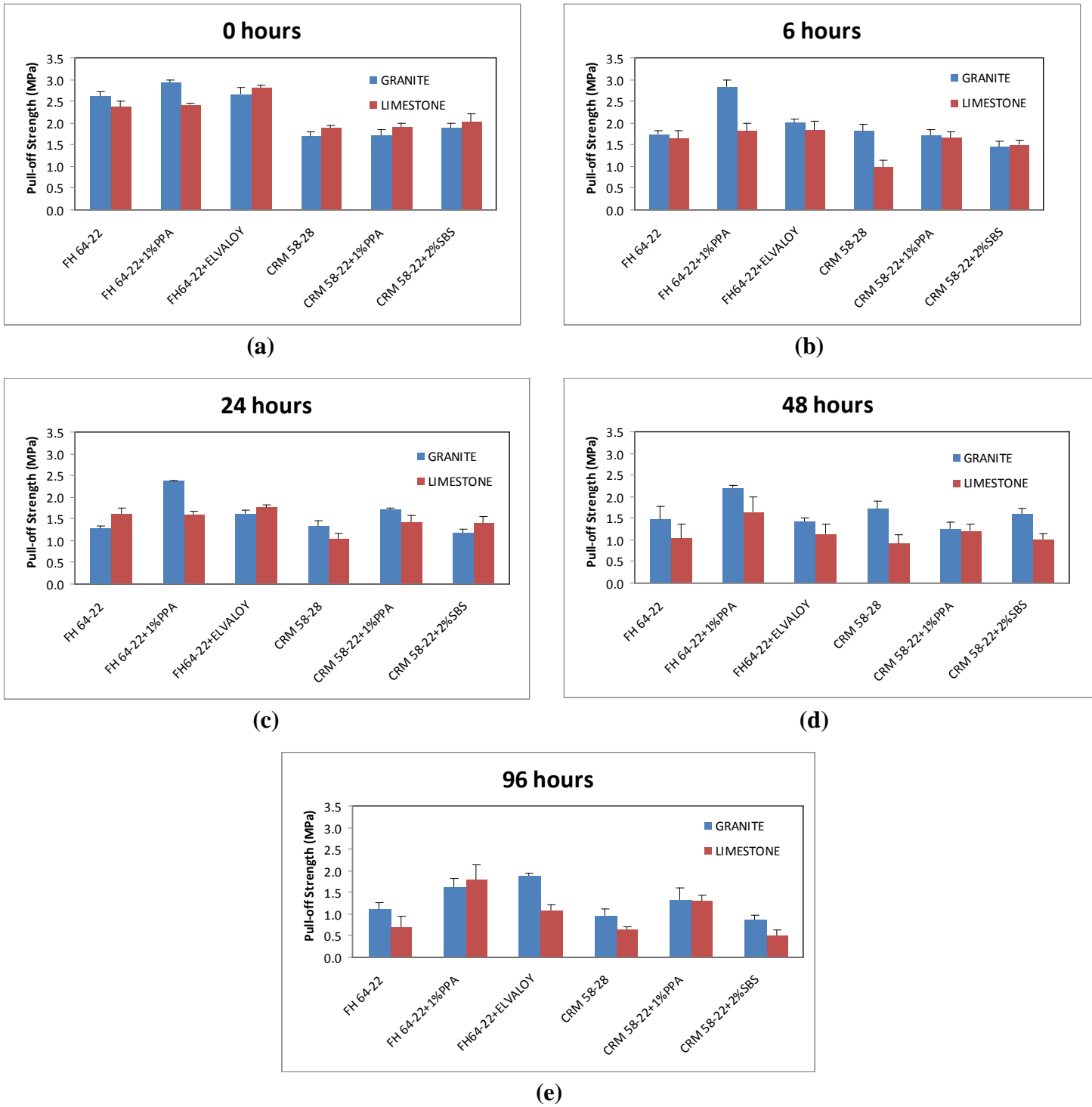


Figure M1a.1. Charts. Influence of conditioning time on the pull-off strength at: (a) 0 hours; (b) 6 hours; (c) 24 hours; (d) 48 hours; and (e) 96 hours.

## Significant Results

The research team obtained promising results regarding characterization of asphalt-aggregate interface by means of a simple-to-perform BBS test. It is observed that the bonding between asphalt and aggregate under wet conditions is highly dependent on binder modification type and conditioning time. Polymers are found to improve the adhesion between the asphalt and aggregate as well as the cohesion within the binder. Also in this quarter, the research team prepared a draft AASHTO standard for the BBS test.

## Significant Problems, Issues and Potential Impact on Progress

The pull-off tensile strength obtained from BBS test performed is highly influenced by the cleanness of the surface of the aggregate plate. Inconsistent and unexpected results for some of the samples conditioned at 48 and 96 hours were obtained when the aggregate plate used was different than the plate used for the 0, 6 and 24 hour tests. It appears that slight changes of the aggregate surface can greatly affect the magnitude of the pull-off tensile strength. Therefore, it is always important to perform moisture susceptibility experiments using aggregates from the same source and to be consistent in sample preparation.

## Work Planned Next Quarter

Efforts for next quarter will focus on investigating the possibility of measuring the surface free energy, zeta potential, and chemical composition of aggregates and binders. These variables may explain the moisture damage mechanisms in asphalt-aggregate systems. The research team will continue working on a comprehensive literature review of moisture damage in asphalt mixtures as related to chemistry of aggregates and binders. Also, the team will start testing according to the experimental matrix proposed in the Year 4 work plan. Validation of the results obtained with the BBS will be accomplished by testing mixtures with the T283 standard test method for moisture susceptibility (e.g., Tensile Strength Ratio) and strain sweep tests in the Dynamic Shear Rheometer (DSR) modified with aggregate plates.

## Cited References

Kanitpong, K., and H. U. Bahia, 2003, Role of Adhesion and Thin Film Tackiness of Asphalt Binders in Moisture Damage of HMA. *Asphalt Paving Technology*,72: 502-528.

## **Work Element M1b: Work of Adhesion Based on Surface Energy**

***Subtask M1b-1: Surface Free Energy and Micro-Calorimeter Based Measurements for Work of Adhesion (TAMU)***

## Work Done This Quarter

The main goal of this subtask is to provide material property inputs required in other work elements as required. Any data obtained from this subtask will be included in the material

properties database. In the last quarter surface free energy of some aggregates and asphalt binders that are being used to develop test methods were measured.

#### Significant Results

None.

#### Significant Problems, Issues and Potential Impact on Progress

None.

#### Work Planned Next Quarter

Work on this subtask will be conducted in conjunction with and as required by other work elements.

#### ***Subtask M1b-2: Work of Adhesion at Nano-Scale using AFM (WRI)***

#### Work Done This Quarter

None

#### Significant Results

None.

#### Significant Problems, Issues and Potential Impact on Progress

None.

#### Work Planned Next Quarter

Continuation: Dynamic wetting experiments will be conducted to study the kinetics of adhesion of asphalts and asphalt chromatographic fractions spin-cast on glass microscope slides. These films will be further studied by AFM imaging and nano-mechanics to investigate microstructuring of wax as a function of the compatibility of the asphalt. Preliminary studies will also be conducted to measure interfacial tensions of asphalts in translucent solvents using a pendent-drop approach (Faour et al. 1996; Hansen and Rødsrud 1991). Acid-Base and van der Waals components of surface tensions will be determined based on this approach.

We have recently observed that as model waxes are added to asphalts at higher and higher concentrations, spin cast solutions of these mixtures phase separate on the glass slide, and do so at different wax-loading concentrations for different asphalts. Figure M1b-2.1 depicts a photograph of solvent spin cast films of: (a) AAA-1, no wax, (b) AAA-1 doped with 4% hexacontane.



Figure M1b-2.1. Photograph of solvent spin cast films of: (LEFT) AAA-1, no wax, (RIGHT) AAA-1 doped with 4% hexacontane.

In addition to this material, SHRP asphalt AAG-1 was also doped with hexacontane wax, but this mixture did not show phase separation until 10% wax was added. We will formally investigate this phenomena to try and study the impact of wax on asphalt aggregate adhesion by studying additional wax-asphalt systems.

#### Cited References

Faour, G., M. Grimaldi, J. Richou, and A. Bois, 1996, Real-Time Pendant Drop Tensiometer Using Image Processing with Interfacial Area and Interfacial Tension Control Capabilities. *J. Colloid Inter. Sci.*, 181, 385–392.

Hansen, F.K., and G Rødsrud, 1991, Surface Tension by Pendant Drop. *J. Colloid Inter. Sci.* 141(1), 1–9.

#### ***Subtask M1b-3: Identify Mechanisms of Competition Between Water and Organic Molecules for Aggregate Surface (TAMU)***

#### Work Done This Quarter

This sub task is investigating the mechanisms responsible for adhesion and debonding of model organic compounds (representing functional groups in asphalt binder) to minerals and representative aggregates. We are measuring the heat of reactions of the chemical mechanisms using a dual-mode flow adsorption calorimeter. Differences in molar heats of reaction of different organics bonding to the same absorbent are indicative of differences in the bonding strength of each absorbate with the absorbent of interest.

Work during this quarter focused on continued development of the instrument. We are currently conducting studies to validate the ability of the instrument to differentiate between bonding characteristics of materials produced under different conditions. These materials are known to have variable surface properties depending on the temperature of formation and other environment conditions. Currently we are evaluating the instrument's ability to accurately measured changes in surface characteristics as a function of the pH of the aqueous environment.

### Significant Results

There are no significant results for this quarter as we focused on aggregate characterizations.

### Significant Problems, Issues and Potential Impact on Progress

There are no significant issues.

### Work Planned Next Quarter

We plan on initiating flow through experiments to measure the molar heat of reaction of the adhesion of model organic compounds that represent asphalt to minerals and aggregates, as well as the molar heats of reactions of water adsorption to organic-coated minerals and aggregates. Adhesion will be modeled in the flow-through calorimeter by organic sorption from nonaqueous phase solvents. Model compounds will be chosen to represent potential functional groups found in asphalt. Potential model compounds include benzoic acid, phenol, valerophenone, benzyl benzoate, quinoline, phenyl sulfoxide, phenyl sulfone, naphthalene, and dibenzanthracene. Solutions containing the model compounds individually, and then together, will be run through the instrument and the sample chamber containing the aggregates samples. The molar hat of reaction of the adsorption reaction will be measured using the temperature difference between the solution entering and exiting the sample chamber. Experimental variables include the chemistry of the model organics, single versus mixtures of model organics, ionic salt content of the nonaqueous phase solvent, and the surface chemistry of the mineral or aggregate. Competition of water and the model organics for the mineral or aggregate surfaces will be characterized using flow-through experiments where increasing concentrations of water in a non-aqueous solution are introduced to aggregates coated with the model organic compounds. Coating will be achieved by dissolving small quantities of the model compound(s) in a volatile organic solvent (hexane). The aggregate will be added to the solution, and following mixing the solvent will be allowed to evaporate. Following coating, the aggregates will be placed in instrument, and increasing amounts of water will be added to the non-aqueous carrier solvent. The instrument will measure any heat generated resulting from water's displacement of the model organic compounds at the aggregate surface. Following each experiment the concentration of the model organic compounds in the carrier solution will be determined using a GC/MS.

## Work Element M1c: Quantifying Moisture Damage Using DMA (TAMU)

### Work Done This Quarter

Software was developed to analyze the DMA test data with the aim of simplifying the analysis procedure to predict fatigue life and evaluate the moisture susceptibility. This software is developed using C++ programming language. In this software the user is required to load the DMA test raw data and specify some test information through a friendly user interface as presented in figure M1c.1. This software has two levels for processing and analyzing the test data based on the available information. Level I is used to calculate the dissipated pseudo-strain energy, and the regression parameters  $a$  and  $b$  from the following relationship (Castelo Branco, 2008):

$$W_R = a + b \cdot \ln(N) \quad (\text{M1c.1})$$

Where  $N$ : the load cycles

Level II is used to calculate the crack growth index as a function of the load cycles  $\Delta R(N)$  in dry and wet conditions as presented in the following equation (Caro et al. 2008).

$$\Delta R(N) = \left[ (2n + 1)^{n+1} \left( \frac{G_R b}{4\pi G_1 \Delta G_f} \right)^n N \right]^{1/2n+1} \quad (\text{M1c.2})$$

Where  $G_R$  is the reference modulus;  $\Delta G_f$  is the work of adhesion between the asphalt binder and the aggregate. Level II can be only executed if the surface energy components of the aggregate and asphalt binder are available. The results of this software will be presented in graphs and charts to simplify the analysis. Figure M1c.2 shows an example of the calculated crack growth index as a function of cycles for an asphalt mixture in dry and wet conditions.

### Significant Results

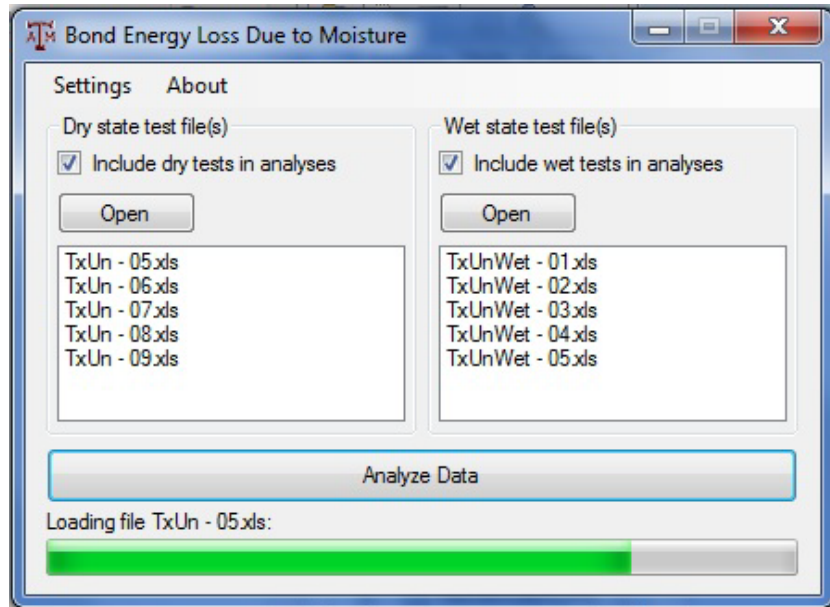
Software development is completed.

### Significant Problems, Issues and Potential Impact on Progress

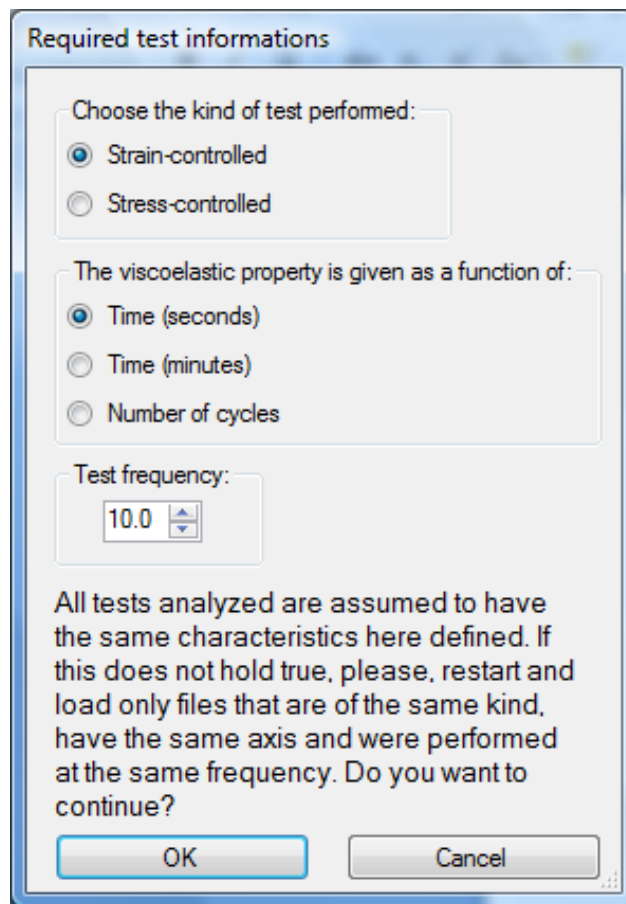
None

### Work Planned Next Quarter

The software will be used to analyze DMA test data with the aim of validation the analysis procedure and fixing any bugs with the software.



(a)



(b)

Figure M1c.1. User input interface.

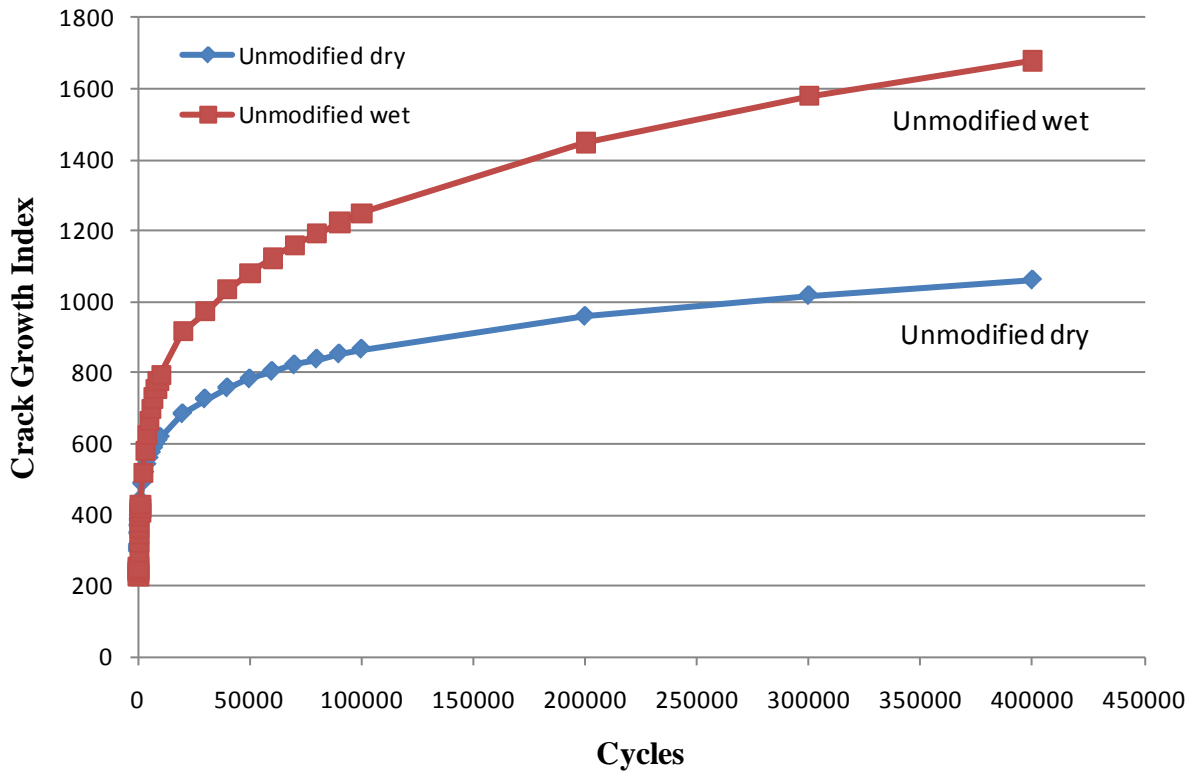


Figure M1c.2. Crack growth index vs. number of cycles.

## CATEGORY M2: COHESION

### Work Element M2a: Work of Cohesion Based on Surface Energy

#### *Subtask M2a-1: Methods to Determine Surface Free Energy of Saturated Asphalt Binders (TAMU)*

##### Work Done This Quarter

No activity was planned for this quarter.

##### Work Planned Next Quarter

Work on this task is anticipated to start in year 4 of the project.

## ***Subtask M2a-2: Work of Cohesion Measured at Nano-Scale using AFM (WRI)***

### Work Done This Quarter

None

### Significant Results

None

### Significant Problems, Issues and Potential Impact on Progress

This work has been delayed due to instrument time and resources which have been devoted to the development of the nano-rheometer as part of the work in the Fundamental Properties subtask 2-3.

### Work Planned Next Quarter

Continuation: Work planned for next quarter will include analysis, using the mechanical models described in the previous quarterly report for this task (Quarterly Technical Progress Report, July 2009), of force curve data collected this quarter. Additional force curve data will be collected for a wider selection of asphalt samples. Tests will be conducted to begin to address the effect of temperature and loading/unloading rates with respect to how “fracture” energy is dissipated as indicated by the various parts of the force curve measurements. These measurements should lead to a better understanding of the ductile-brittle transition that takes place as asphalt is cyclically heated and cooled.

We hypothesize that binder softness-hardness and ductile-brittle characteristics could be coupled but also unrelated where ductile-brittle characteristics may be directly related to the microstructuring that develops in the binder as temperature is varied. Hence, we would like to include in this subtask studies which focus on the propensity of asphalts to develop structure due to wax content and colloidal structuring (asphaltenes-resins), thus, structuring results in immobilization of the solvent characteristics of the binder to reduce self-healing while also resulting in the development of a microstructure resulting in a more brittle material. The approach we will take will involve measuring the variation in mass loss of asphalt and SARA fraction species as a function of temperature and removal of wax from saturate and naphthene aromatics fractions using thermal gravimetric analysis (TGA). Additionally, ultrasound spectroscopy measurements (Schabron et al., 2006) of asphalt and model wax doped asphalt will be conducted to investigate wax-gel structuring of these materials as a function of temperature. Ultrasound spectroscopy is used in the aviation industry to identify metal fatigue in airplanes. As temperature is reduced in asphalt samples, this method may identify structuring in waxy binders which result in stress buildup.

## Cited References

Schabron, J.F., J.F. Rovani, Jr., A.T. Pauli, and A. Beemer, 2006. Initial Studies Using Ultrasonic Spectroscopy for Monitoring Changes in Residua with Pyrolysis. *Fuel*, 85, 2093-2105.

## **Work Element M2b: Impact of Moisture Diffusion in Asphalt Mixtures**

*Subtask M2b-1: Measurements of Diffusion in Asphalt Mixtures (TAMU)*

*Subtask M2b-2: Kinetics of Debonding at the Binder-Aggregate Interface (TAMU)*

### Work Done This Quarter

During this quarter we continued with the literature review of methods to measure the rate of debonding at the binder aggregate interface using spectroscopic methods. We are evaluating the feasibility of using the existing ATR cell with partially exposed interface and the vertical ATR cell with ends that expose the binder-solid interface to water. All tests are currently being conducted using the ZnSe crystal surface initially.

### Significant Results

None.

### Significant Problems, Issues and Potential Impact on Progress

None.

### Work Planned Next Quarter

Based on the preliminary results we plan to draw out a detailed experiment plan to accomplish the goals for this subtask. Preliminary results will also be compared to subtask M1b-3, mechanisms of water-organic molecule competition using the flow calorimeter.

## **Work Element M2c: Measuring Thin Film Cohesion and Adhesion Using the PATTI Test and the DSR (UWM)**

### Work Done This Quarter

In this quarter, finite element simulations of the Bitumen Bond Strength (BBS) test using Abaqus were performed to determine stress distribution in the binder sample for a regular test and to investigate the effect of eccentricity of the pull-off load on the test results. Figure M2c.1 shows the finite element models for the binder sample and the pull-out stub.

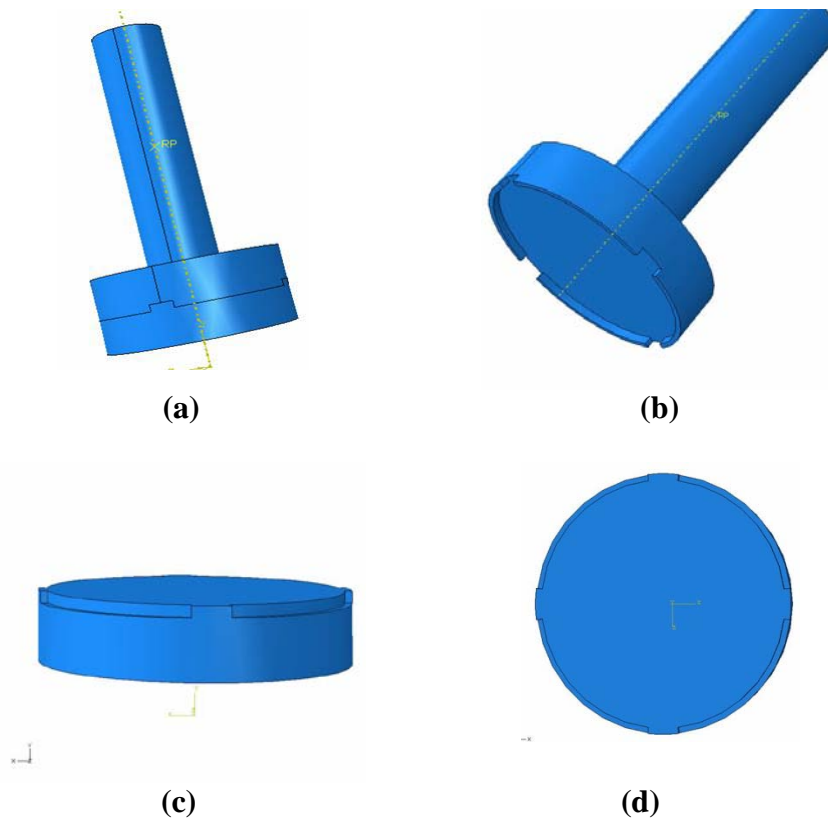


Figure M2c.1. Illustrations. Finite element models for the BBS test: (a) binder and stub; (b) pull-out stub; (c) binder sample; and (d) bottom of pull-out stub.

### Significant Results

The stress distribution in the binder during the BBS test is not uniform due to the sharp edges of the pull-out stub, as shown in figure M2c.2. Without considering eccentricity of the load, a stress concentration factor of approximately 1.64 was calculated. If eccentricity is present during testing (e.g., typical for pull-off tension tests), a significant stress gradient is observed. These results indicate that the asphalt-aggregate bond strength obtained with the BBS test may be underestimated. It is important to note, however, that the results of replicate measurements from the BBS for many binders and emulsions show a relatively low coefficient of variation. In any case, the importance of the stress gradient in terms of measured tension strength will be further evaluated and methods for minimizing the eccentricity during testing will be considered. The focus of this numerical simulation will be to indicate the importance of alignment of the metal stub.

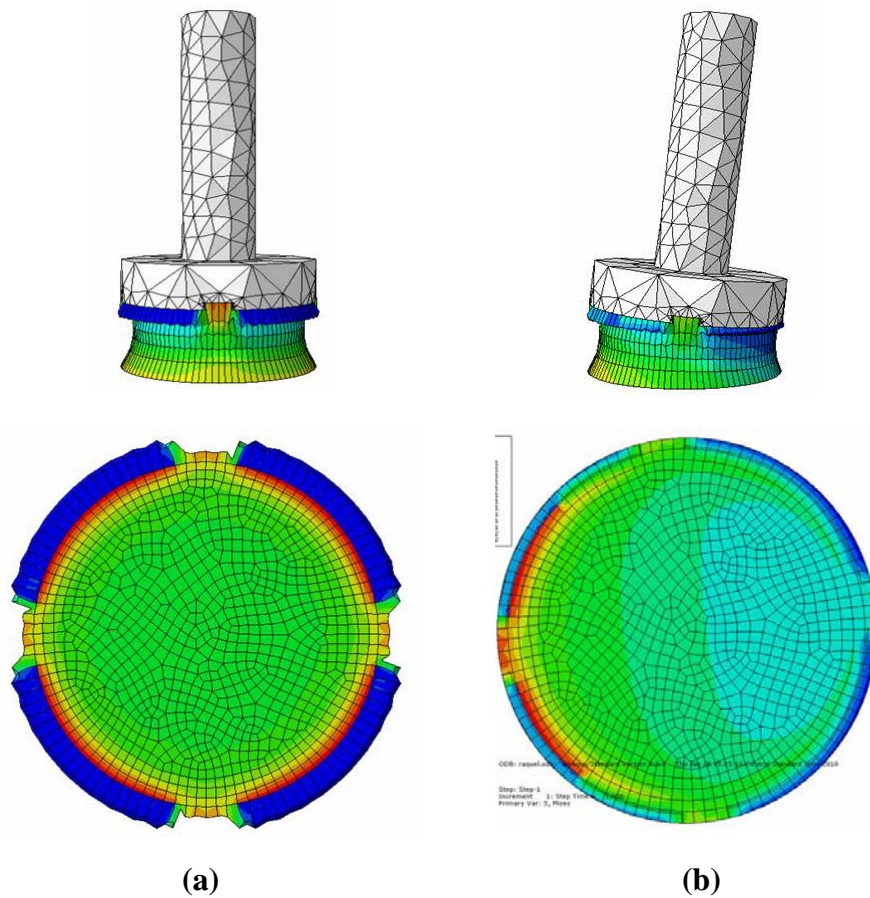


Figure M2c.2. Illustrations. Finite element simulation of eccentric loading for the BBS test: (a) BBS test without eccentricity; and (b) BBS test with eccentricity.

Significant Problems, Issues and Potential Impact on Progress

None.

Work Planned Next Quarter

This is the last quarterly report for this work element. For next quarter the research team will combine the work elements M1a (Affinity of Asphalt to Aggregate) and M2c (Measuring Thin Film Cohesion and Adhesion Using the PATTI Test and the DSR) due to similarities in their objectives. All future research and planned activities for M1a and M2c will be included in the quarterly report for M1a.

## **CATEGORY M3: AGGREGATE SURFACE**

### **Work Element M3a: Aggregate Surface Characterization (TAMU)**

#### Work Done This Quarter

Physical and chemical properties of aggregates at the macro and molecular scale influence the performance of asphalt mixes. These properties control the nature and durability of the bond between aggregates and asphalt in wet and dry conditions and its resistance to moisture induced damage and fatigue cracking. Recent research by Little and colleagues have shown that surface energy of the aggregate-asphalt interface is a reliable predictor of engineering properties of the asphalt mixture. Current understanding of the aggregate and bitumen properties that control and shape surface energy is limited, limiting our ability to *a priori* predict surface energy of any given aggregate-asphalt combination.

Current tasks are organized around the (1) characterization of the chemical composition of the surfaces of reference minerals and aggregates through electron beam spectrometers, including electron microprobe, backscatter electrons and electron-dispersive spectroscopy (EDS), (2) the characterization of the surface energies of reference minerals and aggregates through the universal sorption device and microcalorimetry, (3) quantification of surface (upper 14 nm) atomic species and chemical state with an x-ray photoelectron spectrometer (XPS), and (4) surface topography characterization with scanning electron microscopy (SEM). The results from these tasks will support the development of a predictive model of aggregate surface energies based upon the surface energies of the minerals that compose the aggregate.

Tasks completed this quarter include additional BSE imaging of the basalt (RK) in order to more accurately calculate modal mineralogy, quantitative WDS analyses of the SAz-2 montmorillonite and Georgia kaolinite, image processing of X-ray elemental distribution maps of the aggregates and reference mineral samples, and compilation and organization of the quantitative WDS analyses. Specific accomplishments are highlighted in the tables below.

Surface energy measurements for quartz, microcline, labradorite, biotite, andesine, microcline, albite, augite, hornblende, hematite, siderite, dolomite, and calcite have been collected using the universal sorption device. The components of surface energy were calculated on replicates of the samples.

Sample preparation and aggregate surface characterization tasks completed this quarter are shown in the table below.

Table M3a.1. Status of tasks associated with mineralogical and chemical characterization of aggregates.

<b>SHRP</b>	<b>Name</b>	<b>Yr.Qtr</b>	<b>Thin Section Prep Status</b>	<b>Microprobe Analysis Status</b>
<b>RA</b>	Lithonia Granite	08.1	1 aggr sample prepared, 2 more in progress	1 set of X-ray maps, 1 set of BSE images, 1 preliminary set of WDS quant analyses
		08.2	2 more aggregate samples prepared	2 sets of X-ray maps, BSE images are not needed because of grain size
		09.1		WDS quant analyses of major minerals completed
<b>RC</b>	Limestone (higher absorption)	08.1	2 aggr samples prepared	1 set of X-ray maps, 1 set of BSE images, 1 preliminary set of WDS quant analyses
		08.2	-	No additional analyses
<b>RD</b>	Limestone (low absorp.)	08.1	4 aggr samples prepared,	4 sets of X-ray maps, 1 set of BSE images, 1 preliminary set of WDS quant analyses
		08.2	-	No additional analyses
<b>RK</b>	Basalt	08.1	2 aggr samples prepared, 1 more in progress	2 sets of X-ray maps, 1 set of BSE images, 1 preliminary set of WDS quant analyses
		08.2	1 sample in progress	3 additional sets of X-ray maps, 13 set of BSE images, 1 set of WDS quant analyses for pyroxene, olivine, amphibole
		09.1		WDS quant analyses of feldspar, pyroxene and clay completed.
		09.2		Additional BSE images of thin sections RK1a and RK1b acquired; image processing of X-ray maps in progress
<b>RL</b>	Gulf Coast Gravel	08.1	5 aggr samples prepared, 9 more in progress	4 sets of X-ray maps, 1 set of BSE images, 1 preliminary set of WDS quant analyses
		08.2	9 more in progress	9 sets of X-ray maps
		09.1		WDS quant analyses of mineral grains in 9 gravel particles completed.
		09.2		Image processing of X-ray maps in progress
<b>MM</b>	MM Sandstone	09.1	One 25mm aggr mount prepared with > 20 fragments	1 sets of X-ray maps acquired

Sample preparation and mineral surface characterization tasks completed this quarter are shown in the tables below.

Table M3a.2. Status of tasks associated with mineralogical and chemical characterization of mineral components of aggregates.

Mineral	Group	Yr.Qtr	(1) Acquisition Status (2) Microprobe Mount Status	Microprobe Analysis Status
Quartz	Silica Mineral	08.1	(1) > 200 grams acquired (Arkansas, RNG specimen) (2) Polished microprobe mount in preparation	In progress
		08.2	In progress	In progress
Microcline	Alkali Feldspar	08.1	(1) > 160 grams acquired (G&G collection, B0434) (2) Preliminary polished mount prepared	Preliminary homogeneity and quantitative chemical analysis acquired.
		08.2	In progress	In progress
Albite	Plagioclase Feldspar	08.1	(1) > 100 grams acquired (G&G collection, B0469) (2) Polished mount to be prepared	In progress
		08.2	In progress	In progress
Oligoclase	Plagioclase Feldspar	08.3	> 100 grams acquired (G&G collection, 008)	In progress
Andesine	Plagioclase Feldspar	08.1	(1) > 65 grams acquired (G&G collection, B0513) (2) Preliminary polished mount prepared	Preliminary homogeneity and quantitative chemical analysis acquired.
		08.2	In progress	In progress
Labradorite	Plagioclase Feldspar	08.1	(1) > 160 grams acquired (Naim, Labrador; RNG specimen) (2) Preliminary polished mount prepared	Preliminary homogeneity and quantitative chemical analysis acquired.
		08.2	In progress	In progress
Anorthite	Plagioclase Feldspar	08.1	Samples to be acquired	NA
		08.2	NA	NA

Table M3a 2. Status of tasks associated with mineralogical and chemical characterization of mineral components of aggregates (cont.).

Mineral	Group	Yr.Qtr	(1) Acquisition Status (2) Microprobe Mount Status	Microprobe Analysis Status
Hornblende	Amphibole	08.1	(1) > 350 grams acquired (G&G collection, B0545) (2) Preliminary polished mount prepared	Preliminary homogeneity and quantitative chemical analysis acquired.
		08.2	In progress	In progress
Hornblende	Amphibole	08.1	(1) > 70 grams acquired (G&G collection, Room 008) (2) Polished mount to be prepared	In progress
		08.2	In progress	In progress
		09.1	(2) Polished mount prepared	X-ray map acquired; WDS quant analyses completed.
Augite	Pyroxene	08.1	(1) > 0 (?) grams acquired (G&G collection, B1007) (2) Preliminary polished mount prepared	Preliminary homogeneity and quantitative chemical analysis acquired.
		08.2	In progress	In progress
Augite	Pyroxene	08.1	(1) > 80 grams acquired (G&G collection, Room 008) (2) Polished mount to be prepared	In progress
		08.2	In progress	In progress
		09.2		WDS quant analyses completed.
Forsteritic Olivine	Olivine	08.1	(1) > 280 grams acquired (San Carlos, AZ) (2) Polished mount to be prepared	In progress
		08.2	In progress	In progress

Table M3a.2. Status of tasks associated with mineralogical and chemical characterization of mineral components of aggregates (cont.).

Mineral	Group	Yr.Qtr	(1) Acquisition Status (2) Microprobe Mount Status	Microprobe Analysis Status
Muscovite	Mica	08.1	(1) > 65 grams acquired (G&G collection, Room 008) (2) Polished mount to be prepared	Preliminary quantitative chemical analysis acquired.
		08.2	In progress	In progress
		09.1	(2) Polished mount prepared	X-ray map acquired; WDS quant analyses completed.
Biotite	Mica	08.1	(1) > 175 grams acquired (G&G collection, B0857) (2) Polished mount to be prepared	In progress
		08.2	In progress	In progress
		09.1		WDS quant analyses completed.
Biotite	Mica	08.1	(1) > 150 grams acquired (G&G collection, Room 008) (2) Polished mount to be prepared	Preliminary quantitative chemical analysis acquired.
		08.2	In progress	In progress
Calcite	Carbonate	08.1	(1) > 100 grams acquired (Mexico; RNG specimen) (2) Polished mount to be prepared	In progress
		08.2	In progress	In progress
Dolomite	Carbonate	08.1	Samples to be acquired	NA
		08.2	NA	NA
		09.1	(2) Polished mount prepared	X-ray map acquired; WDS quant analyses completed.
Siderite	Carbonate	09.1		WDS quant analyses completed.

Table M3a.2. Status of tasks associated with mineralogical and chemical characterization of mineral components of aggregates (cont.).

Mineral	Group	Yr.Qtr	(1) Acquisition Status (2) Microprobe Mount Status	Microprobe Analysis Status
Hematite	Iron Oxide	08.1	Samples to be acquired	NA
		08.2	NA	NA
		09.1	(2) Polished mount prepared	X-ray map acquired; WDS quant analyses completed.
Magnetite	Iron Oxide	08.1	Samples to be acquired	NA
		08.2	NA	NA
Ilmenite	Iron Titanium Oxide	08.3	> 100 g sample (Ontario; RNG specimen)	NA
		09.1	(2) Polished mount prepared	X-ray map acquired; WDS quant analyses completed.
Goethite	Iron Oxyhydroxide	08.1	Samples to be acquired	NA
		08.2	NA	NA
Kaolinite (KGA-1B)	Clay Mineral	08.3	Samples acquired	NA
		08.2	Samples acquired	In progress
Kaolinite (Georgia)	Clay Mineral	08.3	Samples acquired	NA
		08.2	Samples acquired	In progress
		09.2	Unpolished flat mount prepared	WDS quant preliminary analyses completed
Montmorillonite (SAz-2)	Clay Mineral	08.3	Samples acquired	NA
		08.2	Samples acquired	In progress
		09.2	Unpolished flat mount prepared	WDS quant preliminary analyses completed
Chlorite	Clay Mineral	08.3	Samples acquired; ~25 g Calumet and New Melones (RNG)	NA
		08.2	Samples acquired	In progress

## Significant Results

### *Establishing a Surface Energy Predictive Model*

One of the first goals will be to establish a model for predicting aggregate bulk surface energies based on mineralogical composition. Improved prediction of aggregate bulk properties pertinent to moisture damage susceptibility can lead to better methods to measure material properties and moisture damage susceptibility of asphalt/aggregate mixes. Development of a simple visual field test of aggregate surface energy properties will aid in on-site evaluation of aggregate moisture damage susceptibility.

We expect the bulk/total surface energy of an aggregate to be a function of the component surface energies of its mineralogical constituents as:

$$Se_{aggregate} = \sum (Se_{Mineral} \cdot SA) + \sigma$$

where Se is surface energy, SA is surface area, and  $\sigma$  is the error term. A visual inspection of rock mineralogy based on percent of constituents can accurately predict total surface energy of the sample.

Methods –A Universal Sorption Device can be used to measure pure phase mineral surface energies by calculating the amount of a reference gas (water, hexane, and methylpropyl ketone in this case) sorbed to the mineral surface at various pressures. The adsorption isotherm for each reference gas is used to calculate equilibrium spreading pressure for each of the vapors along with the specific surface area (SSA) using the BET Equation. The equilibrium spreading pressure of each vapor is then used to calculate the three surface energy components using GvOC Equations. These values will then be used to establish an additive model of total surface energy for previously characterized rock samples based on percent of each constituent at the surface. The validity of the model will be tested by using the same Universal Sorption Device technique on the aggregate samples. A statistical analysis will be performed on the observed measurements versus predicted values.

Experiments – Although rock mineralogy has the capacity to be very complex it is dominated by a relatively small group of minerals of predictable variability in North America. The mineralogy of common aggregates used in hot asphalt mixes across America is outlined in the aggregate analysis data from the Strategic Highway Research Program’s (SHRP) materials reference library. Pure phase minerals are being collected by Dr. Ray Guillemette based on the findings of the SHRP. These minerals are the dominant constituents in all major aggregates of the study. The chosen minerals are listed in table 1.

The surface energies of these pure phase minerals will be calculated using a Universal Sorption Device using three reference gases to determine spreading pressures. Each mineral will be crushed and passed through a number 10 sieve. Minerals will be washed with distilled water and heated for 24 hours at 80° Celsius in a Fisher Isotemp® Oven. Each reference gas will be used on a separate sample of each pure phase mineral. After the test is run each sample will be washed with distilled water and reheated at 80° C for future analysis.

After each of the pure phase mineral surface energies have been quantified the SHRP aggregate samples themselves will be crushed and analyzed on the Universal Sorption Device to statistically determine the linear additive model's validity.

Data- The data gained from this experiment will be in  $erg / (cm)^2$  for each pure phase mineral and SHRP aggregate. In order to calculate mineral surface energy the isotherm for each reference gas must be calculated. To obtain a full isotherm, the aggregate is exposed to ten equal increments of partial probe vapor pressure from vacuum to saturated vapor pressure. At each stage the adsorped mass is recorded after it reaches equilibrium. The adsorped mass of each stage is then used to plot the isotherm. The measured isotherm for hexane is then used to calculate the specific surface area (SSA) using the Branauer, Emmett, and Teller BET equation:

$$A = \left( \frac{N_m N_0}{M} \right) \alpha$$

where  $N_0$ =Avogadro's number;  $M$ =molecular weight of the probe vapor;  $\alpha$  = projected area of a single molecule; and  $N_m$ =monolayer capacity of the aggregate surface. The specific surface area and each adsorption isotherm are then used to calculate three surface energy components using the GvOC equation:

$$W = 2\sqrt{\gamma_s^{lw} \gamma_v^{lw}} + 2\sqrt{\gamma_s^+ \gamma_v^-} + 2\sqrt{\gamma_s^- \gamma_v^+}$$

where  $g^{Total}$  = total surface energy of the material;  $g^{lw}$  = Lifhsitz-van der Waals or dispersive component;  $g^{AB}$  = acid-base component;  $g^+$  = Lewis acid component, and  $g^-$  = Lewis base component.

## Current Results

In order to use the Universal Sorbtion Device as an appropriate measuring device for surface energy the reproducibility must first be known. In order to test the reproducibility one of the SHRP aggregates was chosen at random and the surface energy was measured on the sorption device. The aggregate was RD-7, a shaly limestone composed primarily of calcite. Hexane and methylpropyl ketone were run in triplicate and water vapor was tested four times. The results indicated that there was a good deal of internal consistency between the test runs, and the overall surface energy calculation was within a 95 percent confidence interval to previous study of the aggregate over two years ago. In total, testing of 12 minerals and two clays has either been completed or is in progress. All minerals will be tested in quadruplicate for each vapor. The results to date are included in the following chart.

Sample Surface Energies					
Aggregates	van der Waals	e- Acceptor	e- Donor	Fractional Polarity	Total
RD Limestone	49.98	0.47	469.22	0.37	78.67
MM Sandstone	45.24	2.02	310.96	0.53	95.31
RC Limestone	49.55	2.98	799.29	0.66	147.16
RL Gravel	57.50	23.00	973.00	0.84	356.80
RK Basalt	52.30	0.64	164.00	0.28	72.80
RA Granite	48.80	0.00	412.00	0.02	50.00
RB Granite	52.78	3.28	15744.19	0.90	507.3948
Minerals					
Albite	51.57	0.22	501.69	0.29	72.79
Andesine	40.64	0.40	3755.04	0.66	118.35
Augite	52.67	8.69	3890.33	0.87	420.45
Bassanite	38.27	0.30	3036.03	0.61	98.16
Biotite	52.51	0.07	809.97	0.22	67.41
Calcite	34.94	0.40	85.16	0.25	46.54
Cerussite	35.07	0.11	113.14	0.17	42.11
Dolomite	60.29	0.18	564.05	0.25	80.57
Gypsum	41.13	1.31	65.47	0.31	59.65
Gypsum Hot Deg	42.24	1.32	87.66	0.34	63.73
Hematite	48.99	2.85	558.07	0.62	128.81
Hornblende	51.92	0.91	1338.86	0.57	121.63
Ilmenite	39.76	0.35	318.90	0.35	60.89
Kaolinite	30.48	5.01	80.00	0.57	70.51
Labradorite	46.21	1.81	186.54	0.44	82.92
Microcline	44.00	0.46	202.79	0.31	63.35
Montmorillonite	42.85	1.57	80.43	0.34	65.29
Muscovite	47.55	0.55	544.68	0.42	82.07
Olivine	44.17	1.55	57.52	0.30	63.04
Quartz	50.33	0.02	365.00	0.09	55.37
Rhodochrosite	40.33	0.86	145.76	0.36	62.66
Siderite	61.39	1.59	789.63	0.54	132.18

### Significant Problems, Issues and Potential Impact on Progress

No significant problems at this time.

### Work Planned Next Quarter

Work planned in the next quarter includes continued analysis of the aggregates and minerals, with specific reference to surface energies.

## **CATEGORY M4: MODELING**

### **Work Element M4a: Micromechanics Model (TAMU)**

#### Work Done This Quarter

The reader is referred the work element F3b.

#### Significant Results

The reader is referred the work element F3b.

#### Significant Problems, Issues and Potential Impact on Progress

The reader is referred the work element F3b.

#### Work Planned Next Quarter

The reader is referred the work element F3b.

### **Work Element M4b: Analytical Fatigue Model for Mixture Design**

This work is addressed under Work Elements F1b-1, F3c-1, and E1a.

### **Work Element M4c: Unified Continuum Model**

#### Work Done This Quarter

The development of the TAMU continuum model for capturing the effect of moisture on the degradation of the adhesive and cohesive bond strength is presented in this section. To model the effect of moisture on bond strength degradation two physical mechanisms are considered. The first mechanism is due to the effect of the moisture on bond degradation within the mastic itself (cohesive damage,  $\phi_c^M$ ); whereas, the second mechanism is related to the diffusion of the moisture at the interface of the mastic and aggregate leading to the bond strength degradation at the interface (adhesive damage  $\phi_a^M$ ). These two mechanisms may ultimately lead to erosion of the mastic film due to water imposed by passing traffic (scouring effect). Moisture damage is modeled using the effective (undamaged) configuration concept which makes the numerical implementation very easy. Hence, various damage laws which are linear/nonlinear functions of moisture content are investigated for modeling both cohesive moisture damage and adhesive moisture damage. These continuum-based moisture damage laws are implemented in PANDA. Each damage law is then used to predict the available experimental data in order to verify the moisture damage model and determine the associated material parameters. An attempt is made to relate these material parameters in the moisture damage model with the fundamental properties of the aggregate-mastic interface and the mastic. Furthermore, the developed moisture damage

model is coupled with the viscoelastic, viscoplastic, and viscodamage model developed in work element F3c. This will allow one to investigate the effect of moisture on the viscoelastic, viscoplastic, and damage response of asphalt mixes when subjected to realistic loading conditions. A parametric analysis is conducted to verify that the model captures the main effects of moisture on the response of the asphalt mixtures. In another parametric study the effect of moisture damage on permanent deformation and rutting in asphalt layers subjected to traffic loading while moisture-conditioned is studied.

#### Significant Results

None

#### Significant Problems, Issues and Potential Impact on Progress

None

#### Work Planned Next Quarter

The focus of the coming quarter is on calibrating and validating the moisture damage model. A systematic procedure will be developed for identifying the material parameters associated with the moisture damage model based on well-designed experiments at TAMU. The experiments include moisture conditioned pull-off tests on mastic-aggregate systems using the materials from the ARC 2x2 matrix validation plan. Furthermore, the experimental verification of the moisture damage component of the unified continuum damage model and the constitutive model itself will be initiated by conducting the mixture-level tests after subjecting the specimens to different levels of moisture conditioning. The validated moisture law will be employed in predicting pavement distresses in the presence of the moisture based on the unified viscoelastic, viscoplastic, and viscodamage model.

### **CATEGORY M5: MOISTURE DAMAGE PREDICTION SYSTEM**

This area is planned to start later in the project.

Moisture Damage Year 3		Year 3 (4/09-3/10)													Remarks
		4	5	6	7	8	9	10	11	12	1	2	3		
<b>Adhesion</b>															
<b>M1a</b>	<b>Affinity of Asphalt to Aggregate - Mechanical Tests</b>														
M1a-1	Select Materials														
M1a-2	Conduct modified DSR tests														
M1a-3	Evaluate the moisture damage of asphalt mixtures														
M1a-4	Correlate moisture damage between DSR and mix tests														
M1a-5	Propose a Novel Testing Protocol														
M1a-6	Standard Testing Procedure and Recommendation for Specifications														
<b>M1b</b>	<b>Work of Adhesion</b>														
M1b-1	Adhesion using Micro calorimeter and SFE														
M1b-2	Evaluating adhesion at nano scale using AFM														
M1b-3	Mechanisms of water-organic molecule competition														
<b>M1c</b>	<b>Quantifying Moisture Damage Using DMA</b>														
<b>Cohesion</b>															
<b>M2a</b>	<b>Work of Cohesion Based on Surface Energy</b>														
M2a-1	Methods to determine SFE of saturated binders														
M2a-2	Evaluating cohesion at nano scale using AFM														
<b>M2b</b>	<b>Impact of Moisture Diffusion in Asphalt</b>														
M2b-1	Difusion of moisture through asphalt/mastic films														
M2b-2	Kinetics of debonding at binder-aggregate interface														
<b>M2c</b>	<b>Thin Film Rheology and Cohesion</b>														
M2c-1	Evaluate load and deflection measurements using the modified PATTI test														
M2c-2	Evaluate effectiveness of the modified PATTI test for Detecting Modification														
M2c-3	Conduct Testing														
M2c-4	Analysis & Interpretation														
M2c-5	Standard Testing Procedure and Recommendation for Specifications														
<b>Aggregate Surface</b>															
<b>M3a</b>	<b>Impact of Surface Structure of Aggregate</b>														
M3a-1	Aggregate surface characterization														
<b>Modeling</b>															
<b>M4a</b>	<b>Micromechanics model development</b>														
M4b	Analytical fatigue model for use during mixture design														
M4c	Unified continuum model														
<b>M5</b>	<b>Moisture Damage Prediction System</b>														

**LEGEND**

**Deliverable codes**

- D: Draft Report
- F: Final Report
- M&A: Model and algorithm
- SW: Software
- JP: Journal paper
- P: Presentation
- DP: Decision Point
- [x]

-  Work planned
-  Work completed
-  Parallel topic

**Deliverable Description**

- Report delivered to FHWA for 3 week review period.
- Final report delivered in compliance with FHWA publication standards
- Mathematical model and sample code
- Executable software, code and user manual
- Paper submitted to conference or journal
- Presentation for symposium, conference or other
- Time to make a decision on two parallel paths as to which is most promising to follow through
- Indicates completion of deliverable x
- NOTE 1:** Research team intends to use DSR only for validation purposes.
- NOTE 2:** Delay in the development of binder procedure for moisture characterization is causing the experimental program for mixtures to be delayed.
- NOTE 3:** DSR is not expected to be used as procedure to evaluate moisture damage.

Moisture Damage Year 2 - 5		Year 2 (4/08-3/09)				Year 3 (4/09-3/10)				Year 4 (04/10-03/11)				Year 5 (04/11-03/12)			
		Q1	Q2	Q3	Q4	Q1	Q2	Q3	Q4	Q1	Q2	Q3	Q4	Q1	Q2	Q3	Q4
<b>Adhesion</b>																	
<b>M1a</b>	<b>Affinity of Asphalt to Aggregate - Mechanical Tests</b>																
M1a-1	Select Materials		DP														
M1a-2	Conduct modified DSR tests		P		P					P							
M1a-3	Evaluate the moisture damage of asphalt mixtures				DP					P	P	JP	P				
M1a-4	Correlate moisture damage between DSR and mix tests								P	P							
M1a-5	Propose a Novel Testing Protocol				P					P					JP, F		
M1a-6	Standard Testing Procedure and Recommendation for Specifications										P						
<b>M1b</b>	<b>Work of Adhesion</b>																
M1b-1	Adhesion using Micro calorimeter and SFE							JP									
M1b-2	Evaluating adhesion at nano scale using AFM								JP						JP		JP, F
M1b-3	Mechanisms of water-organic molecule competition				JP								JP	D	F		
<b>M1c</b>	<b>Quantifying Moisture Damage Using DMA</b>												JP	D	F		
<b>Cohesion</b>																	
<b>M2a</b>	<b>Work of Cohesion Based on Surface Energy</b>																
M2a-1	Methods to determine SFE of saturated binders														JP		
M2a-2	Evaluating cohesion at nano scale using AFM								JP								JP, F
<b>M2b</b>	<b>Impact of Moisture Diffusion in Asphalt</b>																
M2b-1	Diffusion of moisture through asphalt/mastic films							JP	D	F	D	F					
M2b-2	Kinetics of debonding at binder-agreagte interface																
<b>M2c</b>	<b>Thin Film Rheology and Cohesion</b>																
M2c-1	Evaluate load and deflection measurements using the modified PATTI test	DP	JP	D	F												
M2c-2	Evaluate effectiveness of the modified PATTI test for Detecting Modification			D	DP, F												
M2c-3	Conduct Testing							JP									
M2c-4	Analysis & Interpretation				P												
M2c-5	Standard Testing Procedure and Recommendation for Specifications					D											
<b>Aggregate Surface</b>																	
<b>M3a</b>	<b>Impact of Surface Structure of Aggregate</b>																
M3a-1	Aggregate surface characterization											JP		P			
<b>Models</b>																	
<b>M4a</b>	<b>Micromechanics model development</b>				JP					JP		JP			D	DP	F, SW
M4b	Analytical fatigue model for use during mixture design															M&A, D	F
M4c	Unified continuum model									JP		JP	DP	M&A	D	DP	F, SW
M5	Moisture Damage Prediction System																

**LEGEND**

**Deliverable codes**

- D: Draft Report
- F: Final Report
- M&A: Model and algorithm
- SW: Software
- JP: Journal paper
- P: Presentation
- DP: Decision Point

[x]

-  Work planned
-  Work completed
-  Parallel topic

**Deliverable Description**

- Report delivered to FHWA for 3 week review period.
- Final report delivered in compliance with FHWA publication standards
- Mathematical model and sample code
- Executable software, code and user manual
- Paper submitted to conference or journal
- Presentation for symposium, conference or other
- Time to make a decision on two parallel paths as to which is most promising to follow through
- Indicates completion of deliverable x



## PROGRAM AREA: FATIGUE

### CATEGORY F1: MATERIAL AND MIXTURE PROPERTIES

#### Work Element F1a: Cohesive and Adhesive Properties

*Subtask F1a-1: Critical Review of Measurement and Application of Cohesive and Adhesive Bond Strengths (TAMU)*

*Subtask F1a-2: Develop Experiment Design (TAMU)*

*Subtask F1a-3: Thermodynamic Work of Cohesion and Adhesion (Year 1 start)*

*Subtask F1a-4: Mechanical Work of Adhesion and Cohesion*

*Subtask F1a-5: Evaluate Acid-Base Scale for Surface Energy Calculations*

#### Work Done This Quarter

Two aggregates with different lithologies and different observed moisture resistance, limestone and andesite, were chosen as the substrate material in place of stainless steel. Three sets of tests were performed this quarter on each asphalt-aggregate combination in order to fully characterize the combination. These tests were a film sweep in which only the film thickness was varied; a series of test to generate the master curve in which loading rate and temperature were varied, but film thickness held constant; and a series of tests to determine the moisture resistance of the asphalt-aggregate combination in which only the moisture conditioning time was varied. Table F1a.1 displays the matrix of tests run with each aggregate substrate.

Table F1a.1. Testing matrix for asphalt-aggregate pull-off tests.

Testing Matrix																		
Replicate	Asphalt	Film Sweep - 45 Tests 0.01 mm/sec @ 23°C					Master Curve - 81 Tests									Moisture Conditioning - 27 Tests 0.01 mm/sec @ 23°C & 30µm		
		Film Thicknesses (µm)					Loading Rate - Temperature Combinations - 30µm									Conditioning Time		
		5	10	30	50	100	0.01 mm/sec			0.02 mm/sec			0.05 mm/sec			12 hrs	24 hrs	48 hrs
						10°C	23°C	36°C	10°C	23°C	36°C	10°C	23°C	36°C				
1	AAB																	
2																		
3																		
1	AAD																	
2																		
3																		
1	ABD																	
2																		
3																		

#### Significant Results

None

#### Significant Problem, Issues and Potential Impact on Progress

None

### Work Planned Next Quarter

The results obtained this quarter will be analyzed to determine how the fracture energy varies with changes in the film thickness, loading rate, temperature, and moisture conditioning time. This task will be completed during the coming quarter.

### **Work Element F1b: Viscoelastic Properties (Year 1 start)**

#### ***Subtask F1b-1: Viscoelastic Properties under Cyclic Loading***

### Work Done This Quarter

In this quarter we obtained results to demonstrate that interaction of stresses significantly influence the viscoelastic response of the asphalt binder at elevated temperatures even at intermediate stress levels. A stress sweep was conducted as a standard procedure to determine the linear viscoelastic limit of the asphalt binder. The frequency of oscillation was 0.1 Hz and 10 cycles were applied at each stress level. The stress amplitude was varied from the minimum of 100 Pa to a maximum of 48.1 kPa. The minimum of 100 Pa was selected to ensure that the lowest stress was well within the linear viscoelastic limit of the binder. The maximum stress amplitude was based on the maximum torque capacity of instrument. One important consideration while running the stress sweep test was that the normal force experienced by the plate was also recorded during the test.

Figure F1b.1 shows the test result for a typical stress sweep test. The figure illustrates both the applied shear stress as well as the average normal stress generated due to large deformation. Test results obtained thus far clearly show that application of shear stresses in torsion using a DSR also results in the generation of a normal force when the specimen is confined and the gap is not allowed to change. Second, the complex modulus is nonlinear even at low stress levels. Based on these observations, we hypothesized that there is an increase in the free volume of the asphalt binder which results in development of the normal force under confined conditions of constant gap. We also hypothesized that this complex stress state was responsible for the deviation from the linear response of the material.

A stress sweep was conducted on the same material in order to verify the increase in free volume without constraining the test specimen with a constant gap. Note that the increase in free volume at molecular scale is not the same as macroscopic increase in volume; however, the two are very strongly related. More details on this will be discussed in future reports. The parallel plate geometry was used to run this test since it allowed adjusting the gap in real time as the test is being conducted such that the normal force was always close to zero. The change in gap size was measured during the test. Test results demonstrate that in the absence of the constraint of a constant gap, the specimen expands partly due to increase in free volume and partly due to geometric nonlinearity.

The following tests were conducted using the cone and plate geometry to verify the hypothesis that the interaction of normal and shear stresses was one of the sources of nonlinear response.

This particular form of non-linearity is referred to as interaction non-linearity. A series of stress-time sweep tests were conducted to eliminate any accumulated normal force during the stress sweep test. The time sweeps were conducted at five different stress levels on the same specimen, using cone and plate geometry. The stress amplitudes were 0.1 kPa, 5 kPa, 10 kPa, 20 kPa, and 40 kPa. The frequency of test was kept the same as before; 0.1 Hz. Time sweep test at each stress level consisted of 10 cycles and the shear complex modulus was measured at the end of each cycle. A rest period of two minute was introduced between each time sweep to allow the normal force developed in the previous time sweep to relax. Each time sweep was repeated twice to allow us to detect any change or damage to material.

Figure F1b.2 shows the test results for time sweep test including the change in normal force. Ten sets of data point each related to one time sweep separated by two minutes of rest period. Data indicate that at low stress levels there is no normal force and the complex modulus remains constant. At higher stress levels, an increase in the normal force is accompanied with a decrease in the complex shear modulus. The interaction between normal force and shear complex modulus can be easily observed in these plots.

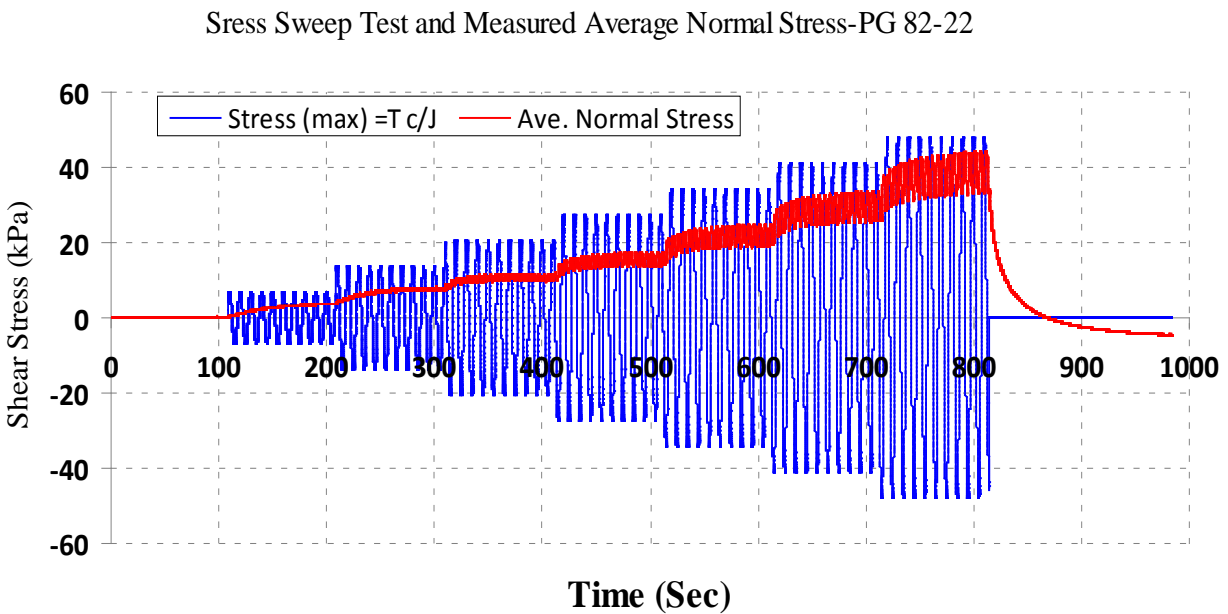


Figure F1b.1. Stress sweep test using cone and plate geometry.

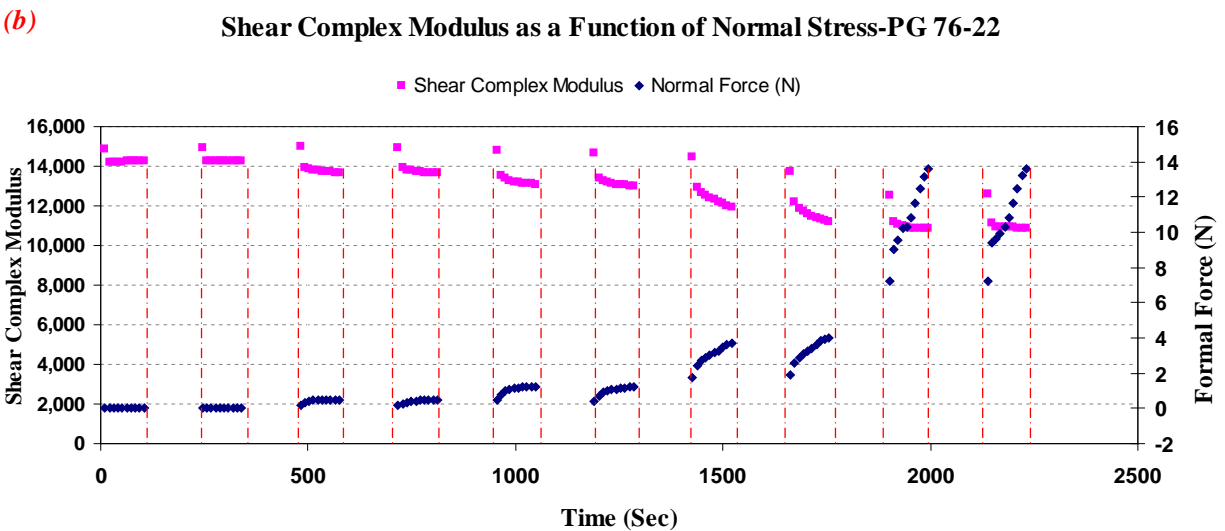
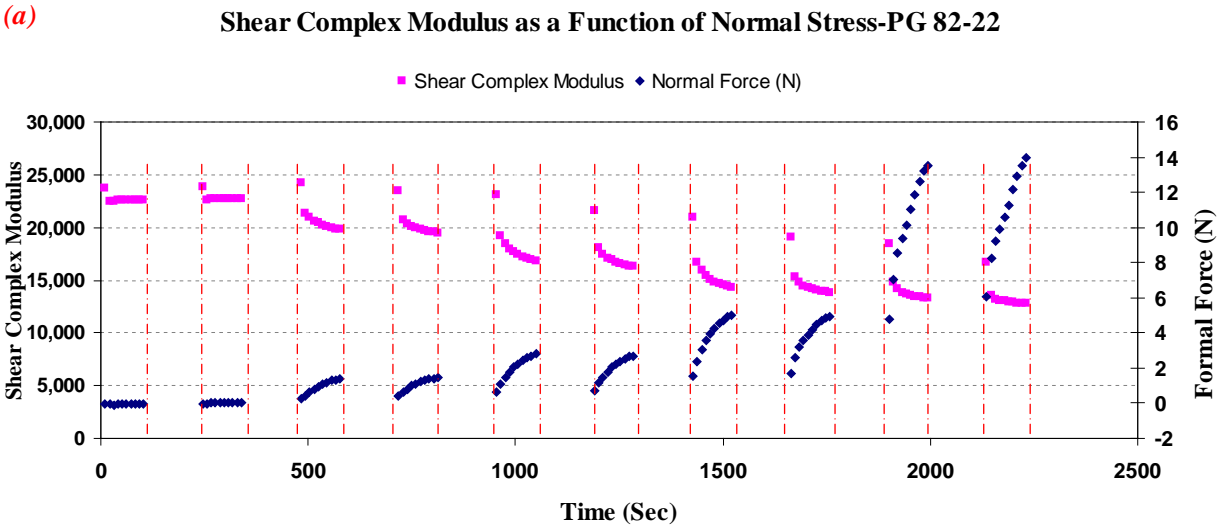


Figure F1b.2. Time sweep tests at different stress levels; with two repeat at each stress level to detect any damage, with two minutes rest period between each time sweep; the interaction between shear and normal stress is clearly demonstrated in these data.

### Significant Results

Based on the results from these tests we hypothesize that at intermediate to high stress or strain levels, the free volume of the binder increases. When subjected to shear stresses, restrictions on the increase in free volume will result in the generation of stresses normal to the shear plane. In the case of a DSR test these restrictions may be due to the constant gap in the test geometry and in the case of asphalt mixtures these restrictions may be due to confinement from surrounding aggregates. Results from this study also demonstrate that the nonlinear response of asphalt binders observed using measurements with the DSR can be explained due to interaction between normal stresses and applied shear stresses.

## Significant Problems, Issues and Potential Impact on Progress

None.

## Work Planned Next Quarter

Initial test results support the hypothesis that normal force induces a non-linear response in the material. This is also referred to as interaction non-linearity in the literature. We will continue with the investigation and modeling of this form of non-linear response. We will also verify the significance of interaction nonlinearity for FAM or asphalt mortars in the next phase of the study. The expectation is that the findings from this subtask will result in a more robust constitutive model for the time and stress state dependent response for asphalt materials that can significantly improve the accuracy of micromechanical models.

### ***Subtask F1b-2: Separation of Nonlinear Viscoelastic Deformation from Fracture Energy under Repeated and Monotonic Loading***

## Work Done This Quarter

Multiple technical presentations were made in international meetings in this quarter. The first two presentations were made in the Transportation Research Board (TRB) 89<sup>th</sup> Annual Meeting that was held in Washington, D.C., January 2010. They were entitled “Viscoelastic and Fatigue Characterization of Asphalt Mixtures” and “Characterization of Damage in Asphalt Mixtures Using Dissipated Pseudo Strain Energy”, respectively. The third presentation, entitled “Characterization of Fatigue Properties of Asphalt Mixtures”, was made in the Fundamental Properties and Advanced Models Expert Task Group of the Federal Highway Administration (FHWA) in Irvine, California, February 2010. All three presentations summarized the characterization of fatigue properties of asphalt mixtures under the repeated tensile loading using an energy balance approach, which was developed in past quarters.

In this quarter, the characterization of asphalt mixtures was further investigated in two aspects: (1) determining the number of cracks at various numbers of repeated loading cycles using the energy balance approach; and (2) testing pilot specimens using the test protocols that were developed in past quarters and are detailed in previous Quarterly Reports and in the technical report entitled “Aging Experiment Design Including Revised CMSE\* Testing Protocols and Analysis to Characterize Mixture Fatigue Resistance” (Luo et al. 2009).

The energy balance approach developed in previous quarters proved its ability to model the growth of fatigue cracks using fundamental material properties measured from the Viscoelastic Characterization (VEC) test and the Repeated Direct Tension (RDT) test. Specifically, this approach determined the amount of energy dissipated to drive the fatigue crack growth and predicted the mean crack radius with the increase of load applications. It was found that, when the number of load cycles increased, the mean crack radius increased while the number of cracks decreased. Both mean crack radius and the number of cracks were desired in order to determine the lost area of the intact material so as to further determine the true stress in the intact material of a damaged asphalt mixture that essentially drove the crack growth. The investigation on the

mean crack radius was documented in previous quarterly reports, and the determination of the number of cracks was developed using the same energy balance approach in this quarter.

The determination of the number of cracks consisted of three steps. The first step was to calculate the true stress in the intact material of a damaged asphalt mixture using the dissipated pseudo strain energy (DPSE) balance equation as shown in equation F1b-2.1:

$$\pi \frac{(\sigma_A)^2}{E_A} \sin(\varphi_A - \varphi_{LVE}) = \pi \frac{(\sigma_T)^2}{E_T} \sin(\varphi_{NLVE} - \varphi_{LVE}) \quad (\text{F1b-2.1})$$

where  $\sigma_A$ ,  $E_A$  and  $\varphi_A$  are the apparent stress, modulus magnitude and modulus phase angle measured from a destructive RDT test, respectively;  $\sigma_T$  is the true stress in the intact material;  $\varphi_{LVE}$  and  $E_T$  are the phase angle and magnitude of the modulus measured from a nondestructive RDT test, respectively; and  $\varphi_{NLVE}$  is the modulus phase angle of the material within the nonlinear viscoelastic region, which is calculated based on the phase angle measured from the destructive RDT test. Solving equation F1b-2.1 for  $\sigma_T$  gives:

$$\sigma_T = \frac{\sigma_A}{\sqrt{\frac{\sin(\varphi_{NLVE} - \varphi_{LVE})}{\sin(\varphi_A - \varphi_{LVE})} \cdot \frac{E_A}{E_{LVE}}}} \quad (\text{F1b-2.2})$$

The second step in the procedure of determining the number of cracks was to apply the force equilibrium condition to the asphalt mastic as shown in equation F1b-2.3. Since the asphalt mixture was under a repeated tensile load, it was the asphalt mastic that took the tensile load. As a result, most cracks developed in the asphalt mastic and the RDT test captured the behavior of the full mixture with most of the damage occurring in the mastic. Therefore, the following equation was established:

$$\sigma_A A_M = \sigma_T (A_M - A_D) \quad (\text{F1b-2.3})$$

where  $A_M$  is the total area of damaged mastic asphalt obtained from the composition of the asphalt mixture; and  $A_D$  is the lost area of mastic asphalt due to crack growth. Substituting equation F1b-2.2 into F1b-2.3 gives:

$$A_D = A_M \left( 1 - \sqrt{\frac{\sin(\varphi_{NLVE} - \varphi_{LVE})}{\sin(\varphi_A - \varphi_{LVE})} \cdot \frac{E_A}{E_{LVE}}} \right) \quad (\text{F1b-2.4})$$

The third step in the calculation procedure is to determine the number of cracks using the formulation of  $A_D$  shown in equation F1b-2.4 and the mean crack radius as follows:

$$A_D = M\pi c^2 \quad (\text{F1b-2.5})$$

where  $M$  is the number of cracks; and  $c$  is the mean crack radius. The calculation of  $c$  was elaborated in previous quarterly reports. The ratio of  $A_D$  to the total cross sectional area of the damaged asphalt mixture was defined as the damage density,  $\phi$ . Plots of  $\phi$  and  $M$  versus the number of load cycles are given in figures F1b-2.1 and F1b-2.2, respectively.

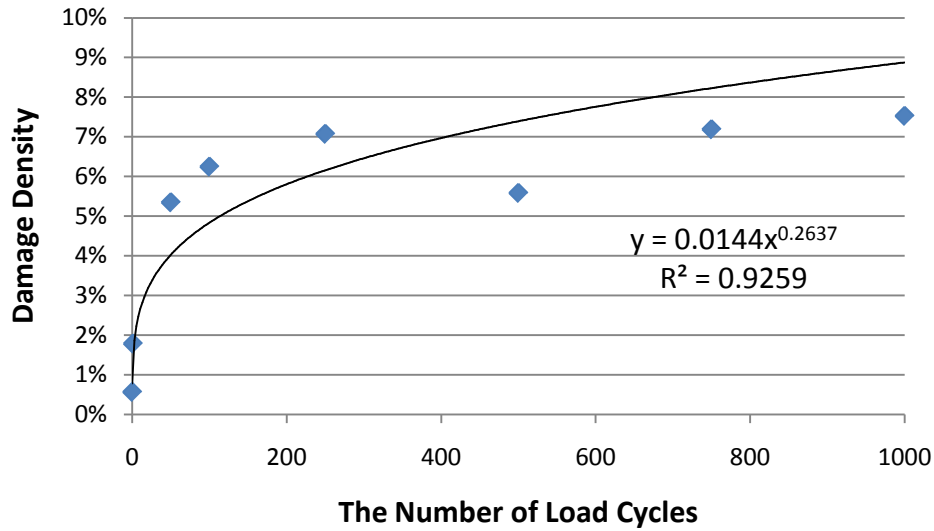


Figure F1b-2.1. The damage density with increase of load cycles.

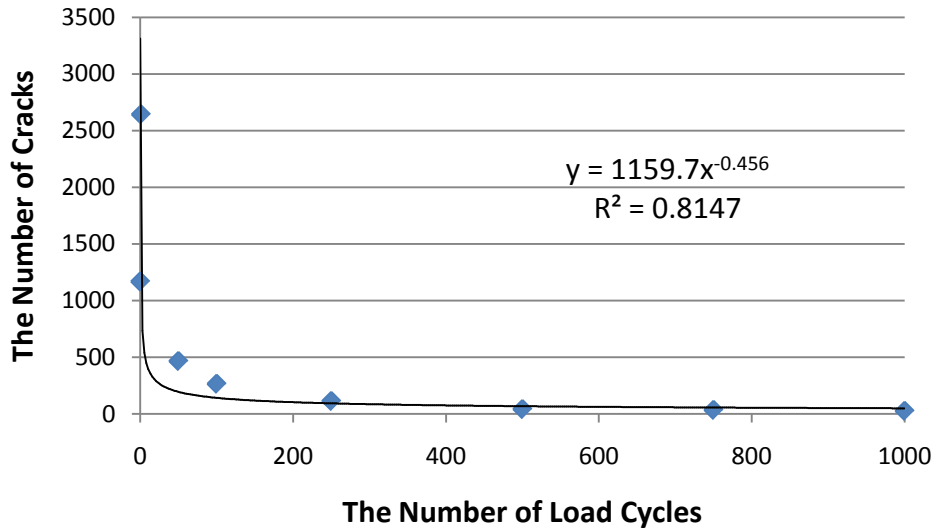


Figure F1b-2.2. The number of cracks with increase of load cycles.

The second major accomplishment in this quarter was testing the pilot specimens. The pilot specimens included two sets of specimens made of two types of binder AAD and AAM, respectively. In each set, there were two air void contents (4% and 7%) and two aging periods (0 and 6 months). Three tests were conducted on the pilot specimens in the sequence of: X-ray Computed Tomography (CT) test, the VEC test, and the RDT test. The X-ray CT test collected the information on the air void distribution and the average air voids size. The value of the average air void size obtained by the X-ray CT was compared to the initial mean crack radius obtained from the energy balance approach. The results from the VEC test included the master curves of the complex modulus magnitude and phase angle as well as the master curves of the complex Poisson's ratio magnitude and phase angle. Based on the RDT test data, the energy balance approach investigated the damage introduced to the asphalt mixture including both fatigue crack growth and permanent deformation.

Two major improvements were made during the testing. The first improvement was to utilize the tensile creep testing method in the VEC test. The original VEC test applied a monotonically increasing tensile load to the specimen. The terminal strain was controlled at  $80 \mu\epsilon$  so as to not introduce any damage, which was realized by watching the displacement of three Linear Variable Differential Transformers (LVDTs) through the computer of the Material Testing System (MTS). In order to simplify the test, a tensile creep testing method was introduced to modify the VEC test. In the tensile creep test, a constant tensile load was applied to the specimen for 1 minute. This tensile load was held at a low level that did not damage the specimen. It is much more convenient and efficient for the MTS to perform the tensile creep test. The data analysis of the tensile creep test data was also programmed in Matlab and Excel so that the master curves of the complex modulus magnitude and phase angle were generated automatically from the raw test data produced by the MTS. Another improvement was made in the data analysis on the RDT test data to reduce the variability of the RDT test results. Usually the variability of the RDT test results was generated in the measurement of the phase angle since the applied stress was not a perfect sinusoidal wave. This error in the measurement was associated with the testing machine and the measuring system. This error could be reduced by performing Fourier transformation to the stress response (Pellinen and Crockford 2003). A comparison between the raw data and transformed data is shown in figure F1b-2.3. After the Fourier transformation, the peak and valley of the wave were more accurately identified; consequently, the measured phase angle was more reliable.

### Significant Results

The energy balance approach was further developed this quarter to obtain the number of cracks in an asphalt mixture at different numbers of load cycles. This approach successfully determined not only the mean crack radius but also the damage density in the material. Half of the pilot specimens were tested. The modified VEC test demonstrated high efficiency compared to the original VEC test protocol. The raw test data of the RDT test were processed using the Fourier transformation, which successfully reduced the variability of the RDT test and enhanced the accuracy of the energy balance approach that characterized the fatigue damage of asphalt mixtures.

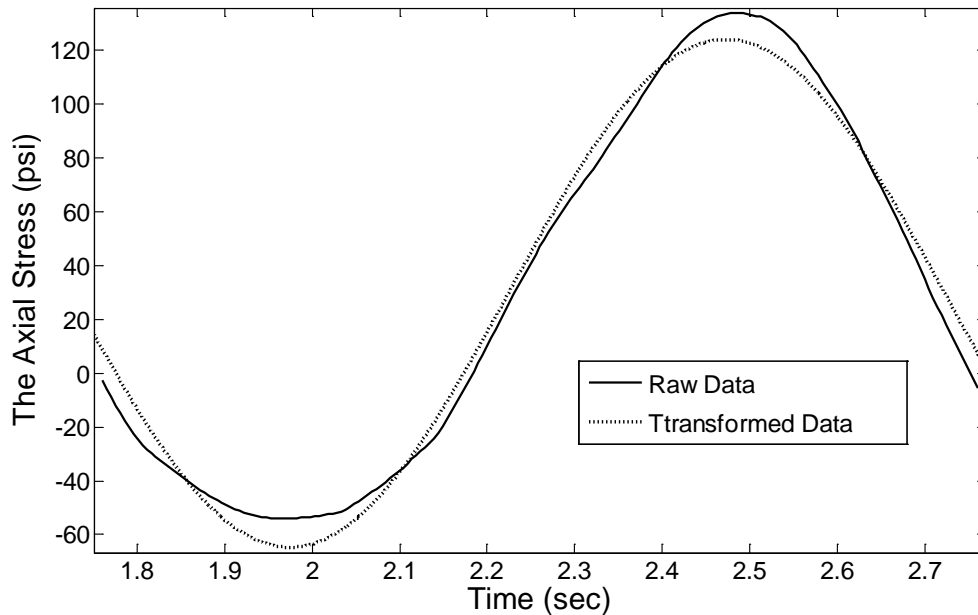


Figure F1b-2.3. The raw data and Fourier transformed data for the stress response.

### Significant Problems, Issues and Potential Impact on Progress

The newly purchased Material Testing System (MTS) is still not ready to use for testing because the software has not been fully installed. It is expected that the new MTS will be ready next quarter so more testing can be accomplished.

### Work Planned Next Quarter

The current characterization of asphalt mixtures in a damaged state is based on the RDT test without rest periods between loading cycles. Therefore, the healing of the asphalt mixture is not investigated in the RDT test. In the next quarter, the current RDT test protocol will be modified to incorporate rest periods in the repeated loading cycles. As a result, the healing of the asphalt mixture will be taken into account using the energy balance approach.

### References

Luo, X., A. Epps Martin, R. Luo, R.L. Lytton, and C.J. Glover, 2009, *Aging Experiment Design Including Revised CMSE\* Testing Protocols and Analysis to Characterize Mixture Fatigue Resistance*. Report No. FHWA-DTFH61-07H-0009, Texas Transportation Institute, College Station, Texas.

Pellinen, T., and B. Crockford, 2003, Comparison of Analysis Techniques to Obtain Modulus and Phase Angle from Sinusoidal Test Data. *Proc.*, 6<sup>th</sup> International RILEM Symposium, April 14-17, Zurich, Switzerland, 307-309.

## Work Element F1c: Aging

### *Subtask F1c-1: Critical Review of Binder Oxidative Aging and Its Impact on Mixtures (TAMU)*

#### Work Done This Quarter

The paper by King (1993) was reviewed for the purpose of developing an understanding of the fast-rate reaction process, to support kinetics measurements. Additionally, measurements of diffusivity in mastics have been reviewed.

#### Significant Results

*Oxycyclic oxidation mechanisms.* King (1993) proposed an oxycyclic mechanism that integrates the research findings of van Gooswilligen, Beaver and Petersen. van Gooswilligen concludes that asphalt oxidation involves catalyst, oxygen, and asphalt as necessary reactants. Beaver postulates the ETIO (Electron Transfer Initiated Oxidation) mechanism for sediment formation in fuels, which is applied by King to asphalt oxidation. Petersen showed that the primary oxidation products are ketones, sulfoxides, carboxylic acids and acid anhydrides. The oxycyclic mechanism provides insight to the net reaction, in terms of reactants and products. However individual mechanistic steps are not defined. One possible reaction pathway is that the catalyst first oxidizes the substrate (asphalt molecule), the resulting catalyst-substrate complex then reacts further with oxygen to form peroxide, and finally the O-O peroxide bond breaks further to form ketones and other products. King shows the capability of the oxycyclic mechanism to explain the formation of ketones from benzylic carbon, carboxylic acids from alcohols, carboxylic acids from ketones, and acid anhydrides from diketones. However, it is unable to explain the formation of sulfoxides, which is reasonable because sulfide oxidation probably follows a different scheme from hydrocarbon oxidation.

The big advantage of King's oxycyclic mechanism is that it involves no free radical chain reaction, which is refuted by several research findings. It also allows the asphalt molecules to oxidize without atom movement, given that asphalt is a stiff viscoelastic material.

While the oxycyclic mechanism is attractive, the proposed theory is based on the assumption that catalyst plays a critical role in oxidation, which is not well established. Furthermore, there is no experimental evidence yet to prove this theory.

*Oxygen Diffusivity in Asphalt.* Oxygen diffusivity in asphalt mastics has been measured on four Texas binders at three temperatures (60 °C, 75 °C, and 90 °C) with three volume fraction levels of aggregate fines (0%, 10% and 25%) (TxDOT project 0-6009). The fine aggregates used in the asphalt mastics range in size from 100 mesh down to 200 mesh. The effect of fines on the diffusion of oxygen in binders is an important issue for modeling binder oxidation in pavements.

A trend of decreasing oxygen diffusivity with increasing volume fraction of fines was observed for each binder at the test temperatures. Other than the volume fraction of filler, oxygen diffusivity in mastics does not show a clear dependence on either test temperature or binder.

Further analysis of the dependence of diffusivity on volume fraction of fines using the average diffusivity values from the different binders and test temperatures shows a good comparison of those average values to predicted values using conventional models (Maxwell, Rayleigh or Non-spherical complex models, Bird et al., 2001), figure F1c-1.1. In this figure, the measured diffusivity for each mastic is normalized by the measured diffusivity of its own neat binder, i.e. without fines, at the same temperature. Although using average values of diffusivity at each level of fines is somewhat problematic because the asphalt-to-asphalt variability appears to be due to more than random measurement error, the results do suggest that with a known volume fraction of fines for a given mixture design, the oxygen diffusivity in mastics can be estimated with reasonable accuracy by using conventional prediction models.

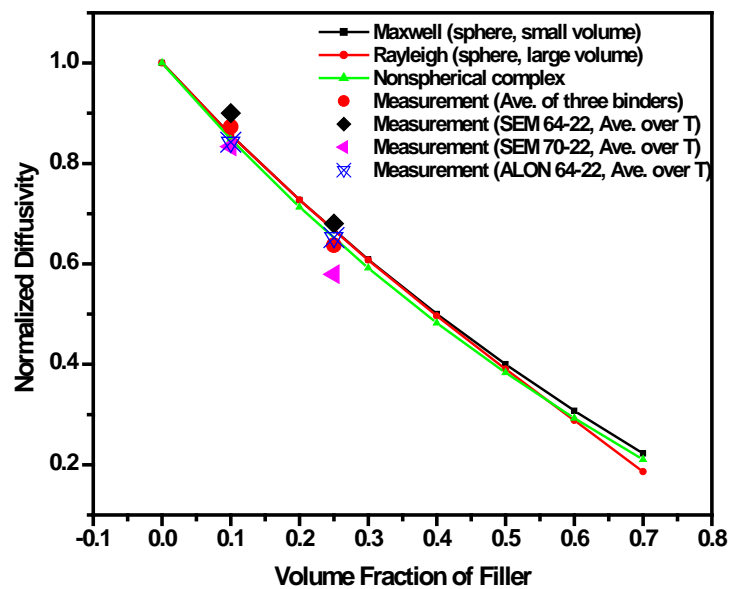


Figure F1c-1.1. Comparison of model prediction with average of measured diffusivity values for each binder over testing temperatures.

Significant Problems, Issues and Potential Impact on Progress

There are no problems or issues.

Work Planned Next Quarter

Review of the literature and work by other researchers is ongoing.

### ***Subtask F1c-2: Develop Experimental Design (TAMU)***

#### Work Done This Quarter

No work this quarter.

#### Significant Results

None.

#### Significant Problems, Issues and Potential Impact on Progress

Conducting the planned experiments using ARC core binders is awaiting the arrival of ARC binders. Measurements on mixtures fabricated using other binders are underway.

#### Work Planned Next Quarter

Measurements of mixture rheology and fatigue continue. Also, rheological measurements of binders extracted and recovered from these mixtures will be made as part of the effort to link binder oxidation to changes in mixture properties.

### ***Subtask F1c-3: Develop a Transport Model of Binder Oxidation in Pavements (TAMU)***

#### Work Done This Quarter

Further development of the transport model is ongoing based upon pavement and mixture measurements of binder oxidation, and based upon laboratory measurements of binder oxidation and diffusion kinetics. Additional data on properties that are required for the model are reported in subtask F1c-1. Measurements using ARC binders are planned for upcoming months.

#### Significant Problems, Issues and Potential Impact on Progress

The effort to obtain cores from pavement sites in different climate zones continues. Discussion with researchers at WRI have been held to evaluate which of their test sites might be best used for providing information on binder and mixture changes in pavements as a function of service time. Cores from such sites will provide 1) data on binder oxidation as a function of time and depth in pavements and 2) data on changes to mixture rheology and fatigue resistance that occur in response to binder oxidation.

#### Significant Results

A paper has been drafted to document the air temperature pattern model that has been developed for accurately calculating air temperature as a function of time for use in the pavement oxidation model. Also, a paper has been submitted to the Journal of Materials in Civil Engineering to document the improved pavement temperature model, a key element of the pavement oxidation model.

### Work Planned Next Quarter

Data on binder kinetics and diffusion, laboratory mixture rheology and fatigue resistance, and field core rheology and fatigue resistance continue.

### ***Subtask F1c-4: The Effects of Binder Aging on Mixture Viscoelastic, Fracture, and Permanent Deformation Properties (TAMU)***

### Work Done This Quarter

A key element of this subtask is to measure the effect of binder oxidative hardening on mixture rheological and fatigue properties. Earlier efforts reported in the literature showed that binder oxidative hardening decreases mixture fatigue resistance, but did not provide enough information to explain why some mixtures are adversely affected more than others, or what mixture parameters are most critical to understanding how binder oxidation decreases mixture fatigue resistance. To state it differently, we do not yet have enough information to be able to model changes to mixture properties, including both rheology and fatigue resistance, that occur as binders oxidize. The work of this subtask is directed at improving that understanding, thereby leading to improved fundamental models of pavement performance.

In Subtask F1c-2, we developed a laboratory experimental protocol for fabricating and testing mixtures of different types and aged to different levels to obtain the type of fundamental data required for such fundamental models. Additionally, specimens aged in the field at different sites around the country will provide similar data on field-aged and field-loaded pavements. These mixture tests are proceeding, although they have been delayed because of issues related to procurement and development of the test equipment and protocols. Work on mixture test analysis is proceeding in parallel and is described below.

The destructive properties of asphalt mixtures in compression were investigated in this quarter. This investigation consisted of: 1) development of comprehensive mechanistic models to characterize the anisotropic and viscoplastic properties of asphalt mixture in compression; and 2) formulation of parameters in the mechanistic models in terms of measurable material properties.

The developed mechanistic models included the following components:

- Anisotropy due to aggregate preferential orientation and aggregate sphericity. A fabric tensor that described the material microstructure was defined to re-derive the vector magnitude,  $\Delta$ , which is shown in equation F2c.1. The value of  $\Delta$  ranged from 0 to 1: a value of 0 indicated the completely random distribution of aggregates that led to an isotropic asphalt mixture; and a value of 1 implied the major axis of all aggregates orients in the horizontal direction or in the vertical direction.
- Modified stress tensor due to anisotropy and cracks/voids. This modified effective stress tensor addressed the effects of both anisotropy and cracks/voids on the true stresses in the intact material. The formulation of the modified effective stress tensor is shown in equation F2c.2.

- Microstructure-based viscoplastic model for asphalt mixture. The microstructure-based viscoplastic model took the separated dissipated pseudo-strain energy (DPSE) for permanent deformation,  $W_{R2}$ , as the driving force of the irrecoverable viscoplastic deformation. The viscoplastic yield properties of an asphalt mixture was described by the modified Drucker-Prager yield surface function that took into account the effects of confinement, internal friction and interlocking on the asphalt mixture. The compressive properties of the asphalt mixture were also separated from the extensive properties using the deviatoric shear stress as shown in equation F2c.7. The application of the non-associated flow rule indicated that the direction of the viscoplastic strain increment is perpendicular not to the yield surface but to the plastic potential surface.

The parameters of the mechanistic models were either regression variables based on experimental data or model parameters dependent on inherent material properties such as anisotropic moduli, internal friction angle and cohesion. Formulations were developed for three model parameters: 1) microstructural vector magnitude,  $\Delta$ ; 2) slope of yield surface function,  $\alpha$ ; and 3) initial yield stress,  $\kappa_0$ . Formulations of the slope of the plastic potential function and of the yield stress ratio of extension to compression will be developed in the next quarter.

### Significant Results

In this quarter, mechanistic models were developed to characterize the anisotropic viscoplastic-damage properties of asphalt mixtures in compression. The anisotropy of the asphalt mixture was captured by the microstructure-based parameter, vector magnitude. The visco-damage properties were characterized by the modified Perzyna's viscoplastic model incorporated with the extended Drucker-Prager yield surface function and non-associated flow rule. Formulations were established to determine the model parameters in terms of material properties.

### Significant Problems, Issues and Potential Impact on Progress

The mechanistic viscoplastic models for asphalt mixtures were not completed in this quarter because of the significant anisotropy of the asphalt mixture in compression and the complexity of the damage density that accounted for the degradation of asphalt mixture properties due to increasing mean crack radius under a compressive load. The test protocols and data analysis program need to be further developed to evaluate and calibrate the proposed viscoplastic-damage models and the formulation of model parameters in terms of material properties.

### Work Planned Next Quarter

In the next quarter, formulations will be developed for the slope of the plastic potential function and for the yield stress ratio of extension to compression. The formulation of the modified vector magnitude will also be calibrated. The DPSE for permanent deformation will be explicitly defined and calculated for an asphalt mixture under the repeated compressive loading. The damage density will also be calculated to address the increase of the mean crack radius with the increase of the number of load cycles.

## ***Subtask F1c-5: Polymer Modified Asphalt Materials (TAMU)***

### Work Done This Quarter

In this quarter, polystyrene (PS), polybutadiene (PB) [36% cis-PB, 55% trans-PB, and 9% vinyl] and styrene-butadiene-styrene tri-block copolymer (SBS) were blended with asphalts at different concentrations, and FTIR absorption and fluorescence microscopy measurements of those blends were evaluated to assess FTIR absorption versus styrene and butadiene content and blend morphology. Then, using these results, the effects of oxidation on polymer degradation and blend morphology were evaluated.

### Significant Results

#### *FTIR absorption and morphology characterization*

In an effort to better understand the relationship of absorption by the various FTIR absorption bands to polymer composition, FTIR absorption of PS at  $699\text{ cm}^{-1}$ , trans-PB at  $966\text{ cm}^{-1}$ , and vinyl at  $911\text{ cm}^{-1}$ , quantified in terms of peak height and area, shows a good correlation to concentration, whereas absorption of cis-PB is heavily interfered with by adjacent asphalt bands. To obtain a quantitative measurement of total polymer content and content of cis-PB, another constraint is required besides FTIR absorption. The PS/PB ratio in SBS might be used as an additional constraint, as this ratio may be available from SBS manufacturers and is rather consistent (approximately 30 percent, ranging from between 23 to 40 percent, according to the literature). Combining all such information, the total polymer content and the content of each SBS component for a given asphalt might be predicted. This effort is continuing.

The polymer morphology of the asphalt-polymer blends was studied with fluorescence microscopy to better understand the phase behavior of polymer blended in asphalt and the changes in morphology that occur with oxidative aging. For asphalt blended with PB, an increase of PB concentration results in an increase of polymer phase separation. Asphalt blended with PS, on the other hand, shows a much better dispersion of the polymer, even at relatively high PS concentration (five percent). For blends of SBS in asphalt, the morphological structure was between that of PS and PB. A representative morphology for each blend at five percent polymer is shown in figure F1c-5.1. These observations suggest that butadiene segments of SBS interact more strongly with other butadiene segments than with asphalt, whereas styrene segments enhance SBS interactions with asphalt. This conclusion is not surprising, especially when the chemical structure of the polymer components versus that of asphalt is considered. These results suggest that the interplay of these two components will decide, to some extent, the polymer network structure formed and the interaction of the polymer network with the asphalt.

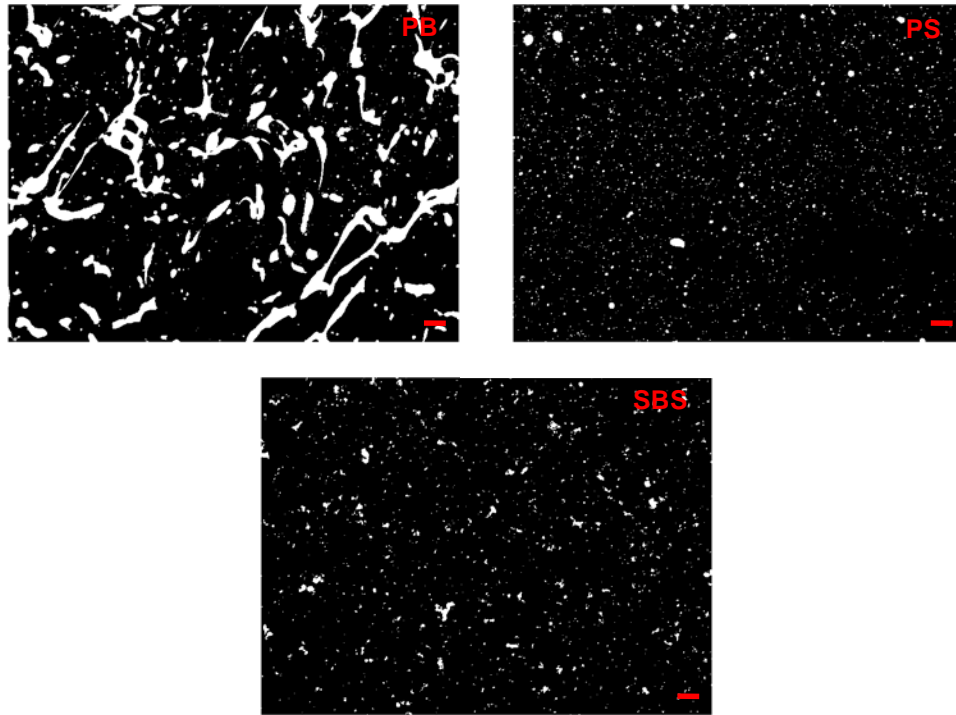


Figure F1c-5.1. Polymer morphology of PS, PB and SBS blended asphalt at a concentration of 5 percent (scale bar represents 20  $\mu\text{m}$ ).

In addition, the polymer morphology for ten commercial polymer-modified asphalts was examined. Probably due to effective additives and good blending techniques, but possibly also due to the specific polymer-asphalt interactions, seven of the asphalts exhibit a very uniform dispersion of polymer in the asphalt; separate polymer phases can barely be observed with fluorescence microscopy. However, the other three blends show a clear polymer phase structure.

#### *Polymer Degradation with Oxidation*

With the polymer characterization tools developed above, morphology and polymer content were evaluated for a number of commercial SBS-modified asphalts that were oxidized at different temperatures.

The effect of oxidation on polymer morphology has been evaluated with one SBS-modified asphalt (Alon 76-22) whose morphology is clearly observed with fluorescence microscopy and one SBS-modified asphalt (SEM 70-22) whose morphology cannot be clearly observed. Both asphalts were oxidized at controlled temperatures for a period of time, and samples were retrieved at different times for morphology imaging. Interestingly, the size of the polymer phase regions for the Alon 76-22 decreases with oxidation time, along with fluorescence intensity. For SEM 70-22, however, which did not exhibit a well-defined SBS phase morphology, fluorescence intensity decrease was also observed with oxidation. A comprehensive imaging analysis process was carried out and further confirmed the fact, as shown in figures F1c-5.2 and F1c-5.3. These observations strongly suggest SBS physically degrades with oxidation.

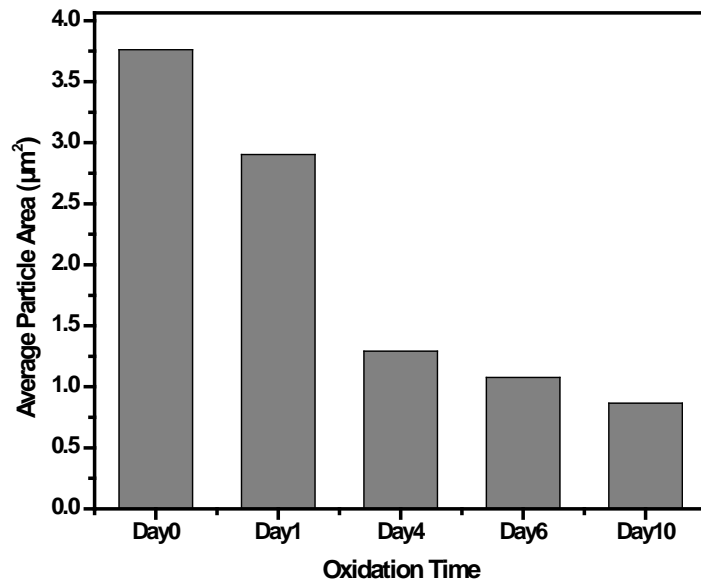
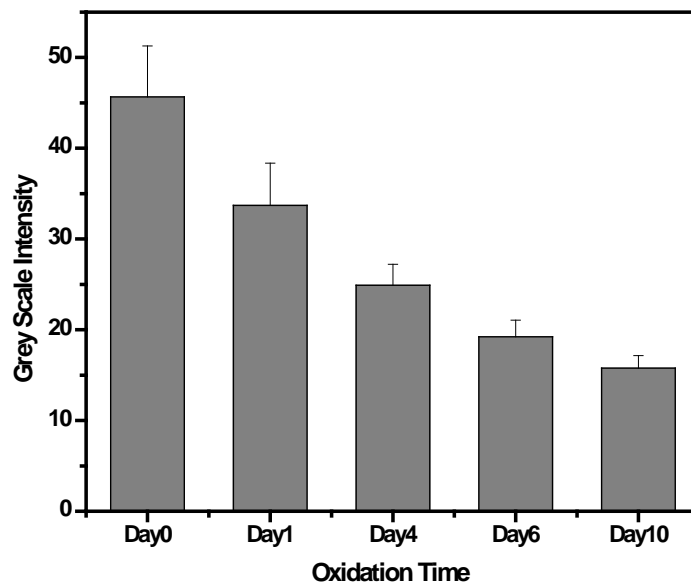


Figure F1c-5.2. Change of average polymer “particle” area with oxidation time at 90 °C.



.Figure F1c-5.3. Change of gray scale intensity of polymer fluorescence with oxidation time at 90 °C.

## Significant Problems, Issues and Potential Impact on Progress

None.

## Work Planned Next Quarter

In next quarter, the effect of asphalt oxidation on polymer morphology and content will be evaluated with additional SBS-modified asphalts.

Evaluating the effect of oxidation on the indicated polymer content is an ongoing effort. The dynamic change of polymer content (as measured by FTIR) for SBS and its components with oxidation is being determined to evaluate the oxidation susceptibility and oxidation kinetics for different polymers. The rheological properties of polymer modified asphalt also are measured, and an index, such as the ratio of the low shear rate limiting viscosity (or the DSR function, as appropriate) for the polymer modified binder to the limiting viscosity (or DSR function, as appropriate) of its base binder will be used to evaluate the oxidation susceptibility and oxidation kinetics for different polymers in terms of polymer functionality.

## References

Beaver, B., C. Gilmore, G. Veloski, and V. Sharief, 1991, Role of indoles in the oxidative degradation of unstable diesel fuels. *Energy and Fuels*, 5, 274-280.

Bird, R.B., W.E. Stewart., and E.N. Lightfoot, 2001, *Transport Phenomena*. John Wiley & Sons. 2nd Edition, p. 281.

King, G. N., 1993, Oxycyclics: Understanding Catalyzed Oxidation Mechanisms in Bitumen and Other Petroleum Products. *Fuel Science and Technology, Intl.*, 11 (1), 201-238.

Petersen, J.C., 1986, Quantitative functional group analysis of asphalts using differential infrared spectrometry and selective chemical reactions – theory and application. *Transportation Research Record*, 1096.

van Gooswilligen, G., H. Berger, and F. Th. De Bats, 1985, Oxidation of bitumens in various tests. *Proc.*, Eurobitume, 95-101.

## Publications and Presentations

Prapaitrakul, Nikornpon, Rongbin Han, and Charles J. Glover, 2009, A Transport Model of Asphalt Binder Oxidation in Pavements. *Road Materials and Pavement Design*, Vol. 10 Special Issue, p. 95-113.

Rongbin Han, Xin Jin, Charles J. Glover. “Modeling Pavement Temperature for Use in Binder Oxidation Models and Pavement Performance Prediction,” submitted July 2009 to *Journal of Materials in Civil Engineering* (resubmitted, under review as of 1/15/10).

Prapaitrakul, Nikornpon, Rongbin Han, Xin Jin, and Charles J. Glover. "Transport Model Calculations of Asphalt Binder Oxidation in Pavements," presented at the 46th Annual Petersen Asphalt Research Conference, July 14, 2009.

Prapaitrakul, Nikornpon, Rongbin Han, Xin Jin, and Charles J. Glover, "A Transport Model of Asphalt Binder Oxidation in Pavements," presented at the 3rd International Conference on Asphalt Materials, Qingdao, Shandong Province, China, August 6, 2009.

## **Work Element F1d: Healing**

*Subtask F1d-1: Critical review of the literature*

*Subtask F1d-2: Material selection*

*Subtask F1d-3: Experiment design*

*Subtask F1d-4: Test methods to measure properties related to healing*

*Subtask F1d-5: Testing of Materials for model validation\* (TAMU)*

### Work Done This Quarter

#### *Test procedure to determine intrinsic healing of asphalt binders using the DSR*

The test procedure to determine intrinsic healing of asphalt binders using the DSR was refined to improve repeatability and reduce artifacts that may appear as healing, especially at lower temperatures. The new test procedure also minimizes the time between bringing the two surfaces into contact with each other and the first measurement for stiffness of the composite (treated as time  $t=0$ ). A document detailing every step of the test procedure is available with the ARC researchers.

#### *Temperature dependence of intrinsic healing in asphalt binders*

Intrinsic healing of asphalt binder can be determined using the DSR based test method as described above. Based on the hypothesis for the healing mechanism it is expected that the intrinsic healing of asphalt binders would be temperature dependent. In order to validate this hypothesis and quantify the rate of intrinsic healing was determined at three different temperatures using the DSR. The testing is currently under progress and includes three binders, three temperatures and two different aging conditions.

Based on the work done this quarter, the influence of temperature on the initial healing and time dependent healing is evident. Two considerations in interpreting this data are as follows. First, the initial healing recorded by the DSR has a 15 second delay from the time the two surfaces of the binder are brought into contact with each other. This is due to practical limitations of the test method. Therefore, even at low temperatures there may be some time dependent healing that may take place as the first reading is being recorded. Second, prior to starting the test a high normal force is applied for a very small duration of time before the target constant normal force of 0.4N is achieved and maintained throughout the test. This is to ensure complete wetting of the two surfaces.

Figures F1d.1 and F1d.2 illustrate the initial and time dependent healing measured using the DSR for a PG 64-22 and a PG 70-22 binder. These binders were selected pending the availability of the core binders for this task. For the PG 64-22 binder, a significant fraction of the healing occurred instantaneously (or within the 15 second interval before starting measurements). The overall healing increased slightly with time but significantly as the temperature was increased from 10C to 20C. Similar results were obtained for the PG 70-22 binder. The last data set for PG 70-22 25C is based on a single replicate, whereas rest of the data are based on at least three replicates. It appears that the time dependent healing for PG 70-22 increased significantly when the temperature was increased from 20C to 25C.

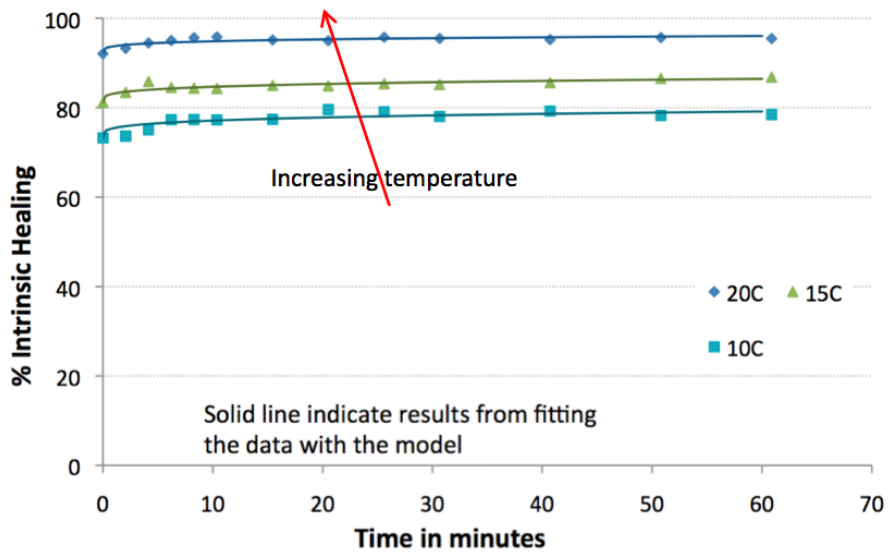


Figure F1d.1. Healing rate for PG 64-22 binder at different temperatures.

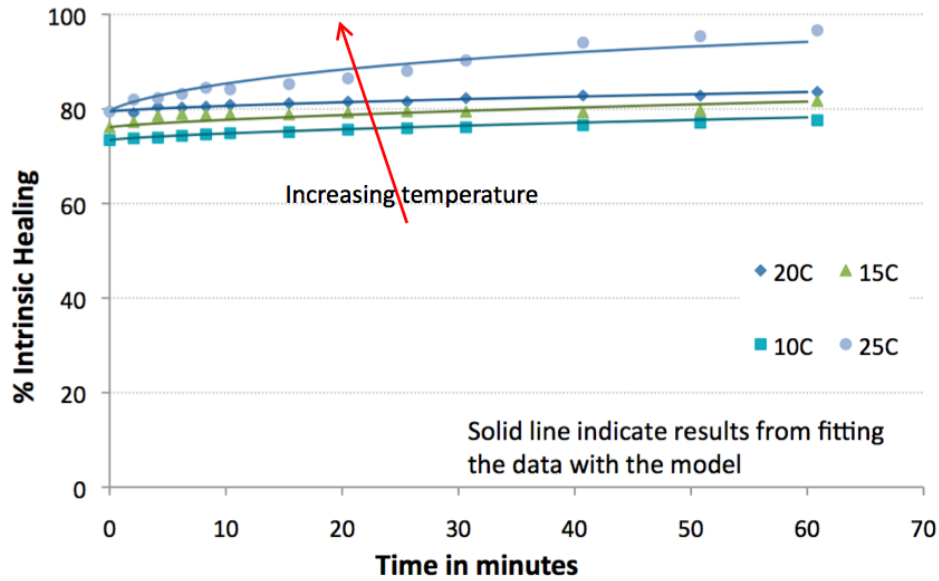


Figure F1d.2. Healing rate for PG 70-22 binder at different temperatures.

In the previous reports we had indicated the use of the Avrami equation to characterize the intrinsic healing function of different asphalt binders. This modified form of the Avrami equation, shown below, introduces a constant,  $R_0$ , to represent the instantaneous strength gain across wetted crack surfaces due to their interfacial work of cohesion:

$$R_h(t) = R_0 + p(1 - e^{-qt^r}) \quad (\text{F1d.1})$$

Equation F1d.1 represents the sum effect of: (i) instantaneous strength gain due to interfacial cohesion at the crack interface, represented by the parameter  $R_0$  which is also equal to  $1-p$ , and (ii) time dependent strength gain due to inter diffusion of molecules between the crack surfaces, represented by  $1 - e^{-qt^r}$ . Accordingly, the term  $R_0$  should not change significantly with slight changes in temperature. However, due to practical limitations of this test method, we may expect small increases in  $R_0$  with increase in temperature. This is corroborated in figure F1d.3 that illustrates the change in  $R_0$  for the two different binders as a function of temperature.

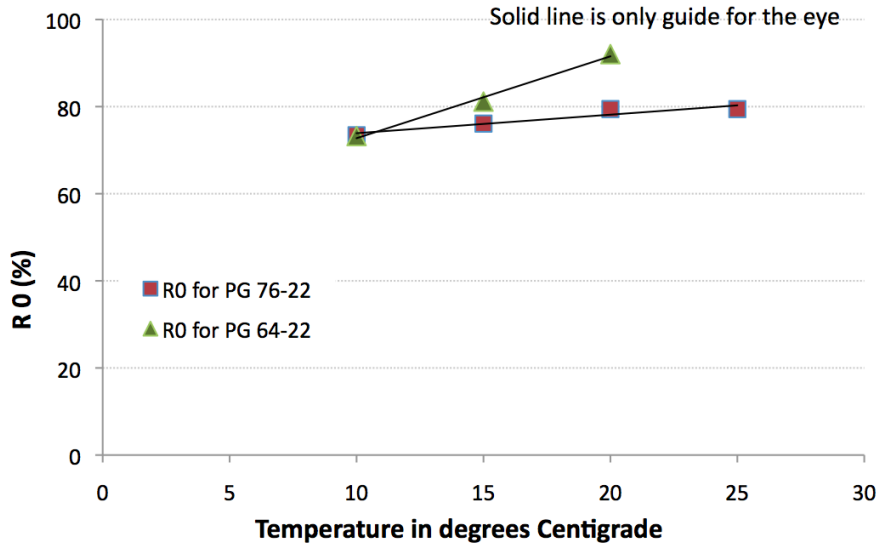


Figure F1d.3. Change in R0 for the two asphalt binders as a function of temperature.

Based on the proposed hypothesis, the parameter “q” in the above expression must be strongly influenced by the temperature. Also, the term “r” is treated as a material constant. Figure F1d.4 illustrates the change in increase in “q” with an increase in temperature. The rate constant has a much higher rate of increase for the PG 64-22 binder as compared to the PG 70-22 binder. These findings are preliminary but encouraging and more work is in progress.

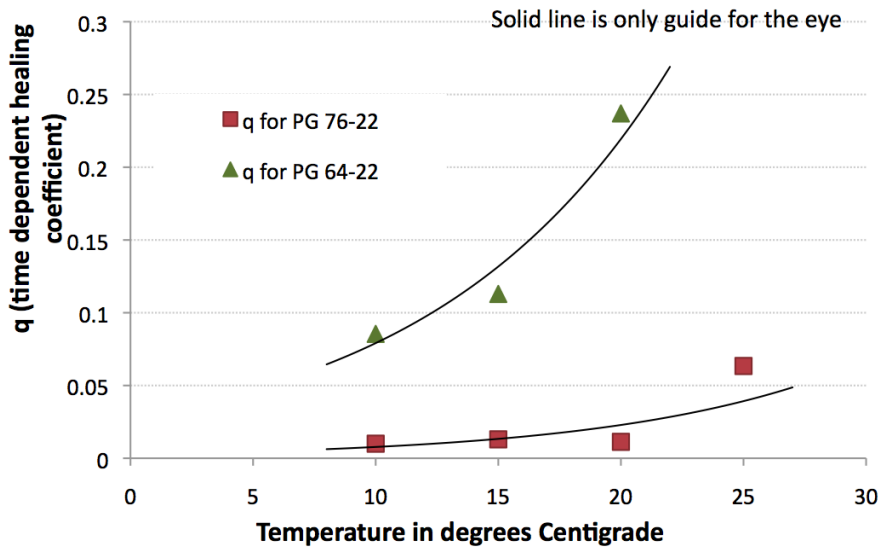


Figure F1d.4. Change in healing rate parameter “q” as a function of temperature.

### *Experiment design to determine wetting characteristics of asphalt binder*

We are continuing with preliminary tests to determine the feasibility of back calculating wetting characteristics using DMA tests on mortars. We hope to complete these tests in this quarter and start executing the experiment design.

### Significant Problems, Issues and Potential Impact on Progress

None.

### Work Planned Next Quarter

We plan to complete the measurements on the healing characteristics of at least three different asphalt binders at different aging conditions and temperatures. We also plan to finalize and start the test plan on the characterization of wetting using the DMA with mortar samples. Finally, we also plan to start the experiments using the synchrotron in this quarter.

### ***Subtask F1d-6: Evaluate Relationship Between Healing and Endurance Limit of Asphalt Binders (UWM)***

### Work Done This Quarter

In this quarter, evaluation of the strain-controlled time sweep with intermittent loading procedure for healing characterization was continued. The research group found that the procedure suggested by Shen (2009), which includes cycling between one second of loading followed by a rest period using a frequency of 10 Hz, is not feasible in the available Dynamic Shear Rheometers (DSRs). The DSR is unable to reach the target strain amplitude within the one-second loading time; rather, it takes several seconds to reach the desired strain amplitude. To solve this problem, efforts in this quarter focused on modifying the testing procedure to accommodate the DSR's limitations. Strain-controlled time sweeps with rest periods using longer loading times and longer rest periods were conducted. The number of loading cycles following each rest period that do not reach the target strain amplitude is negligible when using longer loading times, which in effect minimizes the issue of the time required to reach the target strain amplitude.

Two binders were tested using strain-controlled time sweeps with 10-minute loading periods, followed by two- and five-minute rest periods using a frequency of 10 Hz. Results were compared to tests run with the same loading conditions but without rest to see if this test procedure is capable of capturing healing. The research group tested a PG 64-22 un-aged binder at 25 °C, using a strain amplitude of 4%; test results are shown in figure F1d-6.1. The other binder tested—a PG 64-28 rolling thin film oven (RTFO)-aged binder—was tested at 20 °C using a strain amplitude of 5%; results of this test are shown in figure F1d-6.2. Three replicates were run for each loading condition and repeatable results were obtained. The data for each loading condition in the graphs consist of averages from the three test replicates. It should be noted that the normalized  $|G^*|$  is calculated by dividing the complex modulus measured at a given cycle by the maximum complex modulus measured during the test.

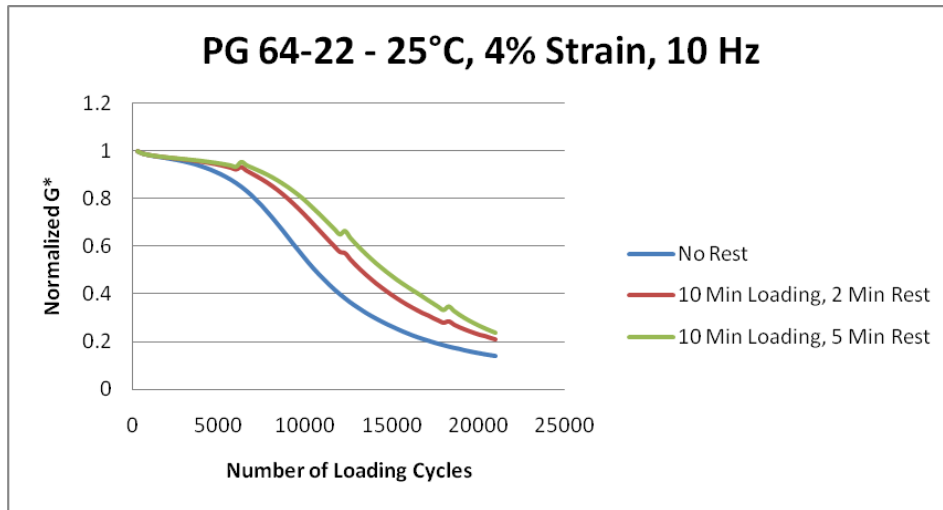


Figure F1d-6.1. Graph. Effect of healing on fatigue life: un-aged PG 64-22 binder.

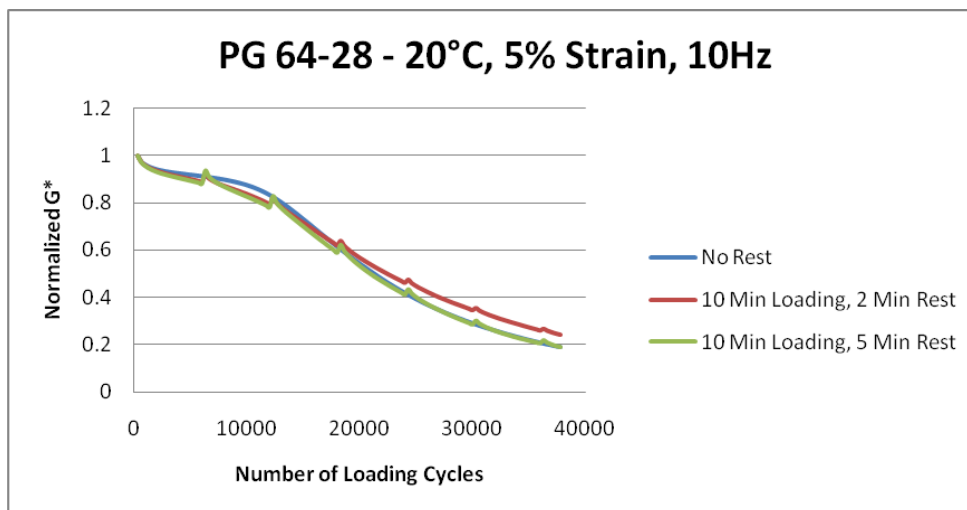


Figure F1d-6.2. Graph. Effect of healing on faigue life: RTFO-aged PG 64-28 binder.

As shown in figure F1d-6.1, the test procedure captured the healing of the PG 64-22 un-aged binder. It can be seen that alternating loading periods of 10 minutes followed by rest periods of different duration allows for healing characterization of the PG 64-22 binder. In particular, fatigue life is extended when the rest period is increased from two to five minutes.

The RTFO-aged PG 64-28 binder shows negligible healing using 10-minute loading periods followed by rest. Because the PG 64-22 un-aged binder displayed healing using this testing procedure, it is reasonable to conclude that the RTFO-aged PG 64-28 binder exhibits negligible healing. Since the binders have similar performance grades but differ in age, it is possible that aging reduced healing. However, it is also possible that the absence of healing is the result of

testing at a lower temperature. More testing is needed to determine if aging is the real cause of lack of healing and if temperature is such an important factor.

In addition to running the strain-controlled time sweeps with intermittent loading, a test to evaluate the effect of strain level, loading frequency and temperature on the time required to reach the target strain amplitude was conducted. Table F1d-6.1 provides a summary of the temperatures, frequencies and strain levels evaluated. For each temperature, testing included all frequency and strain combinations. Thus, for 20 °C and 1.59 Hz, strain levels of 2%, 3% and 5% were evaluated. The binder tested was the PG 64-28 RTFO-aged binder, which is used in the previously described time sweeps.

Table F1d-6.1. Testing parameters.

Temperature (°C)	Loading Frequency (Hz)	Strain (%)
15	1.59, 5, and 10	2,3, and 5
20	1.59, 5, and 10	2,3, and 5
25	1.59, 5, and 10	2,3, and 5

The target strain level does not have a significant effect on the time required to reach the target strain and on the deviatory behavior from the expected strain level. This trend is depicted in figure F1d-6.3.

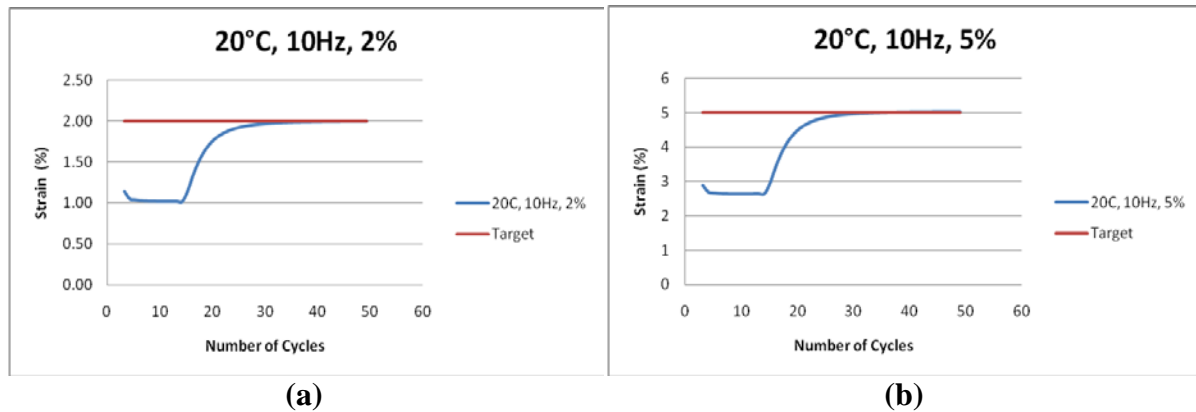


Figure F1d-6.3. Graphs. Depiction of deviation from target strain using testing conditions of 20 °C and 10 Hz for: (a) target strain of 2%; and (b) target strain of 5%.

Regardless of the loading frequency, it took approximately 2.5 seconds to reach the desired strain level. However, it was found that using a frequency of 10 Hz results in the largest deviations from reaching the target strain level, as shown in figure F1d-6.4. The research team noted that raising the temperature reduced the magnitude of deviation from the target strain amplitude but did not have an effect on the time required to reach the target strain level.

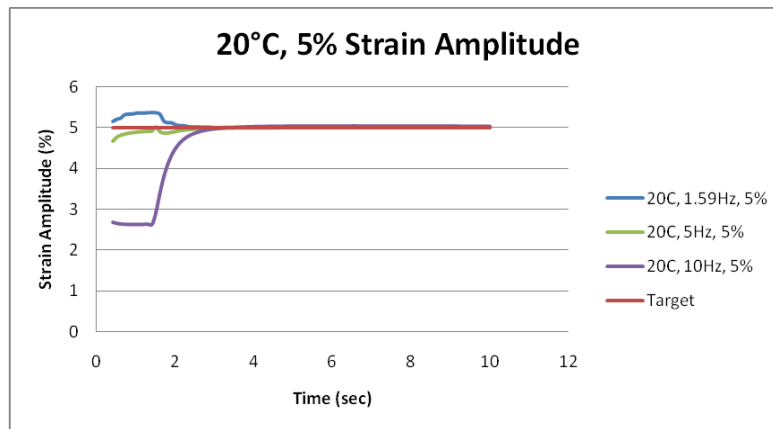


Figure F1d-6.4. Graph. The effect of frequency on deviation from target strain.

Because it was observed that frequencies of 5 Hz and 1.59 Hz (10 rad/s) result in less deviation from the target strain, a trial of strain-controlled time sweeps with intermittent loading will be conducted at lower frequencies for next quarter. Based on these experimental results, a protocol for healing evaluation using time sweep with rest periods will be proposed.

Also in this quarter, the research team focused their efforts on developing a methodology to separate stress relaxation from healing during rest periods. Kim (1988) separated stress relaxation and healing using the concept of pseudo strain for asphalt mixtures. The concept of pseudo strain was developed by Schapery (1984). Schapery stated that constitutive equations for certain viscoelastic materials are identical to those for the elastic case, but strains and stresses are not necessarily physical quantities. Rather, they are pseudo variables. The use of pseudo strain allows for elimination of the hysteretic behavior due to loading and unloading. Thus, for a given pseudo strain applied, stress is constant if damage is negligible. The difference in stress at the same pseudo strain level can thus be attributed to damage. If rest periods are included in a loading sequence and relaxation is the only phenomenon occurring during the rest period, the stress after the rest period should be the same or less than the stress prior to the rest period for the same pseudo strain level. If the stress after the rest period is larger than the stress before the rest period, at the same pseudo strain level, the increase in stress can be attributed to healing.

The research team has placed an emphasis on using mechanical analogs to model strain-controlled time sweeps with rest periods using three different loading patterns (e.g., two triangular patterns and sinusoidal). Preliminary analyses include the use of Maxwell and standard solid models. For all three loading patterns in the simulation of a time sweep with no rest, the model predicts a decrease in the modulus over the first few cycles, followed by a constant modulus. The introduction of rest periods also results in decrease in modulus over the first few cycles to a near constant value higher than that for the no-rest case. This increase in modulus is solely due to stress relaxation and the linear viscoelastic nature of the model and not due to healing, as one might assume. In the next quarter, the research team will propose a framework to separate healing from relaxation in actual time sweep tests with rest periods based on mechanical analog modeling.

### Significant Results

Identification of rheometer limitations for detecting healing when running strain-controlled time sweeps with intermittent loading has been accomplished. Additionally, progress has been made on using modeling with mechanical analogs to separate healing from stress relaxation and introduce a more usable healing test procedure.

### Significant Problems, Issues and Potential Impact on Progress

None.

### Work Planned Next Quarter

Based on these findings, the research team will propose a preliminary procedure for healing characterization using low frequency (e.g., 1.59 Hz and 5 Hz) time sweep tests with rest periods. The effect of aging (e.g., RTFO and pressure aging vessel (PAV)) on healing characteristics will also be evaluated. Further research on the separation of healing and relaxation by using mechanical analog models will be conducted.

### Cited References

Kim, Y. R., 1988, *Evaluation of Healing and Constitutive Modeling of Asphalt Concrete by Means of the Theory of Nonlinear Viscoelasticity and Damage Mechanics*. Ph.D. Thesis, Texas A&M University, College Station, Texas.

Schapery, R. A., 1984, Correspondence Principle and a Generalized J-Integral for Large Deformation and Fracture Analysis of Viscoelastic Media. *International Journal of Fracture Mechanics*, 25: 195-223.

Shen, S. and H. Chiu, 2009, Fatigue and Healing in Asphalt Binders. Presented at the 88th Transportation Research Board Annual Meeting, Washington, D.C.

### ***Subtask F1d-7: Coordinate with Atomic Force Microscopic (AFM) Analysis (WRI)***

#### Work Done This Quarter

A manuscript entitled "Morphology of asphalts, asphalt chromatographic fractions and model wax-doped asphalts studied in thin-films by atomic force microscopy" has been submitted to the *International Journal of Pavement Engineering*.

**Authors:** A.T. Pauli, R.W. Grimes, A.G. Beemer, J.J. Miller, J.D. Beiswenger, J.E. MacNaughton, T.F. Turner, and J.F. Branthaver.

**Abstract:** Asphalts used in the construction of pavements exhibit unique properties at the micron and nanometer scale. In this paper, we report results of investigations pertaining to the study of asphalts and asphalt chromatographic fractions prepared as thin-films and imaged by atomic

force microscopy. The results of these studies clearly show that a variety of "microstructures" can develop on the surface of asphalt thin-film samples. Microstructure is also observed on the surface of various asphalt fractions. Structure develops to different degrees and in different forms depending on the residua crude source from which the asphalt or asphalt fraction is derived and the thermal history of the sample. Microstructure has been observed and reported by a number of independent researchers who have used atomic force microscopy (AFM) to study asphalt samples. These researchers consistently report the observation of similar structural shapes and sizes. Several different interpretations have been proposed to explain the observed microstructure with respect to various aspects of the sample's chemical composition. We believe that, to date, all of these interpretations, including our own in previous publications, are at least partially incorrect. Based upon our current best interpretation of a very large number of AFM images, we hypothesize that the interaction between crystallizing paraffin waxes and the remaining asphalt (when simply considered as an oily solvent phase) are responsible for much of the structuring, including the well-known bee-structures, that has been observed on the surface of asphalt samples. In this paper we report results of experiments in which asphalt film thickness and thermal history were varied systematically, and show how these variables effect structuring at the asphalt surface. These results are shown to be consistent with our hypothesis. Experiments in which structuring and changes in structuring were observed in various asphalt fractions, de-waxed asphalt fractions, and wax-doped asphalts all indicate that paraffin waxes are involved in much of the observed microstructuring. Finally, we report on a set of experiments in which a model wax/oil system (paraffin wax and paraffin oil) was shown to produce structures, including bee-structures, very similar to those seen in the asphalt thin film samples.

### Significant Results

The interaction between crystallizing paraffin waxes and the remaining non-wax asphalt components is responsible for much of the structuring, including the well-known bee-structures that has been observed on the surface of asphalt thin-film samples as imaged by AFM. The observed structuring was shown to occur in non-polar asphalt fractions which would be expected to contain most of the wax-type materials. Previous discussions of microstructuring in asphalts have focused mainly on polar/polar interactions. The appearance of surface structuring was shown to relate to wax type and concentration as well as solvent phase characteristics and crystallizing conditions. Wax crystallization is an important consideration with respect to asphalt as used in road pavements because it takes place in a temperature range that coincides with pavement service temperatures. Waxy materials have long been associated with low-temperature performance properties of asphalt concretes, but may also affect mid temperature properties as well. It is highly probable that crystallization is a primary mechanism through which waxy materials affect asphalt low-temperature properties. Therefore, understanding wax crystallization should lead to a fundamentally better understanding of asphalt low- and mid- temperature properties.

Wax crystallization is frequently associated with a variety of flow problems encountered in the production, transport, and refining of petroleum and petroleum products. Attempts to resolve flow problems associated with wax in crude oils and refined products have generated significant research activities in the petroleum industry. As a result of this research, methods have been developed in the petroleum industry to modify wax crystallization behavior, and thus mechanical properties associated with this phenomenon. Various chemical additives referred to as viscosity

modifiers and pour-point-depressants have been developed for this purpose. These additives are typically comprised of polymers specifically tailored to interfere with the wax crystallization process. We believe that a fundamental understanding of the crystallization behavior of waxes in asphalts could lead to the development of this type of viscosity modifier additives for application to asphalt paving. Controlling wax crystallization behavior in asphalt could lead to significantly improved low- and mid-temperature properties, and potentially provide a method for eliminating fatigue and thermal cracking problems in constructed pavements.

#### Significant Problems, Issues and Potential Impact on Progress

None

#### Work Planned Next Quarter

Continuation: Analysis of existing data will continue in the next quarter. In these analyses, morphological features observed in asphalt and asphalt chromatographic fraction thin films prepared from validation site asphalts will be compared to performance data of the field site pavements. Image analysis of AFM scans will be developed to define a roughness “lumpiness” index.

#### ***Subtask F1d-8: Coordinate Form of Healing Parameter with Micromechanics and Continuum Damage Models (TAMU)***

#### Work Done This Quarter

An evolution equation for the healing micro-damage parameter is formulated based on micromechanics of micro-crack healing and phenomenological aspects. The micro-damage healing model is coupled to the viscoelastic, viscoplastic, and continuum damage mechanics constitutive models in the unified continuum damage mechanics model PANDA. Moreover, the formulated model is validated initially against uniaxial compression and tension fatigue data from the Nottingham database on asphalt mixtures.

#### Work Planned Next Quarter

Thermodynamic aspects of the developed healing model will be explored based on the laws of thermodynamics. Moreover, the micro-damage healing model will be validated against ALF experimental data and other existing data on another asphalt mixture in the Nottingham database. Special emphasis will be placed on relating the associated material parameters to fundamental properties (e.g. surface energy, bond strength, length of the healing process zone) based on micro-mechanical arguments.

## CATEGORY F2: TEST METHOD DEVELOPMENT

### Work Element F2a: Binder Tests and Effect of Composition (UWM)

#### Work Done This Quarter

The research team continued collecting data to check the relation between elastic recovery measured in the Dynamic Shear Rheometer (DSR) and the elastic recovery measured in the ductility bath. In addition, a new test—amplitude strain sweep—was introduced to measure fatigue resistance. The results from this test were compared to fatigue data from time sweep. All fatigue testing was performed at intermediate temperatures.

#### Significant Results

The relationship between elastic recovery measured in the DSR at 25 °C and the elastic recovery measured in the ductility bath at the same temperature is shown in figure F2a.1. The  $R^2$  of 0.98 indicates that there is a strong relation between the two tests. Similar trend was observed for the CRM-based binder with  $R^2$  of 0.96.

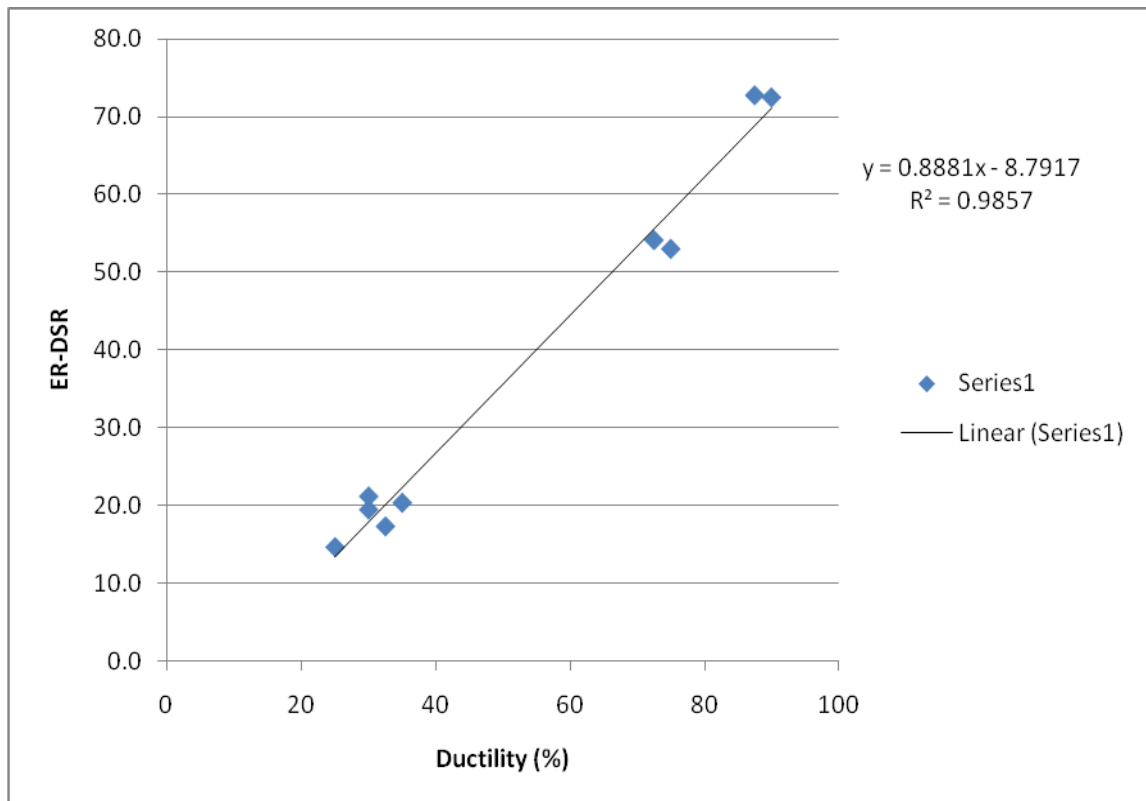


Figure F2a.1. Graph. Relation between elastic recovery measured in the DSR and elastic recovery measured in ductility bath. (ER = elastic recovery.)

The research team used the recently developed amplitude strain sweep test to measure the fatigue properties of the binders, and the results were compared with results from the time sweep testing. The amplitude strain sweep results at two different strain levels are shown in table F2a.1.

Table F2a.1 Amplitude strain sweep results.

Binder Tested	A	B	$\alpha$	Nf at Applied Strain [%]	
				2.5	5.0
FH NEAT 25C	3.18E+06	-4.371	2.186	5.79E+04	2.80E+03
FH+2LSBS 28C	1.31E+07	-4.652	2.326	1.84E+05	7.33E+03
FH+4LSBS 31C	3.65E+07	-4.820	2.410	4.40E+05	1.56E+04
FH+0.7 ELV 28C	1.91E+07	-4.558	2.279	2.94E+05	1.25E+04
FH+1.5 ELV 31C	4.11E+07	-4.613	2.307	5.99E+05	2.45E+04
FH+1PPA 28C	2.74E+07	-4.881	2.440	3.12E+05	1.06E+04
FH+1.5PPA 31C	7.48E+07	-5.062	2.420	6.68E+05	2.33E+04

Nf = fatigue life. LSBS = linear styrene-butadiene-styrene. ELV = Elvaloy. PPA = polyphosphoric acid.

Figure F2a.2 shows the number of cycles to failure at 2.5% strain for different materials. The results show an increase in the fatigue performance with increased level of modification.

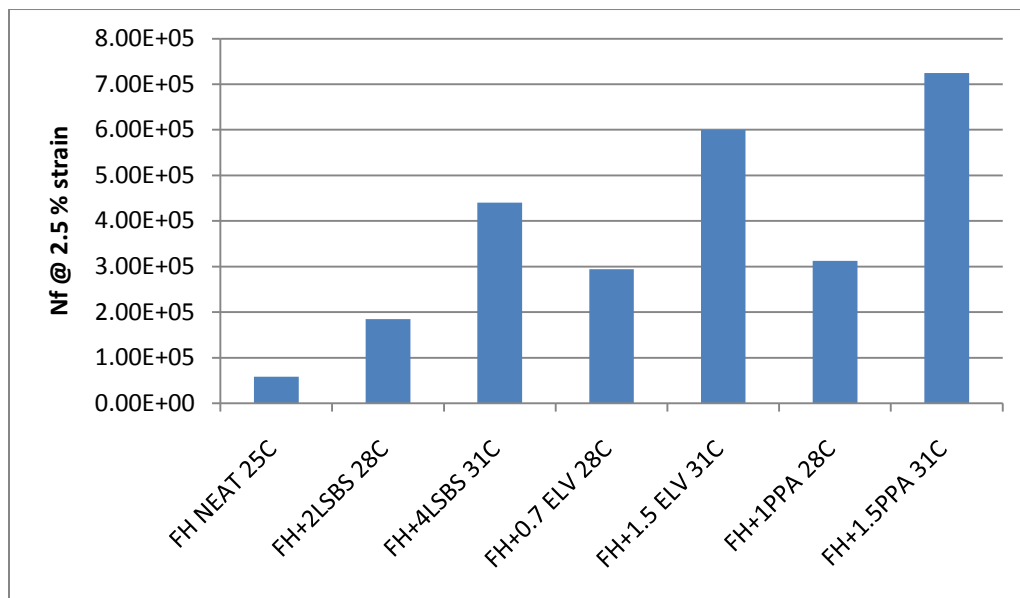


Figure F2a.2. Chart. Fatigue results at 2.5% strain.

The time sweep test results are summarized in table F2a.2 and figure F2a.3.

Table F2a.2 Time sweep results.

Binder Tested	K2	K1	Nf @ 10000 Pa
FH NEAT 25C	8.869E+06	-0.677	1.74E+04
FH+2LSBS 28C	1.000E+07	-0.646	2.61E+04
FH+4LSBS 31C	3.470E+06	-0.488	3.88E+04
FH+0.7 ELV 28C	2.000E+06	-0.511	1.81E+04
FH+1.5 ELV 31C	1.080E+06	-0.416	2.34E+04
FH+1PPA 28C	1.101E+06	-0.449	1.76E+04
FH+1.5PPA 31C	1.361E+07	-0.718	1.83E+04

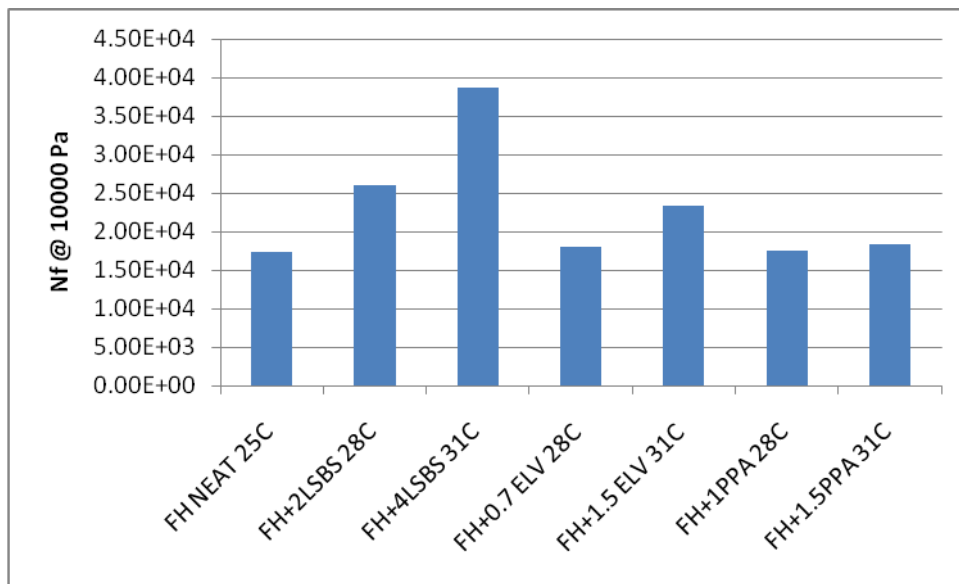


Figure F2a.3. Chart. Fatigue results of the time sweep.

In order to compare the results of the different modifiers, the ratio between the number of cycles to failure for each modifier/modification level and the neat binder was calculated for the two tests. Table F2a.3 summarizes the ratio values.

Table F2a.3 Modified binders: Number of cycles to failure as ratio to neat binder.

Modification Level	Modifier	Time Sweep @ 10 KPa Wi	Strain Sweep 2.5%	Strain Sweep 5%
One Grade Jump (28 °C)	SBS	1.50	3.18	2.62
	ELV	1.04	5.08	4.46
	PPA	1.01	5.40	3.79
Two Grade Jump (31 °C)	SBS	2.23	7.60	5.57
	ELV	1.35	10.35	8.75
	PPA	1.05	12.50	8.32

SBS = styrene-butadiene-styrene.

The results shown in table F2a.3 indicate that for all the different cases the two grade jump have a higher ratio than the one grade jump, and thus higher number of cycles to failure. For the time sweep data, the ranking of the three modifiers was consistent for both one and two grade jumps. SBS showed the highest ratio followed by ELV, and then PPA. On the other hand, the strain sweep results were not as consistent. At 2.5% strain, the PPA showed the highest ratio, followed by ELV, and then the SBS. This trend was the same for both the one and two grade jumps. Finally, for the 5% strain, again, the one and two grade jumps had the same trend, with the highest ratio for the ELV, followed by PPA, and then SBS. Although the two tests ranked the modification techniques differently, it is very important to mention that the testing was done at the intermediate temperature, and thus the two grade jump data was collected at 31 °C while the one grade jump data was collected at 28 °C. Also, a direct comparison between the two tests is not feasible as the test results are at different stress and/or strain levels.

Significant Problems, Issues and Potential Impact on Progress

None.

Work Planned Next Quarter

The research team will continue to investigate the relationship between fatigue data from the amplitude strain sweep with the time sweep data and the most effective method to evaluate effect of modification and type of modification on fatigue life.

**Work Element F2b: Mastic Testing Protocol (TAMU)**

Work Done This Quarter

The reader is referred to work element M1c where a new procedure for preparing FAM specimens and software development is presented.

## Work Planned Next Quarter

Please refer to work element M1c.

## **Work Element F2c: Mixture Testing Protocol (TAMU)**

### Work Done This Quarter

Two technical presentations were made in international meetings in this quarter. The first presentation was entitled “Anisotropic Viscoelastic Properties of Undamaged Asphalt Mixtures” and was made in the “DAWG” Forum on Pavement Performance Data Analysis sponsored by the Transportation Research Board Data Analysis Working Group (the “DAWG”) in Washington, D.C., January 2010. The second presentation, entitled “Characterization of Engineered Properties of Asphalt Mixtures”, was made in the Fundamental Properties and Advanced Models Expert Task Group of the Federal Highway Administration (FHWA) in Irvine, California, February 2010. Both presentations summarized the characterization of anisotropic properties of undamaged asphalt mixtures in compression, which was developed in past quarters.

Based on the findings on the nondestructive properties of asphalt mixtures in compression, the destructive properties of asphalt mixtures in compression were further investigated in this quarter. Two major achievements were accomplished:

- Development of comprehensive mechanistic models to characterize the anisotropic and viscoplastic properties of asphalt mixtures in compression; and
- Formulation of parameters in the mechanistic models in terms of measurable material properties.

The developed mechanistic models capture the anisotropy of asphalt mixture using a newly defined microstructure-based parameter and characterize the viscoplastic properties of asphalt mixture by modified Perzyna’s viscoplastic model that used the extended Drucker-Prager yield surface function and non-associated flow rule. A progressive-damage parameter with respect to load cycle was introduced to the mechanistic models to represent the visco-damaged properties of asphalt mixture. The components of the comprehensive mechanistic models are discussed in detail as follows.

#### **1. Anisotropy due to aggregate preferential orientation and aggregate sphericity**

The existing anisotropic parameter in granular material is the vector magnitude ( $\Delta$ ) that only considers the effect of aggregate orientation on the anisotropy of material (Oda and Nakayama 1989; Masad et al. 2002; Tashman et al. 2004). The use of the vector magnitude is reasonable for fine-grained materials such as soil but is not applicable for materials composed of coarse aggregates like asphalt mixtures. As a result, in order to investigate the anisotropy of an asphalt mixture, the fabric tensor (a tensor describing material microstructure) was redefined and the vector magnitude was re-derived as shown in F2c.1.

$$\Delta = \frac{1}{\sum_{k=1}^M \omega_k} \sqrt{\left( \sum_{k=1}^M \omega_k \sin 2\theta_k \right)^2 + \left( \sum_{k=1}^M \omega_k \cos 2\theta_k \right)^2} \quad (\text{F2c.1})$$

where  $\omega_k = a_k/b_k$ , the sphericity of the  $k^{\text{th}}$  aggregate;  $a_k$  = longest dimension of the aggregate;  $b_k$  = shortest dimension of the aggregate;  $M$  = number of aggregates on an image;  $\theta_k$  = orientation angle of the major axis of the  $k^{\text{th}}$  aggregate measured from the horizontal axis in the images of the vertical section of an asphalt mixture that is obtained by photographing the cut surface or by X-ray CT scanning;  $-90^\circ \leq \theta_k \leq 90^\circ$ , in which the positive sign indicates the counterclockwise measurement from the horizontal axis. Theoretically, the value of  $\Delta$  ranges from 0 to 1:  $\Delta = 0$  indicates the completely random distribution of aggregates leading to an isotropic asphalt mixture; and  $\Delta = 1$  implies the major axis of all aggregates orients in the horizontal direction or in the vertical direction.

## 2. Modified stress tensor due to anisotropy and cracks/voids

A modified effective stress tensor was introduced to combine the effect of anisotropy and cracks/voids on the true stresses in the intact material. Because of the cracks/voids in the asphalt mixture, the area of the intact material in a cross section is less than the whole cross section of the asphalt mixture. As a result, the true stresses in the intact material are different from the apparent stresses that are calculated based on the applied load and the specimen geometry. The modified effective stress tensor is formulated as:

$$\bar{\sigma}_{ij}^e = \frac{3(\sigma_{ik} F_{kj} + F_{ik} \sigma_{kj})}{2[1 - \xi(N)]} \quad (\text{F2c.2})$$

where,

$$F_{ij} = \frac{1}{3 + \Delta} \begin{bmatrix} 1 - \Delta & 0 & 0 \\ 0 & 1 + \Delta & 0 \\ 0 & 0 & 1 + \Delta \end{bmatrix}; \quad (\text{F2c.3})$$

$\Delta$  = vector magnitude;  $\sigma_{ij}$  = apparent stress tensor that can be measured;  $N$  = number of load cycles; and  $\xi$  = damage density at the corresponding load cycle. In this study,  $\bar{\sigma}_{ij}^e$  instead of  $\sigma_{ij}$  was used to develop the viscoplastic models for the asphalt mixture so that the anisotropy and cracks/voids are considered during the viscoplastic deformation.

## 3. Microstructure-based viscoplastic model for asphalt mixture

The permanent deformation of an asphalt mixture is produced by the irrecoverable viscoplastic deformation whose driving force is the separated dissipated pseudo-strain energy for permanent deformation,  $W_{R2}$ . The rate of  $W_{R2}$  is calculated using equation F2c.4:

$$\dot{W}_{R2}(N) = \bar{\sigma}_{ij}^e \dot{\varepsilon}_{ij}^{vp}(N) \quad (\text{F2c.4})$$

in which  $\dot{\varepsilon}_{ij}^{vp}$  is the viscoplastic strain rate (with respect to time) under repeated loading that can be evaluated by a modified Perzyna's viscoplastic model as follows:

$$\dot{\varepsilon}_{ij}^{vp}(N) = \Gamma(f)^n \left[ \int_0^{\Delta t} w^m(t) dt \right] \frac{\partial g}{\partial \bar{\sigma}_{ij}^e} \quad (\text{F2c.5})$$

where  $\Gamma$  = viscosity parameter that is experimentally determined;  $f$  = anisotropic viscoplastic yield surface function;  $n$  = rate dependent parameter to be determined by experiment;  $w(t)$  = cyclic loading wave function;  $m$  = cyclic loading shape factor;  $\Delta t$  = loading time in each load cycle; and  $g$  = anisotropic viscoplastic plastic potential function. The non-associated flow rule applies when  $g \neq f$ .

To evaluate the effect of confinement, internal friction and interlocking on the asphalt mixture, the Drucker-Prager yield surface function was modified to describe the viscoplastic yield properties of an asphalt mixture as:

$$f = \bar{\tau}^e - \alpha \bar{I}_1^e - \left( \kappa_1 \left[ \varepsilon_{ij}^{vp}(N) \right]^{\kappa_2} + \kappa_0 \right) \quad (\text{F2c.6})$$

where  $\bar{\tau}^e$  = anisotropic effective deviatoric shear stress;  $\bar{I}_1^e = \bar{\sigma}_{kk}^e$  = anisotropic effective first invariant of  $\bar{\sigma}_{ij}^e$ ;  $\kappa_1, \kappa_2, \kappa_0$  are material properties, where  $\kappa_0$  is the initial yield stress; and  $\alpha$  = the slope of the yield surface which represents the material frictional properties. In the yield surface function, the term  $\bar{\tau}^e - \alpha \bar{I}_1^e$  indicates the softening effect of loading on the material while the term  $\kappa_1 \left[ \varepsilon_{ij}^{vp}(N) \right]^{\kappa_2} + \kappa_0$  is the hardening effect.

To separate the compressive and extensive properties of an asphalt mixture, the deviatoric shear stress is expressed as (Dessouky et al. 2006; Saadeh et al. 2007):

$$\bar{\tau}^e = \frac{\sqrt{\bar{J}_2^e}}{2} \left[ 1 + \frac{1}{d} + \left( 1 - \frac{1}{d} \right) \frac{\bar{J}_3^e}{(\bar{J}_2^e)^{3/2}} \right] \quad (\text{F2c.7})$$

where  $d$  = a material parameter which represents the ratio of the yield stress in extension to that in compression. The value of  $d$  ranges from 0.778 to 1: when  $d = 1$ ,  $\bar{\tau}^e = \sqrt{\bar{J}_2^e}$ ; when  $d < 1$ ;  $\bar{\tau}^e = \sqrt{\bar{J}_2^e}/d$ . In equation F2c.7,  $\bar{J}_2^e$  is the second invariant of the deviatoric stress  $\bar{S}_{ij}^e$  ( $\bar{S}_{ij}^e = \bar{\sigma}_{ij}^e - 1/3 \bar{\sigma}_{kk}^e \delta_{ij}$ ), and  $\bar{J}_2^e = 3/2 \bar{S}_{ij}^e \bar{S}_{ji}^e$ ;  $\bar{J}_3^e$  is the third invariant of the deviatoric stress  $\bar{S}_{ij}^e$ , and  $\bar{J}_3^e = 9/2 \bar{S}_{ij}^e \bar{S}_{jk}^e \bar{S}_{ki}^e$ .

The non-associated flow rule applies to the asphalt mixture, which means that the direction of the viscoplastic strain increment is perpendicular not to the yield surface but to the plastic potential surface. Therefore, the plastic potential surface has the same form as the Drucker-Prager function but with different coefficients:

$$g = \bar{\tau}^e - \beta \bar{I}_1^e - \kappa_3 \quad (\text{F2c.8})$$

where  $\beta$  = the slope of viscoplastic potential surface and  $\kappa_3$  = material parameter which will vanish during derivation in equation F2c.5.

The second major achievement that was accomplished in this quarter was the formulation of the parameters in the aforementioned viscoplastic models in terms of measurable material properties. In the viscoplastic models shown in equations F2c.4 through F2c.8, the model parameters include  $\Delta$ ,  $\Gamma$ ,  $n$ ,  $\alpha$ ,  $\beta$ ,  $\kappa_0$ ,  $\kappa_1$ ,  $\kappa_2$  and  $d$ , in which  $\Gamma$ ,  $n$ ,  $\kappa_1$ ,  $\kappa_2$  are regression variables based on experimental data and  $\Delta$ ,  $\alpha$ ,  $\beta$ ,  $\kappa_0$ ,  $d$  are model parameters dependent on inherent material properties such as anisotropic moduli, internal friction angle and cohesion. The following formulations were developed to determine the model parameters in terms of material properties.

### 1. Microstructural vector magnitude, $\Delta$

The traditional method to obtain  $\Delta$  is based on the measurements of aggregate orientation angle in the photographs of the cut surface or X-ray CT scanning images of asphalt mixture specimens. In order to more efficiently and more cost-effectively determine  $\Delta$ , a formulation was proposed to estimate  $\Delta$  using the ratio of vertical modulus to horizontal modulus,  $E_{11}/E_{22}$ , as shown in equation F2c.9:

$$\Delta = \frac{3 \left( \frac{E_{11}}{E_{22}} - 1 \right)}{4(q-1) - \left( \frac{E_{11}}{E_{22}} - 1 \right)} \quad (\text{F2c.9})$$

where  $E_{11}$  = vertical modulus in the compaction direction;  $E_{22}$  = horizontal modulus in the direction perpendicular to the compaction direction;  $q$  = maximum value for anisotropic modulus ratio,  $E_{11}/E_{22}$ . This formulation has been mathematically verified based on the linear relation between second invariant of deviatoric fabric tensor and the anisotropic modulus ratio.

### 2. Slope of yield surface function, $\alpha$ and initial yield stress, $\kappa_0$

The slope of the yield surface function and the initial yield stress were formulated in terms of the Mohr-Coulomb parameters, internal frictional angle ( $\varphi$ ) and the cohesion ( $C$ ), by comparing the yield surface function of the Mohr-Coulomb criterion to that of the Drucker-Prager criterion. The formulations of the two parameters are as follows:

$$\alpha = \frac{2 \sin \varphi}{\sqrt{3}(3 + \bar{n} \sin \varphi)} \quad (\text{F2c.10})$$

$$\kappa_0 = \frac{6C \cos \varphi}{\sqrt{3}(3 + \bar{n} \sin \varphi)} \quad (\text{F2c.11})$$

where  $\bar{n}$  = Lode parameter that is introduced to estimate the effect of intermediate principal stress on the yielding of material, and is defined as:

$$\bar{n} = \frac{2\bar{\sigma}_2^e - \bar{\sigma}_1^e - \bar{\sigma}_3^e}{\bar{\sigma}_1^e - \bar{\sigma}_3^e}, \quad -1 \leq \bar{n} \leq 1 \quad (\text{F2c.12})$$

$\bar{n} = 1$  indicates an extension condition and  $\bar{n} = -1$  means a compressive condition.

### 3. Slope of plastic potential function, $\beta$

The formulation of the slope of plastic potential function is to be completed in next quarter.

### 4. Yield stress ratio of extension to compression, $d$

The formulation of the yield stress ratio of extension to compression is to be completed in next quarter.

## Significant Results

In this quarter, the anisotropic viscoplastic-damage properties of asphalt mixtures in compression were characterized by proposed comprehensive mechanistic models. The anisotropy of the asphalt mixture was captured by a newly defined microstructure-based parameter (vector magnitude). The visco-damage properties were represented by a progressive-damage parameter (damage density). The viscoplastic properties were characterized by the modified Perzyna's viscoplastic model incorporated with the extended Drucker-Prager yield surface function and non-associated flow rule. Formulations were established to determine the model parameters in terms of material properties, such as anisotropic modulus, internal friction angle, and cohesion.

## Significant Problems, Issues and Potential Impact on Progress

The comprehensive viscoplastic models for asphalt mixtures have not been completed because: (i) the separated dissipated pseudo-strain energy for permanent deformation ( $W_{R2}$ ) is not well defined and calculated for an asphalt mixture in compression that is significantly anisotropic, and (ii) the damage density ( $\zeta$ ) is not explicitly specified to account for the degradation of asphalt mixture properties due to increasing radius of cracks/voids under a compressive load. In addition, testing protocols and data analysis methods for viscoplastic-damage properties of asphalt mixtures under the repeated compressive loading need to be developed to evaluate and calibrate proposed viscoplastic-damage models and the formulations of model parameters in terms of material properties.

### Work Planned Next Quarter

- Experimental calibration on the relationship between the modified vector magnitude and the anisotropic modulus ratio;
- Mathematical derivation of functions of slope of plastic potential function and yield stress ratio of extension and compression with respect to the material properties;
- Definition and calculation of separated dissipated pseudo-strain energy for permanent deformation in the repeated compressive loading condition; and
- Definition and calculation of damage density due to increasing radius of cracks/voids under the repeated compressive loading.

### References

Dessouky, S., E. Masad, D. Little, K. Chatti, R. Davis, R. Roque, R. Kluttz, N. Gibson, and W. Rongzong, 2006, Mechanistic modeling of permanent deformation in asphalt mixes with the effect of aggregate characteristics. *Association of Asphalt Paving Technologists*, 75, 535-576.

Masad, E., L. Tashman, N. Somedavan, and D. Little, 2002, Micromechanics-Based Analysis of Stiffness Anisotropy in Asphalt Mixtures. *Journal of Materials in Civil Engineering*, 14(5), 374-383.

Oda, M., and H. Nakayama, 1989, Yield function for soil with anisotropic fabric. *Journal of Engineering Mechanics*, 115(1), 89-104.

Saadeh, S., E. Masad, and D. Little, 2007, Characterization of asphalt mix response under repeated loading using anisotropic nonlinear viscoelastic-viscoplastic model. *Journal of Materials in Civil Engineering*, 19(10), 912-924.

Tashman, L., E. Masad, H. Zbib, D. Little, and K. Kaloush, 2004, Anisotropic viscoplastic continuum damage model for asphalt mixes. Geotechnical Special Publication, American Society of Civil Engineers, New York, NY, 111-125.

### **Work Element F2d: Tomography and Microstructural Characterization (TAMU)**

#### Work Done This Quarter

The work related to X-ray CT imaging is being carried out as needed to support other tasks. For example CT images are being used to determine whether or not the damage distribution is isotropic as considered in the continuum model F3c.2.

The work related to microstructure characterization of asphalt binders is also being carried out to determine the distribution of mechanical properties of the asphalt binder at a sub micron scale using the AFM. We have completed some preliminary tests in the previous quarters and we have

also completed a substantial literature review to support this task. The results from the microstructure characterization will help the work related to cracking and healing in Task F1d.

### Major Findings & Status

None.

### Work Planned for Next Quarter

We will continue with the X-ray CT and AFM imaging as required in support of the other tasks in this work plan.

## **Work Element F2e: Verification of the Relationship between DSR Binder Fatigue Tests and Mixture Fatigue Performance (UWM)**

### Work Done This Quarter

Investigation of the applicability and validity of the linear amplitude sweep (LAS) as an accelerated binder fatigue test continued. Analysis of binder and mixture fatigue data was completed using the framework of viscoelastic continuum damage (VECD). LAS results and strain-controlled time sweeps were both performed for comparison and verification purposes. Time sweeps were analyzed using VECD in the same manner as the LAS.

Fatigue data (i.e., LAS and time sweep at 5% and 7% strain levels) of binders from two Transportation Pooled Fund studies (TPF-5(080) and TPF-5(146)) were analyzed this quarter. Binders from the TPF-5(080) study include: 64-28 unmodified, 64-28 styrene-butadiene-styrene (SBS) polymer-modified, 58-34 terpolymer, and 64-34 terpolymer. The binders from the TPF-5(146) study are described in the previous quarterly report. Note that all binders were rolling thin film oven (RTFO)-aged and that the TPF-5(080) binders were tested at an iso-stiffness condition. The iso-stiffness temperature was defined as the temperature where  $|G^*| \cdot \sin \delta$  is equal to 5000 kPa as determined by master curve generation from frequency sweep test results. The TPF-5(146) binders were tested at 20 °C to allow for comparison with fatigue mixture testing conducted at the University of Massachusetts, Dartmouth.

As discussed in previous quarterly reports, the use of the VECD framework for both the time and amplitude sweep tests allows for the estimation of fatigue life ( $N_f$ ).  $N_f$  is calculated based on the parameters A and B and the strain level of the binder ( $\gamma_{max}$ ) in the pavement structure, as shown in equations F2e.1 and F2e.2:

$$A = \frac{f(D_f)^k}{k \left( \pi \frac{D}{|G^*|} C_1 C_2 \right)^\alpha} |G^*|^{-\alpha} \quad (\text{F2e.1})$$

$$B = -2\alpha. \quad (\text{F2e.2})$$

The relationship between time sweep results and LAS test results was investigated by comparing the parameter A and the number of cycles to failure ( $N_f$ ) obtained from both procedures. Results from the ALF binders discussed in the previous quarterly report were also included in the comparison. A plot comparing the parameter A determined from both the LAS and time sweep conducted at 5% strain is shown in figure F2e.1.

There is a statistically significant correlation between the LAS "A" and time sweep "A" obtained from the ALF and TPF-5(080) binders. There is also a strong correlation between the LAS and time sweep "A" for the TPF-5(146) binders, but the relationship differs from the ALF and TPF-5(080) binders. It is also noteworthy that the best correlation between time sweep and LAS results is obtained when the frequency sweep is used to determine the parameter  $\alpha$  used in VECD analysis.

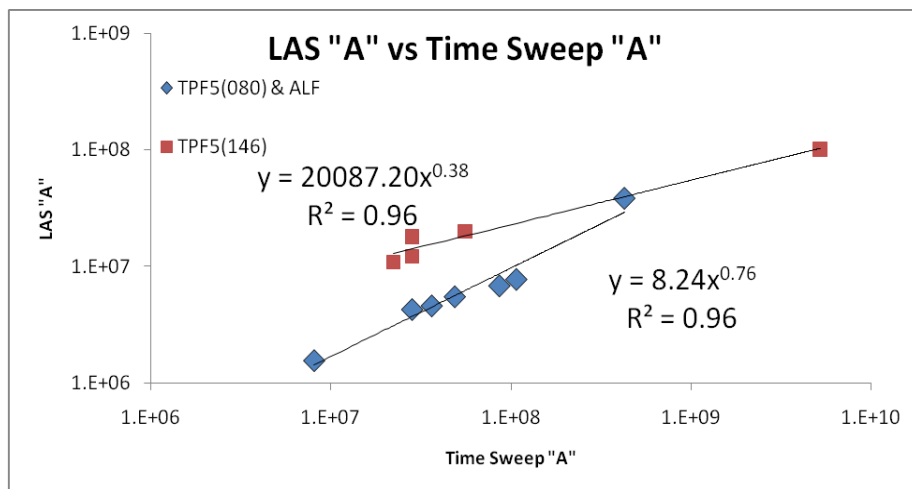


Figure F2e.1. Graph. Correlation between the parameter A determined from LAS and time sweep testing.

The relationship between the  $N_f$  predicted using results from both the LAS and time sweeps conducted at 5% strain for the TPF-5(080) and ALF binders was investigated. A strain level (i.e.,  $\gamma_{max}$ ) of 3% was selected for  $N_f$  prediction. The correlation between the  $N_f$  predicted using the LAS and time sweep is shown in figure F2e.2. There was a strong correlation ( $R^2=0.97$ ) found between the  $N_f$  predicted using LAS and time sweep.

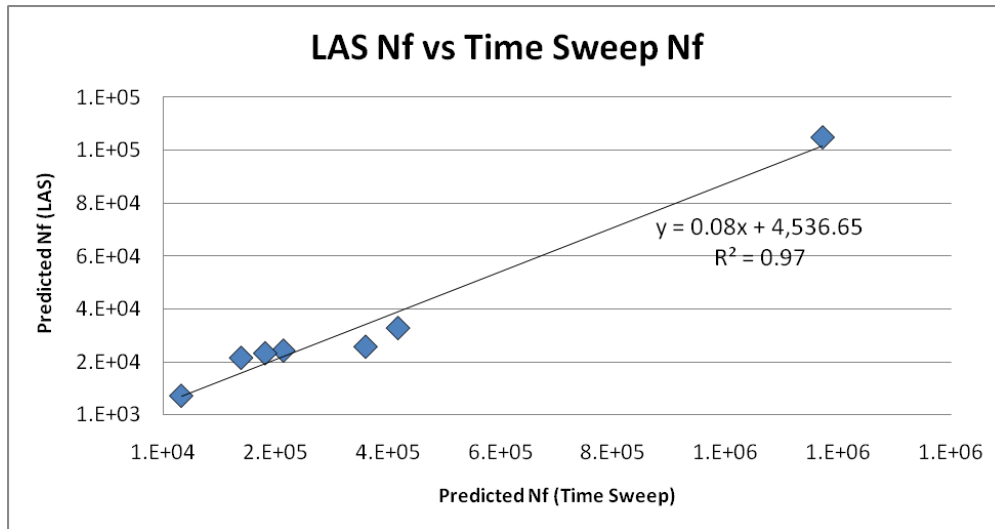


Figure F2e.2. Graph. Correlation between predicted  $N_f$  from LAS and time sweep.

In addition to comparing fatigue performance of binders from LAS and time sweep test, a comparison between binder and mixture results was carried out for the TPF-5(146) binders. Fatigue mixture testing and analyses conducted by Professor Mogawer at the University of Massachusetts, Dartmouth, and Professor Kutay at Michigan State University were used in the comparison. The mixtures were tested using uniaxial push-pull and the experimental data was analyzed based on VECD approach described in Kutay et al. (2008). As shown in table F2e.1, the ranking of the binders based on the LAS parameter A and the ranking of the corresponding mixtures based on the number of cycles to a 50% reduction in stiffness at a strain level of  $350 \mu\epsilon$  is similar. This comparison with mixture performance shows the promising potential of the amplitude sweep procedure for fatigue characterization of binders.

Table F2e.1. Comparison between LAS and mixture uniaxial push-pull VECD results (1 = most fatigue resistant; 5 = least fatigue resistant).

Binder	Average Binder Rankings			Mixture Rankings		
	LAS - A	5%TS - A	7%TS - A	VECD - 75 $\mu\epsilon$	VECD - 175 $\mu\epsilon$	VECD - 350 $\mu\epsilon$
PG64-34	1	1	1	1	1	1
PG76-22	2	2	2	3	2	2
Latex	3	3	3	2	3	3
PPA	4	4	4	4	5	5
TPF Control	5	5	5	5	4	4

PPA = polyphosphoric acid. TPF = Transportation Pooled Fund.

### Significant Results

Based on the results obtained in this quarter, it appears that there is a good correlation between the LAS and time sweep model parameters using VECD. Similar rankings observed for the fatigue performance of binders using LAS and mixtures using uniaxial push-pull indicate the potential of the proposed accelerated procedure. A paper discussing details of the implementation of the LAS has been submitted to *Road Materials Pavement and Design*.

### Significant Problems, Issues and Potential Impact on Progress

None.

### Work Planned Next Quarter

The research team will continue implementation and verification of the LAS test by testing the remaining LTPP binders (eight completed and 22 to be tested). The research team will also focus its efforts on completing the following tasks:

- Further investigate the relationship between LAS results and asphalt mixture testing (uniaxial push-pull) results by testing typical mixtures prepared with locally available aggregates.
- Compare the Binder Yield Energy Test (BYET) at intermediate temperatures and the percent recovery from the Multiple Stress Creep and Recovery (MSCR) test at high temperatures.
- Develop a method to determine damage model coefficients ( $C_0$ ,  $C_1$  and  $C_2$ ) without using solver in Excel (e.g., using closed-form solutions for the least squares problem).
- Send a set of binders from which LAS data is available to Turner-Fairbank Highway Research Center (TFHRC) for Double-Edge Notched Tension (DENT) testing to calculate the equivalent work of fracture (EWF) and its relation to fatigue performance.
- Perform a sensitivity analysis of all the parameters involved in the VECD calculation of the damage curves in LAS procedure.

### Cited References

Kutay, M. E., N. Gibson, and J. Youtcheff, 2008, Conventional and Viscoelastic Continuum Damage (VECD) Based Fatigue Analysis of Polymer Modified Asphalt Pavements. *Journal of the Association of Asphalt Paving Technologists*, 77: 395-425.

## **CATEGORY F3: MODELING**

### **Work Element F3a: Asphalt Microstructural Model**

#### Work Done This Quarter

The interaction between crystallizing paraffin waxes and the remaining non-wax asphalt components is responsible for much of the structuring, including the well-known bee-structures that has been observed on the surface of asphalt thin-film samples as imaged by AFM. The observed structuring occurs in non-polar asphalt fractions which would be expected to contain most of the wax-type materials. Previous discussions of microstructuring in asphalts have focused mainly on polar/polar interactions. The appearance of surface structuring relates to wax type and concentration as well as solvent phase characteristics and crystallizing conditions. Wax crystallization is an important consideration with respect to asphalt as used in road pavements because it takes place in a temperature range that coincides with pavement service temperatures. Waxy materials have long been associated with low-temperature performance properties of asphalt concretes, but may also affect mid temperature properties as well. It is highly probable that crystallization is a primary mechanism through which waxy materials affect asphalt low-temperature properties. Therefore, understanding wax crystallization should lead to a fundamentally better understanding of asphalt low- and mid- temperature properties.

Wax crystallization is frequently associated with a variety of flow problems encountered in the production, transport, and refining of petroleum and petroleum products. Attempts to resolve flow problems associated with wax in crude oils and refined products have generated significant research activities in the petroleum industry. As a result of this research, methods have been developed in the petroleum industry to modify wax crystallization behavior, and thus mechanical properties associated with this phenomenon. Various chemical additives referred to as viscosity modifiers and pour-point-depressants have been developed for this purpose. These additives are typically comprised of polymers specifically tailored to interfere with the wax crystallization process. We believe that a fundamental understanding of the crystallization behavior of waxes in asphalts could lead to the development of this type of viscosity modifier additives for application to asphalt paving. Controlling wax crystallization behavior in asphalt could lead to significantly improved low- and mid-temperature properties, and potentially provide a method for eliminating fatigue and thermal cracking problems in constructed pavements.

#### ***Sub-subtask F3a-1.1. Next Generation Model Asphalts (University of Rhode Island)***

#### Work Done This Quarter

The work done in the January–March 2010 quarter focused on (1) initiating the molecular simulation of larger resin molecules for use in new model asphalts, and (2) devising the methods by which molecular-scale results will be communicated into larger-scale phase field calculations that account for the geometries and microstructures of different phases in a bitumen.

Work continued on initiating simulations of new resin molecules that combine larger size with polarity. These simulations were more challenging than expected due to missing force field

parameters for 5-membered rings containing N-H or C=O and fused to benzene rings, such as dibenzopyrrole or the ketone of cyclopentadiene with fused aromatic rings. These simulations are continuing in the present quarter and are being supplemented with optimizations using quantum mechanics in order to determine appropriate bond lengths and bond angles.

Revisions were requested by the *Journal of Chemical Physics* on a manuscript submitted during the Oct-Dec 2009 quarter. This paper showed the decoupling of rotational relaxation and translational diffusion for asphaltene and polymer molecules in model asphalts as temperature decreased, while these relaxation processes remain coupled for resins, naphthene aromatics, and saturate chains. The revised manuscript better motivated the fundamental chemical physics of the problem and was about to be submitted as the quarter ended.

A followup preprint was written for the Petroleum Chemistry division of the American Chemical Society for presentation and publication in conjunction with the August 2010 national meeting, to be held in Boston. One result shown was a comparison in the rotation-diffusion product among different resin species, reproduced here as figure F3a-1.1. Larger resins showed slightly larger increases in this product, though all increases were small compared to those found for asphaltene molecules.

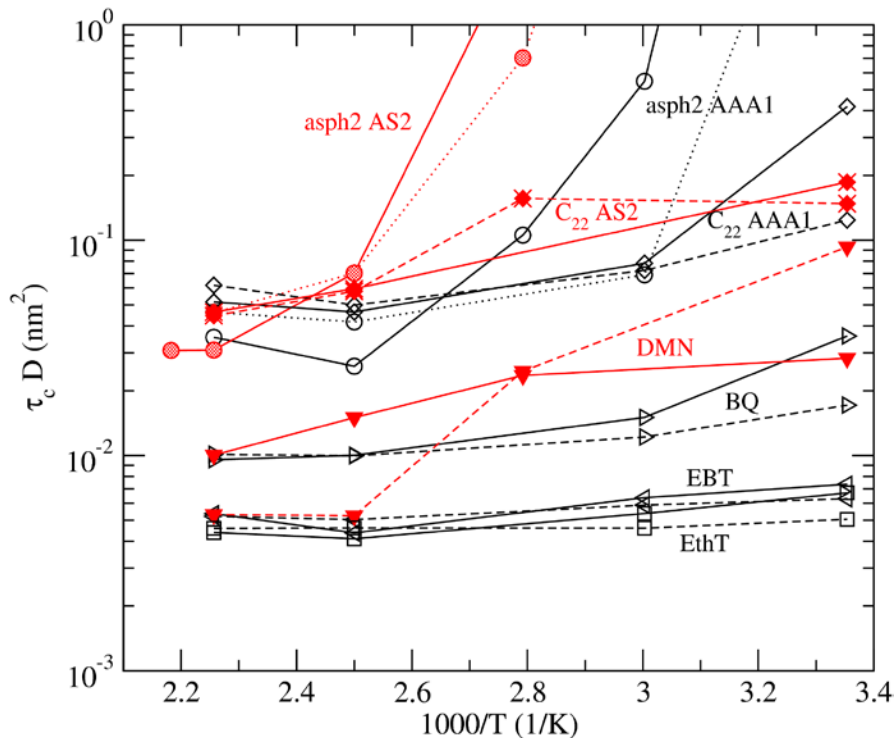


Figure F3a-1.1. Change in rotation-diffusion product in model AAA-1 (black) and asphalt 2 (red) for systems without (dashed) or with (solid) a polymer present. Increases in  $\tau_c D$  as temperature decreases (larger  $1000/T$ ) indicate decoupling between rotation and translation.

Analysis is not yet complete of the alkane crystallization event that had occurred within simulations of model asphalts at 25°C and 85°C and was reported earlier. Some preliminary results were shown at the March 2010 ETG meeting in Irvine. A Letter documenting the crystallization event, the crystal structure, and molecular indicators will be completed in the next quarter.

***Sub-subtask F3a-1.2. Molecular simulation “push” and phase model “pull” (University of Rhode Island)***

The manuscript submitted to *Rheologica Acta* at the end of the Oct-Dec 2009 quarter was rejected without review by the Associate Editor, who felt that a Maxwell model analysis of bitumen rheology was of insufficient interest to *Rheologica Acta* readers. The main point of the manuscript was to compare the relaxation time distributions that underlie the rheology of different bitumens and how those distributions change in response to aging (e.g., RTFO, PAV). Since these topics are of interest in the paving community, the manuscript was submitted with little change to the *Journal of Materials in Civil Engineering* of the ASCE.

Methodology development to relate molecular-level packing and energetics to the inputs required for phase field modeling has continued. The key ideas were communicated at the ETG meeting in Irvine and are listed here:

- 1) Phase field modeling strives to provide the geometries and microstructure that occur in response to thermodynamic phase separation.
- 2) The phase identity (e.g. amorphous bitumen vs. crystalline wax) and concentration at each point  $x$  evolve with time in response to gradients in free energy, which include second derivatives of the phase variable  $\varphi$  and concentration  $c$  with respect to position. The governing differential equations are (Boettinger et al. 2002)

$$\frac{\partial \varphi}{\partial t} = -M_{\varphi} \left[ \frac{\partial A}{\partial \varphi} - \varepsilon_{\varphi}^2 \nabla^2 \varphi \right] \quad (\text{F3a-1.2.1})$$

$$\frac{\partial c}{\partial t} = \nabla \cdot \left[ M_c c(c-1) \nabla \left( \frac{\partial A}{\partial c} - \varepsilon_c^2 \nabla^2 c \right) \right] \quad (\text{F3a-1.2.2})$$

- 3) Phase field calculations require as input the Helmholtz free energy  $A$  as a function of temperature  $T$ , composition, and phase. A typical approach is to impose (1) regular solution theory for the concentration dependence and (2) mathematical step functions and barriers to distinguish between phases; i.e.  $\varphi = 0$  and  $\varphi = 1$  as phases I and II, with a barrier at  $\varphi = 1/2$ .

Bitumen systems could deviate from these assumptions. For example, non-random packing, such as specific interactions among asphalt components, is counter to the assumption of zero excess

entropy  $S^E$  that underlies regular solution theory. A potential impact on chemomechanics is that mechanical calculations could be performed on microstructures that evolved under inaccurate energies and thus are inaccurate representations of the true microstructure.

Method development focused on further study of the SAFT equation of state as a means of relating chemistry to free energy. This equation of state determines the free energy via individual contributions based on an ideal gas reference state plus hard sphere repulsions, van der Waals interactions, chain bonding, and specific associations. A literature study is continuing on applications of this approach to systems related to asphalts. The current plan of attack is to use simulation results from sub-subtask F3a-1.1, *Next Generation Model Asphalts*, as inputs for parameterizing this equation of state. Examples of such results include enthalpy  $H(T,P)$ , energy  $U(T,V)$ , volume  $V(T,P)$  of individual phases, and pair correlation function  $g(r)$  at separation  $r = \sigma_{ij}$  (molecule-molecule contact). This last property equals the ratio of the local nanoscale density in the immediate vicinity of a molecule to the average density of the entire phase. Past works using SAFT in related systems include studies on the precipitation of asphaltenes during crude oil production and refinement by treating the crude oil using a continuous phase model (Gonzalez et al. 2005) or a colloidal model based on specific resin-asphaltene interactions (Wu et al. 2000).

#### Significant Problems, Issues and Potential Impact on Progress (followup to 10-12/2009 quarter)

Methodology developments this quarter were made by Prof. Greenfield. New URI M.S. student Derek Li has been working on simulating the new resins and will work on the new model asphalt. Continuing URI M.S. student Abiodun Olawepo has started making contributions to this project that relate to how differences in bitumen chemistry lead to differences in relaxation time distribution.

Cost sharing accounting is now up-to-date. Cost sharing expenses are currently far ahead of the overall 1:4 ratio compared to project expenditures. As mentioned in past updates, the prior cost sharing plan had assumed an Out-of-state Tuition Award, which is not applicable for Rhode Island residents Li and Olawepo, and modifications will continue to be required. The changes in place had Prof. Greenfield devoting part of his sabbatical to the project, thus contributing his 50% sabbatical salary as cost share. Additional rebudgeting will potentially be necessary in future quarters.

#### Work Planned Next Quarter

The next quarter will again focus on two areas: (1) next-generation model asphalts and (2) molecular/phase model connections.

#### *Sub-subtask F3a-1.1, Next Generation Model Asphalts.*

- Complete Letter about crystallization event and submit for publication.
- Continue communications with WRI beyond those at the ETG meeting about choice of asphalts of interest and corresponding chemical characterization data (NMR, FTIR, etc.).

- Formulate model asphalts using properly sized molecules and conduct initial simulations. Additional asphaltene molecular structures will be considered as well. The choice of compounds will be pursued jointly by URI and WRI.

***Sub-subtask F3a-1.2, Molecular simulation “push” and phase model “pull”.***

- Continue formulation work to describe the detailed path for incorporating molecular simulation outputs into phase field model inputs.
- Complete literature survey about applications of the SAFT equation of state to asphaltenes.
- Communicate beyond discussions at the ETG with phase-field practitioners on this project about how parameters can cross the molecule/phase field scales.

Outcomes from all discussion will be shared at a F3a team meeting, if one occurs during the quarter, or will be distributed by email.

Cited References

Boettinger, W.J., J.A. Warren, C. Beckermann, and A. Karma, 2002, Phase-Field Simulation of Solidification. *Ann. Rev. Mater. Res.*, 32, 163–194.

Gonzalez, D.L., P.D. Ting, G.J. Hirasaki, and W.G. Chapman, 2005, Prediction of Asphaltene Instability under Gas Injection with the PC-SAFT Equation of State. *Energy Fuels*, 19, 1230-1234.

Wu, J., J.M. Prausnitz, and A. Firoozabadi, 2000, Molecular Thermodynamics of Asphaltene Precipitation in Reservoir Fluids. *AIChE. J.*, 46, 197-209.

***Sub-subtask F3a-1.5, Adapting Phase-field Theory for Modeling of Asphalt Fatigue (Virginia Tech University)***

A phase-field model is a mathematical model for solving interfacial problems. It has mainly been applied to solidification dynamics (Boettinger et al. 2002), but it has also been applied to other situations such as viscous fingering (Folch et al. 1999), fracture dynamics (Karma et al. 2001), and vesicle dynamics (Biben et al. 2005). The following is a summary of these efforts.

Work Done This Quarter

During this quarter, the Virginia Tech team has been working on adapting the Phase-Field theory and its general philosophy to the modeling of fatigue of asphalt binder, mastics and mixture; developing the experimental plan for validating multiscale fatigue modeling; and characterization of the void distributions from nano-to-micro and millimeter scales.

## Introduction

Microstructures of materials are heterogeneities which arise during processing of materials. Microstructure evolution is a common phenomenon in many fields, such as biology, hydrodynamics, chemical reactions, and phase transitions. Materials microstructures consist of spatially distributed phases of different compositions and crystal structures, grains of different orientations, domains of different electrical or magnetic polarizations, as well as structural defects. These structural features usually have a mesoscopic length scale between the scale of nanometers and microns. The size, shape, and spatial arrangement of the local structural features play a critical role in determining the physical properties of a material.

Microstructure evolution appears to reduce the total free energy, such as the bulk chemical free energy, interfacial energy, elastic strain energy, magnetic energy, and electrostatic energy. It also appears to reduce materials' total free energy under applied external fields, such as applied stress, electrical, temperature, and magnetic fields. Due to the highly complex and nonlinear nature of microstructure evolution, analytical solutions are not possible. Thus, numerical simulations are employed to perform the phase-field evolution.

During the past decade, the phase-field approach has emerged as a powerful method for modeling many types of mesoscale morphological and microstructure evolution processes in materials. It is based on a diffuse-interface description developed more than a century ago by van der Waals (Rowlinson 1979). It describes a microstructure using a set of conserved and non-conserved field variables that are continuous across the interfacial regions. The temporal and spatial evolution of the field variables is governed by a pair of well-known continuum equations, namely, the Cahn-Hilliard nonlinear diffusion equation (Leo and Johnson 2001) and the Allen-Cahn relaxation equation (Chen 2002). With the fundamental thermodynamic parameters as the input, phase-field method is able to predict the evolution of materials morphologies and complex microstructures. In addition, phase-field method does not need to track the positions of interfaces, which makes it advantageous over macro- and nano- scale methods. Furthermore, this approach solves the microstructural evolution problem by integrating a series of partial differential equations of the system, without an explicit treatment of the boundary conditions at the interface.

## Phase-Field Method

The phase-field model describes a microstructure, both the structural domains and the interfaces, as a whole by using a series of field variables. The field variables are continuous across the interfacial regions (Boettinger et al. 2002). The interfaces in a phase-field model have a diffuse process. There are two types of field variables, conserved and nonconserved. Conserved variables have to satisfy the local conservation condition. In the diffuse-interface description, the total free energy of an inhomogeneous microstructure system described by a set of conserved ( $c_1, c_2, \dots$ ) and non-conserved ( $\eta_1, \eta_2, \dots$ ) field variables is given by

$$F = \int \left[ f(c_1, c_2, \dots, c_n, \eta_1, \eta_2, \dots, \eta_p) + \sum_{i=1}^n \alpha_i (\nabla c_i)^2 + \sum_{i=1}^3 \sum_{j=1}^3 \sum_{k=1}^p \beta_{ij} \nabla_{i\eta k} \nabla_{j\eta k} \right] d^3 r + \iint G(r - r') d^3 r d^3 r' \quad (\text{F3a-1.5.1})$$

where  $f$  denotes the local free-energy density. It is a function of field variables  $c_i$  and  $\eta_i$ .  $\alpha_i$  and  $\beta_{ij}$  are the gradient energy coefficients. The first volume integral represents the local contribution to the free energy from short-range chemical interactions. The origin of interfacial energy comes from the gradient energy terms that are nonzero only at and around the interfaces. The second integral represents a nonlocal term that contains the contributions to the total free energy from long-range interactions, such as elastic interactions, electric dipole-dipole interactions, and electrostatic interactions. The main differences among different phase-field models lie in the treatment of various contributions to the total free energy.

### *Local Free-Energy Function*

One of the key components in a phase-field model is the local free-energy density function. Many of the phase-field models, particularly in solidification modeling, use a double-well form for the function:

$$f(\phi) = 4\Delta f \left( -\frac{1}{2}\phi^2 + \frac{1}{4}\phi^4 \right) \quad (\text{F3a-1.5.2})$$

where  $\phi$  is a field variable. The free-energy function has a doubly degenerating minima represented by  $\phi = -1$  and  $\phi = +1$ . For example, in the case of solidification,  $\phi = -1$  and  $\phi = +1$  represent the liquid and solid states, respectively.  $\Delta f$  is the potential height between the two states with the minimum free energy. If  $\phi$  represents a conserved composition field, the two minima represent the two equilibrium phases with different compositions.  $\Delta f$  is the driving force for the transformation of a single homogeneous phase ( $\phi = 0$ ) to a heterogeneous mixture of two phases represented by  $\phi = -1$  and  $\phi = +1$  during structural decomposition. If  $\phi$  is a long-range order parameter field,  $\phi = -1$  and  $\phi = +1$  are employed to describe two thermodynamically degenerating anti-phase domain states.

### *Elastic Energy*

Phase transitions in solids may produce coherent microstructures at their early stages. In a coherent microstructure, the lattice planes and directions are continuous across the interfaces, and the lattice mismatch between phases and domains are accommodated by elastic displacements. The elastic energy contribution to the total free energy in a phase-field model can be introduced directly by expressing the elastic strain energy as a function of field variables or by including coupling terms between the field variables and the displacement gradients in the local free-energy function (Biben et al. 2005).

Consider a general microstructure described by a conserved composition field  $c(\mathbf{r})$  and a non-conserved order parameter field  $\eta(r)$ , one can assume that the local stress-free strain is linearly proportional to the composition field and has a quadratic dependence on the order parameter field, i.e.,

$$\varepsilon_{ij}^0(r) = \varepsilon_{ij}^c c(r) + \varepsilon_{ij}^\eta \eta^2(r) \quad (\text{F3a-1.5.3})$$

It should be emphasized that the linear dependence of stress-free strain on composition is assumed simply for convenience. The elastic energy of a system with a nonlinear dependence of lattice parameter on composition can be obtained using the same approach. The above stress-free strain contains two pieces of information: one is the microstructure described by the field variables,  $c(r)$  and  $\eta(r)$ , and the other is the crystallographic relationship between the phases or domains in a microstructure through the lattice expansion coefficients with respect to composition and order parameter, i.e.  $\varepsilon_{ij}^c$  and  $\varepsilon_{ij}^\eta$ . The local elastic stress in a coherent microstructure is then given by

$$\sigma_{ij}(r) = \lambda_{ijkl}(r) \varepsilon_{kl}^{el}(r) = \lambda_{ijkl}(r) [\varepsilon_{kl}(r) - \varepsilon_{ikl}^c c(r) - \varepsilon_{kl}^\eta \eta^2(r)] \quad (\text{F3a-1.5.4})$$

where  $\lambda_{ijkl}(r)$  is the elastic modulus tensor, which is inhomogeneous.  $\varepsilon_{kl}(r)$  is the total local strain, which is obtained by solving the following mechanical equilibrium equation,

$$\frac{\partial \sigma_{ij}}{\partial r_j} = 0 \quad (\text{F3a-1.5.5})$$

subject to appropriate mechanical boundary conditions. With the elastic solution of  $\varepsilon_{kl}(r)$ , the total elastic energy of a microstructure can be calculated through the following equation,

$$E = \frac{1}{2} \int_V \lambda_{ijkl}(r) \varepsilon_{ij}^{el} \varepsilon_{kl}^{el} dV \quad (\text{F3a-1.5.6})$$

In the presence of external stress, the mechanical energy contribution to the total free energy becomes

$$E = \frac{1}{2} \int_V \lambda_{ijkl}(r) \varepsilon_{ij}^{el} \varepsilon_{kl}^{el} dV - \int_V \sigma_{ij}^a \varepsilon_{ij}(r) dV \quad (\text{F3a-1.5.7})$$

where  $\sigma_{ij}^a$  is the applied stress and can be inhomogeneous.

### *Evolution Equations*

With the total free energy of a microstructure discussed above, the evolution of field variables in a phase-field model can be obtained by solving the following Cahn-Hilliard (Leo and Johnson 2001) and Allen-Cahn (Allen and Cahn 1972) equations,

$$\frac{\partial c_i(\mathbf{r}, t)}{\partial t} = \nabla M_{ij} \nabla \frac{\delta F}{\delta c_j(\mathbf{r}, t)} \quad (\text{F3a-1.5.8})$$

$$\frac{\partial \eta_p(\mathbf{r}, t)}{\partial t} = -L_{pq} \frac{\delta F}{\delta \eta_q(\mathbf{r}, t)} \quad (\text{F3a-1.5.9})$$

where  $M_{ij}$  and  $L_{pq}$  are related to atom or interface mobility,  $c_1, c_2, \dots$  are conserved fields, and  $\eta_1, \eta_2, \dots$  are non-conserved.

Thus, modeling the microstructure evolution using the phase-field approach is reduced to finding solutions to the above two kinetic equations. A number of numerical methods have been implemented (Benítez and Ramírez-Piscina 2005; McFadden et al. 2000) to solve them. Most phase-field simulations employed the simple second-order finite-difference method on a uniform spatial grid and explicit time-stepping. Additionally, small time step is needed to keep the numerical solutions stable.

#### *Application of phase-field and method being developed*

The application of the phase-field approach to the crack propagation in amorphous solids has been explored by Aranson et al. (2000) and Karma et al. (2001). They introduced a non-conserved phase-field to characterize the local state of matter, either the local density or the degree of atomic bonds broken in the solid. For example, the value of 1 for the phase-field represents the solid regions, and 0 represents the cracks where the density is zero (Aranson et al. 2000) or where all the atomic bonds are broken (Karma et al. 2001). At the crack surface, the phase-field varies from 0 to 1. The Allen-Cahn equation for the phase-field is coupled to the elasto-dynamics equation for the displacement field. While the evolution of the displacement fields is driven by the applied stress or strain, the evolution of the phase-field is determined by a local criterion: either the local density is below a certain critical density (Aranson et al. 2000) or the local strain is above a critical value (Karma et al. 2001). Therefore, it is concerned that the simulations of steady-state crack motion in a strip geometry using the phase-field approach can capture the main phenomenological features of crack propagation observed experimentally. However, the quantitative modeling of the crack propagation dynamics requires further development of this method.

The deformation and fracture phenomena in pavement materials occur from nano to macro scale. Whether or not a material behaves brittle or ductile depends strongly on how the multiscale hierarchical structures are arranged inside the material, and how these structures respond to an applied load. So far, asphalt concrete deformation and failure phenomena are hard to be addressed in standard continuum calculations, like FEM analyses, due to the fact that failure is originated from particle dislocation and bond rupture. On the other hand, atomistic modeling method can predict the nanoscale mechanical properties, but it is hard to be extended to larger domain simulations other than nanoscale due to the time- and length- scale limits. The phase-field method is a promising meso-scale approach to be applied to the pavement materials modeling realm.

In pavement engineering, traffic loads weaken asphalt concrete and cause micro damage. With the fatigue damage progresses, some pavements recover strength by ‘self healing’ in the rest

period. The rates of recovery and loss vary with asphalt composition and aggregate type. Since fatigue cracking from micro damage is a major cause of failure in asphalt pavement, combinations of asphalt concrete that may heal efficiently will lead to construction of more durable and longer-lived roads.

Thus, one innovative research can be proposed to apply the phase-field models to simulate the stability and time-dependent meso-structure of colloidal emulsions, e.g. asphalt binder systems. By formulating the bulk and gradient energy in terms of the system's constitutive variables (e.g., order parameters), one can obtain predictions of phase separation, coarsening, and phase topology in emulsions as a function of temperature and bulk composition. This work will start with deriving the generic form for the free energy functional. This form includes the number and type of relevant order parameters that are required to provide a sufficiently detailed picture of the structural evolution of nano-emulsions. Then, computational algorithms for phase-field models will be employed to solve the above mentioned evolution equations.

Available experimental evidence (Soltani and Anderson 2005; Qiu et al. 2009) indicates the beneficial effects of rest periods in restoring the stiffness and strength characteristics of asphalt subject to fatigue loading. In this effort, the above derived generic form of the phase-field model will be employed to model fatigue cracking and self-healing processes within asphalt. The micro fatigue cracking and self-healing are mesoscale phenomena of the macroscale fatigue effects. Hence, experimental and numerical approaches can be carried out to investigate the mesoscale mechanisms leading to the initiation, propagation and healing of damage in asphalt concrete pavements. Then, by postulating a decomposition of the deformation gradient and a decomposition of the Helmholtz free energy function, one useful formulation will be obtained for the three dimensional visco-plastic responses of asphalt concrete materials. Consequently, the fatigue and self-healing properties of the bituminous material can be simulated by this phase-field model.

### *Fatigue Phenomena of Asphalt Concrete*

Asphalt concrete fatigue distress becomes a critical issue on the state highway and causes national wide attention: a mission of the strategic plan proposed by asphalt research consortium in 2007 is to study fatigue damage of the asphalt pavement. The plan includes the study of a model based on sound principles of the mechanics and considers the impact of the mixture's internal structure on stress distribution.

The Superpave mix design improves the rutting problem of asphalt concrete pavement to a large extent by using less asphalt content and coarse aggregate gradation, but fatigue damage becomes a serious issue and one of the most commonly happened distresses on the state highway. In order to understand the mechanism of fatigue phenomenon of asphalt concrete, the behavior of the components and their impact on the performance of the mixture should be investigated. Aggregate is one of the main components of the mixture which has very high stiffness, its deformation under loading is very small and negligible. Asphalt binder and mastics with voids are the other two main components; they combine together to make the matrix among aggregates. Since their stiffness and strength are much lower compared with aggregates, the

strain level in these areas is much higher; the damage under repeated loading in these areas cannot be ignored and its relationship with asphalt concrete fatigue should be investigated.

Since the crack phenomena are governed substantially by properties of the mastic and the existence of mastics will change the properties of the binder and influence the overall mechanical performance of asphalt mixtures (Kim et al. 2003), a microscopic method is important.

#### *Current Evaluation Methods*

A large number of research projects have been conducted to investigate the fatigue of asphalt mixture from both theoretical and experimental views. At the early stage, the fatigue of asphalt mixture was analyzed based on power-law relationship between excitation level and number of load applications to failure. This method was widely used by many researchers because of its simplicity, but this method doesn't take internal fracture of materials and damage accumulations into account and totally experiment dependent.

Dissipated energy is another concept developed to characterize the fatigue of asphalt mixture. A strain would be induced if a stress is applied to a material; this strain will recover if the stress is removed shown in the figure F3a-1.5.1. If the loading and unloading curves coincide, all the energy put into the material is recovered. If they do not coincide, there is energy lost in this process. The energy loss during a load cycle can be used as an indicator of induced damage.

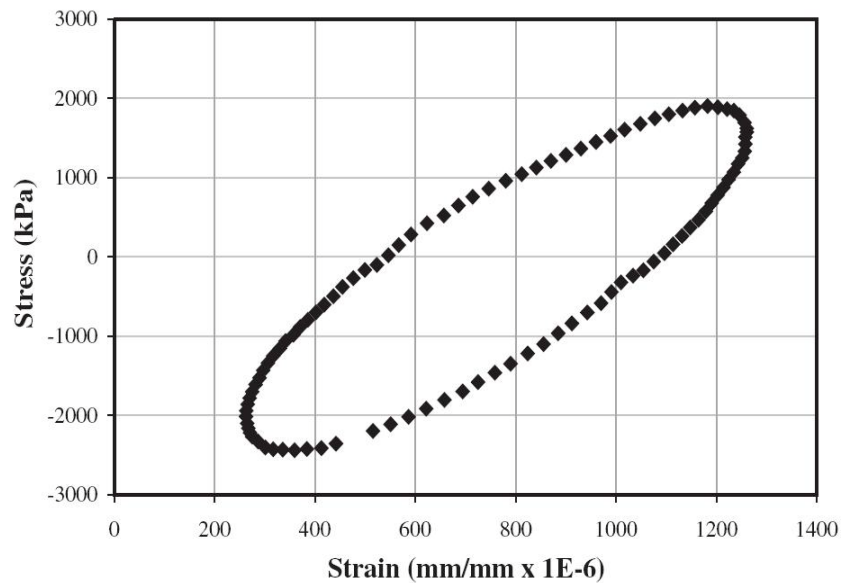


Figure F3a-1.5.1. Stress-strain Hysteresis Loop (Khalid et al. 2006)

Fracture mechanics including linear elastic fracture mechanics and non-linear fracture mechanics is another widely accepted method to model the fatigue of the asphalt concrete. For the linear elastic fracture mechanics, stress intensity factor  $K$  which characterizes the stress distribution in the vicinity of a macro-crack is developed. The crack growth during the fatigue process of the

asphalt pavement under repeated loading is a function of  $K$  (stress intensity) based on the Paris' Law. For the non-linear fracture mechanics, plastic deformation is considered. A commonly used parameter for characterization of non-linear behavior is the  $J$  contour path independent integral, which can be used as both an energy parameter and a stress intensity parameter.

Damage mechanics is also well known method used to model the fatigue of the asphalt mixture. The classical continuum damage mechanics model ignores the micro cracks in details and focus on the macroscopic response, which is the stiffness of the materials. The damage parameter  $D$  based on this method is developed.

Compared to the considerable research efforts to the asphalt mixture, the fatigue of the asphalt binder and mastics were not paid enough attention. In 1996, Boussad et al. did research about the binder rheology and its relationship to the fatigue of the materials. They used an empirical equation to describe the fatigue of asphalt binder and mixture. The equation correlated the number of loading cycles to failure of the binder to the initial strain application. In 1997, Deacon et al. studied the influence of binder loss modulus on the fatigue of AC pavement. Relationships were evaluated between asphalt binder properties and laboratory fatigue life of asphalt-aggregate mixes under third-point controlled-strain flexural beam fatigue testing. In 2002, Bonnetti et al. proposed to use the cumulative dissipated energy ratio (DER) concept as a criterion to determine the fatigue life of asphalt mixture and asphalt binder. Dynamic shear rheometer (DSR) was used to measure the complex modulus  $G^*$  and phase angle  $\theta$  of the asphalt after aging with the rolling thin film oven. The measurements were used to compute the dissipated energy ratio. This method correlates the binder properties to the fatigue of mixture.

The literature review presented above indicates that the main test tool to measure the fatigue response of asphalt binder is DSR test, but the loading mode of DSR test is not close to the field situation and the fatigue of binder is not directly evaluated. The research on mastic fatigue mainly focuses on the filler effect to the property change of the asphalt binder. The mastic performance under cyclic loading and its impact on fatigue initiation are not well understood. The relationships among the binder fatigue, mastic fatigue and mixture fatigue are barely studied.

### *Proposed Methods*

The phase-field theory and its general philosophy present a potential method to unite the fatigue analysis or modeling approach for binder, mastics and mixture. The proposed methods will integrate multiscale microstructure characterization, multiscale modeling and simulation and experimental validation.

### *Experimental Method*

Realizing the limitation of DER, the Direct Tension Tester of Interlaken Company will be utilized to conduct the fatigue test of asphalt binder and mastics. Repeated loading will be designed using the Test Builder coming with the device. The computer controlled loading system could adjust and apply a load so that the specimen experiences a constant level of strain during each load cycle. The loading frequency is at a range of 5 to 10 Hz. This loading mode is more

close to the field condition and the performance of the asphalt binder and mastics and their influence on the mixture behavior can be linked together with this test.

The fatigue of the mixture will be evaluated using flexural beam testing. During each loading cycle, the deflection of the beam specimen, loading cycles and applied load should be recorded to calculate the maximum tensile stress, maximum tensile strain, phase angle, stiffness, dissipated energy, and cumulative dissipated energy. The materials used to prepare the specimen are listed in the table F3a-1.5.1. Three kinds of asphalt binder based on Superpave binder specification will be prepared. The fillers amount used in the mastics is controlled by three filler/ratio content. A proper factorial will be designed soon.

Table F3a-1.5.1. Specimen material specifications.

	Aggregate	Asphalt binder	Filler /Asphalt Ratio
1	Gap graded	PG 64-22	1.5
2	Dense graded	PG 64-28	1.2
3	Uniformly graded	PG 70-28	0.8

### *X-ray Tomography*

The asphalt mastic and mixture samples will be scanned using x-ray tomography to obtain a series of image slices that reflect density variation of the major components of the materials such as asphalt binder, aggregates. When multiple slices are stacked together, they created a digital specimen (figure F3a-1.5.2) visualization of the internal structure of the specimen. Through image processing, the series of images will be transformed into a 3D data array that can be mapped into FEM elements for digital testing. After identification of the material components, proper material properties can be assigned to the corresponding components. The x-ray CT images of the specimen before and after testing will be used to analyze the deformation and crack propagation for specimens.

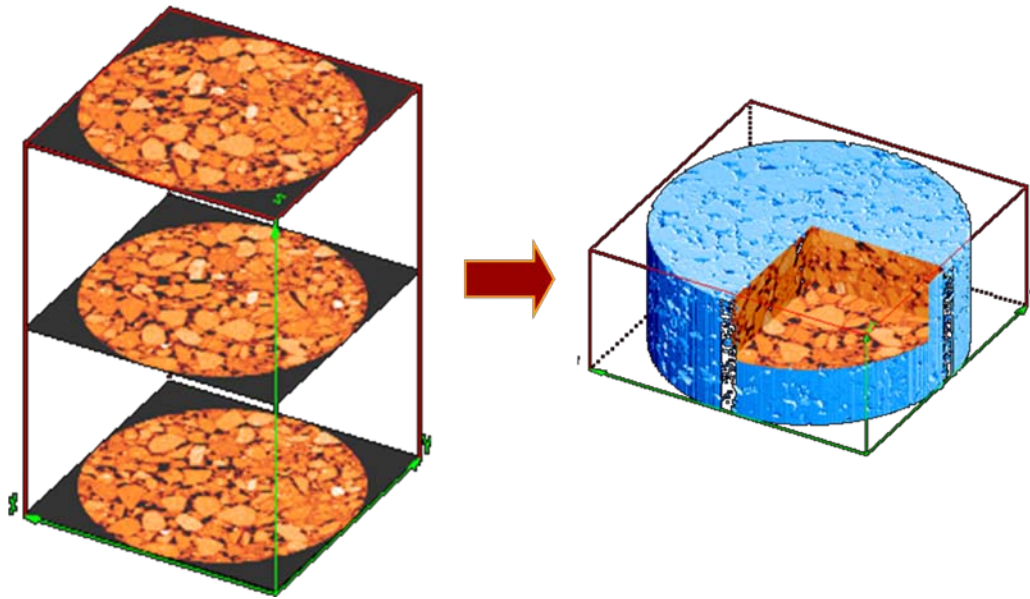


Figure F3a-1.5.2. 3-D reconstruction of the internal specimen.

### *Multiscale Characterization of Void Distribution*

Size and distribution of air voids play an important role in the performance of hot mix asphalt (HMA) mixtures. HMA mixtures with higher air void contents develop fatigue cracks earlier than those with lower air void contents. Mixtures with larger air voids deteriorate faster than those with smaller air voids, because large air voids may cluster, form a weak zone and induce local instabilities in the mixture. In addition mixtures with larger air voids age faster than those with smaller air voids. Aging occurs when air reacts with the asphalt to make it more brittle and more vulnerable to fatigue cracking. Thus, being able to anticipate how an HMA mixture will deteriorate before a pavement is constructed is important to selecting suitable mixtures for prolonging the pavement's service life. In order to predict the effects of the aforementioned deterioration mechanisms in HMA mixtures knowledge of the mean size and distribution of air voids is required. Currently, X-Ray CT along with image analysis techniques has been used extensively for the quantification of air void distribution in HMA at a millimeter scale. However, little or no information of the air voids size and distribution is available at micro and nano-scale level. Awareness of air void size and distribution at these scales can lead to better tracking of cracks in the HMA mixture as the air voids begin to grow under repeated loading and thus better understanding of fatigue in HMA. In this regard, a nano and a micro X-Ray CT and image analysis will be used to characterize the size and distribution of air voids in bitumen and mastics.

### *Computational Simulation*

The strain controlled fatigue test described above will be simulated using finite element method on ABAQUS, shown in figure F3a-1.5.3. The digital specimen prepared with the assistance of X-ray scanned image will be incorporated. The binder and the mastics will be simulated by analyzing the lab test results and using suitable material properties (ie. visco-elastic and visco-

plastic) computed through Phase-field analysis and modeling. The internal cracks will be incorporated into simulation with the assistance of scanned image of mixtures at different stages of the test and different cracking models will be used to analyze the crack propagation during the fatigue process. The digital test prepared will provide a useful tool to study the fatigue phenomenon of AC concrete.

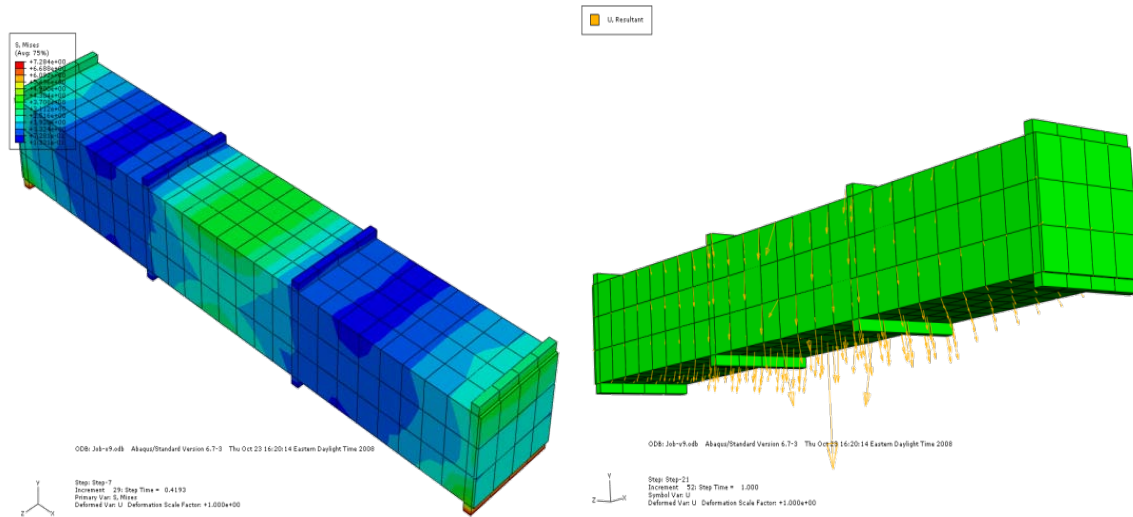


Figure F3a-1.5.3. Abaqus simulation of the lab test.

## Work Planned Next Quarter

### *Major Tasks being conducted*

A very important objective of this research is to link the fatigue of the asphalt binder and asphalt mastics to the performance of the AC mixture. From the results of lab test and computational simulations, the relationship between the microstructure, fatigue of binder and mastics, and the macro performance will be analyzed. The major tasks of being pursued during this quarter include:

1. Adapting the Phase-field theory into a multiscale formulation (**Ongoing**).
2. Conduct the fatigue test of asphalt binder, mastics and mixture using modified Direct Tension Tester (**Ongoing**).
3. Conduct the X-ray scan of the specimen to obtain the internal structure and crack propagation at multiscale (**Ongoing**).
4. Prepare the Digital test incorporated with the realistic sample internal structure (**Ongoing**).

## Cited References

- Allen, S.M., and J.W. Cahn, 1972, Ground State Structures in Ordered Binary Alloys with Second Neighbor Interactions. *Acta Metallurgica*, 20 (3), 423-433.
- Aranson, I.S., V.A. Kalatsky, and V.M. Vinokur, 2000, Continuum Field Description of Crack Propagation. *Physical Review Letters*, 85 (1), 118-121.
- Benítez, R., and L. Ramírez-Piscina, 2005, Sharp-Interface Projection of a Fluctuating Phase-Field Model. *Physical Review E*, 71 (6), 061603.
- Biben, T., K. Kassner, and C. Misbah, 2005, Phase-Field Approach to Three-Dimensional Vesicle Dynamics. *Physical Review E*, 72 (4), 041921.
- Boettinger, W.J., J.A. Warren, C. Beckermann, and A. Karma, 2002, Phase-Field Simulation of Solidification I. *Annual Review of Materials Research*, 32 (1), 163-194.
- Bonnetti, K.S., K. Nam, and H.U. Bahia, 2002, Measuring and Define Fatigue Behavior of Asphalt Binders. *Transportation Research Record*, 1810, 33-43.
- Boussad, N., P. DesCroix, and A. Dony, 1996, Prediction of Mix Modulus and Fatigue Law from Binder Rheology Properties. *Association of Asphalt Paving Technologists*, 65, 40-65.
- Chen, L.-Q., 2002, Phase-Field Models for Microstructure Evolution. *Annual Review of Materials Research*, 32 (1), 113-140.
- Deacon, J.A., J.T. Harvey, A. Tayebali, and C.L. Monismith, 1997, Influence of Binder Loss Modulus on Pavement Fatigue Performance of Asphalt Concrete Pavement. *Journal of the Association of Asphalt Paving Technologists*, 66, 633-685.
- Folch, R., J. Casademunt, A. Hernández-Machado, and L. Ramírez-Piscina, 1999, Phase-Field Model for Hele-Shaw Flows with Arbitrary Viscosity Contrast. II. Numerical Study. *Physical Review E*, 60 (2), 1734.
- Karma, A., D.A. Kessler, and H. Levine, 2001, Phase-Field Model of Mode III Dynamic Fracture. *Physical Review Letters*, 87 (4), 045501.
- Kim, Y.R., D.N. Little, and I. Song, 2003, Effect of Mineral Fillers on Fatigue Resistance and Fundamental Material Characteristics: Mechanistic Evaluation. *Transportation Research Record*, 1832, 1-8.
- Leo, P.H., and W.C. Johnson, 2001, Spinodal Decomposition And Coarsening Of Stressed Thin Films On Compliant Substrates. *Acta Materialia*, 49 (10), 1771-1787.

McFadden, G.B., A.A. Wheeler, and D.M. Anderson, 2000, Thin Interface Asymptotics for an Energy/Entropy Approach to Phase-Field Models with Unequal Conductivities. *Physica D: Nonlinear Phenomena*, 144 (1-2), 154-168.

Qiu, J., M.F.C. van de Ven, S. Wu, J. Yu, and A.A.A. Molenaar, 2009, Investigating the Self Healing Capability of Bituminous Binders. *Road Materials and Pavement Design*, 10, 81-94.

Rowlinson, J.S., 1979, Translation of Vanderwaals, JD The Thermodynamic Theory of Capillarity under the Hypothesis of a Continuous Variation of Density. *J. Stat. Phys.*, 20 (2), 197-244.

Soltani, A., and D.A. Anderson, 2005, New Test Protocol to Measure Fatigue Damage in Asphalt Mixtures. *Road Materials and Pavement Design*, 6 (4), 485-514.

***Sub-subtask F3a-1.8. Asphalt Molecular Structure and Correlation to Experimental Physical-Chemical Properties of Asphalts (WRI).***

Work Done This Quarter

Experimental measures of equilibrium wax melting temperature were determined for model paraffin waxes, a commercial microcrystalline wax, and wax separated from two asphalts. These temperature values should serve as input for the phase field model presented in this sub-task.

*Background*

Wax re-crystallization in thin-films of asphalt and asphalt fractions may be described by a phase-field model originally derivation by [Guenther and Kyu 2000; Kyu et al. 2000; Mehta et al. 2004a, 2004b; Xu et al. 2005]. In this work Mehta, Kyu and Xu describe the "Growth Dynamics of Isotactic Polypropylene Single Crystals During Isothermal Crystallization from a Miscible Polymeric Solvent". Specifically, the authors derive a functional of the free energy of crystal ordering,

$$\mathcal{F}_{crystal} = \int_V \left( f_0(\varphi, T) + \frac{(\mathbf{\kappa} \nabla \varphi)^2}{2} \right) d\Omega \quad (\text{F3a-1.8.1})$$

expressed in terms of a local free energy term

$$f_0(\varphi, T) = \Phi_\varphi \left[ \zeta \frac{\varphi^2}{2} - (1 + \zeta) \frac{\varphi^3}{3} + \frac{\varphi^4}{4} \right] \quad (\text{F3a-1.8.2})$$

defined by an asymmetric double well potential function, and a potential field strength,  $\Phi_\varphi$ , where  $\varphi$  is the crystal order parameter (non-conserved), and  $\zeta$  is the energy barrier to crystallization. A free energy gradient term is further defined as

$$\frac{(\mathbf{\kappa}\nabla\varphi)^2}{2} \quad (\text{F3a-1.8.3})$$

which quantifies the “diffuseness” of the liquid-solid crystal interfaces which develop during crystal formation, where  $\mathbf{\kappa}$  -values are tensor symmetry components of the crystal-lattice [Cahn and Hilliard 1958, 1959a, 1959b].

Correspondence of phase field modeling parameters to thermodynamics quantities is key to the success of this approach in terms of distinguishing between asphalts derived from different crude sources. This may be shown, based on the thermodynamic description of nucleation, in terms of the equilibrium transition free energy,

$$\Delta f(\varphi) = 2A\sigma - Ar\Delta H_u(1 - T/T_m^*) \quad (\text{F3a-1.8.4})$$

where  $T$  is a crystallization temperature at which a crystal begins to form,  $T_m^*$  is the equilibrium melting temperature of the polymer (in this case polymethylene-wax),  $r_z$  is the lamellar thickness of the crystal,  $\Delta H_u$  is the enthalpy of transition (crystallization),  $A$  is a unit area, and  $\sigma$  is the surface free energy per unit area of the folded or lamellar crystal surface.

The limiting expression is given as

$$\frac{\Delta f(\varphi)}{V} = \frac{2\sigma}{r_z} - \Delta H_u(1 - T/T_m^*)\varphi = 0 \quad (\text{F3a-1.8.5})$$

re-written in terms of the critical lamellar thickness,  $r^*$ , and the crystal melting temperature,  $T_m$  as a free energy per unit volume,  $V$ ,

$$0 = \frac{2\sigma}{r^*} - \Delta H_u(1 - T_m/T_m^*)\varphi \quad (\text{F3a-1.8.6})$$

The non-conserved "critical" phase field parameter,  $\varphi^*$ , is then expressed as a function of the ratio of the critical and variable lamellar thicknesses,

$$\frac{(1 - T/T_m^*)}{(1 - T_m/T_m^*)} = \frac{r^*}{r_z} = \varphi^* \quad (\text{F3a-1.8.7})$$

The energy barrier to crystallization is then shown to be related to the change in free energy of crystallization by

$$\Delta f(\varphi) = \frac{\Phi}{6}(\zeta - 1/2) \quad (\text{F3a-1.8.8})$$

where

$$\zeta = \frac{\left[ \varphi^* \left( 4\zeta_0 - 3(\varphi^*)^2 \right) \right]}{(6\zeta_0 - 4\varphi^*)} \quad (\text{F3a-1.8.9})$$

and where  $\zeta_0 = T_m / T_m^*$ . Hence,

$$\Delta f(\varphi) = f(\varphi) - f(0) = \Phi \zeta_0^3 \left( \frac{\zeta}{6} - \frac{\zeta_0}{12} \right) \quad (\text{F3a-1.8.10})$$

$$\frac{2\sigma}{nRT r_z} - \frac{\Delta H_u}{nRT} (1 - T / T_m^*) = \Phi \zeta_0^3 \left( \frac{\zeta}{6} - \frac{\zeta_0}{12} \right) \quad (\text{F3a-1.8.11})$$

The surface free energy per unit area of the diffuse interface constituting the folded or lamellar crystal surface is solved as

$$\sigma = nRT \int_0^1 \kappa \sqrt{2f(\varphi)} d\varphi = (nRT \kappa / 6) \sqrt{\Phi / 2} \quad (\text{F3a-1.8.12})$$

Equations F3a-1.2.1 or F3a-1.5.9 express the rat law expression of the developing crystal phase given  $\zeta$  as an input parameter in equation F3a-1.8.2.

### *Experimental*

Again, correspondence of phase field modeling parameters to thermodynamics quantities is key to the success of this approach in terms of distinguishing between asphalts derived from different crude sources. Thus, methods are being developed to measure phase transition temperatures of waxy species in asphalt, (e.g., equilibrium wax melting/crystallization temperatures, and wax appearance temperatures in asphalts).

A simple method of measuring wax crystallization temperatures and the change in specific volume of wax at the transition temperature, based on the change in refractive index as a function of changing temperature (Harrison et al. 1958) was considered during this quarter. In this method a temperature controlled refractometer is used to measure the refractive index of melted wax as it is cooled through the crystallization temperature regime. Model paraffins, paraffin mixture, a microcrystalline wax, and waxes separated from asphalts were considered. Model waxes octacosane ( $C_{28}H_{58}$ ) and docosane ( $C_{22}H_{46}$ ), purchased from Analabs, Inc., and a microcrystalline wax (IGI 5788A) from the International Group, Inc. were used in these studies.

Waxes were separated from chromatograph fractions (saturates, naphthene aromatics, neutral fractions) using a procedure employed during the SHRP program (Branthaver et al. 1993). Wax separations were conducted by initially dissolving 1-gram of the sample material in 10-mL of toluene. The asphalt/toluene solutions were cooled in an ice/acetone bath to a temperature of 0°C. Cold (0°C) methyl ethyl ketone (MEK, HPLC-grade, JT Baker) was then added to the flask containing the sample solution. The resulting mixture was stirred, then cold-filtered using a water-jacketed funnel w/fritted-glass disk. The filter temperature was maintained at 0°C. The

material retained on the filter constituted a wax filter cake. The eluted liquid contained the wax-free fraction. Each filter cake was washed with additional cold MEK, air dried, then removed from the filter with a plastic or rubber spatula and stored in a sealed vial. The eluate was recovered via rotary-vacuum-distillation. No additional drying of the eluted material was conducted.

Corbett (SARA) separations (ASTM D4124-09, *In Press*) were carried out by dissolving 1-g of isooctane-type maltenes in 10-mL of n-heptane and injecting the solution onto a 70-cm long, 1.5-cm diameter glass LC-column filled with approximately 110-g of CG-20 chromatographic grade activated alumina (cat#AXO612-3, 80-200 mesh, Chromatographic grade, EMD). Fractions (i.e., saturates-aromatics-then resins) were eluted by introducing the following solvents onto the column; 50-ml n-heptane, 100-mL of toluene (HPLC-grade, Fisher Scientific), 75-mL of methanol (HPLC-grade, Fisher Scientific)/toluene (50:50 by vol.), and 150-mL trichloroethylene (TCE, HPLC-grade, Alfa Aesar). Saturates were collected prior to elution of a fluorescent band migrating up the column. Naphthenic aromatics characterized by the fluorescent band were collected prior to a dark band migrating up the column below the fluorescent band. TCE was finally introduced to strip the column of any remaining “dark band” material defined as the polar aromatics fraction. Fractions were recovered by roto-evaporation and dried to constant weight.

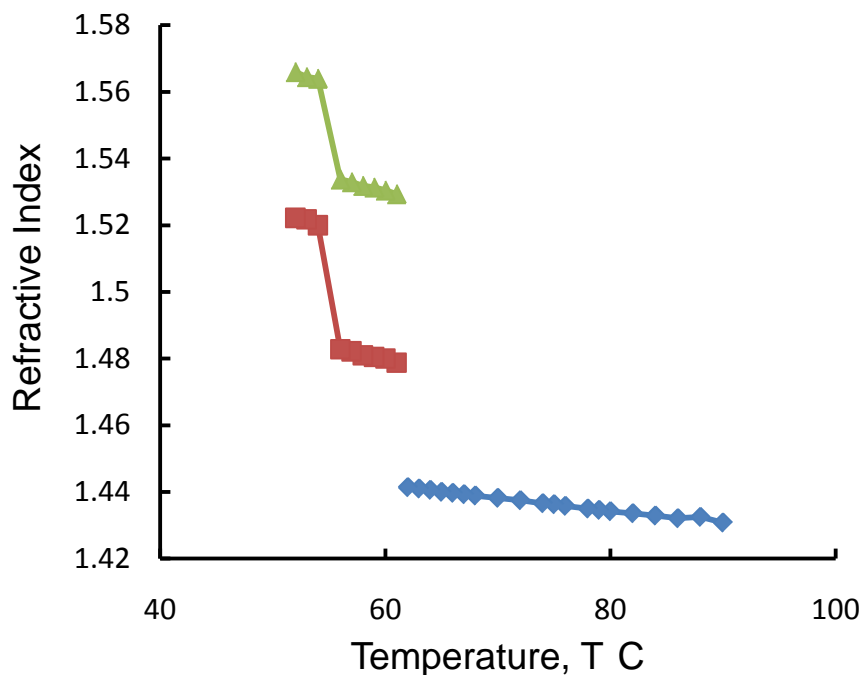


Figure F3a-1.8.1. Refractive index versus temperature plot for the model paraffin wax octacosane, where multiple lines below the crystallization temperature are related to birefringence.

Figure F3a-1.8.1 depicts a refractive index versus temperature plot for the model paraffin wax octacosane. In this plot both ordinary and extraordinary refractive indices,  $n_o$  and  $n_e$ , respectively are used to calculate the effective refractive index,  $n$ , as

$$n = \frac{(2n_o + n_e)}{3} \quad (\text{F3a-1.8.13})$$

Density of the wax as a function of changing temperature may then be calculated as

$$\rho_{i+1} = \rho_i \left[ \left( \frac{n_i^2 + 2}{n_i^2 - 1} \right) \left( \frac{n_{i+1}^2 - 1}{n_{i+1}^2 + 2} \right) \right] \quad (\text{F3a-1.8.14})$$

where the initial density,  $\rho_i$ , is initially given the value of unity, but later adjusted so that the density value at 25°C is approximately equal to the true density values of the waxes considered. Specific volumes (mL/g) were determined as the inverse of density  $\bar{v} = 1 / \rho$ .

In the present study densities of paraffin waxes in the carbon number range of C30 to C60 may vary between 0.775 to 0.8-g/mL, while densities of microcrystalline waxes, (branched or iso-alkanes and alkanes with naphthenic character), may vary between 0.8 to .98-g/mL, thus,  $\rho_i$  values were adjusted to give a density value of 0.8 at 25°C for all samples studied. Figure F3a-1.8.1. depicts a plot of specific volume as a function of temperature for model waxes, model wax mixtures and waxes separated from two asphalts.

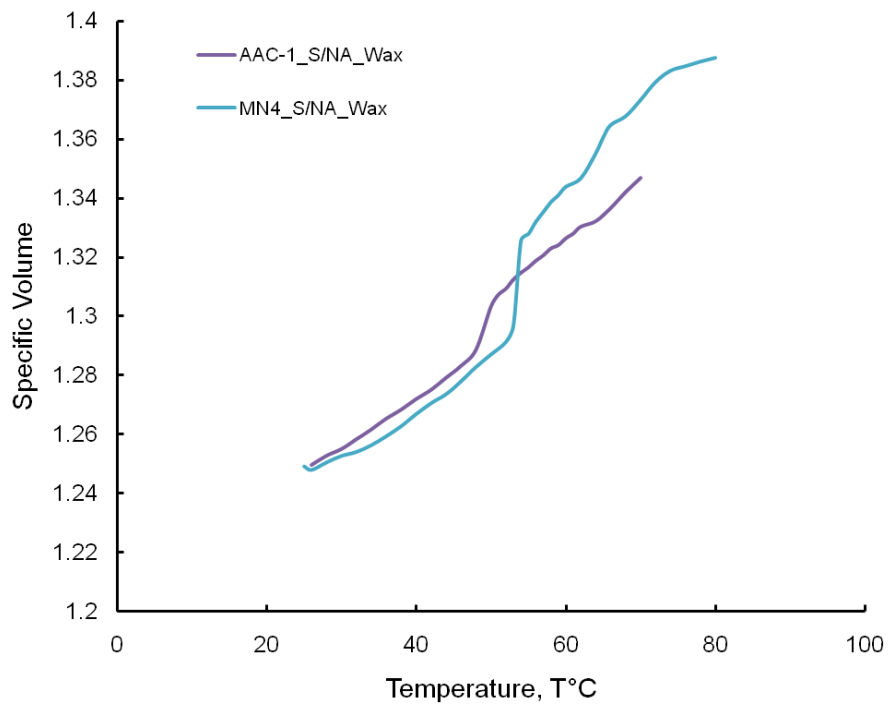
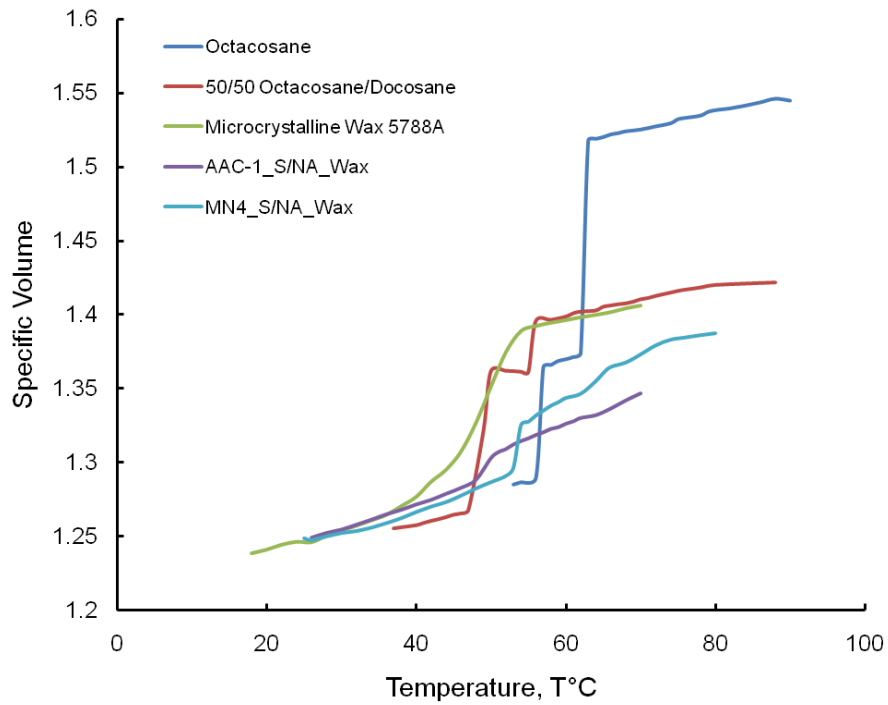


Figure F3a-1.8.2. Specific volume versus temperature plot for the model paraffin and microcrystalline waxes, and waxes derived from two asphalts.

### Work Planned Next Quarter

Separate waxes from comparative performance site asphalts and measure wax transition characteristics based on the method discussed in this subtask. Characterize wax and wax free materials by high performance gel-permeation chromatography (HP-GPC), thermal gravimetric analyses, and modulated differential scanning calorimetry. Data determined from these methods will serve as input into phase field modeling approaches.

### Cited References

ASTM D4124-09, (*In Press*). Standard test method for separation of asphalt into four fractions. Annual book of ASTM standards, road and paving materials; vehicle-pavement systems, section 4, vol. 04.03, West Conshohocken, PA: ASTM International, 397-403.

Branthaver, J.F., J.C. Petersen, R.E. Robertson, J.J. Duvall, S.S. Kim, P.M. Harnsberger, T. Mill, E.K. Ensley, F.A. Barbour, and J.F. Schabron, 1993, SHRP-A-368, Binder Characterization and Evaluation, Volume 2: Chemistry. Strategic Highway Research Program, National Research Council, Washington, DC.

Cahn, J.W., and J.E. Hilliard, 1958, Free Energy of a Nonuniform System. I. Interfacial Free Energy. *J. Chem. Phys.*, 28 (2), 258-267.

Cahn, J.W., and J.E. Hilliard, 1959a, Free Energy of a Nonuniform System. II. Thermodynamic Basis. *J. Chem. Phys.*, 30 (5), 1121-1124.

Cahn, J.W., and J.E. Hilliard, 1959b, Free Energy of a Nonuniform System. III. Nucleation in a Two-Component Incompressible Fluid. *J. Chem. Phys.*, 31 (3), 688-699.

Guenther, A.J. and T. Kyu, 2000, Formation of banded textures in liquid crystalline polymers with extended curvature elasticity. *Macromolecules*, 33, 4463-4471.

Harrison, D.V., A.M. Reigold, and W.R. Turner, 1958, Volume Changes in Petroleum Waxes as Determined from Refractive Index Measurements. *Industrial and Engineering Chemistry*, 3(2), 352-359.

Kyu, T., R. Mehta, and H-W. Chin, 2000, Spatiotemporal growth of faceted and curved single crystals. *Phys. rev. E.*, 61 (4), 4161-4170.

Mehta, R., W. Keawwattana, and T. Kyu, 2004a, Growth dynamics of isotactic polypropylene single crystals during isothermal crystallization from a miscible polymeric solvent. *J. chem. phys.*, 120 (8), 4024-4031.

Mehta, R., W. Keawwattana, A.L. Guenther, and T. Kyu, 2004b, Role of curvature elasticity in sectorization and ripple formation during melt crystallization of polymer single crystals. *Phys. rev. E.*, 69, 061802.

Xu, H., R. Matkar, and T. Kyu, 2005, Phase-field modeling on morphological landscape of isotactic polystyrene single crystals. *Phys. rev. E.*, 72, 011804.

## **Work Element F3b: Micromechanics Model (TAMU)**

### ***Subtask F3b-1: Model Development***

#### Work Done This Quarter

During this quarter we have mainly progressed towards two activities:

- We have worked on the implementation of a cohesive zone model that is capable of accounting for the rate-dependent fracture process in asphaltic materials. More specifically, we have implemented two different UEL codes (customized *ABAQUS* USER ELEMENT subroutines) available in the open literature into the *ABAQUS* main frame and have tested one UEL (four-node bilinear cohesive zone model) by comparing model simulation results obtained from the newly implemented UEL with simulation results from the customary bilinear model that exists in the original *ABAQUS*. The idea is to extend the UEL subroutine, after successful implementation, for predicting the rate-dependent fracture characteristics, since none of cohesive zone models featured in the current *ABAQUS* can be applied to the rate-dependent fracture problems.
- Another primary task we focused on during this quarter was the development of a proper mixing-compaction-production practice of the fine aggregate matrix (FAM) phase in asphalt concrete mixtures. This effort is to provide more accurate mechanical properties (viscoelastic properties and cohesive zone properties of matrix phase) of the FAM phase to accomplish the finite element-based micromechanics modeling. Some significant findings obtained during this quarter are presented in this report.

The research outcomes were presented in two recent conferences: the 2010 TRB annual meeting and the ASCE GeoFlorida conference and at the Advanced Models ETG meeting held in Irvine CA. In addition, one paper was written and submitted for the ASCE Engineering Mechanics Special Publication (EMSP), and two journal papers under review process have finally been accepted for publication. Work progress and significance of each activity can be summarized as follows.

- UEL implementation into *ABAQUS* main frame

During this quarter we started working on the development of a rate-dependent cohesive zone model. This is an essential part of our work as it will allow us to simulate fracture in asphalt mixtures in a more realistic way by accounting for the rate-dependent fracture characteristics. Towards this challenging task, the first step we took was to implement rate-independent cohesive zone models in a form of UEL (USER ELEMENT) subroutine into the *ABAQUS* main frame. The cohesive zone models implemented are the ones that have already been featured in the current version of *ABAQUS*; therefore, simulation results between two can be compared to check

if the UEL implementation is correctly accomplished. Then, as mentioned earlier, the newly implemented UEL will be extended to address the rate-dependent fracture characteristics.

Among many available models, we have implemented two UEL codes (i.e., an exponential model provided by Gao and Bower (2004) and a bilinear model provided by Song (2006)) into the main frame of *ABAQUS*. To check if the implementation is made correctly, a uniaxial bar in tension (shown in figure F3b-1.1) was simulated. The bar is elastic with a four-node cohesive zone element in the middle of the bar. Simulation results were compared, and as clearly seen in figure F3b-1.1, both results were identical, which indicates that the new UEL model has been successfully implemented into *ABAQUS*. The UEL is now being expanded to allow the prediction of rate-dependent fracture process.

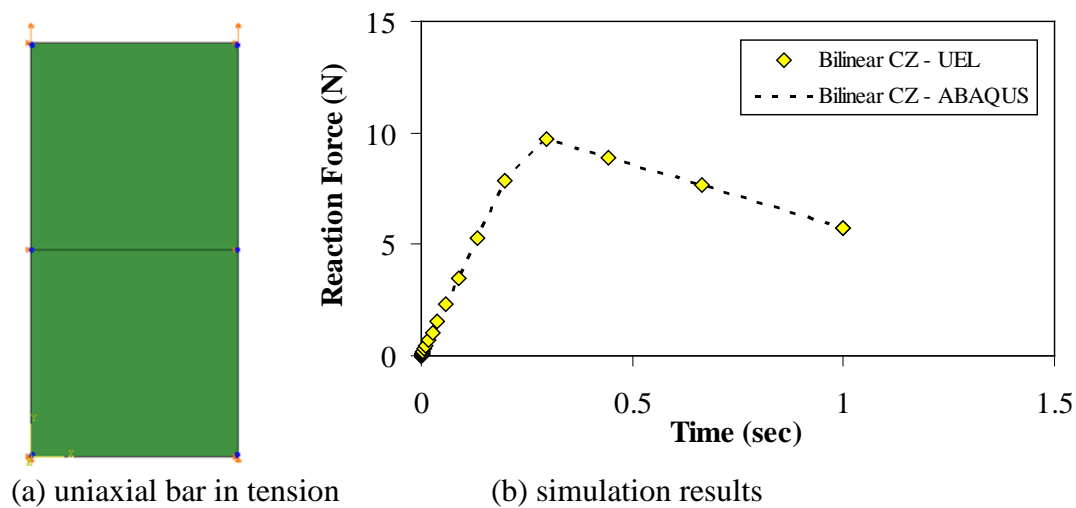


Figure F3b-1.1. A uniaxial bar problem to check the accuracy of UEL implementation.

- Development of a protocol for mixing, compaction, and production of FAM phase to provide mechanical properties for the micromechanical modeling

To accomplish our computational micromechanics modeling based on the finite element method, individual phases in asphalt mixtures need to be characterized for their mechanical properties as model inputs. The more accurate characterization of phase properties will guarantee the more accurate predictions of mixture behavior. FAM is considered one of primary phases constituting the asphalt concrete mixture as shown in figure F3b-1.2; however, the characterization of mechanical properties of the FAM phase has been performed somewhat carelessly because of many unknowns such as the volumetric characteristics of the FAM. For example, accurate estimation of binder content, air voids, aggregate particle sizes and distributions in the FAM phase is not easy to make; probably it is impossible. Nevertheless, in order to improve model accuracy based on the more accurate characterization of constituent properties (model inputs), we have attempted to develop an approach that is more articulate and scientific than pre-existing

approaches (Kim et al. 2003, 2006; Song et al. 2005; Masad et al. 2006; Castelo et al. 2008) in the process of mixing-compaction-production of the FAM specimen.

Unlike conventional asphalt concrete volumetric systems, we assumed that the asphalt concrete mixtures consist of two primary material phases – the elastic phase of aggregates and the viscoelastic phase of FAM, which is composed of asphalt binder, fine aggregates passing sieve No. 16 (mesh size of 1.19 mm), and entrained air voids. The maximum fine aggregate size of 1.19 mm in the FAM mixture was determined based on two-dimensional digital image analyses of cross sections obtained from various compacted asphalt concrete samples. The digital images could not properly capture aggregates approximately less than 1.0 mm, which is close to the mesh size of sieve No. 16. The mix design of the FAM phase has been postulated on the basis of the sharing of binder by the coarse and fine aggregates in the asphalt concrete mixture. The mix design considered binder content that is absorbed into aggregates and that covers aggregates with a fixed binder film thickness. Algebraically, the required binder content to produce the FAM specimen was proposed as the one remaining after excluding binder absorbed in the coarse aggregates and the thin film (12 micron for the current approach) of binder covering coarse aggregates from the total binder in the bulk asphalt concrete mixtures.

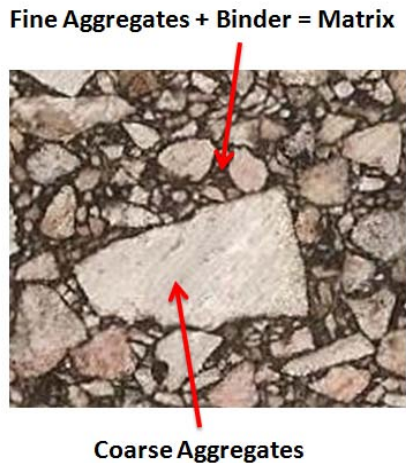


Figure F3b-1.2. Typical microstructure of asphalt concrete mixtures.

The new protocol also incorporated the extraction of small DMA specimens out of Superpave gyratory bulk samples that were compacted with different amounts of FAM mixtures to represent different levels of air voids. Each DMA specimen produced was tested to characterize linear viscoelastic properties (in a form of dynamic modulus master curve) at each different level of air voids. The aggregate phase was considered an elastic material of which property (Young's modulus) was obtained by performing the nano-indentation tests using a Berkovich diamond indenter. Test results (DMA tests for the FAM and nano-indentation tests for the coarse aggregates) were then incorporated with the micromechanical finite element simulations to predict linear viscoelastic dynamic moduli of the corresponding bulk asphalt concrete mixture. Simulated dynamic moduli from the micromechanical model were finally compared to dynamic

moduli obtained from laboratory tests, so that the appropriate level of FAM density (i.e., the amount of air voids) can be determined. Figure F3b-1.3 briefly illustrates the process employed for this study.

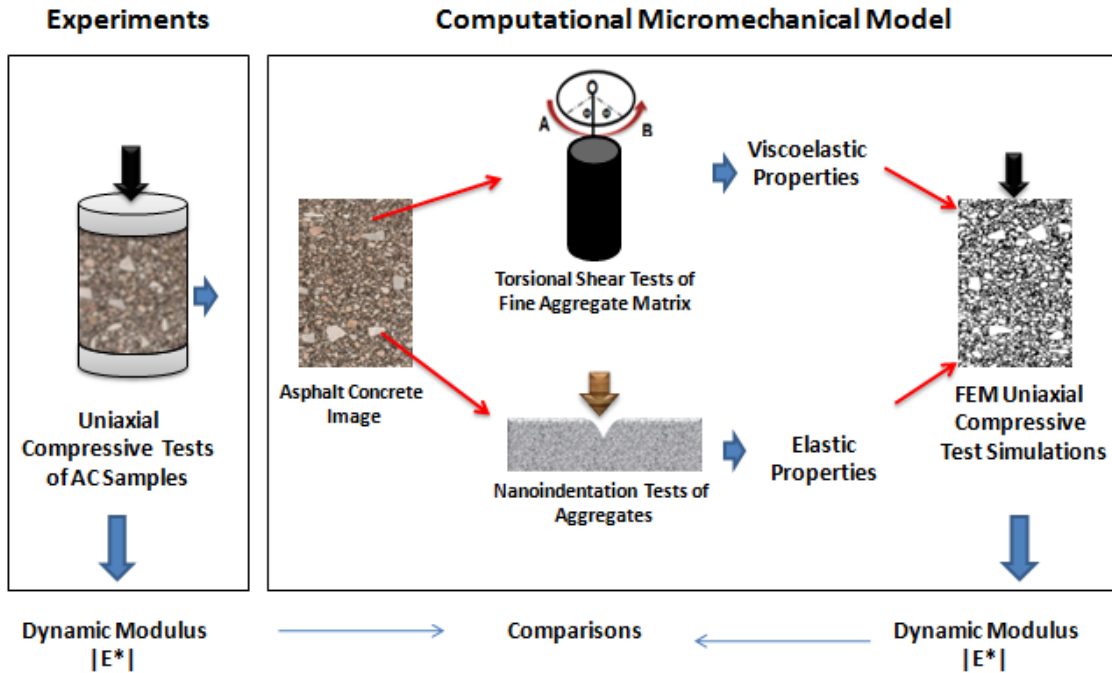


Figure F3b-1.3. Research method employed for the characterization of FAM phase.

DMA test results for the viscoelastic properties of the FAM phase and the nano-indentation test results for the elastic property of coarse aggregates are presented in figure F3b-1.4 and figure F3b-1.5, respectively. Five different air voids (from 0.00 % to 1.75 %) were attempted for the production of FAM specimens. Clearly, as shown in figure F3b-1.4, FAM mixtures with lower air voids presented stiffer behavior than the mixtures with higher air voids. Twenty nano-indentation measurements were made for the elastic property (Young's modulus) of coarse aggregates and it resulted in a mean value of 60.9 GPa, as presented in figure F3b-1.5.

With the treated digital image of asphalt concrete mixture microstructure and the properties of each phase, computational micromechanics modeling was then conducted. Figure F3b-1.6 shows the digital image of the mixture used to construct finite element meshes. For this study, a two-dimensional approximation of the three-dimensional mixtures was adopted because of the significant geometric complexity. Furthermore, as mentioned earlier, air voids were not explicitly considered in the microstructure, but were considered an entrained form in the matrix phase. Figure F3b-1.6 also presents boundary conditions applied to the sample. Vertical displacements ( $U_Y$ ) were constrained at the bottom face of the sample, and a compressive haversine traction ( $T_Y$ ) was evenly applied to the top nodes. To construct a dynamic modulus master curve, a wide spectrum of loading frequencies was simulated ( $10^{-4}$  to  $10^3$  Hz).

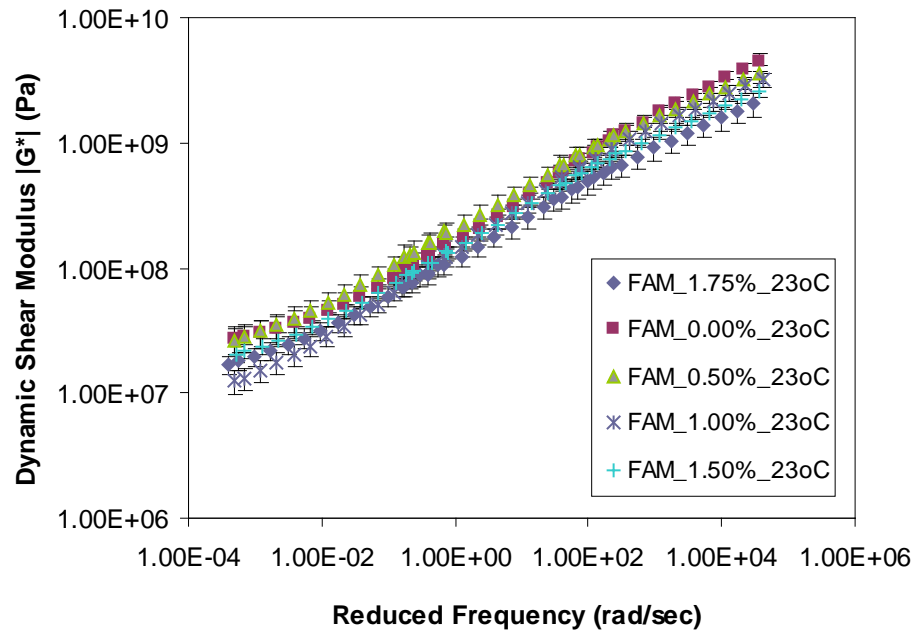


Figure F3b-1.4. DMA test results of FAM mixtures with different air voids.

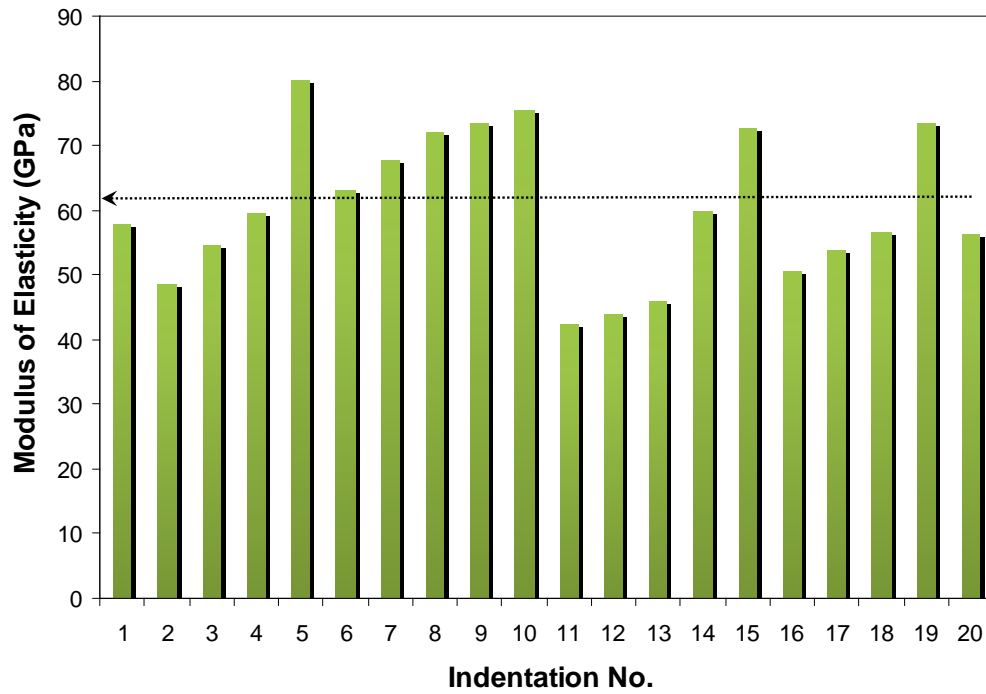


Figure F3b-1.5. Nano-indentation test results (modulus of elasticity) of coarse aggregates.

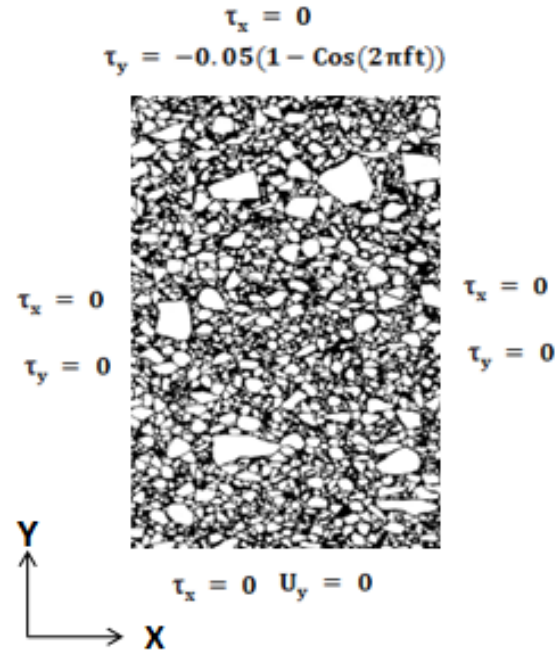


Figure F3b-1.6. Finite element mesh of the digital image treated and boundary conditions imposed.

As presented in figure F3b-1.3, dynamic modulus tests were also performed on the cylindrical asphalt concrete specimens in the uniaxial cyclic compressive testing mode. The loading levels were carefully adjusted until the strain levels were within the range of 0.00005-0.000075. Three linear variable differential transformers (LVDTs) were mounted onto the surface of the specimen at 120° radial intervals with a 100-mm gauge length. Vertical deformations averaged from the three LVDTs were used to calculate the dynamic modulus, defined simply as the ratio of the sinusoidal stress amplitude to the sinusoidal strain amplitude. Three temperatures (4, 20, and 40°C) with varying frequencies were used. The frequency-temperature superposition concept was then applied in order to develop the master curve at 23°C. Three replicates were tested and test results are presented in figure F3b-1.7. As error bars embedded in the master curve show, test results between replicates were fairly consistent at high loading frequencies, whereas greater variations of the moduli were observed at lower loading frequencies (high testing temperatures).

Figure F3b-1.8 shows dynamic modulus comparisons between model simulations from each different FAM cases and the experimental results. In general, all predictions at the different levels of air voids were in fair agreement with the test results. Comparison between experimental results and the model simulations presented a relatively higher deviation at lower loading frequencies but better agreement when the loading frequency was larger.

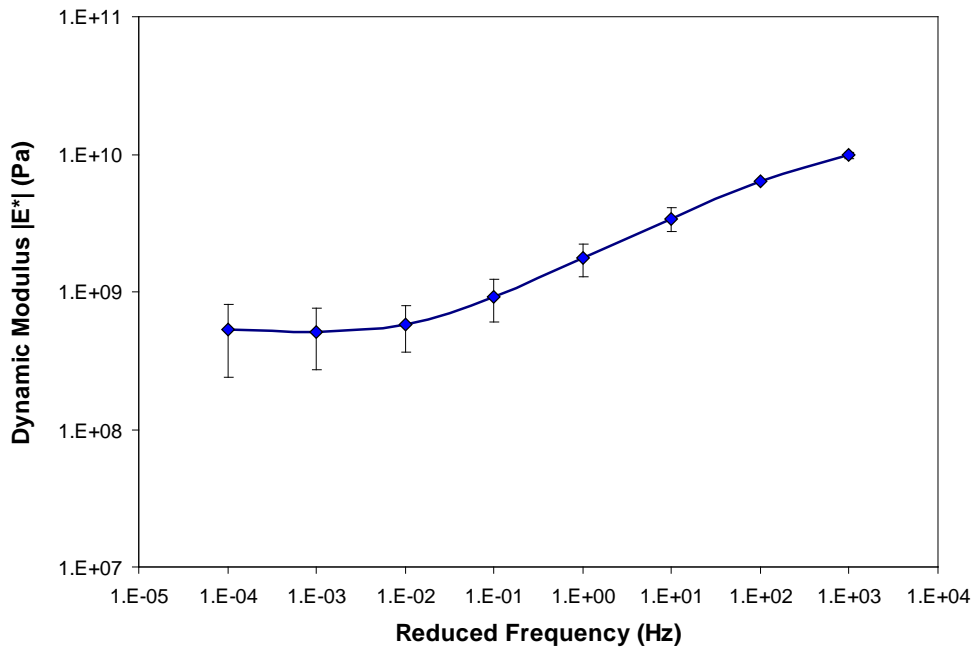


Figure F3b-1.7. Dynamic modulus test results of asphalt concrete cylinders (three replicates).

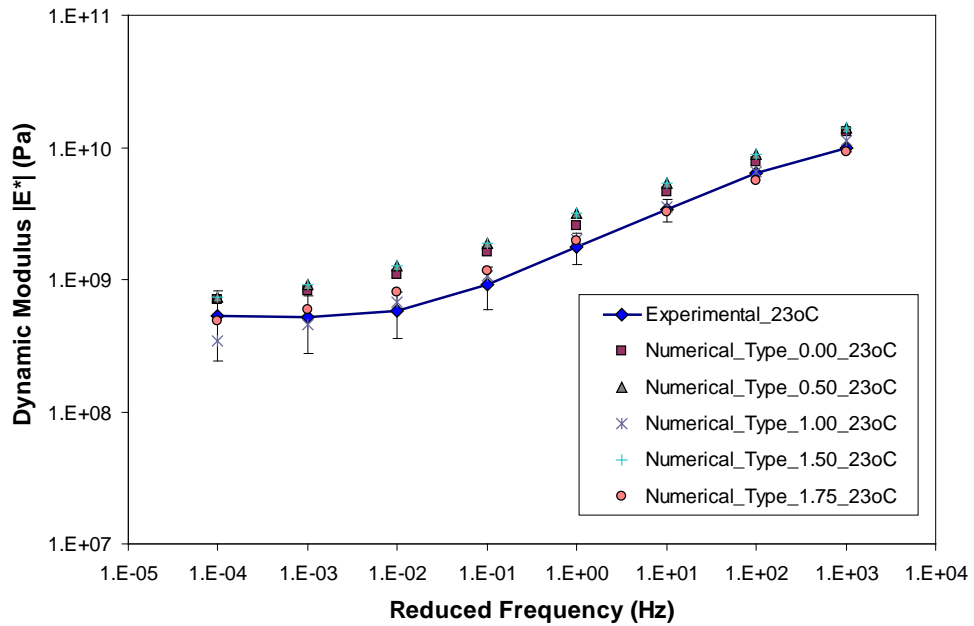


Figure F3b-1.8. Dynamic modulus comparisons between model simulations and test results.

Figure F3b-1.9 plots the upper and lower limits of experimental tests along with the two extreme cases of FEM simulations that are placed within the limits. As shown, the dynamic modulus master curves predicted by FEM simulations were within the range of experimental variations for the samples with those FAM phase which had 1.00 to 1.75 % of air voids. The master curves of asphalt mixtures containing the FAM of 0.00 % and 0.50% air voids were not within the upper-lower limits. This implies that the FAM phase must contain air voids to certain extent for representing mixture properties more accurately.

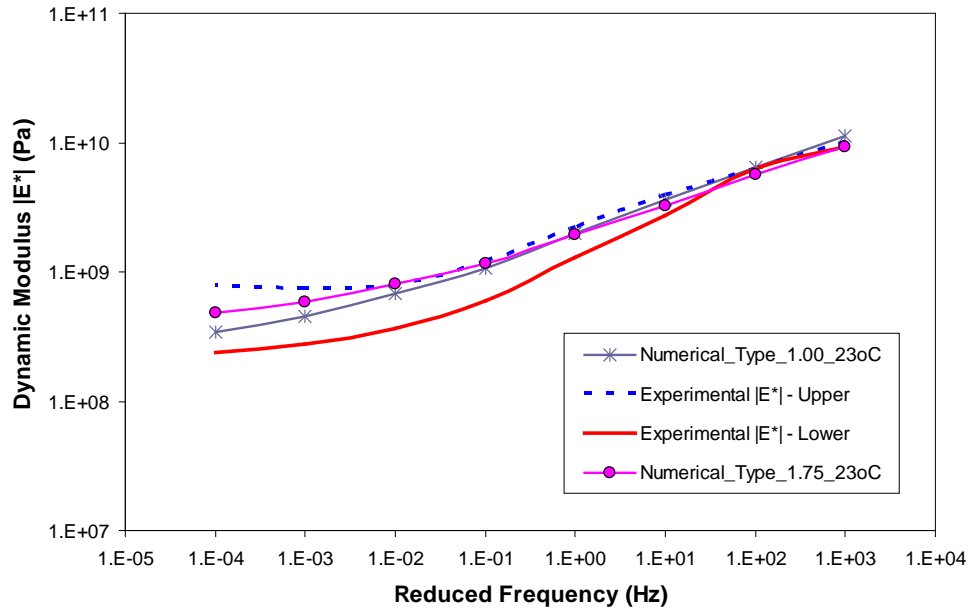


Figure F3b-1.9. Dynamic modulus comparisons: Upper-lower limits of experimental data vs. simulation placed within the upper-lower limits.

### Significant Problems, Issues and Potential Impact on Progress

None.

### Work Planned Next Quarter

In the next quarter we will work on the following activities:

- Extension of the current rate-independent UEL code to incorporate the rate-dependence of the cohesive zone fracture parameters;
- Analysis of the SCB (Semi-Circular Bending) fracture test results (presented in the previous quarters) to more accurately identify rate-dependent fracture characteristics of FAM materials; and
- Development of the mixing-compaction-production practice of the FAM phase with more test data and simulation results to reach more conclusive findings.

## References

Castelo, B.V., E. Masad, A. Bhasin, and D.N. Little, 2008, Fatigue analysis of asphalt mixtures independent of mode of loading. *Transportation Research Record*, 2507, 149-156.

Gao, Y.F. and A.F. Bower, 2004, A Simple Technique for Avoiding Convergence Problems in Finite Element Simulations of Crack Nucleation and Growth on Cohesive Interfaces. *Modeling and Simulation in Materials Science and Engineering*, 12, 453-463.

Kim, Y., D.N. Little, and R.L. Lytton, 2003, Fatigue and healing characterization of asphalt mixtures. *Journal of Materials in Civil Engineering*, 15 (1), 75-83.

Kim, Y., H.J. Lee, D.N. Little, and Y.R. Kim, 2006, A simple testing method to evaluate fatigue fracture and damage performance of asphalt mixtures. *Journal of the Association of Asphalt Paving Technologists*, 755-787.

Masad, E., C. Zollinger, R. Bulut, D.N. Little, and R.L. Lytton, 2006, Characterization of HMA moisture damage using surface energy and fracture properties. *Journal of the Association of Asphalt Paving Technologists*, 75, 713-754.

Song, I., D.N. Little, E. Masad, and R.L. Lytton, 2005, Comprehensive evaluation of damage in asphalt mastics using X-ray CT, continuum mechanics, and micromechanics. *Journal of the Association of Asphalt Paving Technologists*, 74, 885-920.

Song, S.H., 2006, Fracture of Asphalt Concrete: A Cohesive Zone Modeling Approach Considering Viscoelastic Effects. Ph.D. dissertation at University of Illinois at Urbana-Champaign.

## Work Done This Quarter

### *Lattice Micromechanical Model*

In the previous quarter, the lattice modeling was enhanced to model the dependence of strength on rate with the help of continuum damage theory applied to individual lattice links. The objective for this quarter was to quantitatively verify the new lattice model and incorporate air voids in the model.

With respect to the quantitative verification of the model, an experimental investigation was undertaken at various scales to obtain the stress-strain relationships, followed by an attempt to use lattice modeling to predict the experimental results. This step turned out to be significantly more challenging than expected, because the experimental data showed a gradual change in time dependence with scaling up; this change was not seen in the lattice models. We are in the process of further investigating the reasons for this changing time dependence as well as other model approaches that can capture this effect.

With respect to the inclusion of air voids in the model, work has begun on incorporating air voids in the virtual fabrication framework. This work, as well as the incorporation of air voids into the lattice models and the seamless integration of this process into the MS-VFLM software, is expected to be completed in the next quarter.

#### *Continuum Damage to Fracture*

Work is continuing on the micromechanical understanding of damage with the eventual goal of linking damage to localization and fracture. Specifically, a quantitative model that can capture the onset of localization (the point of departure from continuum damage theory) is being investigated. Specific results will be reported once the model is successfully developed and tested using some preliminary experimental data.

#### Significant Results

##### *Lattice Micromechanical Model*

None.

#### Significant Problems, Issues and Potential Impact on Progress

Time dependency appears to vary gradually over various scales, and this issue is being actively investigated.

#### Work Planned Next Quarter

##### *Lattice Micromechanical Model*

- Investigate the gradual change in time dependence at various scales.
- Complete the inclusion of air voids in the MS-VFLM framework.

##### *Continuum Damage to Fracture*

Continue to develop the micromechanical understanding of damage and quantifiable criteria for the onset of localization.

### **Work Element F3c: Development of Unified Continuum Model (TAMU)**

#### **The Analysis Procedure of ALF data**

#### Work Done This Quarter

In this quarter, a systematic and consistent thermodynamic-based framework for constructing a temperature-, time-, and rate-dependent constitutive model for bituminous materials, which provides a coupling amongst temperature, viscoelasticity, viscoplasticity, and viscodamage, is

formulated. These derived constitutive equations based on the laws of thermodynamics are the main equations that are implemented in the Pavement Analysis using a Nonlinear Damage Approach (PANDA) code. Therefore, the thermodynamic consistency of unified continuum damage model is verified. The viscodamage model is coupled to other parts of the constitutive model (i.e. to viscoelasticity and viscoplasticity) through using the concept of the effective (undamaged) configuration within the continuum damage mechanics framework. Hence, the Helmholtz free energy density is expressed in terms of the internal state variables in the effective configuration. This procedure simplifies the numerical implementation of the presented nonlinear model to a great deal since it avoids the complexities associated with the direct couplings of the damage to the rest of the constitutive equations and allows natural coupling of viscoelasticity and viscoplasticity to damage evolution.

Moreover, a straightforward procedure for identifying the associated material parameters of the formulated constitutive equations is proposed. The viscodamage model is formulated to be a function of stress, total strain, and the damage history. Also, both viscoplasticity and viscodamage models are enhanced by incorporating a parameter that accounts for the difference in viscoplastic and damage responses in compression and in extension. The temperature coupling is brought into the model explicitly by introducing multiplicative temperature coupling terms in the Helmholtz free energy density function.

One set of material parameters identified from some specific tests is then used to validate the model for different tests. Validation is based on a comprehensive set of experimental data on a hot asphalt mix that include creep-recovery, creep, monotonic constant strain rate, and repeated creep-recover tests in both tension and compression and over a wide range of temperatures, stress levels, and strain rates. These experimental data are obtained from the Nottingham experimental database. Comparing the experimental measurements with the model predictions show that the model can predict the complex mechanical responses of the bituminous materials reasonably well for the majoring of the test data. Also, creep tests show that the model is capable of predicting the time of failure in both tension and compression. The constant strain rate tests at different temperatures and strain rates show that the model is able to capture the peak point, post-peak behavior, and initial response in the stress-strain diagram. It is shown that the dependence of the viscodamage model on the history makes the damage density-strain diagram to have an S-like shape. Hence, one can consider the inflection point of the damage-strain curve as the point after which the post-peak behavior occurs. Moreover, the comparisons between the model predictions and experimental measurements for repeated creep-recovery test show that the model is capable of predicting well the experiments for low rest period times. However, once the rest period increases the model predictions and experimental measurements deviate significantly. This is attributed to micro-damage healing during the resting period. Therefore, it is shown that the formulated healing model corrects this behavior and allows one to get very close agreements between fatigue data and the fatigue damage predictions. This is clearly shown in one of the example simulations shown in figure F3c.1.

The current validation has considered various experimental tests that include creep-recovery, repeated creep-recovery, creep, and uniaxial constant strain rate tests at different temperatures, stress levels, and strain rates in both tension and compression. However, more tests are still

needed to fully validate the proposed model. This is critical at high temperatures specially for calibrating the viscoelastic-viscoplastic temperature coupling terms more accurately.

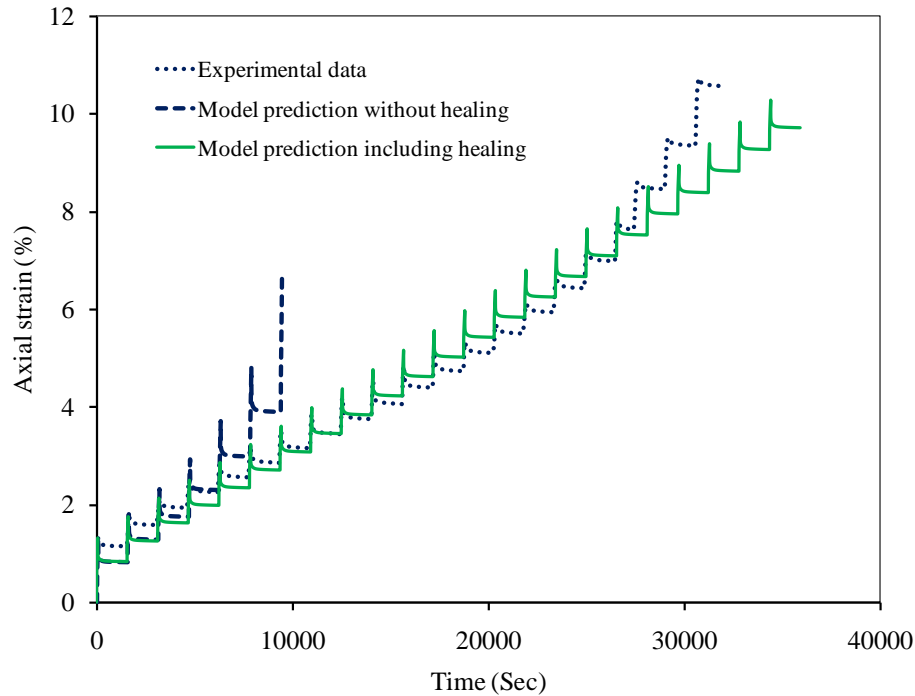


Figure F3c.1. Predictions of repeated creep-recovery experimental data in compression with loading time of 60 seconds and resting periods of 1500 seconds considering the damage model without healing and the damage model with healing.

### Significant Results

None

### Significant Problems, Issues and Potential Impact on Progress

Due to delay in getting the processed ALF tensile and compressive data, the validation of the unified continuum damage model based on the ALF experimental data has been delayed for the coming quarter.

### Work Planned Next Quarter

The next quarter work plan for the unified continuum damage model will focus initiating extensive calibration and validation of the coupled viscoelastic, viscoplastic, and viscodamage model based on the ALF data. Detailed description of the ALF data is available in the final report of project DTFH61.05.RA.00108, which was submitted by North Carolina State University to the Federal Highway Administration on May 2008.

## **Aging**

### Work Done This Quarter

In this quarter, initial steps have been taken for formulating a phenomenological aging model for asphaltic mixtures based on phenomenological aspects derived from experimental data and observations based on oxidation of asphalt binders. The aging model incorporates the effect of oxygen content, air voids, and damage evolution. The aging model is coupled to the developed unified continuum damage mechanics constitutive equations such that viscoelasticity, viscoplasticity, and damage evolution are strongly affected by aging.

### Significant Results

None

### Significant Problems, Issues and Potential Impact on Progress

None

### Work Planned Next Quarter

The focus in the coming quarter is on finalizing the form of the aging model and its implementation into PANDA. Moreover, the model will be initially validated and verified against existing experimental data from other FHWA projects.

## **Analysis of ALF Data**

### Work Done this Quarter

During the past quarter, we worked on the analysis of the ALF data provided by North Carolina State University. The analysis is according to the chart shown in figure F3c.2 and is based on the results of the following test results:

- 1 Dynamic Modulus Test (DMT) with no confinement to form the master curve using time-temperature superposition principle. This step will obtain the linear viscoelastic (LVE) properties (Prony series coefficients) and time-temperature shift factors ( $a_T$ ).
- 2 Repeated Creep Recovery Test (RCRT) with 140 kPa confinement at temperature 55 0C using the decoupling procedure to separate the recoverable and irrecoverable components. The irrecoverable component is analyzed to obtain the viscoplastic parameters.
- 3 Monotonic Test (MT) with 0 and 500 kPa confinements at low temperatures such as 5 and 25 0C to obtain the damage evolution.
- 4 Monotonic Test at high temperatures of 40 and 55 0C to verify the viscoelastic-viscoplastic-viscodamage model.

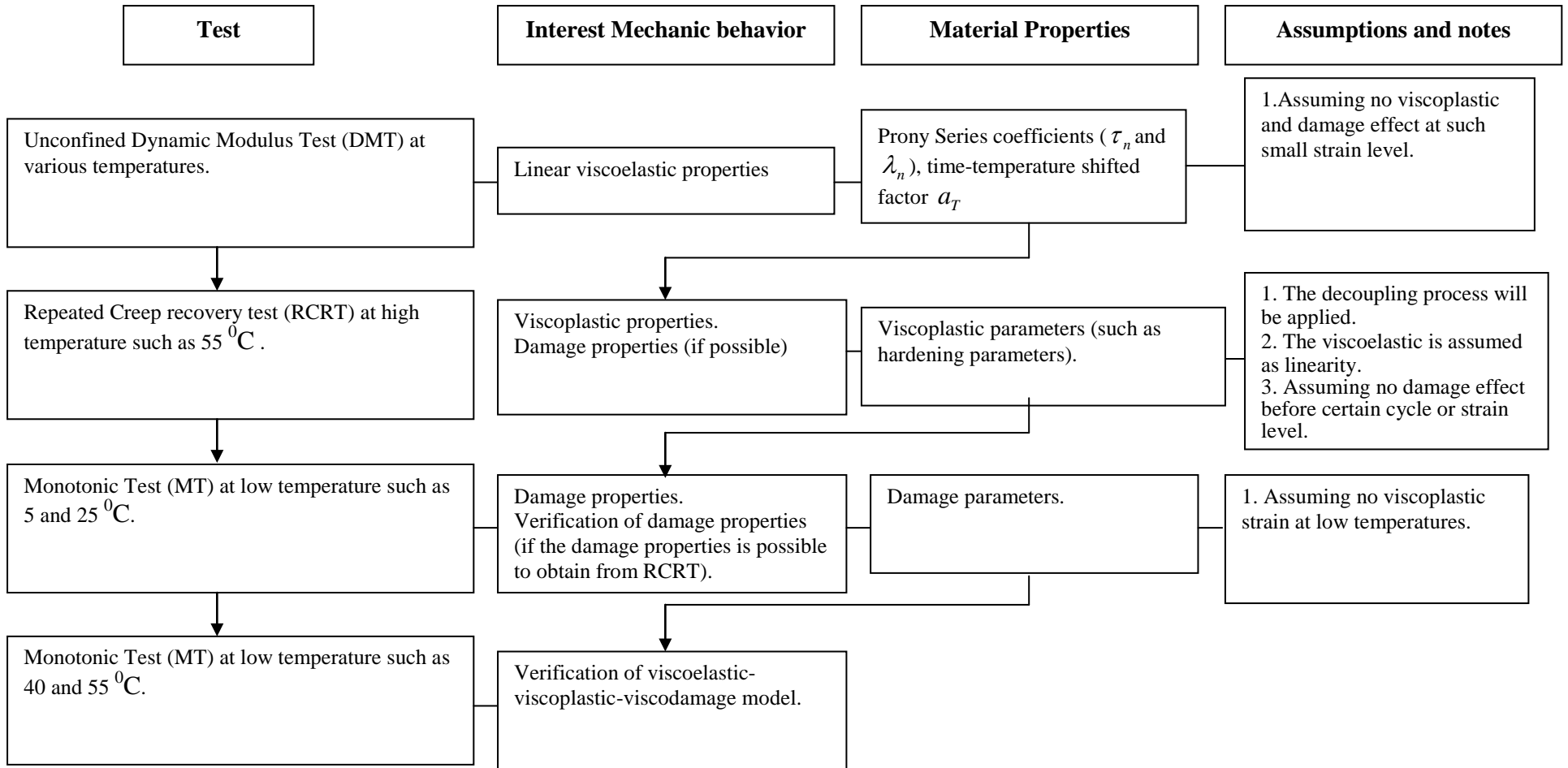


Figure F3c.2. The flow chart of the analysis procedure.

Significant Results

None

Significant Problems, Issues and Potential Impact on Progress

None

Work Planned Next Quarter

The analysis of the ALF data will be completed during the coming quarter and the PANDA model will be verified using the ALF comprehensive database.

**Work Element F3d: Calibration and Validation**

This work element is planned to start later in the project.

Fatigue Year 3		Year 3 (4/09-3/10)											
		4	5	6	7	8	9	10	11	12	1	2	3
<b>Material Properties</b>													
<b>F1a</b>	<b>Cohesive and Adhesive Properties</b>												
F1a-1	Critical review of literature												
F1a-2	Develop experiment design												
F1a-3	Thermodynamic work of adhesion and cohesion												
F1a-4	Mechanical work of adhesion and cohesion			JP			JP			D			F
F1a-5	Evaluate acid-base scale for surface energy calculations												
<b>F1b</b>	<b>Viscoelastic Properties</b>												
F1b-1	Separation of nonlinear viscoelastic deformation from fracture energy under cyclic loading												JP
F1b-2	Separation of nonlinear viscoelastic deformation from fracture energy under monotonic loading			P, JP									JP
<b>F1c</b>	<b>Aging</b>												
F1c-1	Critical review of binder oxidative aging and its impact on mixtures												
F1c-2	Develop experiment design		F										
F1c-3	Develop transport model for binder oxidation in pavements					P, JP	P						
F1c-4	Effect of binder aging on properties and performance					JP				D			F
F1c-5	Polymer modified asphalt materials												
<b>F1d</b>	<b>Healing</b>												
F1d-1	Critical review of literature												
F1d-2	Select materials with targeted properties												
F1d-3	Develop experiment design												
F1d-4	Test methods to determine properties relevant to healing												JP
F1d-5	Testing of materials												
F1d-6	Evaluate relationship between healing and endurance limit of asphalt binders			DP			JP			DP			
F1d-7	Coordinate with AFM analysis												
F1d-8	Coordinate form of healing parameter with micromechanics and continuum damage models												
<b>Test Methods</b>													
<b>F2a</b>	<b>Binder tests and effect of composition</b>												
F2a-1	Analyze Existing Fatigue Data on PMA												
F2a-2	Select Virgin Binders and Modifiers and Prepare Modified Binder												
F2a-3	Laboratory Aging Procedures												
F2a-4	Collect Fatigue Test Data							P					P
F2a-5	Analyze data and propose mechanisms									P			
<b>F2b</b>	<b>Mastic testing protocol</b>												
F2b-1	Develop specimen preparation procedures												
F2b-2	Document test and analysis procedures in AASHTO format												
<b>F2c</b>	<b>Mixture testing protocol</b>												
<b>F2d</b>	<b>Tomography and microstructural characterization</b>												
F2d-1	Micro scale physicochemical and morphological changes in asphalt binders							JP					
<b>F2e</b>	<b>Verify relationship between DSR binder fatigue tests and mixture fatigue performance</b>												
F2e-1	Evaluate Binder Fatigue Correlation to Mixture Fatigue Data												
F2e-2	Selection of Testing Protocols			DP						D			
F2e-3	Binder and Mixture Fatigue Testing												
F2e-4	Verification of Surrogate Fatigue Test												
F2e-5	Interpretation and Modeling of Data					JP					P		
F2e-6	Recommendations for Use in Unified Fatigue Damage Model												
<b>Models</b>													
<b>F3a</b>	<b>Asphalt microstructural model</b>												
<b>F3b</b>	<b>Micromechanics model</b>												
F3b-1	Model development												
F3b-2	Account for material microstructure and fundamental material properties												
<b>F3c</b>	<b>Develop unified continuum model</b>												
F3c-1	Analytical fatigue model for mixture design												
F3c-2	Unified continuum model			JP						JP			
F3c-3	Multi-scale modeling												

**LEGEND**

**Deliverable codes**

- D: Draft Report
- F: Final Report
- M&A: Model and algorithm
- SW: Software
- JP: Journal paper
- P: Presentation
- DP: Decision Point
- [x]

- Work planned
- Work completed
- Parallel topic

**Deliverable Description**

- Report delivered to FHWA for 3 week review period.
- Final report delivered in compliance with FHWA publication standards
- Mathematical model and sample code
- Executable software, code and user manual
- Paper submitted to conference or journal
- Presentation for symposium, conference or other
- Time to make a decision on two parallel paths as to which is most promising to follow through
- Indicates completion of deliverable x

Fatigue Year 2 - 5		Year 2 (4/08-3/09)				Year 3 (4/09-3/10)				Year 4 (04/10-03/11)				Year 5 (04/11-03/12)			
		Q1	Q2	Q3	Q4	Q1	Q2	Q3	Q4	Q1	Q2	Q3	Q4	Q1	Q2	Q3	Q4
<b>Material Properties</b>																	
<b>F1a</b>	<b>Cohesive and Adhesive Properties</b>																
F1a-1	Critical review of literature			JP													
F1a-2	Develop experiment design																
F1a-3	Thermodynamic work of adhesion and cohesion																
F1a-4	Mechanical work of adhesion and cohesion						JP			D	F						
F1a-5	Evaluate acid-base scale for surface energy calculations														JP		
<b>F1b</b>	<b>Viscoelastic Properties</b>																
F1b-1	Separation of nonlinear viscoelastic deformation from fracture energy under cyclic loading			D,JP	M&A				JP	M&A,F,	JP		P		JP,M&A,D		F
F1b-2	Separation of nonlinear viscoelastic deformation from fracture energy under monotonic loading			JP	M&A				JP				JP		JP,M&A,D		F
<b>F1c</b>	<b>Aging</b>																
F1c-1	Critical review of binder oxidative aging and its impact on mixtures																
F1c-2	Develop experiment design			D		F											
F1c-3	Develop transport model for binder oxidation in pavements		P		P, JP		2P,JP			JP	P		P, JP			D, M&A	F
F1c-4	Effect of binder aging on properties and performance				JP, P		JP	D	F	JP	P		P,JP		JP	D	F
F1c-5	Polymer modified asphalt materials										P					D	F
<b>F1d</b>	<b>Healing</b>																
F1d-1	Critical review of literature																
F1d-2	Select materials with targeted properties																
F1d-3	Develop experiment design																
F1d-4	Test methods to determine properties relevant to healing				JP				JP	D	F						
F1d-5	Testing of materials						JP			JP				M&A,D	JP, F		
F1d-6	Evaluate relationship between healing and endurance limit of asphalt binders	DP				DP	JP	DP			JP		P		JP	D	F
F1d-7	Coordinate with AFM analysis									JP							
F1d-8	Coordinate form of healing parameter with micromechanics and continuum damage models															JP,D	F
<b>Test Methods</b>																	
<b>F2a</b>	<b>Binder tests and effect of composition</b>																
F2a-1	Analyze Existing Fatigue Data on PMA		DP														
F2a-2	Select Virgin Binders and Modifiers and Prepare Modified Binder		DP														
F2a-3	Laboratory Aging Procedures																
F2a-4	Collect Fatigue Test Data		P		JP		P	P					JP, DP, F				
F2a-5	Analyze data and propose mechanisms				P		P					P			P	D	F
<b>F2b</b>	<b>Mastic testing protocol</b>																
F2b-1	Develop specimen preparation procedures		D								F						
F2b-2	Document test and analysis procedures in AASHTO format		D								F						
<b>F2c</b>	<b>Mixture testing protocol</b>		D, JP	F													
<b>F2d</b>	<b>Tomography and microstructural characterization</b>																
F2d-1	Micro scale physicochemical and morphological changes in asphalt binders						JP					JP					
<b>F2e</b>	<b>Verify relationship between DSR binder fatigue tests and mixture fatigue performance</b>																
F2e-1	Evaluate Binder Fatigue Correlation to Mixture Fatigue Data																
F2e-2	Selection of Testing Protocols					DP,D				D	F						
F2e-3	Binder and Mixture Fatigue Testing																
F2e-4	Verification of Surrogate Fatigue Test											D	F, DP				
F2e-5	Interpretation and Modeling of Data		JP		P		JP		P		JP		M&A				
F2e-6	Recommendations for Use in Unified Fatigue Damage Model											P				D	F
<b>Models</b>																	
<b>F3a</b>	<b>Asphalt microstructural model</b>							JP								M&A	F
<b>F3b</b>	<b>Micromechanics model</b>																
F3b-1	Model development				JP			JP		JP		P	D	DP	F, SW		
F3b-2	Account for material microstructure and fundamental material properties													D		F	
<b>F3c</b>	<b>Develop unified continuum model</b>																
F3c-1	Analytical fatigue model for mixture design														M&A,D		F
F3c-2	Unified continuum model				JP			JP			JP	M&A	D	DP	F, SW		
F3c-3	Multi-scale modeling									DP	DP,JP	JP	M&A	D		F	

**LEGEND**

**Deliverable codes**

- D: Draft Report
- F: Final Report
- M&A: Model and algorithm
- SW: Software
- JP: Journal paper
- P: Presentation
- DP: Decision Point
- [x]

- Work planned
- Work completed
- Parallel topic

**Deliverable Description**

- Report delivered to FHWA for 3 week review period.
- Final report delivered in compliance with FHWA publication standards
- Mathematical model and sample code
- Executable software, code and user manual
- Paper submitted to conference or journal
- Presentation for symposium, conference or other
- Time to make a decision on two parallel paths as to which is most promising to follow through
- Indicates completion of deliverable x



## PROGRAM AREA: ENGINEERED MATERIALS

### CATEGORY E1: MODELING

#### Work element E1a: Analytical and Micro-mechanics Models for Mechanical Behavior of Mixtures (TAMU)

##### Work Done This Quarter

Multiple technical presentations were made in international meetings in this quarter and are listed as follows:

1. Two presentations were made in the “DAWG” Forum on Pavement Performance Data Analysis sponsored by the Transportation Research Board Data Analysis Working Group (the “DAWG”) in Washington, D.C., January 2010. The titles of the presentations were:
  - a. “Viscoelastic Characterization of Aged Field Asphalt Mixtures Using Direct Tension Test”; and
  - b. “Anisotropic Viscoelastic Properties of Undamaged Asphalt Mixtures”.
2. A presentation was made in the International Society for Asphalt Pavements (ISAP) Technical Committee on Constitutive Modeling of Asphaltic Materials Annual Meeting held in Washington, D.C., January 2010. The presentation was entitled: “Viscoelastic Characterization of Aged Asphalt Field Cores”.
3. Three presentations were made in the Transportation Research Board (TRB) 89<sup>th</sup> Annual Meeting in Washington, D.C., January 2010. They were entitled:
  - a. “Viscoelastic and Fatigue Characterization of Asphalt Mixtures”;
  - b. “Characterization of Damage in Asphalt Mixtures Using Dissipated Pseudo Strain Energy”; and
  - c. “Characterization of the Tensile Viscoelastic Properties of an Undamaged Asphalt Mixture”.
4. Two presentations were made in the Fundamental Properties and Advanced Models Expert Task Group of the Federal Highway Administration (FHWA) in Irvine, California, February 2010. They were entitled:
  - a. “Characterization of Fatigue Properties of Asphalt Mixtures”; and
  - b. “Characterization of Engineered Properties of Asphalt Mixtures”.

All of the listed presentations summarized the characterization of properties of lab mixed lab compacted (LMLC) asphalt mixtures and field cores, which was developed in past quarters.

In this quarter, the characterization of asphalt mixtures was further investigated on both LMLC full mixtures and field cores. In addition, LMLC fine mixtures were fabricated in this quarter for future testing using the Dynamic Mechanical Analyzer (DMA). The progress on the characterization of LMLC full mixtures has been documented under Work Elements F1b-2, F1c-

4 and F2c. The efforts made on testing field cores and fabricating LMLC fine mixtures are detailed as follows.

The test protocol on field cores was improved in this quarter in order to obtain more accurate LVDT measurements. During the test, a monotonically increasing tensile load was applied to the prismatic specimen. The increasing rate of the tensile load was controlled at a constant rate, which was different from the previous testing protocol in which the increasing rate of the loading frame displacement was controlled at a constant rate. Using the improved test protocol, a smoother tensile load curve was obtained that led to a smoother tensile stress curve of the specimen.

When using the improved test protocol, significant oscillation was still found in the corresponding strain curves. In order to reduce the oscillation possibly due to the specimen position in the Material Testing System (MTS), the prismatic specimen was rotated around the loading frame by 90 and 180 degrees, respectively, to make a different specimen surface facing the window of the environmental chamber. At each specimen position, the same tensile load was applied to the specimen and the LVDT readings were recorded. No significant difference was identified when comparing the results of the three tests with different specimen positions. It was confirmed that the major reason of the oscillation in the strain curves was the stiffness gradient of the specimen with pavement depth.

The data analysis method was also improved to better analyze the test data of field core specimens. A macro was made in Excel to calculate the oscillation amplitude band width of each strain curve that was used to calculate the two model parameters  $k$  and  $n$  of the stiffness gradient model. Figure E1a.1 shows an output of the band width calculation. The values of  $k$  and  $n$  were found to be complex numbers with a small imaginary part. The improved data analysis method produced more reasonable values of  $k$  and  $n$  that resulted in a more accurate stiffness gradient function. Typical values of the magnitudes of  $k$  and  $n$  are: 2 and 3.5.

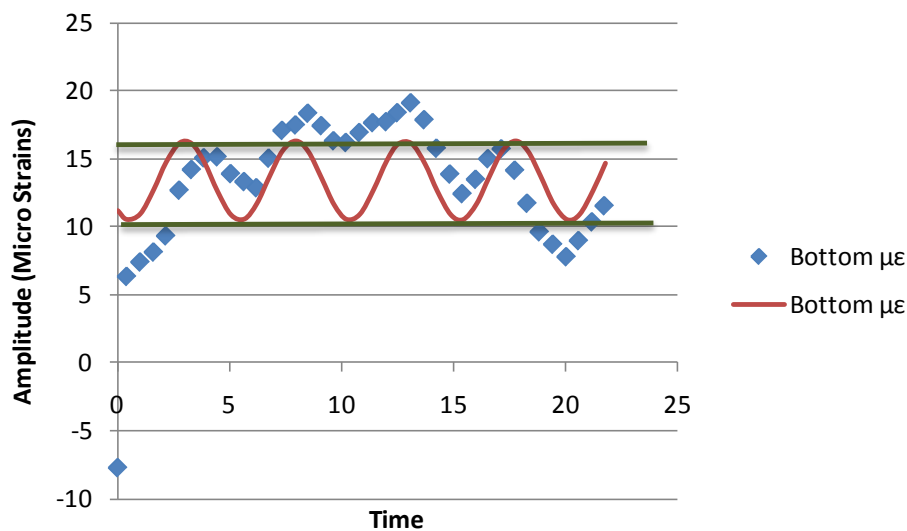


Figure E1a.1. Measured and modeled oscillation band widths of strain curve at bottom of construction lift.

In addition to the improvement on the testing of field core specimens, significant improvements were also made on the fabrication of LMLC fine mixtures. In order to accurately represent the composition and structure of the fine aggregates in the corresponding full mixture, a new method was developed to determine the asphalt content of a fine mixture with the assumption that the asphalt binder was proportionally distributed on the aggregate surface area. The aggregate surface area was calculated based on the sieve size with the assumption that the aggregate was perfectly spherical. The following equations were used to calculate the aggregate surface area (Radovski et al. 2003):

$$S_i = \pi D_i^2 \quad (\text{E1a.1})$$

$$m_i = v_i r_i = \frac{\pi}{6} D_i r_i \quad (\text{E1a.2})$$

$$CR_i = \frac{1}{2} \left( \frac{S_i}{m_i} + \frac{S_{i-1}}{m_{i-1}} \right) \quad (\text{E1a.3})$$

$$CR_i = \left( \frac{1}{r_i D_i} + \frac{1}{r_{i-1} D_{i-1}} \right) \quad (\text{E1a.4})$$

where  $CR_i$  = specific surface area of the particles with diameter in the range between  $D_i$  and  $D_{i-1}$ ;  $r_i$  = effective density of aggregate,  $\text{kg/m}^3$ ;  $S_i$  = surface of each spherical particle retained on the  $i^{\text{th}}$  sieve;  $v_i$  = volume of each spherical particle retained on the  $i^{\text{th}}$  sieve; and  $m_i$  = mass of each particle retained on the  $i^{\text{th}}$  sieve.

The assumption of perfectly spherical aggregate was calibrated using a shape factor  $K$ , which was obtained using the following equation:

$$V_i = KM \frac{4}{3} \pi \left[ \frac{1}{2} (D_i + D_{i-1}) \right]^3 = V_t \quad (\text{E1a.5})$$

in which  $V_i$  = measured volume of aggregate retained on the  $i^{\text{th}}$  sieve;  $M$  = number of aggregate particles retained on the  $i^{\text{th}}$  sieve; and  $K$  = shape factor. The obtained shape factor  $K$  was then used to calibrate the specific surface area  $CR_i$  as follows:

$$CR_i = K \left( \frac{1}{r_i D_i} + \frac{1}{r_{i-1} D_{i-1}} \right) \quad (\text{E1a.6})$$

The aggregates used for the fine mixtures were weighed in accordance with the design of the corresponding full mixture. Then the aggregates were sieved to obtain the retained weight for each sieve size according the gradation of the fine mixtures. The asphalt binder content was then determined based on the aggregate surface area.

The fine mixture was compacted as a specimen with a diameter of 6 in, which was cored into a number of samples with a diameter of 0.5 in and a height of 2 in. These samples were conditioned in vacuum desiccators at five levels of relative humidity: 0%, 25%, 50%, 75% and 100%, separately. The relative humidity in each vacuum desiccator was achieved by controlling the molality of salt in water in the closed desiccator based on the following model (Lang 1967):

$$\phi = \frac{\rho_w}{vmw} \ln \left( \frac{P}{P_0} \right) \quad (\text{E1a.7})$$

where  $\Phi$  = osmotic coefficient;  $v$  = number of ions from one molecule of salt,  $v = 2$  for NaCl and KCl;  $m$  = molality;  $w$  = molecular mass of water; and  $\rho_w$  = density of water. Lower levels of relative humidity (less than 90%) are achieved with different densities of sulfuric acid in the vacuum desiccators. The moisture conditioning of the fine mixture specimens will require two weeks in order to achieve equilibrium.

### Significant Results

Multiple technical presentations were made in international meetings. Significant improvements were made on the characterization of LMLC full mixtures and field cores. The testing protocol on LMLC full mixtures and field cores were improved to be more practical. The data analysis procedures were programmed in Matlab and Excel to automatically generate the material properties taking as input the raw test data produced by the MTS. The LMLC fine mixtures were fabricated. A new method was developed to determine the asphalt binder content in the fine mixture. Fine mixture specimens were conditioned in vacuum desiccators at a variety of levels of relative humidity.

### Significant Problems, Issues and Potential Impact on Progress

The newly purchased DMA has not arrived yet. The new DMA will be used to test the fine aggregate mixture specimens.

### Work Planned Next Quarter

More field core specimens are expected from Western Research Institute (WRI) with known binder properties with pavement depth. The field cores will be tested using the MTS nondestructively to determine the stiffness gradient of the specimens with the pavement depth. Then the overlay tester will be used to characterize the fatigue properties of field core specimens. The self-consistent micromechanics models will take as input the measured mixture and binder properties as well as the volumetric concentrations of binder, aggregate and air void to estimate the aggregate properties of the specimens with pavement depth.

### References

Lang, A.R.G., 1967, Osmotic Coefficient and Water Potentials of Sodium Chloride Solutions from 0 to 40°C. *Australian Journal of Chemistry*, 17 (2), 185-194.

Radovski. B., 2003, Analytical Formulas for Film Thickness in Compacted Asphalt Mixture. *Transportation Research Record*. 1829, Transportation Research Board, National Research Council, Washington, D.C., 26-32.

## **Work element E1b: Binder Damage Resistance Characterization (DRC) (UWM)**

### ***Subtask E1b-1: Rutting of Asphalt Binders***

#### Work Done This Quarter

Work completed this quarter included trial blends of one neat binder with two modifiers to determine affect of percentage of modifier on PG. Two trial blends of the elastomeric and plastomeric modifiers—as well as the elastomeric combined with a cross-linking agent—were produced and the true grade was determined. The relationship of the two blends for each combination allows for the determination of percent modifier required to achieve the target PG grade. The targeted grades include two grade bumps  $+0.5\text{ }^{\circ}\text{C}$  ( $\pm 0.5\text{ }^{\circ}\text{C}$ ) for each neat binder. This allows for comparison of the binders based on traditional selection criteria of PG.

A further review of literature showed mixed results for Repeated Creep and Recovery (RCR) testing of asphalt binders. The distinction in behavior appears to be due to selected stress level. Since this task incorporates multiple stress levels into the RCR testing of binders and mastics, it has been determined that the commonly accepted 100-cycle test will be extended to 1000 cycles for early testing to determine if behavior is accurately represented by the first cycle beyond 100 cycles.

Mix design had significant variability and it was determined that additional contributing factors could be eliminated. For this reason, the coarse and fine gradations used will target the control points of a 19.5-mm nominal maximum aggregate size (NMAS) mix as described by the Wisconsin DOT. These same gradations will be used for each aggregate source regardless of natural gradation.

#### Significant Results

The significant results pertaining to percent modifier are shown in table E1b-1.1.

Table E1b-1.1. Calculation of percent modifier required to achieve target PG.

	Elastomer + Cross-Linking Agent			Elastomer			Plastomer		
	% modifier	True Grade		% modifier	True Grade		% modifier	True Grade	
Un- aged	0	67.03		0	67.03		0	67.03	
	2	74.05		2	72.43		2	73.76	
	4	83.76		4	77.7		3.5	79.79	
	<b>2.37</b>	<b>76.5</b>		<b>3.54</b>	<b>76.5</b>		<b>2.65</b>	<b>76.5</b>	<b>TARGET</b>
RTFO	0	67.65		0	67.65		0	67.65	
	2	73.36		2	71		2	72.62	
	4	79.94		4	79.73		3.5	80.89	
	<b>2.93</b>	<b>76.5</b>		<b>3.23</b>	<b>76.5</b>		<b>2.58</b>	<b>76.5</b>	<b>TARGET</b>

RTFO = rolling thin film oven.

The coarse and fine gradations and targeting control points to be used for each aggregate source are shown in figure E1b-1.1.

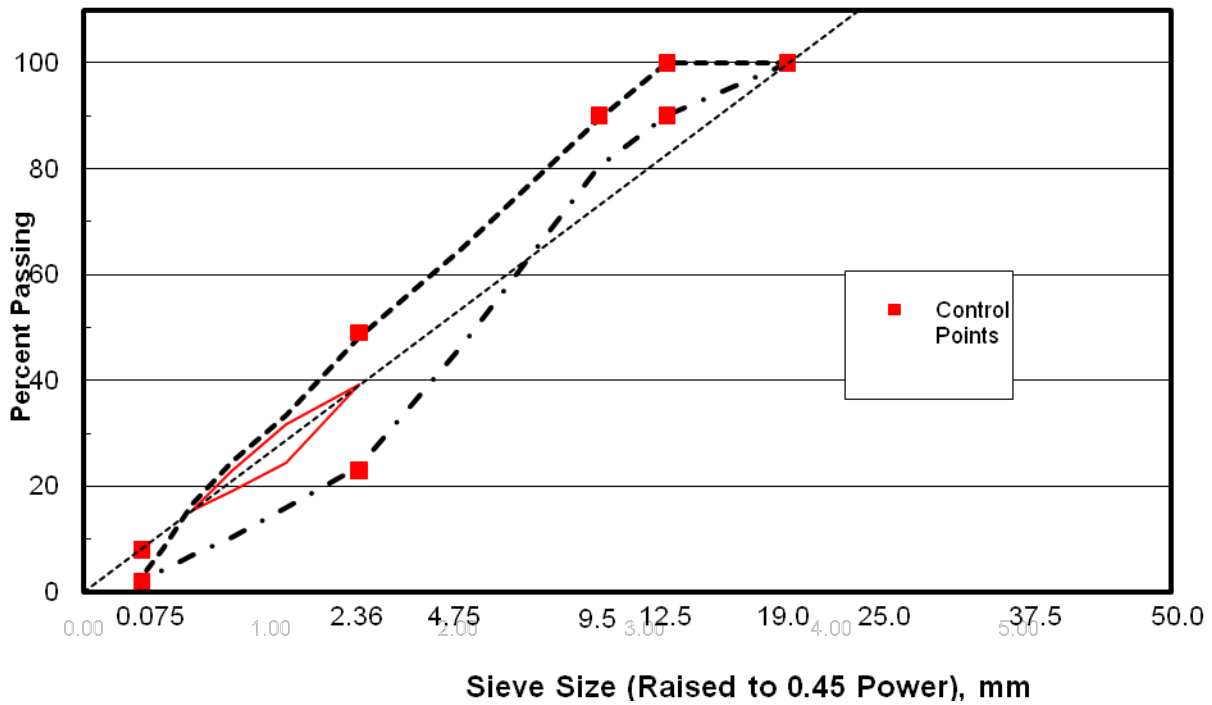


Figure E1b-1.1. Graph. Fine and coarse gradations to be used for mixtures.

The fine and coarse gradations include equivalent amounts of P200 material (material passing No. 200 sieve), which corresponds to the dust-to-binder ratio (DTBR) of the mastics.

Significant Problems, Issues and Potential Impact on Progress

Washing of aggregate stock to ensure control of P200 material takes additional time prior to batching of material. This washing process has added time to the mixture preparation process and not allowed mixing and compacting of this material to commence. This is not a significant problem and is not expected to significantly alter the schedule of this task.

Work Planned Next Quarter

The determined percentage of modifiers will be blended and tested to confirm PG of the material. If material meets the targeted grade  $\pm 0.5$  °C, RCR to 1000 cycles will begin at the intermediate temperature and results will be used to verify if additional cycles are required. Multiple Stress Creep and Recovery (MSCR) of the modified binder will also commence at this time. All testing of binder and mastic is intended to be run on RTFO-aged material to better represent the mixing and compacting processes of mixture preparation. Mixtures of the neat binder at the coarse and fine gradations for two aggregate sources will be produced and tested for performance at the high and low stress levels of flow number (FN) testing. Tables E1b-1.2, E1b-1.3 and E1b-1.4 summarize the testing plan for the next quarter.

Table E1b-1.2. Binder testing matrix.

Binder	Temperature (°C)	MSCR*	RCR (stress in Pa)		
			100	3200	10000
FH Neat PG 64	70				
	58				
	46				

Table E1b-1.3. Mastic testing matrix.

Binder	Filler	Temperature (°C)	MSCR*	RCR (stress in Pa)		
				100	3200	10000
FH Neat PG 64	G	70				
		58				
		46				
	LS	70				
		58				
		46				

Table E1b-1.4. Mixture testing matrix.

Materials			Tests	
Binder	Aggregate	Gradation	FN (stresses in psi)	
			50	150
FH Neat PG 64	LS	F		
		C		
	G	F		
		C		

***Subtask E1b-2: Feasibility of Determining Rheological and Fracture Properties of Thin Films of Asphalt Binders and Mastics using Simple Indentation Tests***

Work Done This Quarter

The research team continued testing according to the experimental plan developed last quarter. Table E1b-2.1 shows the experimental plan with the list of tests completed thus far. As an example, figure E1b-2.1 shows the indentation results obtained for NuStar binder modified with 4 CBE (plastomer modification) at 20 °C.

Table E1b-2.1. Tests completed in the experimental plan.

Binder Name	Modification	Temperature	Sample Height		
			5.1 cm	3.4 cm	1.7 cm
FH 64-22	Neat	20 °C	X	X	X
		30 °C	X	X	X
	SBS-Modified	20 °C			
		30 °C	X	X	X
	CBE-Modified	20 °C	X	X	X
		30 °C	X	X	X
NuStar 64-22	Neat	20 °C	X	X	X
		30 °C	X	X	X
	SBS-Modified	20 °C	X	X	X
		30 °C	X	X	X
	CBE-Modified	20 °C	X	X	X
		30 °C	X	X	X

SBS = styrene-butadiene-styrene.

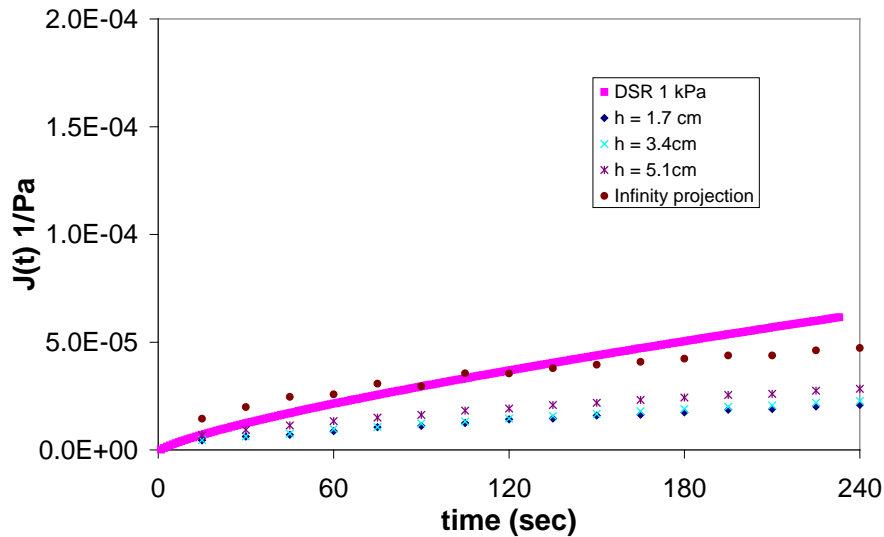


Figure E1b-2.1. Graph. Creep compliance obtained for NuStar 4 CBE at 20 °C. ( $J(t)$  = creep compliance; DSR = Dynamic Shear Rheometer;  $h$  = depth of binder in testing container.)

Also in this quarter, the research team developed the load-controlled indentation finite element (FE) model in Abaqus. The load-controlled indentation model is capable of simulating the experimental conditions of the indentation test. To simulate the dead weight of the indenter in the actual experiment, a static load is applied on the centroid of the simulated indenter. The indenter is modeled as a rigid analytical surface and the sample is meshed using linear Q4 elements.

The size effects observed in the experiment were simulated using finite element modeling (FEM). The two sizes used in the analysis are shown in figures E1b-2.2 and E1b-2.3. Note that the displacement of the indenter follows the same trend as that observed in the experiments.

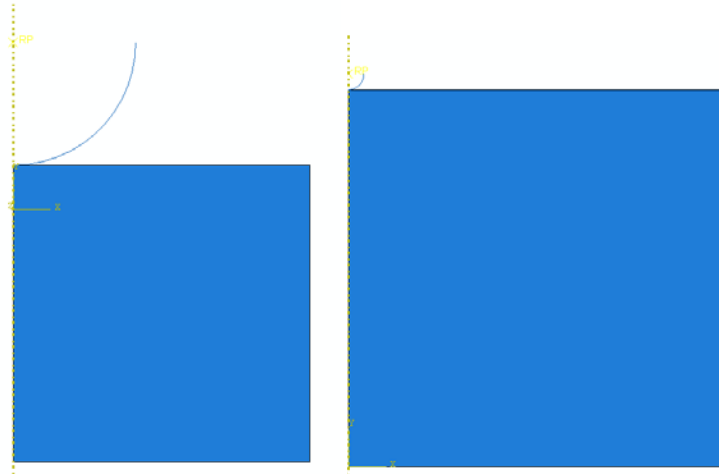


Figure E1b-2.2. Illustration. Different sample sizes (smaller and bigger size, respectively) used in FEM simulation.

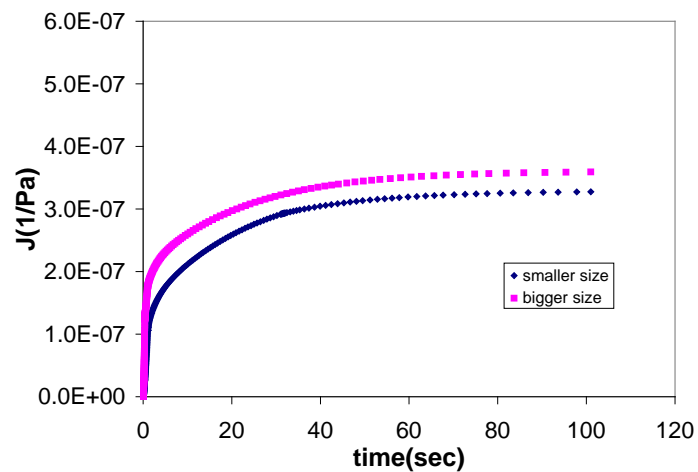


Figure E1b-2.3. Graph. Displacement versus time for different samples sizes obtained from FEM.

The load is applied instantaneously in the experiment. However, in the FEM the load cannot be applied instantaneously in order to avoid singularities and convergence problems. Therefore, the load is applied with an initial ramp (Step 1) and then maintained constant (Step 2). Preliminary FE simulations indicated that the initial ramp seems to have a significant effect on the observed displacement, as shown in figure E1b-2.4. It is observed that the steeper the ramp and closer the simulation gets to experimental setup, the material becomes stiffer. The two cases shown are: Case I, where the ramp is for 1 second; and Case II, where the ramp is for 0.1 second. After the ramp, the load is applied and kept constant for 100 seconds.

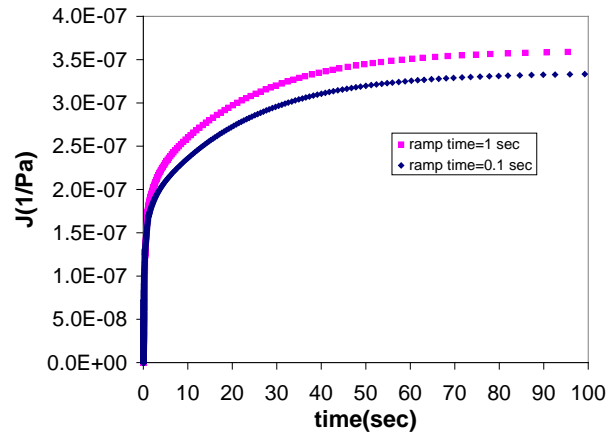


Figure E1b-2.4. Graph. Effect of loading rate on the creep compliance obtained from Abaqus.

Note that the ramping time is very significant and that the appropriate ramping condition needs to be chosen to minimize its effect. Such an effect is dependent on the material in consideration. The research team is investigating this issue.

#### Significant Results

The research team made significant advances in modeling the indentation test using finite elements. The model for load-controlled indentation has been developed. The effect of sample sizes and ramping time were also identified in the numerical simulations and are currently being investigated.

#### Significant Problems, Issues and Potential Impact on Progress

None.

#### Work Planned Next Quarter

In the next quarter the research team plans to focus on the following tasks:

- Finalize the testing matrix for indentation test and complete the Dynamic Shear Rheometer (DSR) creep compliance tests to be used for validation purposes.
- Study the effects of loading ramp and fix the appropriate loading rate.
- Define the appropriate element type and mesh density for the FE model to be used to build the database.
- Build a database of FE simulations of indentation tests of materials with a wide variety of mechanical properties. This database can be used to backcalculate the creep compliance of binders from displacements measured in the proposed indentation test.

## **Work Element E1c: Warm and Cold Mixes**

### ***Subtask E1c-1: Warm Mixes***

#### Work Done This Quarter

Efforts this quarter focused on further development of the asphalt lubricity test, evaluation of the use of a laboratory foaming device for warm mix asphalt (WMA) mix design (NCHRP 9-43 procedure), and synthesis of the data collected for the Manitoba Infrastructure and Transportation (MIT) field project. Further development of the asphalt lubricity test was needed to allow for evaluation of different asphalt binders and warm mix additives at higher temperatures.

Based on results published in the ARC Q4 2009 report, measurement of coefficient of friction is required at higher temperatures to capture the three lubrication regimes: boundary lubrication, mixed lubrication and hydrodynamic friction. The test method previously developed was only able to capture the regime of hydrodynamic friction. Under these conditions, increases in friction coefficient are due to viscous drag from increasing viscosity, increasing speed, decreasing normal force, or a combination of these factors. The research team felt that this behavior does not fully correspond to field conditions, thus the need to consider higher testing temperatures in the new lubricity procedure. Previously measured results were also compared to coefficient of friction values measured by a commercially available tribology cell.

Two mix designs were provided by the NCHRP 9-43 project team to evaluate the use of a laboratory foaming device according to the mix design procedure provided in the NCHRP 9-43 Interim Report (Bonaquist 2008). Both mix designs had a nominal maximum aggregate size (NMAS) of 9.5 with one containing 30% recycled asphalt pavement (RAP). Field mixing and compaction temperatures were reported as 121 °C/110 °C for the 100% virgin aggregate mix and 135 °C/127 °C for the 30% RAP mix. (These temperatures were used during the laboratory mix production and compaction.) Mix design verification consisted of determination of the optimum asphalt content, verification of the estimated asphalt content, and evaluation of mixture workability/aggregate coating. Performance testing samples for flow number and moisture damage testing were also prepared. Work was completed this quarter and samples were shipped to the NCHRP 9-43 project team for testing, and a report summarizing the mixture production and compaction results was submitted to the NCHRP 9-43 project team for review.

A portion of the binder testing and analysis of aggregate coating and mixture workability results for the surface course mix for the MIT field project's Bituminous B (Bit B) was completed. Results were presented at the ARC/MIT Warm Mix Workshop held March 3 in Winnipeg, Manitoba, Canada. A detailed report summarizing the Bit B results will be submitted to MIT before construction of the Bit B surface course commences. The contractor experienced delays last construction season that resulted in approximately 30% of the binder course being placed before the project was closed for the winter. Therefore, submittal of this report will be coordinated with the construction schedule for this season.

## Significant Results

### *Asphalt Binder Workability (Lubricity Testing)*

The research team focused on developing a new procedure to allow lubricity testing to be conducted at higher temperatures, with an upper limit of 150 °C. Limitations of the heating system in the Anton Paar Dynamic Shear Rheometer (DSR) previously used necessitated the manufacturing of a new testing fixture sized to fit in the TA Instruments DSR, which has an oven-heating system that allows for testing at higher temperatures. The new apparatus follows the previously presented “four-ball” testing concept and the dimensions of the balls (12.5 mm) used to conduct the test, except that the dimensions of the cup used were reduced to fit into the TA Instruments DSR. Initial evaluation of the new apparatus was conducted under the following experimental conditions:

- Temperature (°C): 90, 105, 120, 135 and 150.
- Normal force (N): 10, 20 and 30.
- Speed (rpm): 1, 5, 10 and 20.

Combinations of speed and normal force were selected based on testing temperature. Each speed for a given set of conditions was held constant for 3 minutes to assess the repeatability of the coefficient of friction measurements, which was calculated using the torque measured by the machine. Four replicates of the PG 76-22 binder were tested with data collected at a high sampling rate. An example of the results is presented in figure E1c-1.1.

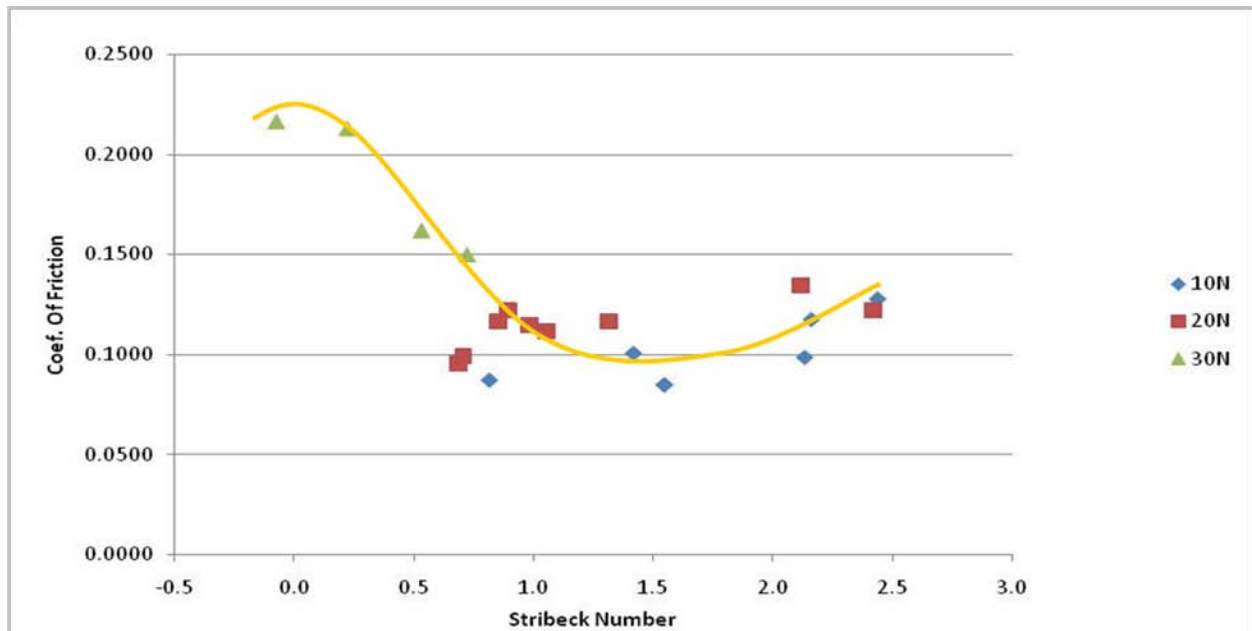


Figure E1c-1.1. Graph. Results of lubricity testing at higher temperatures demonstrating the three lubrication regimes.

In general, results demonstrated the expected behavior in terms of capturing values of the coefficient of friction in all three lubrication regimes. However, the repeatability of these values measured for a given set of conditions and between replicates has thus far been unacceptable. The coefficient of variation (COV) for the coefficient of friction measured at a given temperature, speed and normal force averaged 20%. It is believed that this variability is due to inadequate control of normal force and erratic measurement of torque by the TA Instruments rheometer.

The research team had the opportunity to conduct testing on a commercially available tribology cell using a new Anton Paar DSR. A PG 76-22 styrene-butadiene-styrene (SBS)-modified binder with the WMA additives Revix and Rediset was used to evaluate the ability of the fixture to detect the effect of WMA additives on lubricity. Results for a constant speed (20 rpm), three temperatures (90 °C, 120 °C and 150 °C), and differing levels of normal force are presented in figure E1c-1.2. To construct figure E1c-1.2, the viscosity at a given testing temperature, testing speed and normal force were used to calculate the Stribeck number, a commonly used index in the evaluation of lubricating fluids. The equation for the Stribeck number is provided below:

$$\text{Stribeck number} = \log (R \cdot \eta / P) \tag{E1c-1.1}$$

where R is the speed,  $\eta$  is the viscosity, and P is the normal force.

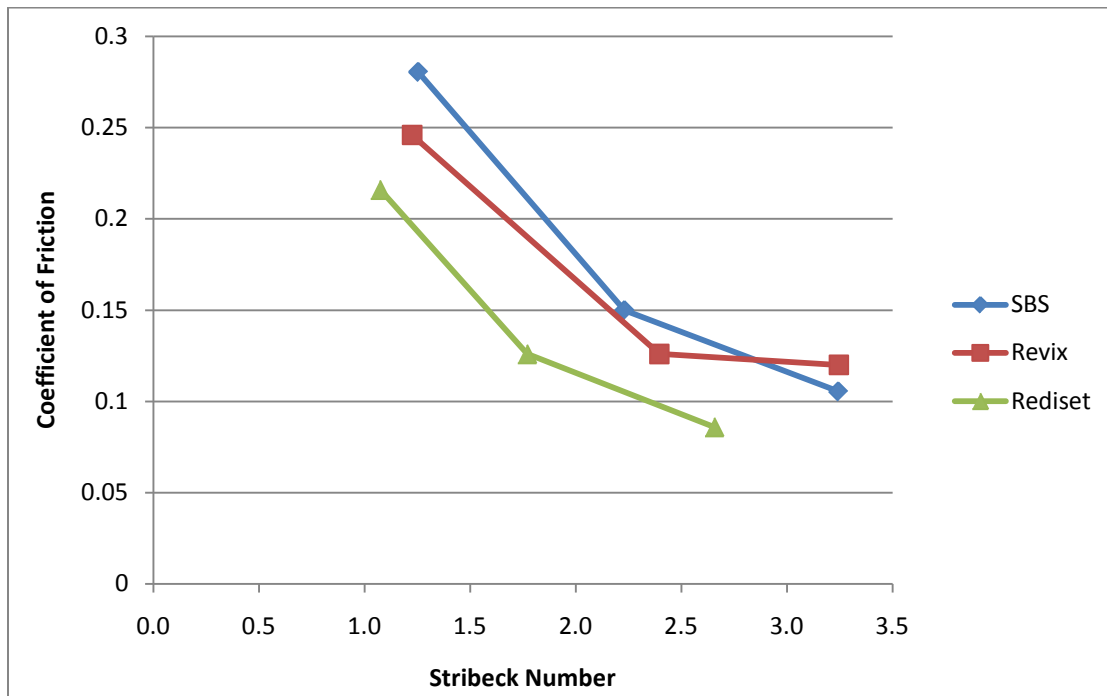


Figure E1c-1.2. Graph. Coefficient of friction versus Stribeck number measured using a commercially available tribology cell.

Results presented in figure E1c-1.2 indicate the lubricating effects of WMA additives, especially at lower values of the Stribeck number, which correspond to higher temperatures and levels of normal force. Under these conditions there is a very thin binder film between the rotating chuck and clamped balls.

The manufacturer testing protocol recommends that speed be logarithmically increased at a constant normal force and temperature to develop the Stribeck curve for a given lubricant. For testing conducted on the conventional and WMA-modified binders, the speed sweep was implemented at different temperatures and normal forces. Pooled standard deviations between the two replicates for each material ranged from 0.03 to 0.04, which relates to COVs between 17% to 30%. Test results were used to construct full Stribeck curves; however, the expected relationship was not achieved.

The source of variability was investigated by testing at a constant speed rather than the incremental speed recommended in the DSR manufacturer procedure. Results indicate that repeatable values of coefficient of friction can be obtained using this geometry, with a pooled standard deviation of 0.01. However, approximately 50 data points are needed for the measurement to stabilize, indicating that a more accurate value of coefficient of friction could be obtained using the average of measurements taken at a constant speed for 2 to 3 minutes rather than the single measurement provided by the incremental speed increase. It is hypothesized that the speed sweep procedure is inappropriate for asphalt because, unlike conventional lubricating oils, there is a viscous component to the behavior of asphalt binders that requires an equilibration time before consistent values are observed.

Results from the commercially available tribology cell were compared to previous measurements taken using the four-ball geometry developed for use in the Anton Paar DSR. A common data set was available for the SBS-modified PG 76-22 and the PG 76-22 with the WMA additive Revix. Testing conditions included one temperature (90 °C), two normal forces (10N and 20N), and four speeds (5, 20, 50 and 75 rpm), giving a total of 16 points for comparison. Use of the Stribeck number allowed for the effect of these different conditions on coefficient of friction to be evaluated using one curve. Results of the comparison are provided in figure E1c-1.3.

Preliminary results presented in figure E1c-1.3 indicate that at higher Stribeck numbers there is a significant difference in the coefficient of friction values measured by the two testing devices. In terms of the testing conditions, high Stribeck numbers are found at lower testing temperatures or normal forces and relate to behavior in the hydrodynamic lubrication regime. In this regime, the coefficient of friction increases with increasing Stribeck number due to viscous drag. This effect is observed for the original testing device (“Cup”), but not in the Tribocell. At this time the cause of this discrepancy is unclear. However, it may be related to the inadequacy of the speed sweep in measuring coefficient of friction for asphalt binders. The data collected using the original testing device represents the average coefficient of friction after a testing time of 2 minutes at a given set of conditions. As a result, these values are more reliable and also relate well with the expected relationships between coefficient of friction and temperature, speed and normal force.

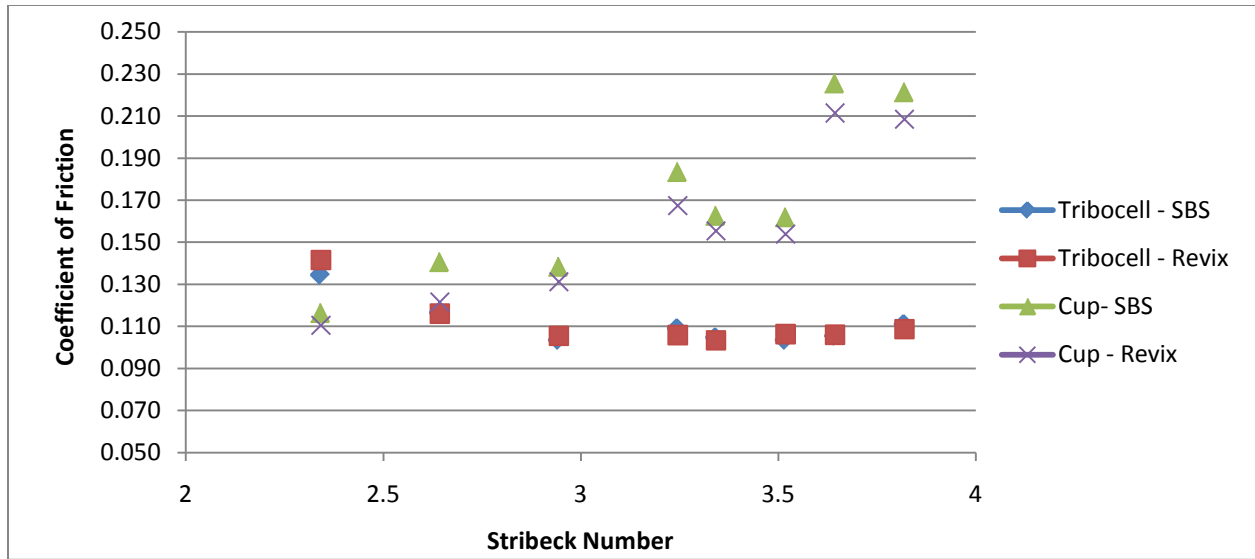


Figure E1c-1.3. Graph. Comparison of coefficient of friction results measured using two testing devices. (Tribocell = commercially available geometry; Cup = original prototype testing device.)

#### *Laboratory Mix Design for Foamed Asphalt*

The use of the laboratory foaming machine to conduct a mix design following the NCHRP 9-43 protocol revealed additional issues for a foamed mix design related to both the operation of the machine and performance of the mix. The intended application of the machine is to produce foamed asphalt designs of asphalt stabilized base course and cold in-place recycling. Both of these activities use approximately 10% to 15% water by weight of the binder; conversely, foaming for WMA only requires 1% to 3%. To accommodate these differences, a more precise flow controller must be used to add a consistent amount of water to the asphalt before foaming. Also, aggregate weights of >3,000 must be used because the flow controller that meters the asphalt into the mixing bucket is not of adequate sensitivity to provide an accurate quantity of asphalt below this weight. From a technical standpoint, the consistency of the foamed asphalt between separate runs of the machine has come into question. For both mix designs, the samples compacted at the optimum asphalt content determined from the trial blends did not meet Superpave volumetric criteria. It is believed that these differences were due to inconsistency of the foamed asphalt produced between two different days of production; however, further investigation is needed.

#### *MIT Field Project*

The work presented for the MIT field project included binder testing and evaluation of aggregate coating and mixture workability for both the binder and surface courses. Data for the binder course—Bituminous C (Bit C)—was presented in the ARC Q4 2009 report. Results of binder testing showed no effect of Evotherm or Advera on the high-temperature properties with true grades of 59.3 °C. As expected, Sasobit caused an increase in high-temperature performance, exhibiting a true grade 62.9 °C. Adhesion testing was also conducted on a limestone substrate on

both dry and moisture-conditioned samples. Moisture-conditioned samples were submerged in a water bath for 24 hours at 40 °C. The Evotherm and Advera WMA additives showed a marginal improvement in performance, increasing the ratio of wet to dry adhesive strength from 0.6, an increase of 0.1 relative to the base binder. Conversely, the Sasobit caused a slight decrease in the adhesive strength ratio, with a value of 0.4. It should be noted that the aggregate substrate used is a limestone from Wisconsin that is known to be moisture-sensitive. Moisture damage testing on mixtures is needed to evaluate the significance of the adhesion testing results.

Aggregate coating conducted at 125 °C and 150 °C for the Bit B mix design and all WMA additives were all above 95%. In terms of mixture workability, no difference in the parameter N92 (number of gyrations to 92%  $G_{mm}$ ) was observed until a compaction temperature of 90 °C. At 90 °C, the N92 value of the HMA and WMA Advera mixes was 15 gyrations, whereas for the mixes prepared using Sasobit and Evotherm, N92 values were 22 and 23, respectively. The NCHRP 9-43 mixture workability criteria requires that  $N92 < 0.35 N_{design}$ . Based on the design traffic, the design gyration level was defined as 100 gyrations for the Bit B mix. Relative to the NCHRP 9-43 protocol, it is clear that all these mixes are workable across all temperatures; therefore, the differences observed between the HMA and WMA additives are not significant.

#### Significant Problems, Issues and Potential Impact on Progress

The only problem impacting progress is the development of a lubricity testing procedure for high temperatures. To date the research team has been unable to consistently measure reliable coefficient of friction values for a given set of testing conditions. It is believed that this is due to limitations of the DSRs used. The procedure will be improved and a limited set of materials tested in early April 2010 to allow the research team to decide if pursuit of high-temperature lubricity test using this machine should continue.

University of Wisconsin–Madison recently purchased a new DSR that allows for measurements at higher testing temperatures. The fixture initially used routinely provided reliable coefficient of friction values for a given set of conditions, and repeatability between replicates at lower testing temperatures was very good. The original fixture and testing procedure will be used to test at higher temperatures, allowing the research team to make up for the delays experienced in developing this test.

#### Work Planned Next Quarter

Development of the lubricity test for higher temperatures will continue. It is anticipated that a procedure will be finalized by the end of April 2010, with full testing beginning in May 2010. As discussed in the Year 4 work plan, lubricity testing will be conducted on both neat and modified asphalts with a variety of WMA additives. The research team will also explore the possibility of evaluating lubricity on rolling thin film oven (RTFO)-aged materials. Viscosity at different temperatures and shear rates will also be conducted. Test results will be compared to mixture workability results. The objective of these efforts will be to determine the relative contribution of lubricity and viscosity to mixture workability and how the relationship changes for different WMA additive types.

Work in the next quarter will also focus on methods of moisture damage evaluation. The adhesive/cohesive properties of the bond between the asphalt and aggregate will be investigated using the Bitumen Bond Strength (BBS) test. Different moisture conditioning methods will be investigated to replicate the mechanism for diffusion of moisture into the asphalt aggregate system realized in the field. In the field it is believed that the moisture damage occurs due to remaining moisture in the aggregate. The BBS test will also allow for investigation of the effects of WMA additives on the adhesive properties of binders. The relevance of the BBS test for this application will be evaluated through comparison to mixture testing results. The research team plans to conduct mixture testing per AASHTO T283 specifications.

The Wisconsin DOT has approved a pilot program for construction of WMA projects. WisDOT has approved a work plan submitted by the research team to evaluate the WMA projects in terms of emissions/energy consumption, laboratory performance, and field measurements of density. The research will be led by Dr. Robert Schmitt of University of Wisconsin–Platteville. It is anticipated that six projects will be constructed throughout Wisconsin. Industry in Wisconsin uses three WMA additives/methods: Revix, Advera, and foaming by injection of water and air during production. Each project will include both HMA and WMA using one additive. The research team hopes to collect field data from two projects for each additive. The research team will present the work plan at the WisDOT Tech Team meeting at the end of April 2010. At this time it is unknown when or where these projects will be constructed.

#### Cited References

Bonaquist, R., October 31, 2008, NCHRP 9-43: Mix Design Practices for Warm Mix Asphalt. Interim Report, National Research Council, Washington D.C.

#### ***Subtask E1c-2: Improvement of Emulsions' Characterization and Mixture Design for Cold Bitumen Applications***

#### Work Done This Quarter

Efforts this quarter focused on conducting Bitumen Bond Strength (BBS) testing. Five emulsified binders were tested at four curing intervals on three substrate types. Table E1c-2.1 shows the experimental testing matrix. The pullout tensile strength is recorded while the pullout rate and other experimental parameters are controlled at constant levels. Substrate types are comprised of three surfaces:

- Aggregate level, which refers to a solid rock plate that has been cut and lapped to achieve a smooth, uniform surface. Prior investigations reported under this work element have utilized this substrate type.
- Chips level, which refers to substrates prepared using a combination of aggregate chips and a quick-setting cement paste. This alternative substrate was chosen for potential reproducibility in field applications.
- Glass level, which refers to a smooth glass plate, is used as a control because it allows full adhesion and forces a cohesive failure mode.

As shown in table E1c-2.1 below, emulsion types are differentiated by type, with the CRS-2 types further differentiated by location of sampling. *CRS-2 (lab)* refers to an emulsion prepared at the suppliers' laboratory mill, while *CRS-2 (field)* refers to samples collected from a field site.

Table E1c-2.1. Experimental matrix for the emulsion bond strength experiment.

<b>Experimental Factors</b>	<b>Levels</b>
Substrate Type	Aggregate
	Chips
	Glass
Emulsion Type	CRS-2 (lab)
	CRS-2 (field)
	CRS-2P
	HFRS-2
	HFRS-2P
Curing Interval (hours)	2
	6
	24
	48

Efforts this quarter also focused on collaborating with a second lab to establish a bias and repeatability statement in an effort to standardize the BBS test protocol. The partnering lab, located at the University of Stellenbosch in South Africa, tested two hot binders that were also tested at the University of Wisconsin–Madison. Hot binders were chosen for this calibration experiment due to extended storage stability and transportability compared to emulsions. Table E1c-2.2 shows the experimental testing matrix for the calibration experiment.

Table E1c-2.2. Experimental matrix for the calibration experiment.

<b>Experimental Factors</b>	<b>Levels</b>
Laboratory	Univ. of Stellenbosch, South Africa
	UW–Madison
Binder Type	PG 64-28
	PG 58-28

### Significant Results

Results for the emulsion bond strength experiment are shown in figures E1c-2.1 and E1c-2.2. These figures show the effect of substrate and emulsion type on the pullout tension response over extended curing intervals. Figure E1c-2.1 demonstrates that the solid aggregate plates perform better than both the chip and glass substrates. While a statistically significant difference is not observed between the chips and glass, a significant difference is observed for both chip and glass substrates and the aggregate substrate. Based on results from previous quarterly reports, a power

fit is observed to adequately model the relationship between curing interval and pullout tension, with  $R^2 > 0.98$  for the entire data set.

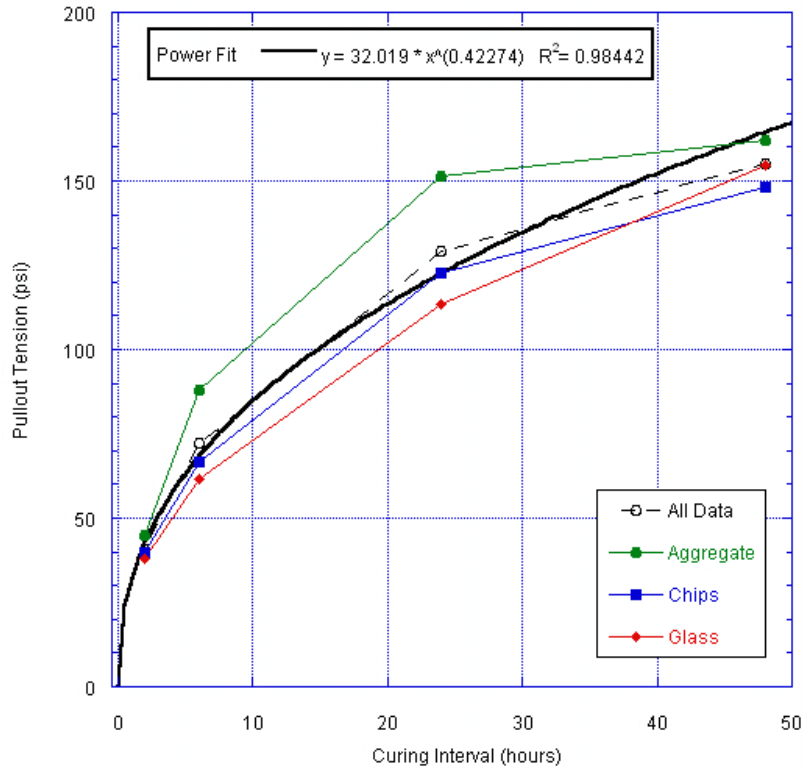


Figure E1c-2.1. Graph. Substrate types are differentiated by bond strength development.

Figure E1c-2.2 compares the pullout tension of different emulsion types over extended curing intervals. Both CRS-2-type emulsions perform better than CRS-2P- and HFRS-2-type emulsions. The HFRS-2P-type emulsion is observed to perform the worst. All emulsion types are observed to exhibit sharp increases in pullout tension initially, with relative gains in tensile strength diminishing over time. These results suggest that the BBS test protocol can be used to effectively evaluate bond strength of different emulsion and substrate types. Again, a power fit is observed to adequately model the data set. These results also indicate that the test protocol is able to rank different emulsion types in terms of bond strength, which may lead to the eventual inclusion of the test protocol in surface treatment specifications currently under development.

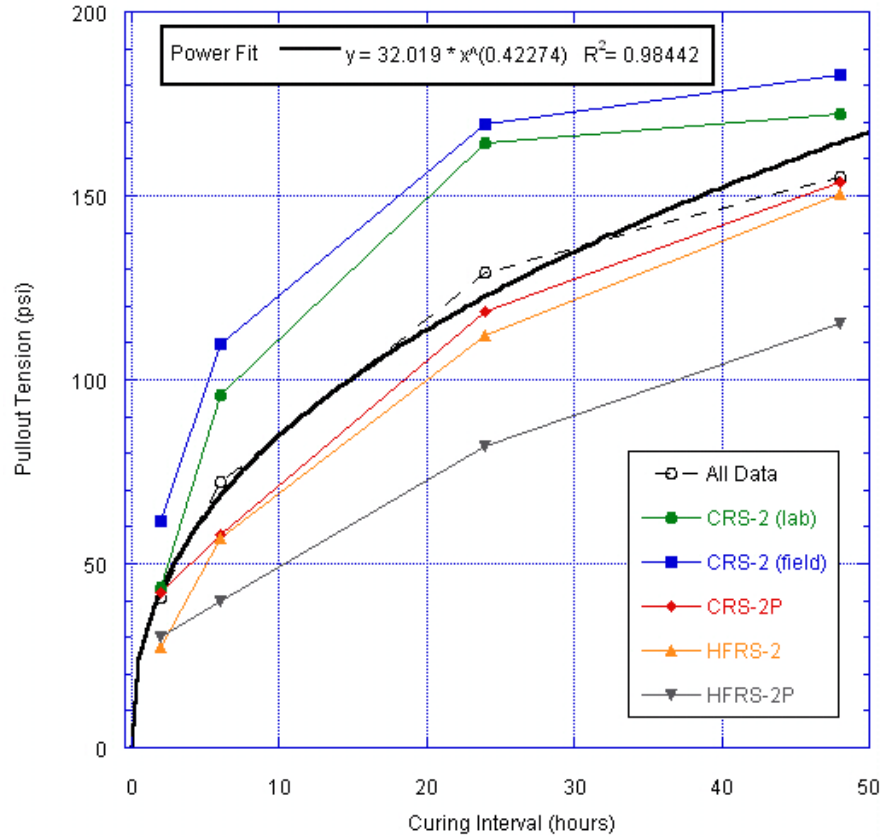


Figure E1c-2.2. Graph. Emulsion types are differentiated by bond strength development.

Results from the calibration experiment indicate that there is more work to do in terms of synchronizing data collection procedures and test protocols between labs. Test results, depicted in figure E1c-2.3, demonstrate that for the given pair of PG binders, labs are producing different response values. Results for UW–Madison show minimal variations in loading rate, indicating that load control is possible for BBS testing. Typical variance is seen in the pullout response. Results from the University of Stellenbosch show wide variations in loading rate for the first trial, with much smaller variations in loading rate observed in the second trial. Pullout tension values are characteristically lower for tests conducted at the University of Stellenbosch compared to tests conducted at UW–Madison.

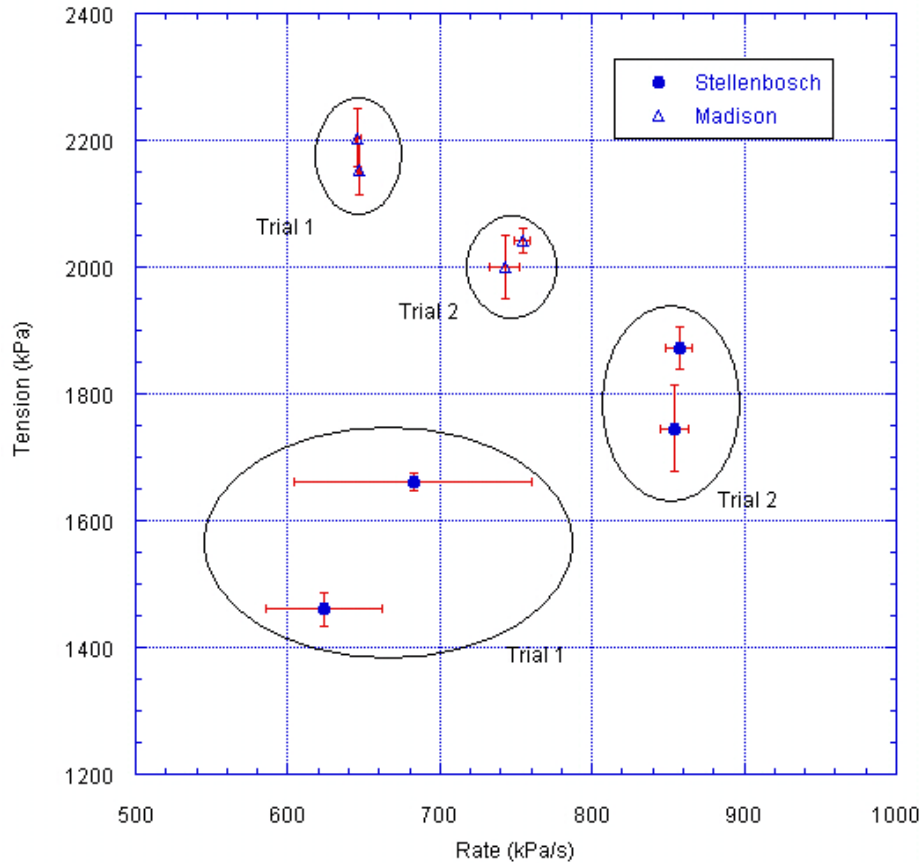


Figure E1c-2.3. Graph. Results from the calibration experiment conducted by the two labs.

### Significant Problems, Issues and Potential Impact on Progress

Results from the calibration experiment demonstrate that while both labs are able to effectively control loading rate, discrepancies exist in pullout tension values for identical binders. A statistical analysis confirms that a significant difference exists between results produced at each lab. The nature of this discrepancy is not immediately evident, though it may be related to the method of sample preparation. The difference in response values may also be attributed to the testing device in use at the University of Stellenbosch laboratory not being able to achieve higher pullout tension values, indicating that there is an issue with the device itself. Until this issue is resolved, further comparisons between emulsified binders tested at each lab will not be possible.

Other issues related to material supplies also hindered progress this quarter. Sweep testing has not advanced due to a lack of aggregate chips and fresh emulsion binders. Both of these issues should be resolved in the next quarter as contractors resume construction operations in warmer weather and are better able to provide the necessary materials on a regular basis.

### Work Planned Next Quarter

Work next quarter will focus on the following tasks:

- *Emulsion construction properties.* The research team will continue to test new emulsion types using the BBS test protocol as they continue to become available. Results from BBS testing and rotational viscometer (RV) testing will also be synthesized into an emulsion evaluation report that will be submitted during the next quarter.
- *Emulsion residue properties.* The research team will continue to identify potential test procedures for evaluating emulsion residue properties in the context of surface treatment performance.
- *Cold mix asphalt.* The research team will review the Cold Mix Literature Review document submitted by UNR and coordinate testing activities accordingly based on the results of this report.
- *ARC Project Advisory Group and Emulsion Task Force activities.* The research team will continue to hold advisory group meetings and support Emulsion Task Force activities.

## **CATEGORY E2: DESIGN GUIDANCE**

### **Work element E2a: Comparison of Modification Techniques (UWM)**

#### Work Done This Quarter

The research team continued testing the binders included in the material library developed for this study. This library includes 17 binders from six sources, five base binder grades and 12 modified binder grades. Tests performed to date include rheological measurements using the Dynamic Shear Rheometer (DSR) according to AASHTO TP5, Multiple Stress Creep and Recovery (MSCR) tests according to ASTM D7405-08a, and storage stability tests according to ASTM D7173-05. The collected binders were also tested after aging according to laboratory aging techniques such as rolling thin film oven (RTFO) (AASHTO T240) and pressure aging vessel (PAV) (AASHTO R28).

#### Significant Results

Table E2a.1 shows the continuous high-temperature grade determined for the binders included in the material library, and the progress in aging the binders for testing.

Table E2a.1. Continuous grade for tested binders and progress in aging.

Material #	Base	Modifier	Class of Modifier	Continuous Grade	RTFO	PAV
1	A0	None	None	65.1	Done	
2	A1	Functionalized PE	Plastomer: Nonreactive	71.1		
3	A2	Functionalized PE	Plastomer: Nonreactive	77.4		
4	A3	SBS with cross-linking	Elastomer: Reactive	70.8	Done	Done
5	A4	SBS with cross-linking	Elastomer: Reactive	77.2	Done	
6	B0	None	None	58.5	Done	
7	B1	Terpolymer	Elastomer: Reactive	65.2	Done	Done
8	B2	Terpolymer	Elastomer: Reactive	71.9	Done	
9	C0	None	None	60.0	Done	Done
10	C1	PPA	Chemical: Reactive	64.7	Done	
11	C2	PPA+SBS+cross-linking	Elastomer: Reactive	72.9	Done	
12	D0	None	None	61.2	Done	
13	D1	Functionalized PE+SBS	Hybrid: Reactive	65.8	Done	
14	D2	Functionalized PE+SBS	Hybrid: Reactive	72.1		
15	E0	None	None	66.2	Done	Done
16	E1	SBS with cross-linking	Elastomer: Reactive	72.4	Done	
17	E2	SBS with cross-linking	Elastomer: Reactive	76.1	Done	

PE = polyethylene. SBS = styrene-butadiene-styrene. PPA = polyphosphoric acid.

The MSCR results for binders tested thus far are summarized in table E2a.2. Highlighted cells indicate that less than three replicates were tested, while empty cells indicate that no testing has been completed. More testing is still required to complete the data set. Results to date show that some binders are extremely sensitive to stress level, as shown by significant decreases in the % recovery (%R) and increases in nonrecoverable creep compliance (J<sub>nr</sub>) values.

Table E2a.2. MSCR results.

	Binder	RTFO				OB			
		100 Pa Stress		3200 Pa Stress		100 Pa Stress		3200 Pa Stress	
		Jnr	% Recovery	Jnr	% Recovery	Jnr	% Recovery	Jnr	% Recovery
Testing at Target Modified PG Grade	A0	2.726	3.6	2.954	1.1	8.654	0.4	9.1	0.007
	A1	2.890	14.6	4.761	1.2				
	A2	1.202	44.4	5.486	1.5				
	A3	2.675	11.1	3.591	4.6	5.715	25.9	9.3	4.4
	A4	1.572	17.2	2.307	8.3	5.408	24.7	9.6	2.9
	B0	2.666	4.4	2.930	1.2	8.364	0.4	8.9	0.0
	B1	1.583	32.6	1.895	23.4	5.578	19.8	7.5	6.9
	B2	0.968	53.0	0.928	51.7	3.339	38.5	4.2	26.3
	C0	2.848	4.0	3.108	1.1	7.002	0.7	7.4	0.0
	C1	2.844	9.1	3.447	1.8	8.758	1.4	9.9	0.0
	C2	0.804	52.0	0.918	44.8	4.639	23.7	7.1	6.6
	D0	2.131	6.1	2.386	1.9	6.623	1.1	7.1	0.0
	E0	3.119	3.4	3.379	0.9	7.160	0.6	7.4	0.0
	E1	2.290	19.0	2.919	8.3	4.691	16.1	6.2	4.8
E2	2.453	26.9	3.475	12.2	4.885	25.8	7.7	7.3	
	Binder	RTFO				OB			
		100 Pa Stress		3200 Pa Stress		100 Pa Stress		3200 Pa Stress	
		Jnr	% Recovery	Jnr	% Recovery	Jnr	% Recovery	Jnr	% Recovery
Testing at Original Binder PG Grade	A0								
	A1					2.082	20.9	4.140	1.6
	A2								
	A3					3.565	11.2	4.180	4.8
	A4					1.397	17.6	1.758	8.2
	B0								
	B1					2.617	23.9	3.170	14.3
	B2					0.872	47.1	0.897	44.9
	C0								
	C1					2.950	5.2	3.300	1.1
	C2					0.715	42.7	0.830	36.1
	D0								
	E0								
	E1					1.796	29.8	2.377	14.3
E2					1.076	28.6	1.287	26.3	

OB = original binder.

Figure E2a.1 illustrates the test results for the RTFO binder tested at the target PG temperature at 3200 Pa stress level, while figure E2a.2 summarizes the results for the un-aged binder tested at the original binder PG temperature. The specification line in figures E2a.1 and E2a.2 followed the guidelines from the recent Binder ETG presentation by John D’Angelo. The relationship between %R and Jnr that separates the elastic from nonelastic behavior was defined by the equation E2a.1:

$$Y = 29.371X^{-0.2631} \tag{E2a.1}$$

Although the current specification requires testing the RTFO binder at the original binder PG temperature, figures E2a.1 and E2a.2 show a similar trend for binders B2 and C2, as both binders had a %R higher than the specification line. Both binders are modified with a reactive elastomer. The figures show many data points that fall below the required limits for elastic modifiers. It should be noted that the majority of these binders are tested at the target PG temperature rather than the original PG temperature. The difference in grade between base and modified grade in some cases was three grades (18 °C) and thus testing the RTFO binder at the target PG temperature resulted in a very low %R. Testing at the base PG grade is required before further analysis can be conducted.

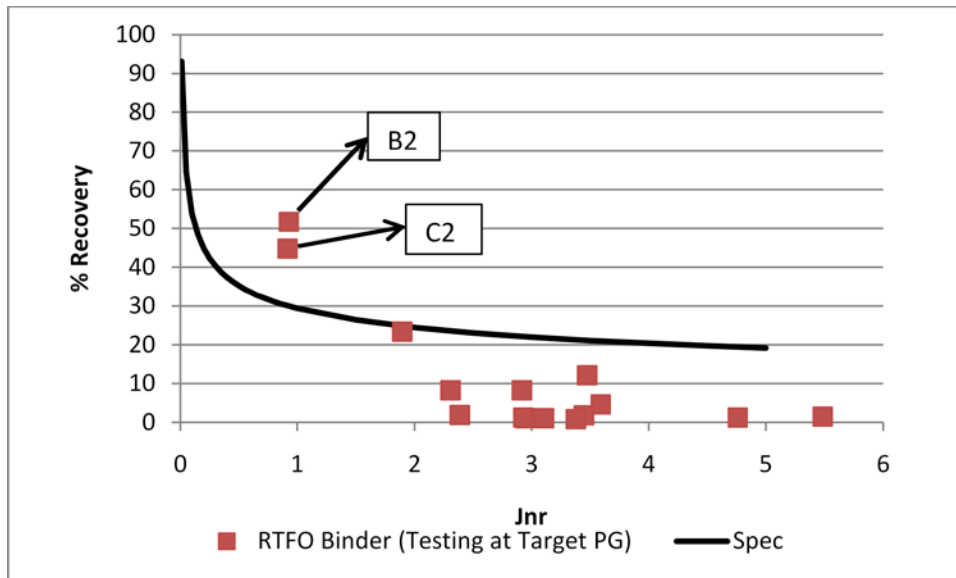


Figure E2a.1. Graph. MSCR results for RTFO binder tested at 3200 Pa and at target PG temperature.

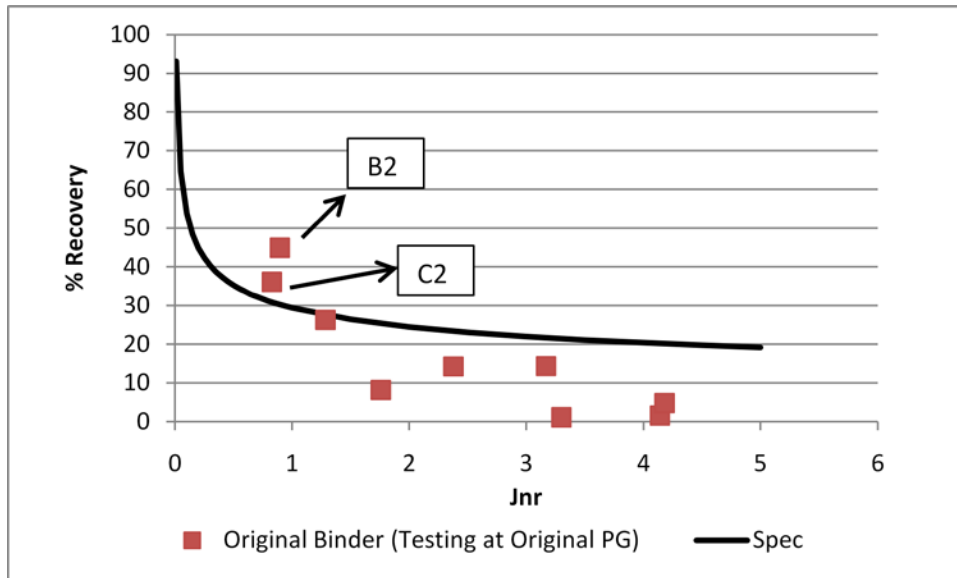


Figure E2a.2. Graph. MSCR results for un-aged binder tested at 3200 Pa and original PG temperature.

### Significant Problems, Issues and Potential Impact on Progress

DSR used for completing the frequency sweep tests was not operational for the majority of this quarter. It was recently repaired and testing will resume in early April 2010.

### Work Planned Next Quarter

The research team will continue aging and testing binders included in the materials database.

### **Work element E2b: Design System for HMA Containing a High Percentage of RAP Material (UNR)**

#### Work Done This Quarter

This work element is a joint project between the University of Nevada, Reno, the University of Wisconsin–Madison, and Western Research Institute.

#### *Subtask E2b-1.a*

The laboratory experiments evaluated the impact of extraction methods on the properties of extracted aggregates and binder content of laboratory simulated RAP mixtures using four different aggregate sources. The evaluated extraction methods were: centrifuge, reflux, and ignition oven. The laboratory simulated RAP mixtures consisted of short term aging of loose mixtures for 4 hours at 275°F following by long term aging of the same mixture for 5 days at 185°F. The aggregate sources evaluated in the study were: Alabama (hard limestone), California

(granodiorite), Florida (soft limestone), and Nevada (rholite). The following summarizes the major findings of this experiment:

The analysis of the extracted asphalt binder contents led to the following conclusion:

- The asphalt binder contents measured by the three extraction methods were statistically significantly lower than the true asphalt binder contents except for the Nevada and California aggregates using the reflux method which showed contents similar to their corresponding true levels.

The impact of the extraction methods on the combined aggregate specific gravity was method-dependent:

- Centrifuge: slightly lower combined specific gravity for the FL and NV aggregates and higher for the AL and CA aggregates.
- Reflux: higher combined specific gravity for all four aggregates.
- Ignition Oven: lower combined specific gravity for the AL and FL aggregates and higher for the NV and CA aggregates.

The final impact of these changes was also evaluated in terms of their impact on the calculated volumetric properties of the mixtures (i.e. Voids in Mineral Aggregates).

#### *Subtask E2b-1.b*

#### *Verification Procedure for the low, intermediate and high temperatures estimation of RAP Binder*

Two RAP sources were available for use in the verification procedure. The first is from Reno, Nev., labeled *Reno*, and the second is from a contracting company in Wisconsin, which is labeled *Wisconsin*. RAP from both sources was sieved and the  $R_{100}$  material was collected, as required in the standard procedure. Two binder sources were also available for use: a PG 64-22 and PG 58-28. Artificial RAP was created by mixing one of the heavily aged binders with burned  $R_{100}$  aggregates from one RAP source at an asphalt content equal to the original RAP asphalt content. The following is a summary of the different combinations tested.

*Artificial RAP<sub>1</sub> + PG 64 – 22 fresh binder* (Case I)

*Artificial RAP<sub>2</sub> + PG 58 – 28 fresh binder* (Case II)

where

Artificial RAP<sub>1</sub>: 2 PAV cycle aged PG 64-22 binder + burned  $R_{100}$  *Reno* aggregates with 10% asphalt content.

Artificial RAP<sub>2</sub>: 2 PAV cycle aged PG 58-28 binder + burned  $R_{100}$  *Wisconsin* aggregates with ~7.5% asphalt content.

The standard procedure was found to accurately predict binder stiffness at critical low PG temperatures. Table E2b.1 summarizes the stiffness results for the different artificial RAP cases tested at different low temperatures. A negative percent difference indicates that the procedure underestimates the measured value, while a positive difference indicates overestimating it. As shown in the table, the difference in the estimated stiffness and measured stiffness was 4% or less for all cases.

Table E2b.1. Stiffness verification test results.

	Estimated S(60), MPa	Measured S(60), MPa	Percent Difference
Case I, -6 °C	2.102	2.025	3.8%
Case I, -12 °C	2.391	2.299	4.0%
Case II, -12 °C	2.442	2.354	3.7%
Case II, -18 °C	2.552	2.513	1.5%
Case II, -24 °C	2.748	2.767	-0.7%

The procedure, however, was found to result in binder m-value that underestimates the measured values by a significant margin. Table E2b.2 shows the estimated and measured m-values along with the percent difference. The percent difference ranged from -14% to -23.7%. The fact that all the estimated values were lower than the measured values indicates that a possible shift is caused by the aggregates in the mortar and that a numerical solution to this could be possible by using composite theory principles. It was also debated if an empirical solution could be found by using an average shift factor. By calculating the average of the ratios between the measured m-value and the estimated m-value, it was determined that a shift factor value of 1.20 could be used.

Table E2b.2. M-value verification test results.

	Estimated m-value	Measured m-value	Percent Difference
Case I, -6 °C	0.221	0.261	-15.3%
Case I, -12 °C	0.171	0.224	-23.7%
Case II, -12 °C	0.224	0.270	-17.0%
Case II, -18 °C	0.217	0.253	-14.2%
Case II, -24 °C	0.185	0.215	-14.0%

Table E2b.3 shows the shifted m-values compared to the measured m-values. The percent difference is less than 10%. Although the shifting factor helped in reducing the percent difference, the research team believes that a difference of 10% is not acceptable as an accurate estimate and that an empirically calculated shift could be misleading. More research is needed to investigate the reason behind the shift of the m-value.

Table E2b.3. Shifted m-value verification test results.

	Estimated m-value	Measured m-value	Percent Difference
Case I, -6 °C	0.265	0.261	-1.6%
Case I, -12 °C	0.205	0.224	+9.2%
Case II, -12 °C	0.269	0.270	+0.4%
Case II, -18 °C	0.260	0.253	-2.8%
Case II, -24 °C	0.222	0.215	-3.2%

Tables E2b.4 and E2b.5 summarize the procedure results for the intermediate- and high-temperature testing. The intermediate-temperature estimation was reasonably close to the measured values, with a percent difference less than 4%. On the other hand, the high-temperature percent difference ranged from about 10% to 20%. Such high values indicate that the current procedure for the high temperature requires further examination.

Table E2b.4. Intermediate-temperature properties estimation.

	Testing Temp. (°C)	Measured RAP Binder $G^*\sin(\delta)$ , kPa	Estimated RAP Binder $G^*\sin(\delta)$ , kPa	Percent Difference
Case I	25.0	3.68	3.80	-3.2%
	28.0	3.59	3.71	-3.5%
Case II	25.0	3.79	3.73	1.4%
	28.0	3.62	3.60	0.5%

Table E2b.5. High-temperature properties estimation.

	Testing Temp. (°C)	Measured RAP Binder $G^*/\sin(\delta)$ , kPa	Estimated RAP Binder $G^*/\sin(\delta)$ , kPa	Percent Difference
Case I	64.0	1.65	2.00	-21.7%
	70.0	1.32	1.46	-11.2%
Case II	58.0	1.45	1.26	13.6%
	64.0	1.09	0.89	17.7%

### *Effect of Burning on Aggregate Properties*

Table E2b.6 and figure E2b.1 summarize the results for this testing program. The results at critical low PG temperatures have indicated that after one burn cycle, very little change occurs in the aggregate gradation and mass weight. Results showed that mortars produced with burned aggregates show a lower stiffness value compared to mortars with unburned aggregates, but the m-value was unaffected by the burning. The differences in stiffness values, however, are fairly

minimal. Two burning cycles did not result in larger differences in the stiffness, m-value or gradation. It should be recognized that the results are based on using one source of manufactured sand. Other sources could show different results, thus program will be expanded to include aggregates that are known to change in ignition oven.

Table E2b.6. Burn adequacy check results.

Comparison			
	Unburned	Burned	2 Burn Cycles
Time (sec)	S(t)	S(t)	S(t)
8	424	375	377
15	361	319	320
30	298	263	264
60	243	215	214
120	196	173	171
240	155	136	134
Time (sec)	m-value	m-value	m-value
8	0.248	0.248	0.247
15	0.266	0.266	0.268
30	0.285	0.286	0.292
60	0.305	0.306	0.315
120	0.325	0.326	0.339
240	0.344	0.346	0.362

S(t) = creep stiffness at time *t*.

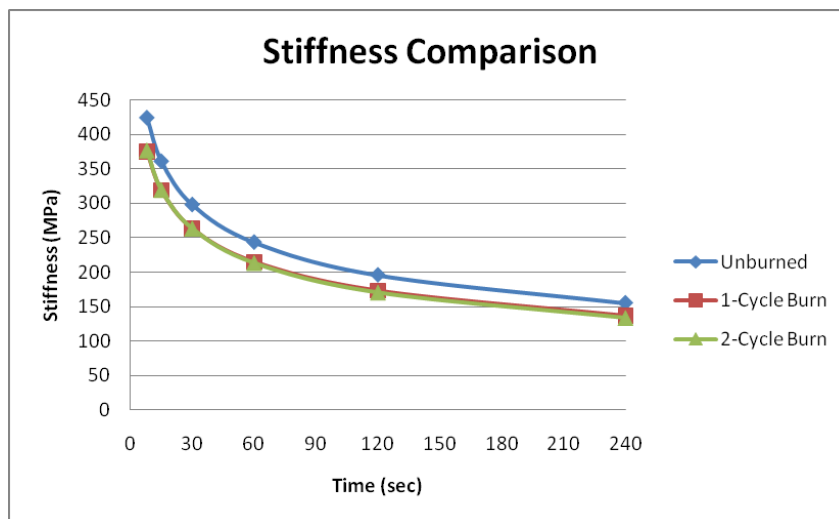


Figure E2b.1. Graph. Burn adequacy check at -6 °C.

*Subtask E2b-2: Compatibility of RAP and Virgin Binders*

Work Done This Quarter

The four field mixes collected from the Manitoba RAP field site were extracted using two different solvents/solvent mixtures, cyclohexane and toluene/ethanol. The RAP material was also extracted in a similar manner. The hypothesis is that extracting RAP with cyclohexane should give an indication of how much of the RAP asphalt actually mixes with a virgin binder and what is retained on the original RAP aggregate. Similarly, extracting the field mixes with the two solvents/mixtures should provide a comparison of binder material that is representative of the binder that is actually effective (cyclohexane) and the total binder (toluene/ethanol). The Manitoba mixes (and sections) are conventional hot-mix using 150/200 pen asphalt, a section with 15% RAP, a section with 50% RAP using the 150/200 pen asphalt, and a section with 50% RAP using 200/300 pen asphalt from the same source.

Results from the solvent extractions of the Manitoba field mixes are shown in table E2b.7. The trend of the extraction results are that the cyclohexane tends to extract similar amounts of binder in plant-aged mixes but less amount of binder in long-term aged mixes like RAP. This trend follows the hypothesis stated in the work plan.

Table E2b.7. Solvent Extraction Recovery of Manitoba Mixes.

Asphalt/Mix	RAP, %	Solvent	% Recovery
150/200	0	Toluene/EtOH	5.18
	0	Cyclohexane	5.09
150/200	15	Toluene/EtOH	4.86
	15	Cyclohexane	4.88
150/200	50	Toluene/EtOH	4.54
	50	Cyclohexane	4.35
200/300	50	Toluene/EtOH	4.44
	50	Cyclohexane	4.45
RAP	100	Toluene/EtOH	6.00
	100	Cyclohexane	5.23

The rheology of the extracted binders from the 0% RAP mix with the 150/200 pen asphalt using the two solvents is shown in figure E2b.2. The figure shows that the binder material extracted from the fresh mix with the two solvents is essentially identical. Since the mix has only mix-plant aging, the result is as expected, that both solvents are effective at removal of the binder material.

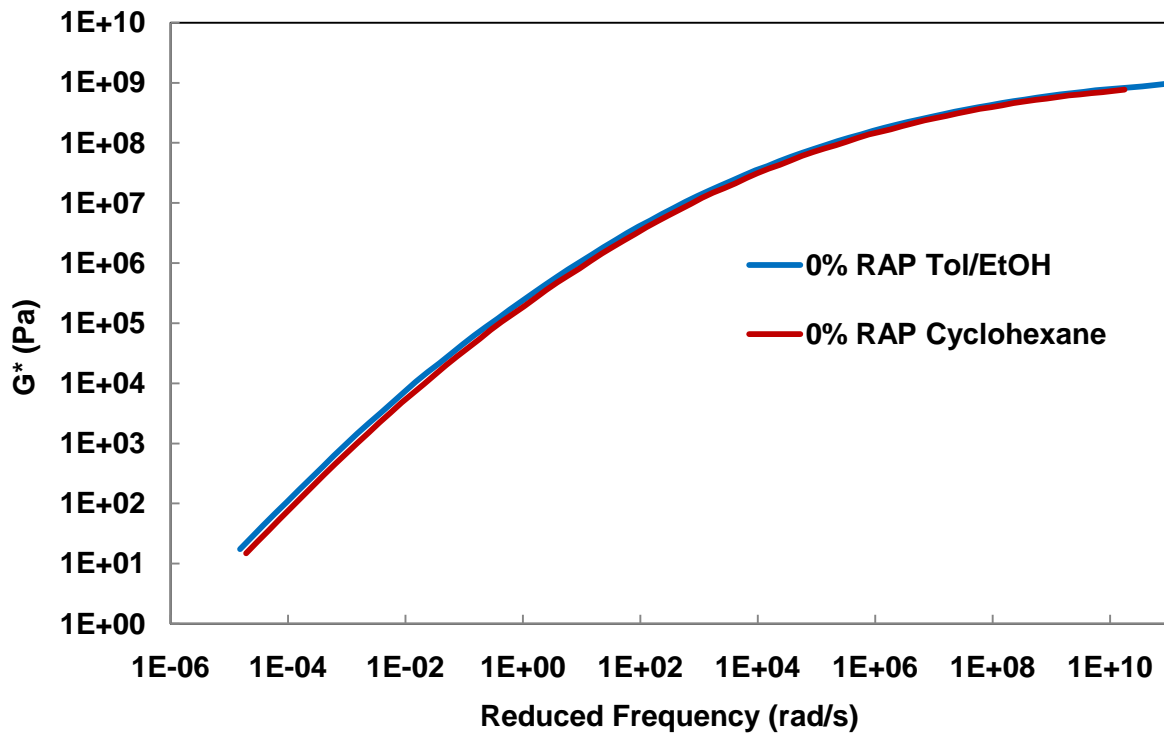


Figure E2b.2. Graph. Rheology of the binder material from the Manitoba 0% RAP mix extracted with two different solvents.

The rheology of the extracted binder material from the 100% RAP material using the two solvents is shown in figure E2b.3. In this case, the cyclohexane solvent has extracted much less material than toluene/ethanol (table E2b.8) and the material extracted has a substantially lower  $G^*$  value. The rationale is that the cyclohexane extract of the 100% RAP material should represent the binder material that is solublized with new asphalt.

A comparison was also made between the RTFO 150/200 pen asphalt and the 200/300 pen asphalt. The results are shown in figure E2b.4. Figure E2b.4 shows that the 200/300 pen asphalt is only marginally softer than the 150/200 pen asphalt but previous data reported by the UNR team shows that the 150/200 pen asphalt grades as a PG 58-28 whereas the 200/300 pen asphalt grades as a PG 52-34 asphalt.

Comparison of the rheology of the RTFO-aged 150/200 pen Manitoba asphalt, the RTFO-aged 200/300 pen Manitoba asphalt, and the cyclohexane extracted 0% RAP field mix is shown in figure E2b.5. The figure indicates that there is good agreement between the cyclohexane-extracted binder material from the 0% RAP mix and the RTFO-aged asphalts. A similar comparison and result can be made with the toluene/ethanol extracted binder material from the 0% RAP mix.

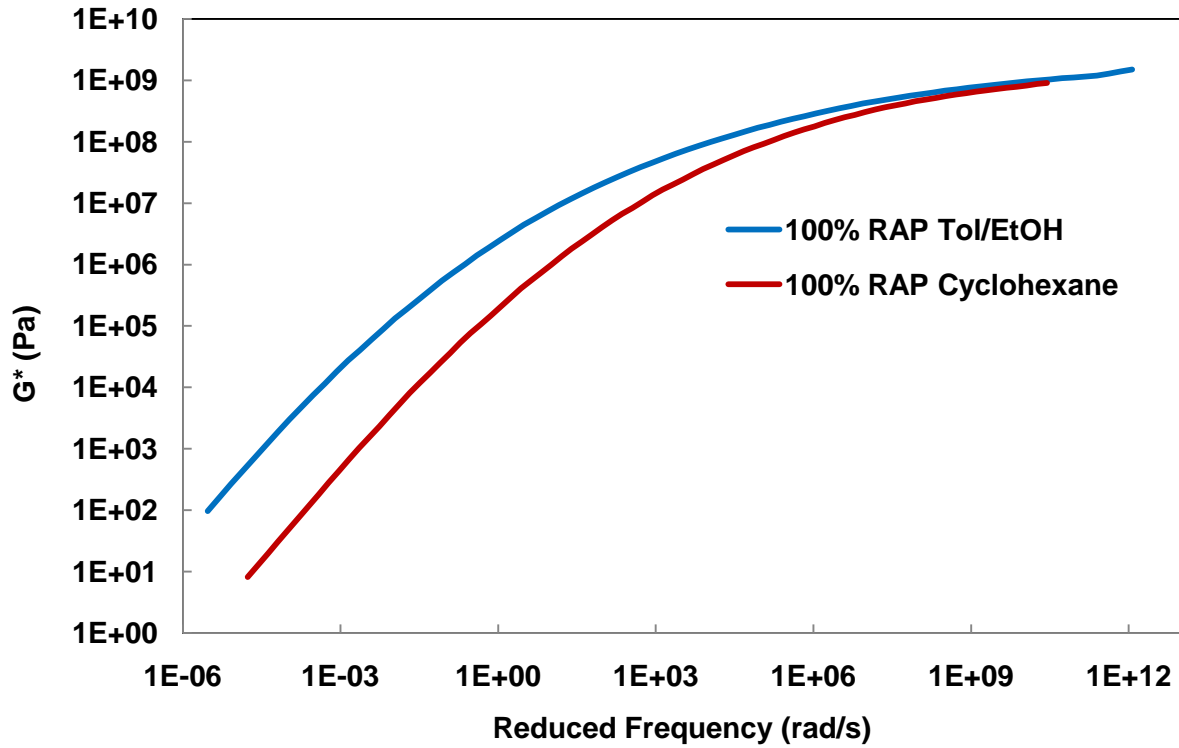


Figure E2b.3. Graph. Rheology of the binder material from the Manitoba 100% RAP material extracted with two different solvents.

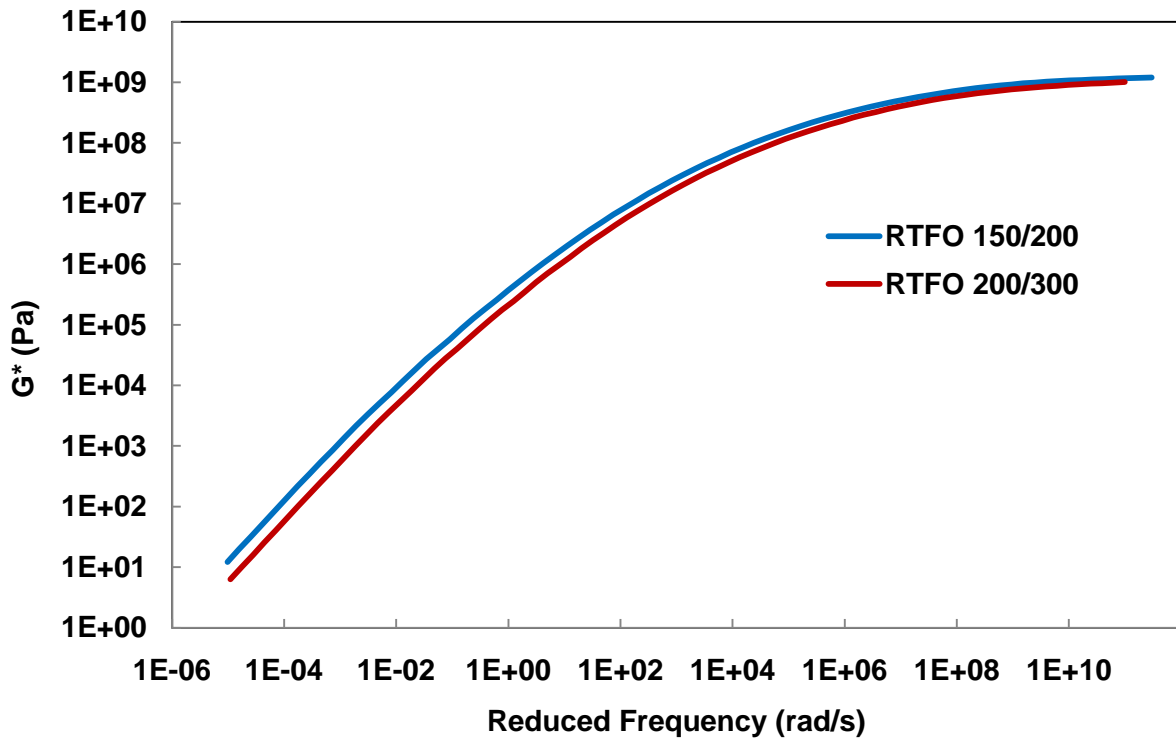


Figure E2b.4. Graph. Comparison of the Manitoba 150/200 pen asphalt and the 200/300 pen asphalt after RTFO aging.

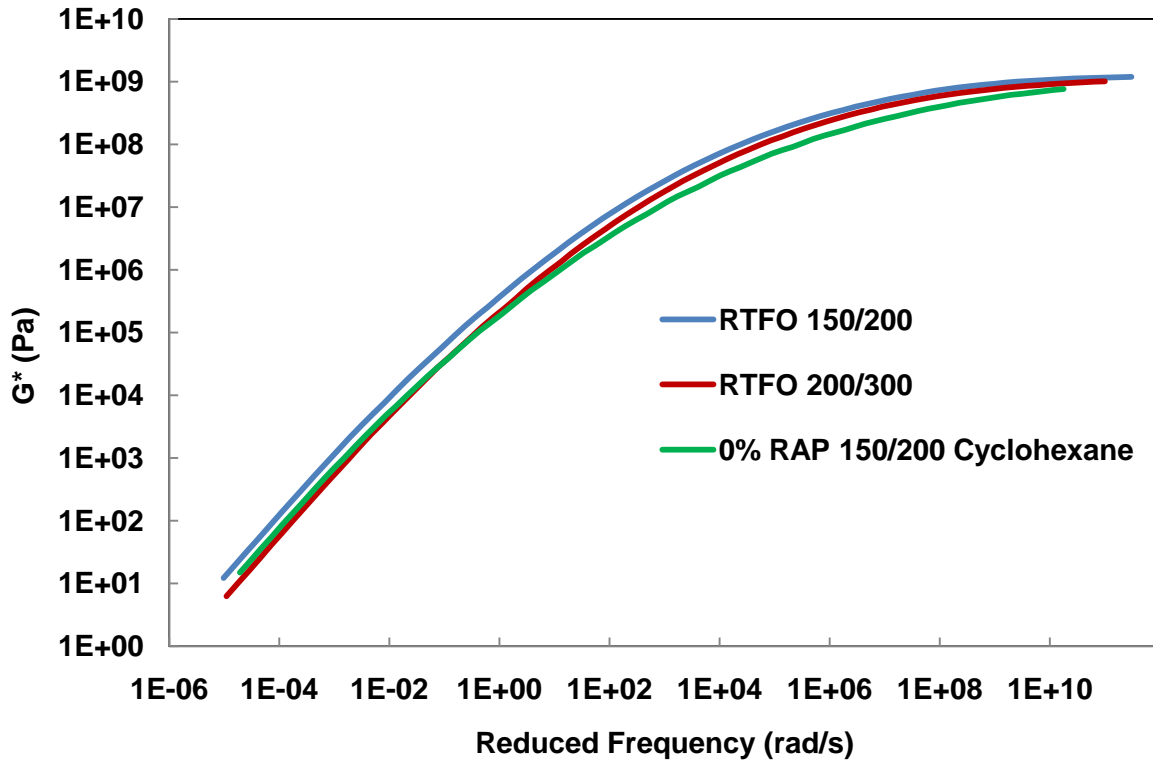


Figure E2b.5. Graph. Comparison of RTFO-aged 150/200 pen asphalt, RTFO-aged 200/300 pen asphalt and the cyclohexane extracted 0% RAP mix.

Extraction of the 15% RAP field mix and the two 50% RAP field mixes with the two different solvents has also been completed. The rheological analysis of these samples follows the trend just described. Chemical characterization of the extracted binder materials from Manitoba using Differential Scanning Calorimetry (DSC), and the WRI Asphaltene Determinator® has also been completed, and all data is being compiled and analyzed.

Extraction of the RAP materials from South Carolina and California has recently been completed and rheological analysis and chemical characterization is underway.

#### *Subtask E2b-5*

The mixtures from the Manitoba RAP sections were evaluated in terms of their resistance to moisture damage and thermal cracking. Table E2b.8 shows the completed testing matrix for the laboratory mixed laboratory compacted (LMLC) and the field mixed laboratory compacted (FMLC) virgin and RAP-containing HMA mixtures.

Table E2b.8. Testing matrix for the Manitoba mixtures.

Property	Spec. size	Mixture ID*							
		F-0%-150	F-15%-150	F-50%-150	F-50%-200	L-0%-150	L-15%-150	L-50%-150	L-50%-200
Resistance to Moisture Damage - TS vs. F-T cycles: 0, 1 and 3 F-T - TSR at 1 and 3 F-T - E* vs. F-T cycles: 0, 1 and 3 F-T	4"x2.5" 4"x2.5" 4"x6"	√	√	√	√	√	√	√	√
Resistance to Thermal Cracking - TSRST: 0 and 3 F-T (long-term oven aged)	2"x2"x10"	√	√	√	√	√	√	√	√

\* F denotes "Field Mix Lab Compacted",  
L denotes "Lab Mix Lab Compacted",  
0%, 15% and 50% denotes the RAP content, and  
150 and 200 denotes Pen 150-200 and Pen 200-300, respectively.

The resistances of the various HMA mixtures to moisture damage were evaluated in terms of measuring the indirect tensile strength and the dynamic modulus of the mixtures under multiple freeze-thaw (F-T) cycling. The multiple F-T cycling followed the procedure outlined in AASHTO T-283: Standard Method of Test for Resistance of Compacted Hot Mix Asphalt (HMA) to Moisture-Induced Damage, at multiple stages.

Figures E2b.6 and E2b.7 show the indirect tensile strength and the tensile strength ratio for the various mixtures as a function of the number of F-T cycles, respectively. Figure E2b.8 shows the dynamic modulus for the various mixtures at 77°F and 10 Hz after 0, 1 and 3 F-T cycles. Figures E2b.9 and E2b.10 show the fracture temperatures for LMLC and the FMLC mixes at the 0 F-T cycles, respectively.

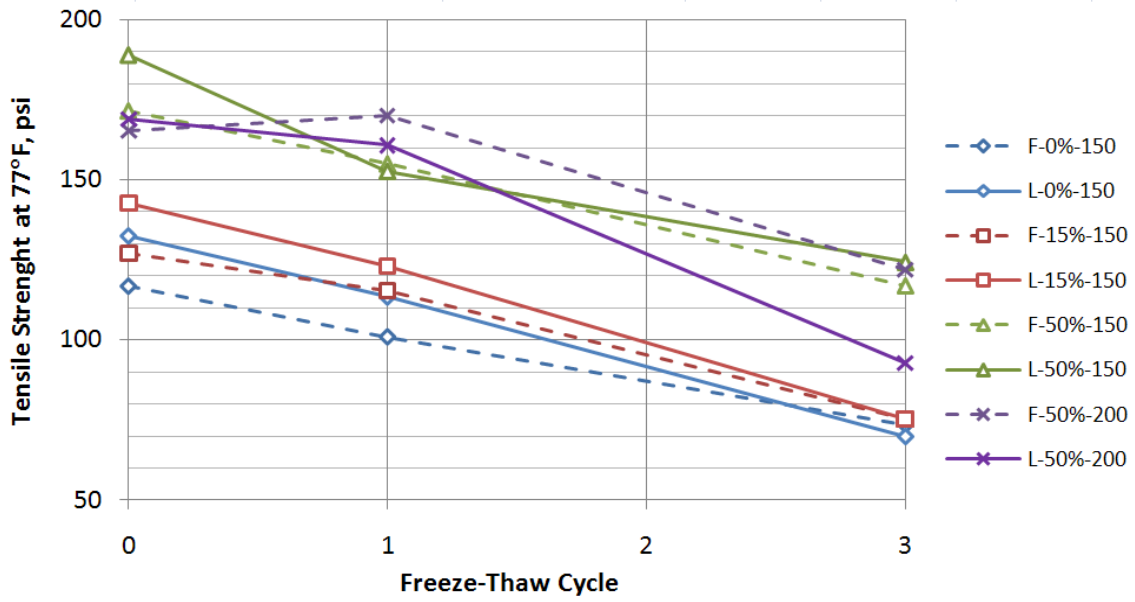


Figure E2b.6. Graph. Indirect tensile strength at 0, 1 and 3 F-T cycles.

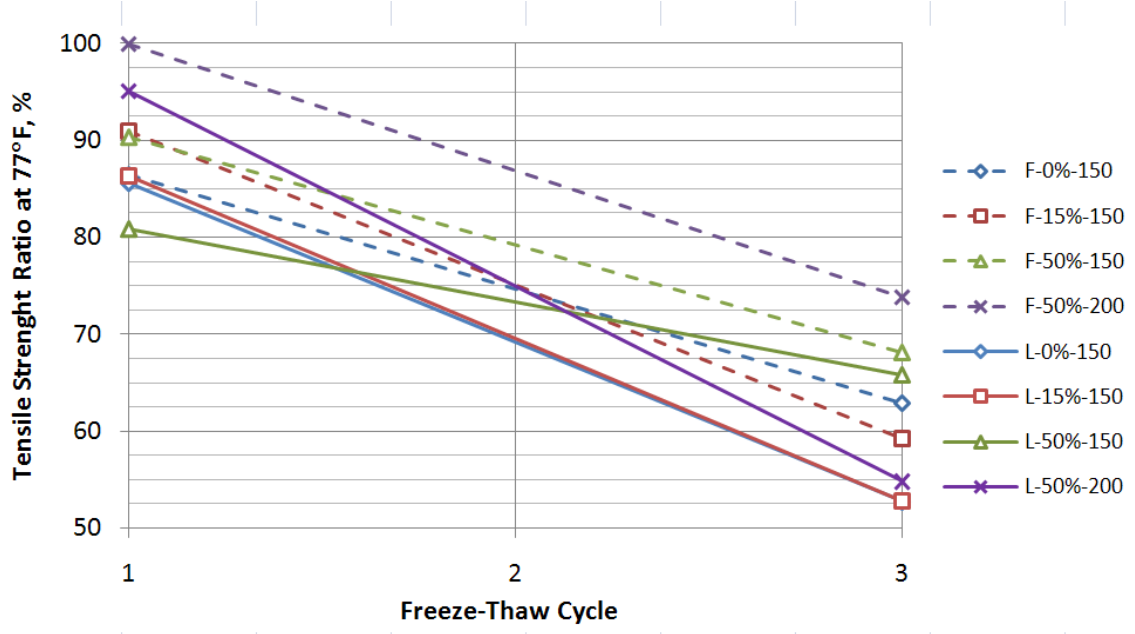


Figure E2b.7. Graph. Tensile strength ratio at 0, 1 and 3 F-T cycles.

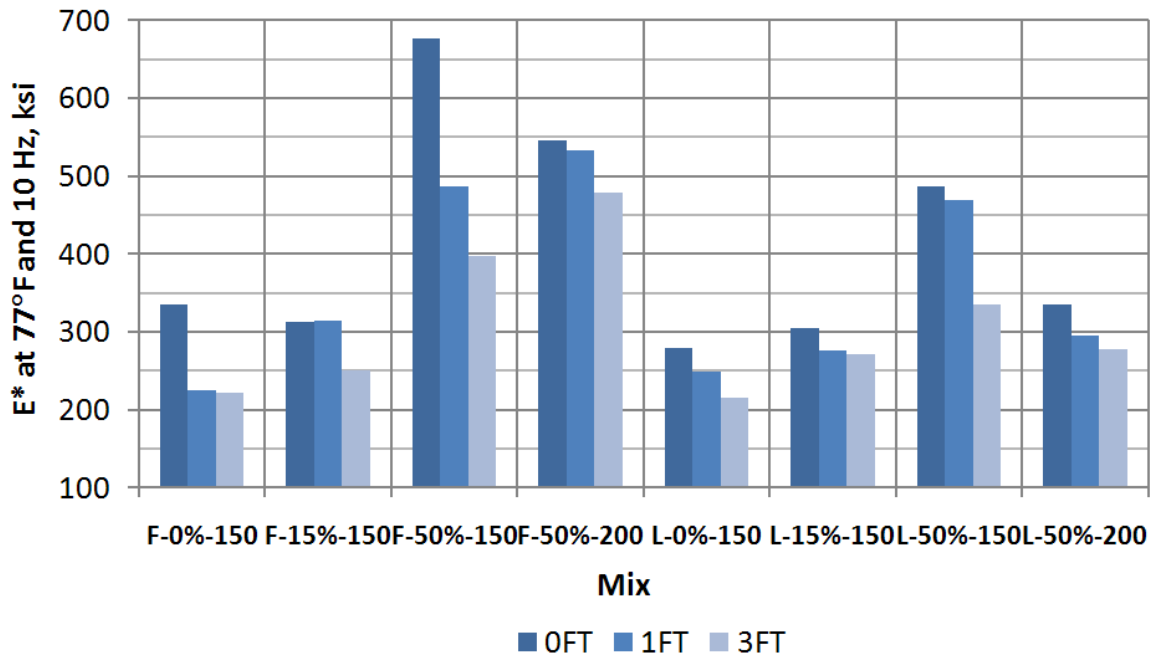


Figure E2b.8. Graph. Dynamic modulus at 77°F and 10 Hz after 0, 1 and 3 F-T cycles.

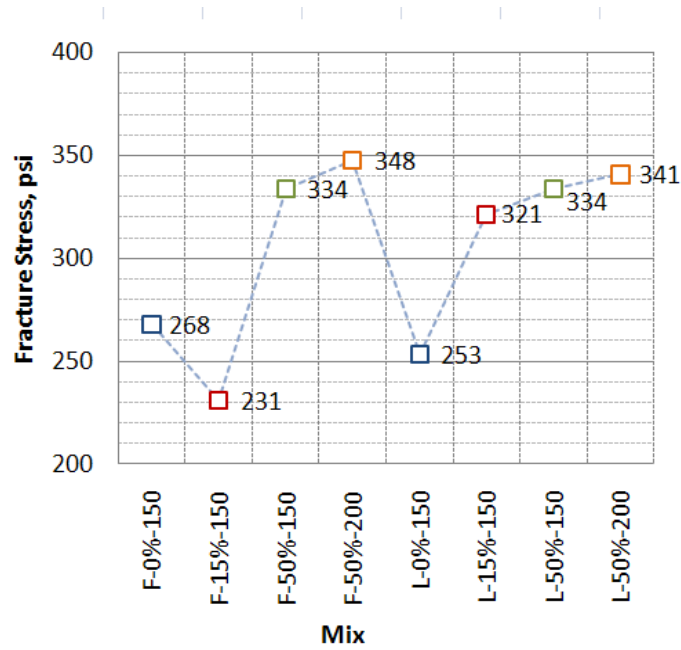


Figure E2b.9. Graph. Fracture temperatures for the LMLC mixes after 0 F-T cycle.

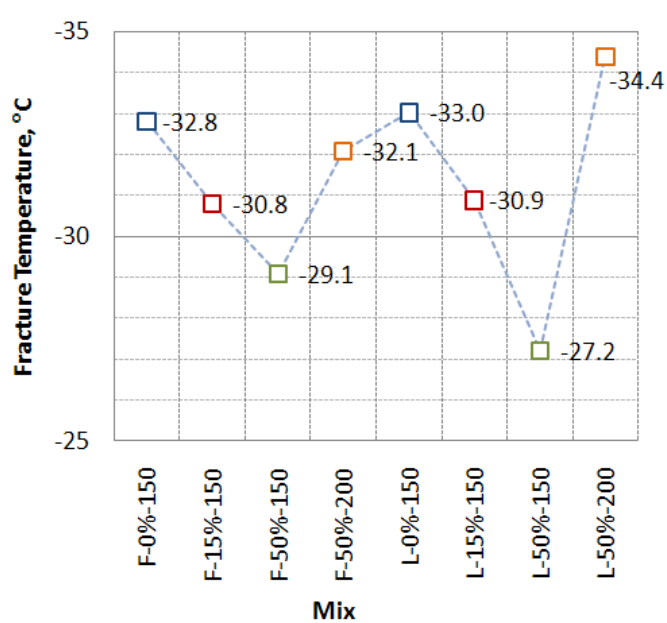


Figure E2b.10. Graph. Fracture temperatures for the FMLC mixes after 0 F-T cycle.

Additionally the Pen 150-200 and Pen 200-300 asphalt binders were graded according to the Superpave system.

A summary of the test results was presented to the Manitoba Infrastructure & Transportation (MIT) personnel on March 03, 2010 at the meeting in Winnipeg, Manitoba.

### Significant Results

Under subtask E2b-1.a, the impact of the current extraction techniques (i.e. ignition, centrifuge, and reflux) on the properties of the extracted recycled asphalt pavement (RAP) aggregates experiment was completed and a report is being finalized for submission. A paper presenting the impact of the findings of this subtask on voids in mineral aggregates (VMA) of HMA mixes containing RAP has been presented at the Transportation Research Board annual meeting in January 10-14, 2010.

Under subtask E2b-1.b, an extensive verification testing program was completed for low, intermediate and high temperatures using two artificial RAP materials and two virgin binder grades. The program was designed to verify that estimated values are equal to the known values of laboratory-aged binders used in producing the artificial RAP. The artificial RAP material was made by mixing burned R<sub>100</sub> aggregates with heavily aged binder (2 to 3 pressure aging vessel (PAV) cycles) at a typical RAP asphalt content (7% to 10%). The artificial RAP was then tested using the original procedure, and the estimated RAP binder properties were then compared against the true binder properties by testing the heavily aged binder. Two artificial RAP-virgin binder combinations were tested at low, intermediate and high PG temperatures.

The RAP binder grade estimation procedure assumes that burning the R<sub>100</sub> (passing No. 50 sieve; retained on No. 100 sieve) RAP material to determine the asphalt content does not alter the aggregate properties or aggregate gradation, and hence will not affect the testing results. Concerns were raised by experts regarding the effect of burning the RAP on interaction between binders and aggregates. Last quarter a procedure check was completed to evaluate the adequacy of using the burned aggregates and verify this assumption. Sieved manufactured sand taken from granite aggregate source (m-sand) was subjected to one and two typical ignition-oven burn cycles and tested against the unburned m-sand mixed at an asphalt content typically noted when using the original procedure (approximately 40%). A sieve analysis was also completed after each burn cycle to check for gradation change. The mortar samples prepared with the m-sand were tested in the Bending Beam Rheometer (BBR) for low-temperature PG. Similar testing for high and intermediate temperatures will be conducted next quarter.

In addition to the above steps used for verification and a procedure check, the research team started a user reproducibility and sample repeatability study. This study is still in its initial phase.

Under subtask E2b-3, an experimental plan was developed to evaluate the laboratory mixing process of RAP-containing HMA mixtures. Granite construction in Utah was contacted for mixtures sampling.

Under subtask E2b-5, the mixtures from the Manitoba RAP sections were evaluated in terms of their resistance to moisture damage and thermal cracking.

#### Significant Problems, Issues and Potential Impact on Progress

The Dynamic Shear Rheometer (DSR) used for completing the frequency sweep tests was not operational for the majority of this quarter. It was recently repaired and testing will resume in early April 2010.

#### Work Planned Next Quarter

Work will continue on the laboratory evaluation of the Manitoba RAP mixes and the evaluation of the extracted/recovered asphalt binders from the virgin and the RAP-containing asphalt mixtures.

The materials for the experimental plan will be collected for subtask E2b-3 “Develop a Mix Design Procedure,” and testing will commence.

Work will continue on four new RAP sources to complete full procedures for each. Variability statistics will also be completed for the standard procedure. Two users will complete the full procedure for the same RAP source and virgin binder. One user will also complete the same procedure twice for a RAP material. The testing plan will be fully developed next quarter. Investigating the feasibility of using the Single-Edge Notched Bending (SENB) and glass transition temperature testing equipment for investigating RAP materials will also begin. The research team will also work on investigating the shift in the predicted m-value curve, and further evaluation of the high-temperature testing procedure. The work on the burning adequacy

check will continue by testing different sand materials, as well as testing at high and intermediate temperatures.

Chemical characterization of the Manitoba extracted samples will be continued using NMR, the WRI Waxphaltene Determinator®, and compatibility testing using Automated Flocculation Titrimetry (AFT). The new AFT is expected to be delivered in the next few weeks.

Chemical and rheological characterization of the South Carolina and California RAP extracted materials will be continued. Blending experiments and subsequent characterization of the blends of the South Carolina and California RAP extracted materials with SHRP asphalts AAC and AAD will commence.

### **Work element E2c: Critically Designed HMA Mixtures (UNR)**

#### Work Done This Quarter

Work continued to evaluate the applicability of the recommended deviator and confining stresses for the flow number test. A report summarizing the findings of the work completed under subtask E2c.1 was submitted to FHWA for review and publication.

The UNR team collaborated with the Flow Number Task Force of the Asphalt Mixture and Construction Expert Task Group to develop a work plan for the evaluation of flow number (repeated load test) criteria for asphalt concrete mixture design. The objective of the proposed experiment is to perform an evaluation of the five promising flow number approaches summarized in table E2c.1 to recommend an approach for use in mixture design. The scope of the proposed experiment includes collecting appropriate flow number test data, analyzing the rutting resistance using the various approaches, then comparing the rutting resistance for a limited number of field mixtures which are known to have acceptable rutting performance for their design traffic level.

Table E2c.1. Promising approaches for rutting resistance from flow number test data.

Method	Air Voids	Temperature	Confining Stress, psi	Deviatoric Stress, psi	Pulse	Criteria
NCHRP 9-33 (AAT, 2009)	7 %	50 % reliability high pavement temperature from LTPPBind at depth of 20 mm for surface courses and top of layer for other layers	0	87	0.1 sec with 0.9 sec dwell	Flow number > critical value as a function of traffic
NCAT (Willis et al. 2009)	7 %	50 % reliability PG grade – 6 °C	10	70	0.1 sec with 0.9 sec dwell	Flow number > critical value as a function of traffic and allowable rut depth
NCHRP 9-30A (NCHRP, 2010)	Avg.; In Place (Specs.)	Option A: 3 Temps. (50% reliability PG minus 5°C, 20°C, mid-range). Option B: Effective temperature based on rutting (MEPDG).	10	70	0.1 sec with 0.9 sec dwell	Slope and intercept of permanent deformation curve < critical values as a function of traffic (rut depth < threshold value).
UNR (Hajj et al. 2010)	7 %	Effective temperature for rutting	Variable*	Variable*	Variable *	Slope and intercept of permanent deformation curve < critical values as a function of traffic
NCHRP 9-26A	7%	3 temperatures: Binder high PG, PG minus 6°C, PG minus 12°C	0	29	0.1 sec with 0.9 sec dwell	Rutting calculated from Minimum Strain Rate at 3 temperatures, aging index, and pavement temperature frequencies < critical rutting

\* using developed predictive equations.

The basic experiment for evaluating the promising flow number approaches is shown in table E2c.2. The primary variables in the experiment are the design traffic level (3, 10, and 30 million equivalent single axle loads); and high pavement temperatures ranging from northern to southern states. For each of the nine cells in table E2c.2, mixtures designed for the specified traffic level and known to have adequate rutting resistance will be nominated by members of the FHWA Mixtures and Construction Expert Task Group. Flow number data will be collected and analyzed using each of the five promising approaches listed in table E2c.1 and a confined flow number test with higher deviatoric stress as suggested by Mathy Engineering and Technical Services (MTE). The primary methods of analysis will be a graphical analysis to compare rutting resistance for each of the six approaches and statistical analysis of the rankings of the rutting resistance from the six approaches for the 9 mixtures included in the experiment. Information on the repeatability and reproducibility of unconfined and confined flow number tests that is

currently being collected in NCHRP Project 9-29 will also be used in recommending a flow number approach for mixture design.

Table E2c.2. Basic experimental design.

Design Traffic Level, MESAL <sup>2</sup>	Standard Binder Grade <sup>1</sup>	Promising Approaches from Table 1					High Deviatoric Stress Confined Flow Number
		NCHRP 9-33	NCAT	NCHRP 9-30A	UNR	NCHRP 9-26A	
3	PG 58-XX	X	X	X	X	X	X
	PG 64-XX	X	X	X	X	X	X
	PG 67-XX or greater	X	X	X	X	X	X
10	PG 58-XX	X	X	X	X	X	X
	PG 64-XX	X	X	X	X	X	X
	PG 67-XX or greater	X	X	X	X	X	X
30	PG 58-XX	X	X	X	X	X	X
	PG 64-XX	X	X	X	X	X	X
	PG 67-XX or greater	X	X	X	X	X	X

<sup>1</sup> Performance grade that would be used if bumping for traffic or speed is not considered. 10 and 30 MESAL designs will likely use binders with higher PG grade.

<sup>2</sup> NCHRP 9-30A defines design traffic as the total number of trucks (Vehicle Classes 4 through 13 based on FHWA classification).

Flow number testing will be performed at the AASHTO Materials Reference Laboratory (AMRL) by Dr. Haleh Azari and at the University of Nevada Reno (UNR) by Dr. Elie Hajj. The experimental plan requires the nine mixtures to be evaluated using each of the six approaches. Five of the approaches: NCHRP 9-33, NCAT, NCHRP 9-30A, NCHRP 9-26A, and high deviatoric stress confined flow number test each require testing three specimens at specific temperatures, confining pressure, and deviatoric stress. The 9-26A method requires 3 additional samples for each mix for developing the aging index. The UNR evaluation of mixture rutting resistance requires dynamic modulus testing to determine stresses in the pavement and flow number tests at multiple temperatures. The UNR evaluation requires testing 12 specimens; three for dynamic modulus, and nine for flow number. Thus for each of the nine mixtures, sufficient material for 30 AMPT specimens will be required. Sufficient material for 1000 lb of each mixture will be collected. From this amount, 500 lb will be shipped to UNR and 500 lb will be shipped to AMRL.

The testing will be conducted at AMRL and UNR. Funding for this testing will be provided by NCHRP for the testing at AMRL and the Asphalt Research Consortium for testing at UNR. Nine months have been provided for the testing analysis; assuming that the work will proceed at the rate of approximately one mixture per month. Final statistical analysis of the rankings of rutting resistance will be completed after all mixtures have been tested. The results will be evaluated by

the members of the Flow Number Task Force, and a report with recommendations will be submitted to the FHWA Mixtures and Construction Expert Task Group for further action.

### Significant Results

None

### Significant Problems, Issues and Potential Impact on Progress

None

### Work Planned for Next Quarter

The calculations of the 3D-Move model will continue to cover all the loading conditions that were described in the experimental plan for this work element.

Work will continue on the evaluation of the permanent deformation characteristics of laboratory-produced and field-produced mixtures under the testing conditions identified in Subtask E2c-1. The impact of air-voids, gradation, and binder type on the asphalt mixture critical temperature will also be evaluated.

Collect the material for the experimental plan developed by the Flow Number Task Force to develop criteria for asphalt concrete mixture design.

### Cited References

Advanced Asphalt Technologies, LLC, 2009, "Draft Final Report to the National Cooperative Highway Research Program (NCHRP) on Project NCHRP 9-33: A Mix Design Manual for Hot Mix Asphalt."

Willis, J.R., A. Taylor, N. Tran, A. Kvasnak, and A. Copeland, 2009, "Correlations Between Flow Number Test Results and Field Performance at the NCAT Pavement Test Track," Paper Submitted to the Transportation Research Board 89<sup>th</sup> Annual Meeting, 2010, Washington, D.C.

NCHRP, 2010, *Calibration of Rutting Models for HMA Structural and Mixture Design*, NCHRP Project 9-30A, Draft Final Report, National Cooperative Highway Research Program, Washington, DC.

Hajj, E. Y., A. Ullao, P.E. Sebaaly, and R.V. Siddharthan, 2010, "Characteristics of Dynamic Triaxial Testing of Asphalt Mixtures," Draft Final Report, Federal Highway Administration.

## **Work element E2d: Thermal Cracking Resistant Mixes for Intermountain States (UNR & UWM)**

### Work Done This Quarter

This work element is a joint project between University of Nevada Reno and University of Wisconsin–Madison.

The UNR team has been writing a final report for Subtask E2d-1 that is related to the analyses of the air and pavement temperature profiles data from LTPP Seasonal Monitoring Program (SMP) and WesTrack pavement sections. Six additional LTPP sections have been added to the project and analyzed. These 6 additional sections are located outside the intermountain region and are located at the following locations with the regions corresponding climatic classification:

- Opelika, AL (Wet, no-freeze)
- Ellendale, DE (Wet-freeze)
- East Dixfield, ME (Wet-freeze)
- Dawsonville, GA (Wet, no-freeze)
- Elizabeth City, NC (Wet, no-freeze)
- Oak Lake, Manitoba, CANADA (Dry-freeze)

A total of 20 LTPP sections have been made available for analysis which consist of 7 sections that are outside the intermountain region and 13 that are situated within. Analysis was conducted to determine any differences between the environmental conditions within the intermountain region and for areas outside this region. It was important to select areas throughout the U.S. and Canada that have different climatic regions.

The long-term oven aging process continued for the binders as described in the experimental plan for this work element. Table E2d.1 shows the work progress for the binder aging. Additionally, the completed aged binders are under testing for their rheological properties.

In this quarter, final adjustments were made to the new dilatometric test device of binders. A second dilatometric cell was added to the system to run two dilatometric tests simultaneously. The new cell was calibrated and, similar to the first cell, no volumetric corrections were deemed necessary.

A series of 11 binders, which includes eight binders extracted from the MnROAD test track and four binders extracted from sections in Olmsted County Road 112 near Rochester, Minn., was tested with two to three replicates. These binders are part of a thermal cracking study led by Western Research Institute, Mn/DOT and FHWA. The glass transition temperature ( $T_g$ ) was calculated using the nonlinear model proposed and tested as described in previous quarterly reports. Good repeatability was generally observed between replicates. The considerable difference in the measured  $T_g$  of different binders highlighted the ability of this test to discriminate the properties of the binders.

To better relate the  $T_g$  to low-temperature performance, all binders were also tested using the Asphalt Binder Cracking Device (ABCD). To account for variability, four replicates of each binder were tested in the ABCD system.

Table E2d.1. Binder aging matrix.

Aging Temp (°C)	Aging Period Unit	Aging Period	Binder Grade/Type				
			PG64-22	PG64-28NV	PG64-22 + 10% Lime	PG64-22 + 20% Lime	PG64-22 + 3% SBS
135	hours	8	AC	AC	AC	AC	AC
		15	AC	AC	AC	AC	AC
		30	AC	AC	AC	AC	AC
		44	AC	AC	AC	AC	AC
100	hours	44	AC	AC	AC	AC	AC
		90	AC	AC	AC	AC	AC
		150	AC	AC	AC	AC	AC
		240	AC	AC	AC	AC	AC
85	days	7.5	AC	AC	AC	AC	AC
		15	AC	AC	AC	AC	AC
		25	AC	AC	AC	AC	AC
		40	AC	AC	AC	AC	AC
60	days	30	AC	AC	AC	AC	AC
		60	AC	AC	AC	AC	AC
		100	AC	AC			
		160	AC	AC			
50	days	60	AC	AC	AC		AC
		120	AC	AC			
		200	AC	AC			
		320	AC	AC			
AC = Aging Completed							

Also in this quarter, the research team focused their efforts on development of the Single-Edge Notched Bending (SENB) test. The adhesion problem between the binder and the metal bars reported in the previous quarterly report for some binders was addressed by proposing new sample geometry, as shown in figure E2d.1. The new geometry adds a notch to the beams made using common Bending Beam Rheometer (BBR) molds, thus addressing the adhesion problem by eliminating the need for metal bars. Note that the sample preparation procedure is less time-consuming and simpler for the proposed BBR geometry.

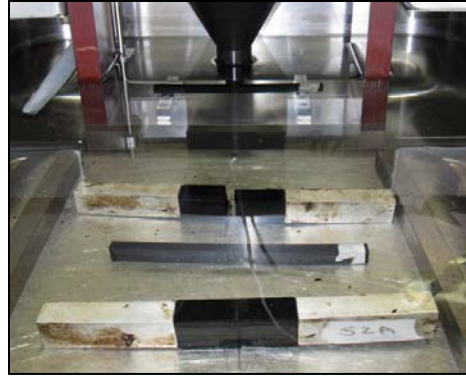


Figure E2d.1. Photograph. Current and newly proposed SENB geometry.

Comparing the cross sections of the existing SENB geometry (1-inch by 1/2-inch) to the BBR beams (1/2-inch by 1/4-inch), it can be seen that the proportions remain unchanged and that the new geometry scales the dimensions by one-half. Thus, it is expected that the stress and strain distributions of both geometries are similar. Finite element simulations of both geometries indicate that the stress distributions around the notch are very similar, as shown in figure E2d.2. Furthermore, the current SENB geometry shows stress discontinuity in the interface between the metal bars and the binders, which may have a significant effect on the results of the test.

The proposed beams can be prepared by making a notch of approximately 3 mm—corresponding to 20% to 25% of beam depth, similar to previous geometry—in the width (12.7 mm) of the BBR mold side beams. The mold can still be used for regular BBR beam fabrication, as the notch is very thin and it can be covered with plastic sheets used in molding.

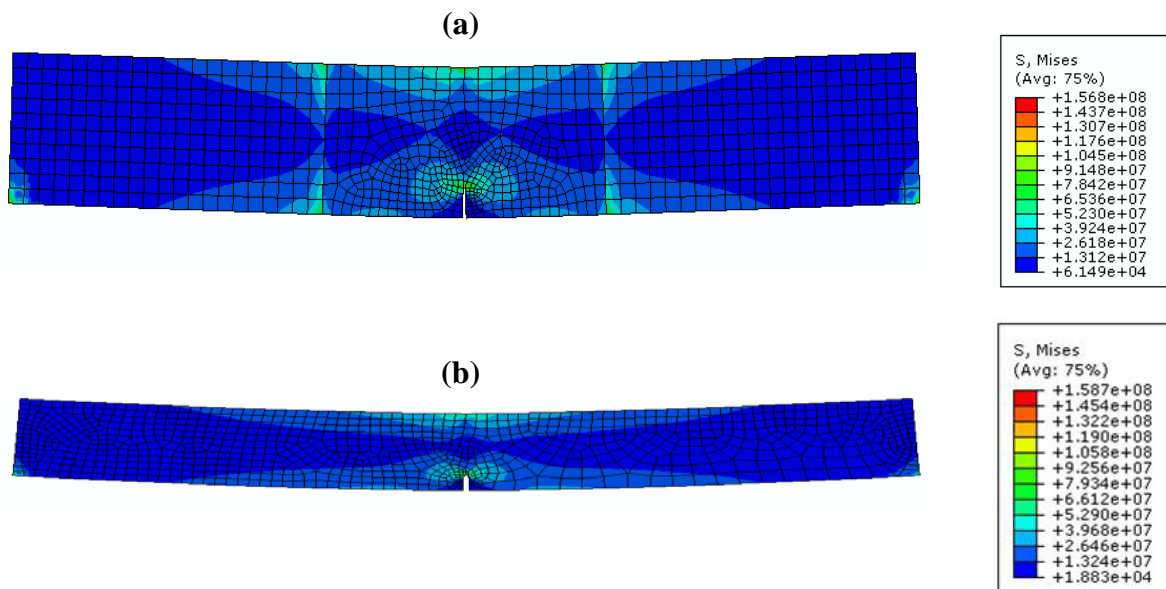


Figure E2d.2. Illustration. Stress distribution from finite element simulations: (a) the original SENB geometry; and (b) the proposed SENB geometry.

A series of tests were done to validate the use of such geometry. Some of the results are shown in figures E2d.3 and E2d.4. It can be seen in figure E2d.3 that a mastic sample with the previous geometry showed lower stiffness in comparison to the BBR sample. This may be due in part to compliance in the bond between the sample and the metal bars. Tests also showed that the repeatability of results using the new geometry is good and comparable to the repeatability of the previous geometry. Figure E2d.4 shows preliminary SENB test results using the new BBR geometry on the NCHRP Flint Hills binders with two modifiers. It can clearly be seen that the test is able to differentiate between the binders based on the type of modification.

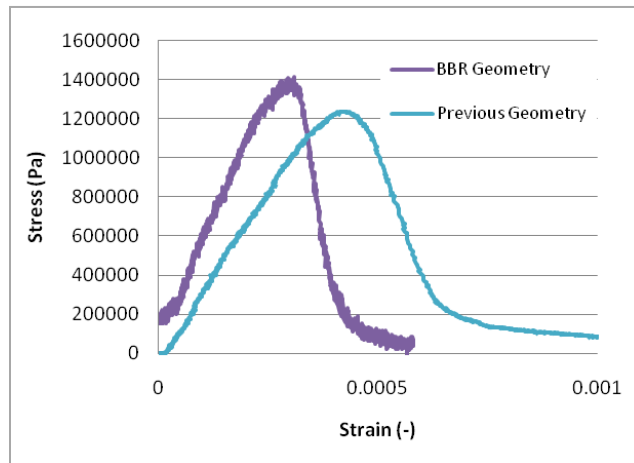


Figure E2d.3. Graph. Comparison between stress-strain curves for a mastic tested at -6 °C using the current and newly proposed SENB geometry.

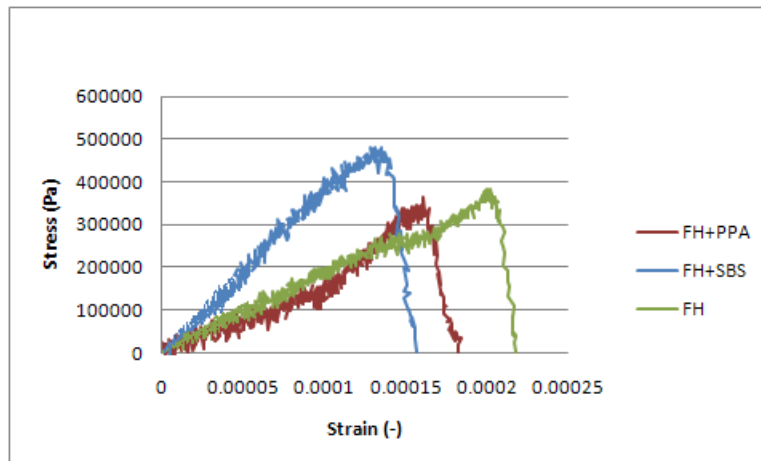


Figure E2d.4. Graph. SENB test results using the new BBR geometry on the NCHRP Flint Hills binders modified with polyphosphoric acid (PPA) and styrene-butadiene-styrene (SBS).

Also in this quarter, the research team worked on incorporating the Thermal Stress Restrained Specimen Test (TSRST) fixture into the  $T_g$  device. A rig was designed and built for TSRST testing. This frame restrains an asphalt mixture sample from contracting while it is subjected to cold temperatures. The research team plans to finalize the design and setup of a unified system to measure  $T_g$  of binders and mixtures as well as fracture strength of mixtures by the end of next quarter.

The current status of the aggregate absorption portion of subtask E2d3.b indicates all the mix designs have been completed with all the samples prepared and in the aging process in the oven.

Significant progress has been made in the  $E^*$ -compression testing with nearly all the testing being complete for this subtask, except for California which has only recently begun the aging process.

Further progress has been made in the  $E^*$ -tension area, with a useable test method being provided by Texas A&M University. Further work is still required to get the procedure ready for production testing as mechanical setbacks have slowed the progress in this area. However, it does now appear that it is possible to conduct this testing at UNR.

Significant progress has been made with the binder extraction process with final adjustments being made to the extraction and recovery process. These adjustments are necessary to assure adequate removal of the extraction solution, a toluene/ethanol blend. Verification of solvent removal is being checked utilizing chromatography techniques (GPC) with the assistance of Texas A&M University.

Further progress has also been made with the extracted binder testing. Previously the binder testing consisted of determining  $G^*$  and  $\delta$  over a range of high and intermediate temperatures using the traditional AASHTO M320 testing procedure. Efforts are now being exerted to complete binder master curves that include both temperature and strain dependency parameters. Considerations are also going to include zero shear or low shear viscosity, ZSV or LSV respectively. A testing and calculation program for the frequency sweep testing and calculation of the master curves is nearing completion with efforts on the complex viscosities to follow shortly.

The subtask E2d.3c: "Mix Characteristics," has seen significant progress in the area of sample preparation and  $E^*$  testing. Currently all the mix designs are complete with the samples having been prepared and are undergoing the aging process.

$E^*$ -compression testing is nearly 75% complete with the same efforts being extended to the  $E^*$ -tension, extraction/recovery procedure, binder master curves, and LSV determinations.

### Significant Results

A set of 11 binders was tested using the ABCD and the new dilatometric device to measure their critical cracking temperature and  $T_g$ , respectively. Figure E2d.5 shows a comparison between the results from these tests. It is observed that as the critical cracking temperature decreases, the  $T_g$

of the binder decreases as well. This preliminary observation indicates that there is a relationship between the  $T_g$  and the low-temperature cracking. More replicates are needed to further validate this conclusion for some of the binders that did not show satisfactory repeatability in the first set of tests. Also, the nature of the relationship of the two parameters must be further analyzed. The use of nonlinear models, such as a quadratic polynomial, improves the observed correlation.

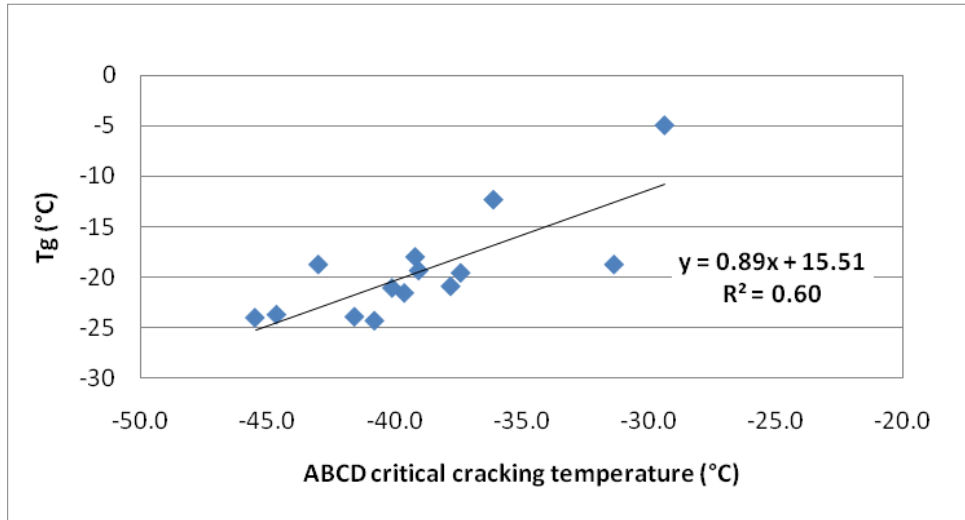


Figure E2d.5. Graph.  $T_g$  versus critical cracking temperature from the ABCD test.

### Significant Problems, Issues and Potential Impact on Progress

None.

### Work Planned Next Quarter

Continue the experiment to evaluate the aging characteristics (oxidation and hardening kinetics) of asphalt binders when aged in forced convection (horizontal airflow) ovens.

The research team will further investigate the relationship between  $T_g$  and low-temperature cracking in the next quarter, extending the scope to SENB tests as well.

Finite element analysis along with further validation testing will be carried out to finalize the SENB test procedure using the new proposed BBR beam geometry. The research team will begin conducting the test matrix for SENB of asphalt binders and mastics once the procedure is finalized.

Work will also continue on incorporating the TSRST fixture into the  $T_g$  device, allowing for a unified system that characterizes both binders and mixtures in terms of  $T_g$  and strength for estimation of resistance to thermal cracking.

Continue the work on the impact of aggregate absorption and gradation on the aging of the asphalt binder. Activities on the mixtures will include continuation of sample aging in ovens, E\* testing in compression, and implementation of E\* tension testing. Following the mixture tests, the samples will then be extracted and recovered for DSR and FTIR testing.

A thermal cracking meeting will be hosted by Granite construction in Reno Nevada on Friday May 7, 2010. The purpose of the meeting is to discuss the details of the binders aging model, mixtures aging model, and thermal stresses model. The meeting will be attended by Drs. Hussain Bahia from University of Wisconsin, Adam Hand from Granite Construction Inc., Charles Glover from Texas A&M, Raj Siddharthan, Peter Sebaaly and Elie Hajj from University of Nevada Reno.

## **Work element E2e: Design Guidance for Fatigue and Rut Resistance Mixtures (AAT)**

### Work Done This Quarter

An extended uniaxial fatigue experiment was conducted to verify that the analytical techniques being used by AAT over the past several years can be used to collapse uniaxial fatigue data gathered over a wide range of temperatures, frequencies and strains. This verification was necessary because recent uniaxial fatigue data collected using the Interlaken AMPT did not collapse nearly as cleanly as data gathered previously using AAT's larger Interlaken servo-hydraulic test system. It was determined that part of the problem was that initial tests using the AMPT were done using strain control mode; this causes a problem during testing because the loading tends to gradually drift into compression, which can reduce the damage rate and cause damage curves to flatten in an unpredictable way. After changing the testing mode to stress control, the damage curves improved, but still did not appear to collapse quite as well as data gathered earlier. Several explanations for the problem are possible: (1) experimental error; (2) a problem with fatigue loading using the AMPT; (3) the analytical approach used by AAT is not always accurate; or (4) there is a transition in behavior—perhaps a brittle-ductile transition—that requires a slightly different analysis depending on which region the test data is gathered in. This extended test program was performed to verify that the analytical techniques being used are effective, and also to evaluate whether or not there is a brittle-ductile transition in HMA fatigue data that requires a slightly different analytical approach, for example, different  $\alpha$  values and/or different shift factors.

### *Experiment Design*

A total of 21 specimens of an HMA were tested using AAT's large Interlaken servo-hydraulic test system. Test conditions are as listed in Table E2e.1.

Table E2e.1. Extended uniaxial fatigue experiment, test temperatures, frequencies and strain levels.

Nominal Test Temperature °C	Test Frequency Hz	Low Strain, Initial Strain Level × 10 <sup>6</sup>	High Strain, Initial Strain Level × 10 <sup>6</sup>	Very High Strain, Initial Strain Level × 10 <sup>6</sup>
-5	1	160	330	---
-5	10	155	300	---
4	1	170	390	---
4	10	160	360	---
10	1	170	410	---
10	10	170	420	---
20	1	215	620	1,400
20	10	180	510	---
30	1	580	910	---
30	10	200	540	---

*Material and Test Procedure*

The HMA used in the experiment was a 9.5 mm mixture that was sampled from during plant production. Table E2e.2 summarizes pertinent design properties for the mixture.

Table E2e.2. Design Properties for HMA Mixture.

Properties		Value
Design Traffic Level, MESAL		<3
Design Gyration Level		75
Gradation	Sieve Size, mm	
	25	100
	19	100
	12	100
	9.5	98
	4.75	72
	2.36	46
	1.18	26
	0.6	17
	0.3	11
	0.15	8
0.075	5.0	
Binder Content, wt %		5.9
Fine Aggregate Angularity, vol %		45.2
Crushed Aggregate Fractured Faces, %		100/100
Design VMA,%		16.2
Design VFA,%		75.5

The specimens were prepared to an air void content of  $7\pm 1$  % using gyratory compaction. Specimens 100 mm in diameter were cored from 150 mm diameter gyratory specimens. Final nominal dimensions of the specimens were 100 mm diameter by 150 mm high. The gauge length used in testing was 100 mm.

The number of loading cycles used to test each specimen varied with frequency and strain level. Specimens tested at low strain and 10 Hz were typically loaded for about 108,000 cycles; low strain specimens tested at 1 Hz were typically loaded for about 10,800 cycles. Specimens tested at high strains usually failed prior to reaching the end of the planned loading. Total loading cycles for these specimens typically ranged from about 1,000 to about 10,000 cycles.

### *Analysis*

The reduced cycles analytical approach was used, as described in Christensen and Bonaquist's AAPT Paper (Christensen and Bonaquist 2008). The original approach suggested by Christensen and Bonaquist involved using a constant  $\alpha$  value of 2.20. However, some evidence was seen during the analysis that the value of  $\alpha$  in fact varied depending upon the properties of the HMA at the given test temperature and frequency. For this reason, two alternate approaches were also evaluated. In the first,  $\alpha$  was calculated from the measured initial phase angle of the specimen. In the second approach,  $\alpha$  was calculated from the phase angle value as estimated from the measured initial modulus. This last approach was included in the analysis because in many cases fatigue test data does not include measurements of phase angle; this last approach can be used to analyze such data using the variable- $\alpha$  approach.

An important aspect of analyzing fatigue data using continuum damage methods is the determination of the initial modulus value. This can have a significant effect on the results of the analysis. Several different methods can be used to determine the initial modulus value. One that AAT has often used is non-linear least squares—initial modulus values are included in the analysis as variables that are determined by statistical methods. This approach could not be used in this case because of the very large size of the experiment—the number of initial modulus values in combination with the large number of other variables made this approach impractical. The other method most often used by AAT in analyzing continuum damage data—and the approach ultimately used in this experiment—is the simple graphical method; modulus values are plotted as a function of loading cycles, and the initial value estimated from these plots. Values can be further refined during the analysis to form a better collapse of the data curve, as long as these adjustments are minor and consistent with the plots of modulus versus loading cycles.

### *Results*

The results of the extended fatigue experiment are illustrated graphically in figures E2e.1 through E2e.3. Figure E2e.1 shows the master fatigue damage curve as generated using a single value of  $\alpha$  (2.20). The collapse of the individual curves in this case was adequate, although there are several high-strain damage curves that fall below the master curve, hanging down like “tails” from most of the other data. This could be evidence of poor collapse of the data, but could also

indicate that these specimens had begun to localize (fail), and that continuum damage analysis no longer applied for these cases. It should be noted that the 1 Hz data at 30°C was not used in any of the analyses; the damage curves for these data was not at consistent with the other damage curves and was eliminated from the data set. The reasons for this inconsistency are not clear, but the modulus values were quite low (about 100,000 lb/in<sup>2</sup>) and the applied strain values very high (580 × 10<sup>-6</sup> and 910 × 10<sup>-6</sup>). It could be that the HMA under these conditions is too soft to test properly in fatigue, or that continuum damage theory no longer applies under these conditions. It is also possible that self heating becomes significant at such high strains and affects the resulting data, although some of the strains used in the data collected at 20°C were just as high or even higher. For the time being, it is suggested that uniaxial fatigue data gathered at initial modulus values less than about 150,000 lb/in<sup>2</sup> is in general suspect.

Figure E2e.2 shows the master fatigue curve as generated using variable  $\alpha$  values—in this case,  $\alpha$  values calculated from the measured initial values for the phase angle. The equation used was found through trial and error:

$$\alpha = 2.00 + 0.10 \left( \frac{90}{\delta} \right) \quad (\text{E2e.1})$$

Where  $\delta$  is the initial phase angle in degrees. Phase angle values in the data set varied from 6.4° at -5°C and 10 Hz to 37.0° at 30°C and 10 Hz. From equation E2e.1, this resulted in  $\alpha$  values ranging from 2.25 to 3.41. In this plot, the “tails” have largely been removed, with the exception of one point (4°C, 10 Hz, high strain). The fact that significantly better collapse of the data was achieved using variable  $\alpha$  values suggests that this is a more appropriate approach than using a fixed value for  $\alpha$ . On the other hand, the range for  $\alpha$  is relatively narrow, and for moderate temperatures and many HMA mixes using a typical value of 2.20 will probably provide adequate results.

Figure E2e.3 is similar to figure E2e.2 in that  $\alpha$  values were allowed to vary. However, in this case phase angle values were estimated from modulus values, and these estimated phase angle values were then used to calculate  $\alpha$ . The reason this analysis was included was because in many fatigue data sets—such as the large amount of data collected during NCHRP Projects 9-25/31—phase angle data does not exist. This approach would be very useful in analyzing such data. In fact, the collapse of the data appears to be as good as in the analysis where measured phase angles were used to calculate  $\alpha$ . However, a different equation had to be used to achieve good collapse:

$$\alpha = 1.50 + 0.25 \left( \frac{90}{\delta} \right) \quad (\text{E2e.2})$$

The method used for estimating the phase angle was based upon data used in NCHRP 9-25/31 to develop the Hirsch model for estimating the modulus of HMA (Christensen et al. 2003; Christensen and Bonaquist 2006). Two different equations are used to estimate the phase angle, depending on the HMA modulus values:

For modulus values less than 270,000 lb/in<sup>2</sup>:

$$\delta = -15.55 + 9.649 \log |E^*| \quad (\text{E2e.3})$$

Where  $\delta$  is the phase angle in degrees, and  $|E^*|$  is the dynamic modulus in lb/in<sup>2</sup>. For modulus values greater than or equal to 270,000 lb/in<sup>2</sup>:

$$\delta = 180.6 - 26.46 + 9.649 \log |E^*| \quad (\text{E2e.4})$$

Where  $\delta$  and  $|E^*|$  are as defined for equation E2e.2.

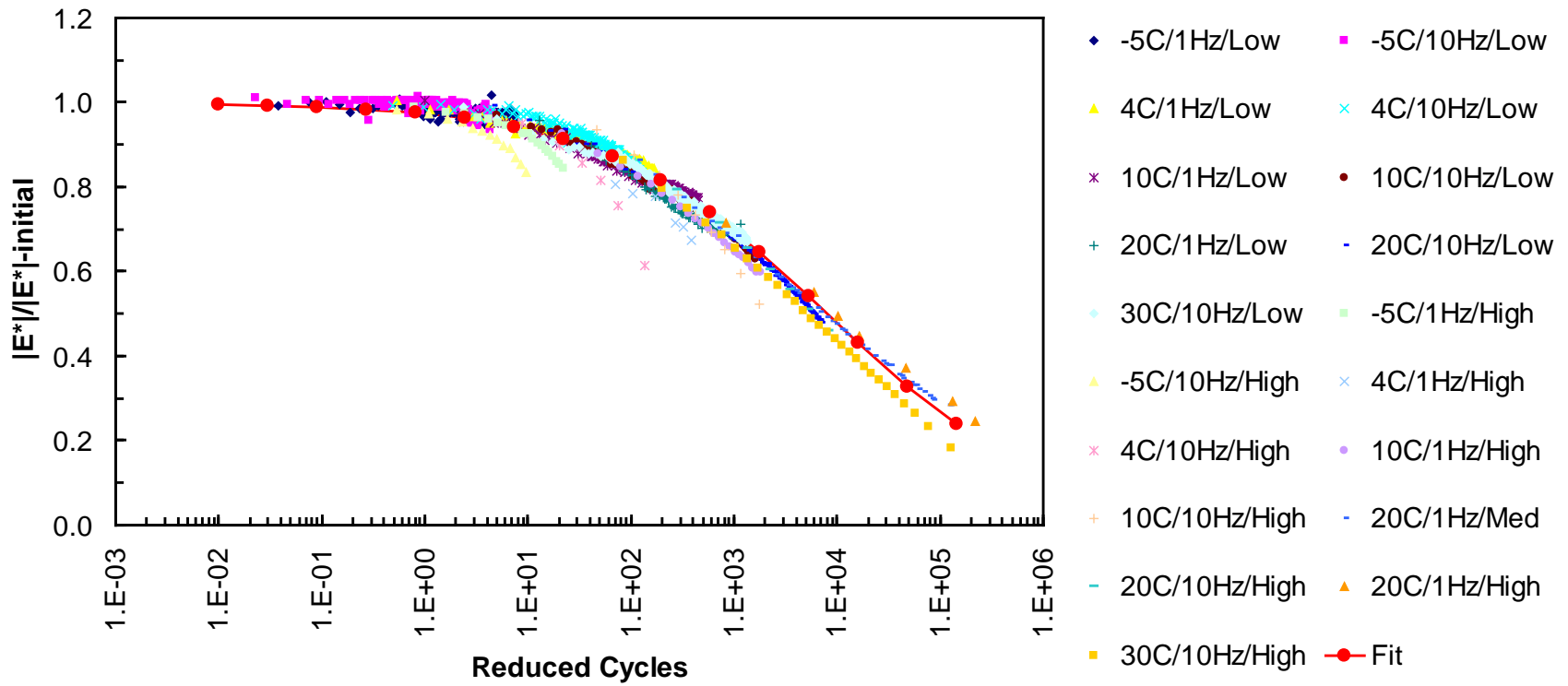


Figure E2e.1. Data curve for extended fatigue experiment as generated using single  $\alpha$  value of 2.2.

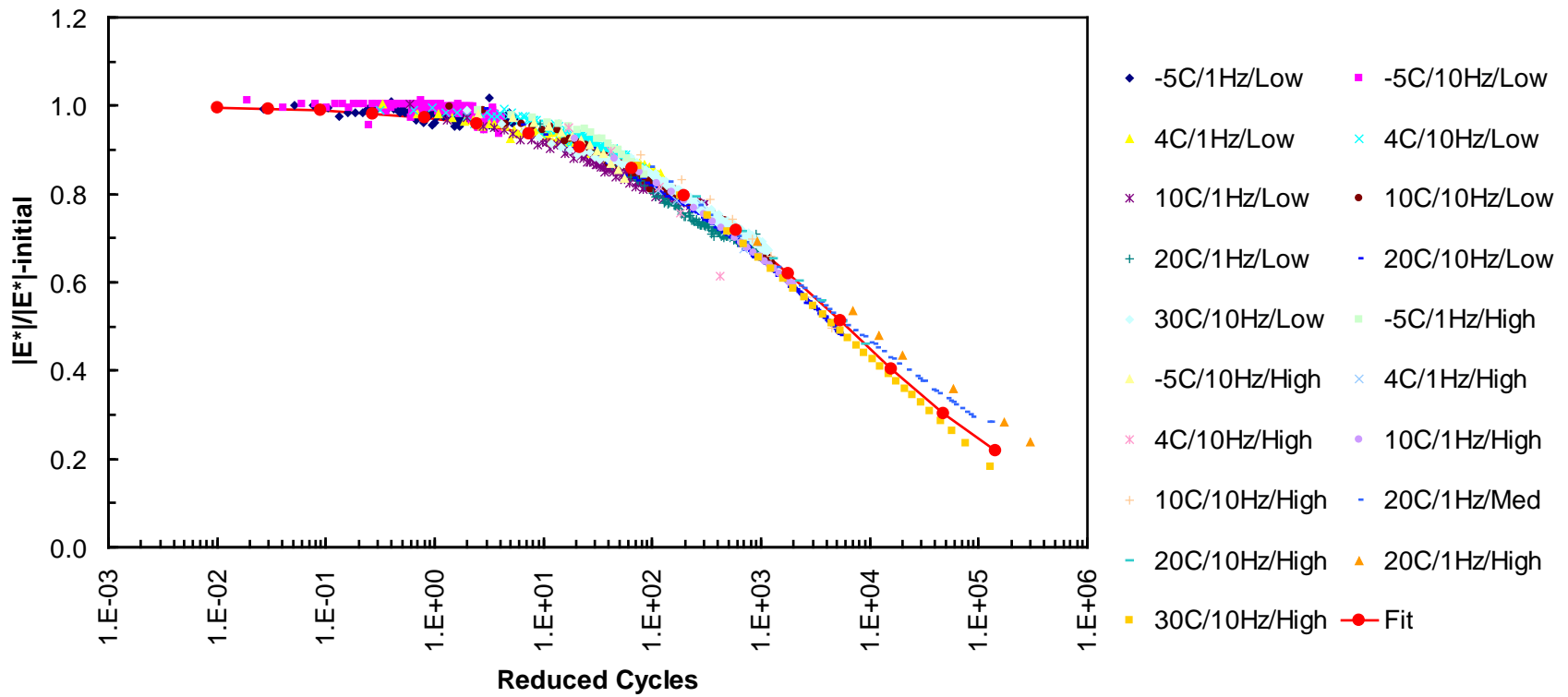


Figure E2e.2. Damage curve for extended fatigue experiment as generated using  $\alpha$  values calculated from measured initial phase angles.

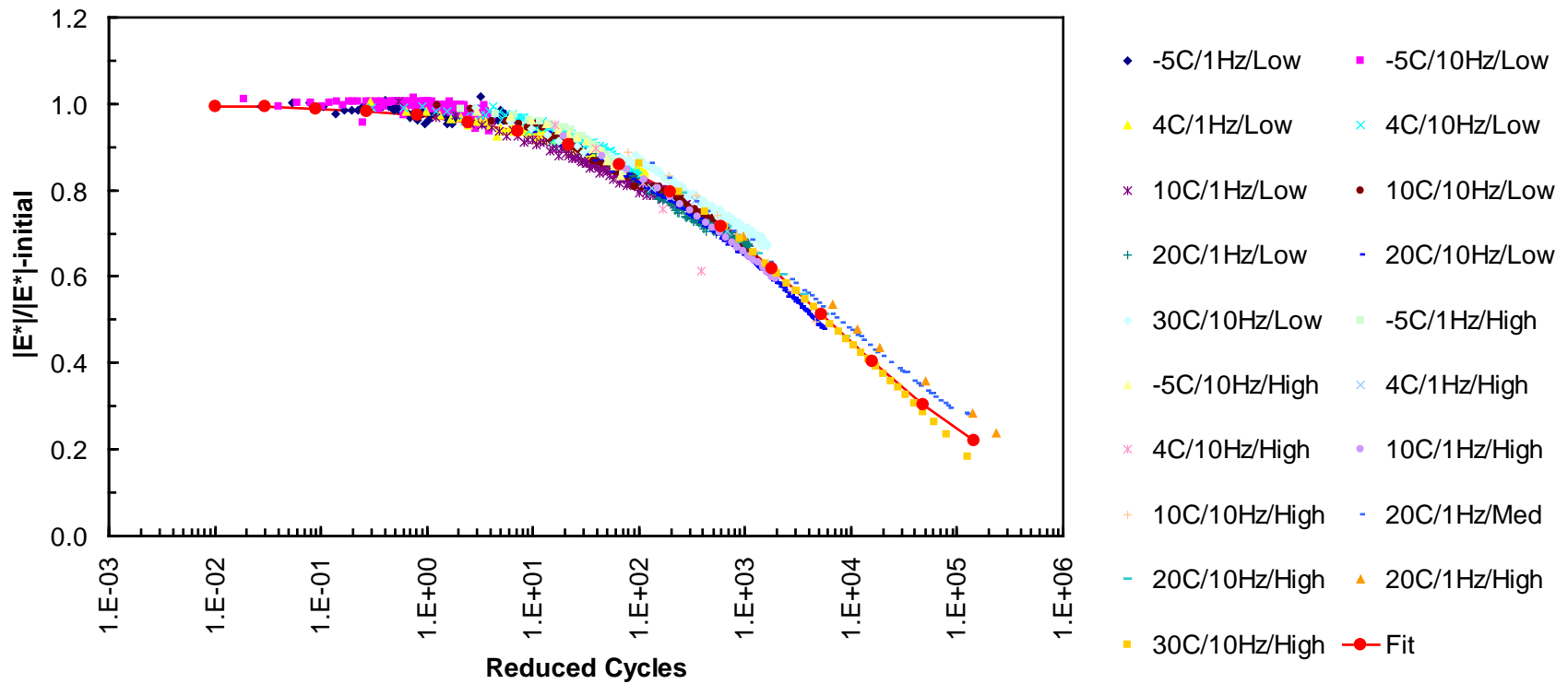


Figure E2e.3. Damage curve for extended fatigue experiment as generated using  $\alpha$  values calculated from initial phase angles estimated from initial modulus values.

## Discussion

It is essential to note that when using variable  $\alpha$  values in the analysis, it was found that selecting an appropriate value for the reference modulus and strain was essential to achieving proper collapse of the data. The theoretical reasons for this are not clear at this time. However, it is clear that applying different values of  $\alpha$  to the reference values of modulus and strain will tend to shift the damage curves towards higher or lower values of reduced cycles. Similarly, using different reference values will result in larger or smaller shifts as  $\alpha$  varies. It is hypothesized here that damage curves do in fact shift with changes in  $\alpha$ , and that reference values for modulus and strain must be selected to account for this shift. Note that it is not the individual values of reference modulus and strain that matter in this situation, but the product of the reference values. For this reason, it might be more appropriate to speak of a reference stress, since modulus  $\times$  strain = stress. In this particular data set, it was found that good collapse was generated when the reference value for modulus was  $2.0 \times 10^6$  lb/in<sup>2</sup> and the reference value for strain  $200 \times 10^{-6}$ . This corresponds to a reference stress of 400 lb/in<sup>2</sup>.

In the experiment design, tests at two different frequencies were included—10 Hz and 1 Hz. It was found that there was a slight mismatch in damage curves found from the two different frequencies. This difference could be reconciled by raising the frequency factor, given as  $(f_R/f)$  to the 1.40 power. The source of this correction is not known at this time, but might result from some minor error in the derivation of existing equations based on continuum damage theory.

Another important question stemming from this analysis is the relationship between  $\alpha$  and the phase angle. It was proposed by Schapery and has been more or less confirmed by other researchers that a relationship exists between  $\alpha$  and the log-log slope of the master curve  $m$ . Lee and Kim have reported that for their analyses  $\alpha = 1 + 1/m$ , while Kim, Little and Litton have reported  $\alpha = 1 + m$  (Kim et al. 2002). The relationships given above in equations E2e.1 and E2e.2 are much different from these (remembering  $m = \delta/90$ ), suggesting a much weaker relationship between  $\alpha$  and the phase angle or  $m$  value. It is possible that rather than relating to the phase angle of the mix that  $\alpha$  should relate to the phase angle of the binder, since the only visco-elastic material in the mix is the binder. To evaluate this possibility, binder modulus values were back-calculated for the test data using the Hirsch model, and these binder modulus values were in turn used to calculate binder phase angle values using the Christensen-Anderson model, assuming a typical  $R$  value of 2.0 (Christensen et al. 2003; Christensen and Bonaquist 2006; Christensen and Anderson 1992). These phase angle values were then used to estimate values for  $\alpha$ , to determine if good collapse could be achieved using this approach, and if the resulting relationship seemed more reasonable than that between the mix phase angle and  $\alpha$ . The results are shown in figure E2e.4; although the collapse is not quite as good as in figures E2e.2 and E2e.3, it is nevertheless quite good, especially considering the binder phase angles have been back-calculated using a number of assumptions of unknown accuracy. The relationship between  $\alpha$  and  $m$  implied in this figure is  $\alpha = 3/2m$ , which is closer to relationships reported in the literature.

In all four analyses, the shift factors were calculated using the Williams Landel Ferry (WLF) as developed by Christensen and Anderson for use in characterizing asphalt binders (Christensen

and Anderson 1992), with a defining temperature (glass transition temperature) of 0°C. The equation for calculating the damage ratio  $C$  as a function of reduced cycles is as given by Christensen and Bonaquist, but with a value of  $K_2$  of 0.4 rather than 0.5 (Christensen and Bonaquist 2008). The values for  $K_1$  are given in Table E2e.2.

Table E2e.2. Values of  $K_1$  for different analyses of the extended fatigue experiment data.

Figure	Analytical Method	Value of $K_1$
1	Alpha fixed at 2.2	8,000
2	Alpha varies with phase angle	6,000
3	Alpha varies with phase angle as estimated from modulus	6,000
4	Alpha varies with estimated binder phase angle	6,000

Preliminary attempts were made to analyze data from this experiment using a traditional approach to continuum damage analysis. However, reasonable collapse of the data could not be achieved. The reason for this is not clear. It should be noted that damage master curves reported in the literature have all been shown using a log scale for the damage parameter  $S$ . In general, these types of plots totally hide any lack of fit in most of the data, so it is possible that traditional methods of collapsing continuum damage curves produce significantly poorer collapse than the reduced cycles approach used here. As an example of how poor collapse of damage curves may not be clear when a linear horizontal scale is used, figures E2e.5 and E2e.6 are shown below. For both plots, the value for the reference modulus was set incorrectly to  $3.0 \times 10^5$  lb/in<sup>2</sup>, resulting in a very poor collapse of the individual damage curves. However, this poor collapse is not really clear in figure E2e.5, where a linear scale for reduced cycles is used. However, when a log scale for reduced cycles is used (figure E2e.6), it is clear that the collapse of the damage curves is very poor. It is clear that both linear and log scales must be used when evaluating the quality of master damage curves generated using continuum damage methods.

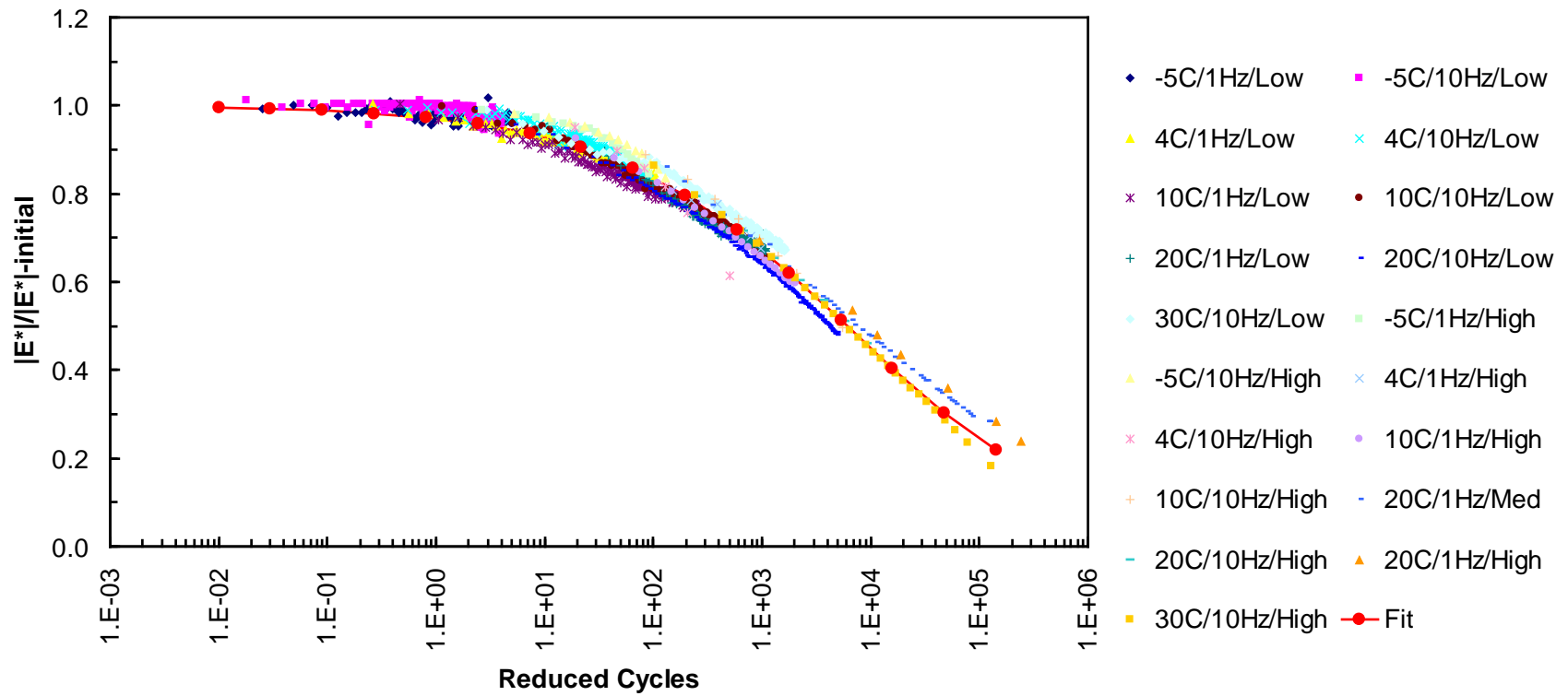


Figure E2e.4. Damage curve for extended fatigue experiment as generated using  $\alpha$  values calculated from estimated binder phase angles.

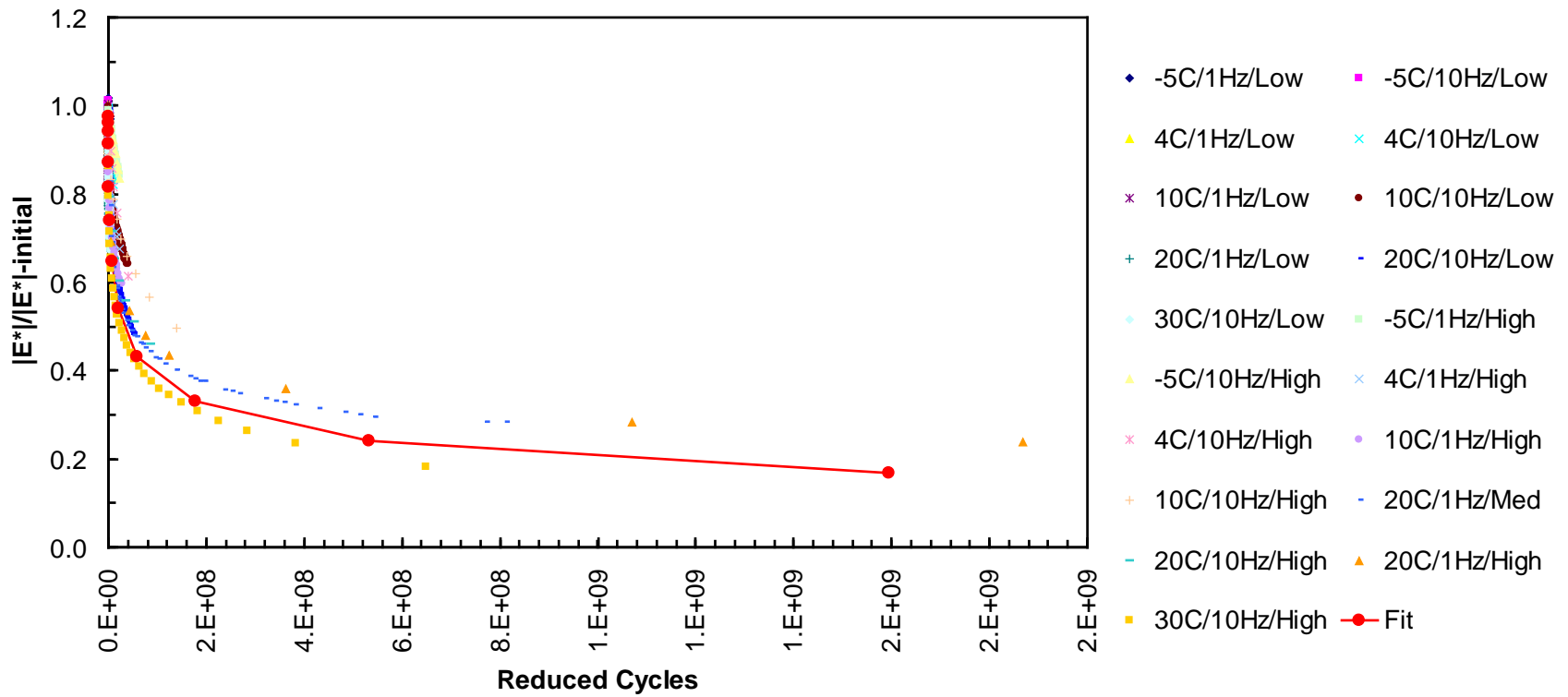


Figure E2e.5. Damage curve for extended fatigue experiment as generated using inappropriate value for the modulus reference value ( $3.0 \times 10^5 \text{ lb/in}^2$ ), linear horizontal scale.

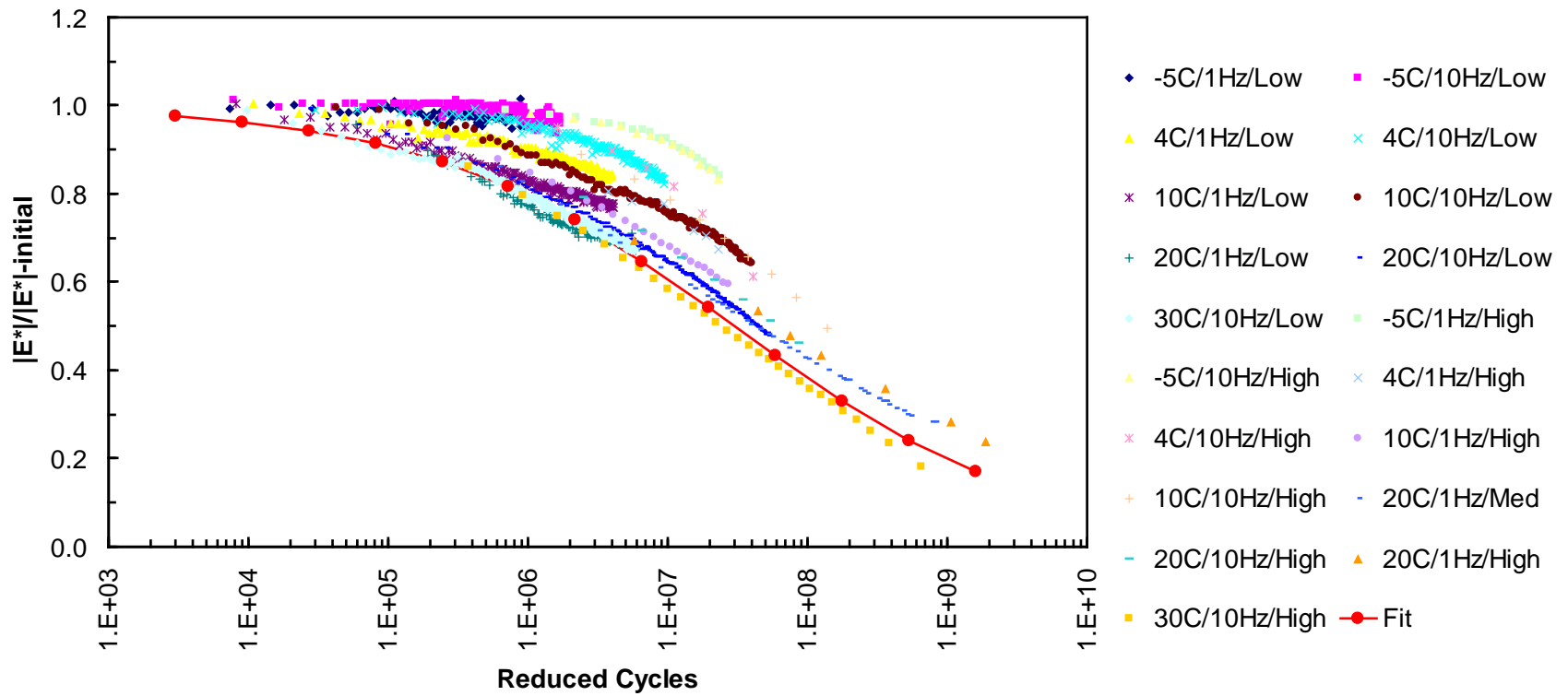


Figure E2e.6. Damage curve for extended fatigue experiment as generated using inappropriate value for the modulus reference value ( $3.0 \times 10^5 \text{ lb/in}^2$ ), log horizontal scale.

### Significant Results

The extended uniaxial fatigue experiment confirmed that the reduced cycles approach could be used to generate master fatigue curves using tests conducted over a wide range of temperatures, frequencies, and strain levels.

### Significant Problems, Issues and Potential Impact on Progress

None.

### Work Planned Next Quarter

Additional work generating master damage curves using standard methods (as opposed to reduced cycles) will be performed in the coming quarter. This work will focus on whether or not standard methods in fact result in appropriate collapse of damage curves to a single damage function.

### Cited References

Christensen, D.W., and D.A. Anderson, 1992, Interpretation of Dynamic Mechanical Test Data for Paving Grade Asphalt Cements. *Journal of the Association of Asphalt Paving Technologists*, Vol. 61.

Christensen, D.W., and R.F. Bonaquist, 2008, Analysis of HMA Fatigue Data Using the Concepts of Reduced Loading Cycles and Endurance Limit. *Journal of the Association of Asphalt Paving Technologists*, Vol. 77.

Christensen, D.W., and R.F. Bonaquist, 2006, *NCHRP Report 567: Volumetric Requirements for Superpave Mix Design*, Final Report for NCHRP Projects 9-25 and 9-31, Washington, D. C.: Transportation Research Board, 57 pp.

Christensen, D.W., T. Pellinen, and R.F. Bonaquist, 2003, Hirsch Model for Estimating the Modulus of Asphalt Concrete. *Journal of the Association of Asphalt Paving Technologists*, 72, 97-121.

Kim, Y.R., Dallas N. Little, and Robert R. Lytton, 2002, Use of Dynamic Mechanical Analysis (DMA) to Evaluate the Fatigue and Healing Potential of Asphalt Binders in Sand Asphalt Mixtures. *Journal of the Association of Asphalt Paving Technologists*, 71, 176-199.

Engineered Materials Year 3	Year 3 (4/2009-3/2010)												Team
	4	5	6	7	8	9	10	11	12	1	2	3	
<b>(1) High Performance Asphalt Materials</b>													
E1a: Analytical and Micro-mechanics Models for Mechanical behavior of mixtures													TAMU
E1a-1: Analytical Micromechanical Models of Binder Properties													
E1a-2: Analytical Micromechanical Models of Modified Mastic Systems													
E1a-3: Analytical Models of Mechanical Properties of Asphalt Mixtures			JP	P	JP(2)				P(2)	P	P	M&A	
E1a-4: Analytical Model of Asphalt Mixture Response and Damage				P	JP(2)				P(3)	P(5)	P		
E1b: Binder Damage Resistance Characterization													UWM
E1b-1: Rutting of Asphalt Binders													
E1b-1-i. Literature Review													
E1b-1-ii. Select Materials & Develop Work Plan													
E1b-1-iii. Conduct Testing					JP						P		
E1b-1-iv. Analysis & Interpretation					JP						P		
E1b-1-v. Standard Testing Procedure and Recommendation for Specifications													
E1b-2: Feasibility of determining rheological and fracture properties of asphalt binders and mastics using simple indentation tests (modified title)													UWM
E1b-2-i. Literature Review													
E1b-2-ii. Proposed SuperPave testing modifications						P							
E1b-2-iii. Preliminary testing and correlation of results										D			
E1b-2-iv. Feasibility of using indentation tests for fracture and rheological properties										D	P	JP	
E2a: Comparison of Modification Techniques													UWM
E2a-1: Identify modification targets and material suppliers					DP							P	
E2a-2: Test material properties													
E2a-3: Develop model to estimate level of modification needed and cost index													
E2a-4: Write asphalt modification guideline/report on modifier impact over binder properties													
E2c: Critically Designed HMA Mixtures													UNR
E2c-1: Identify the Critical Conditions					JP		D				F		
E2c-2: Conduct Mixtures Evaluations											D		
E2c-3: Develop a Simple Test													
E2c-4: Develop Standard Test Procedure													
E2c-5: Evaluate the Impact of Mix Characteristics													
E2d: Thermal Cracking Resistant Mixes for Intermountain States													UWM/UNR
E2d-1: Identify Field Sections									D				
E2d-2: Identify the Causes of the Thermal Cracking			D										
E2d-3: Identify an Evaluation and Testing System		DP						DP		D		JP	
E2d-4: Modeling and Validation of the Developed System													
E2d-5: Develop a Standard													
E2e: Design Guidance for Fatigue and Rut Resistance Mixtures													AAT
E2e-1: Identify Model Improvements												P	
E2e-2: Design and Execute Laboratory Testing Program													
E2e-3: Perform Engineering and Statistical Analysis to Refine Models													
E2e-4: Validate Refined Models													
E2e-5: Prepare Design Guidance													
<b>(2) Green Asphalt Materials</b>													
E2b: Design System for HMA Containing a High Percentage of RAP Material													UNR
E2b-1: Develop a System to Evaluate the Properties of RAP Materials		D			JP				F	P			
E2b-2: Compatibility of RAP and Virgin Binders													
E2b-3: Develop a Mix Design Procedure										D			
E2b-4: Impact of RAP Materials on Performance of Mixtures													
E2b-5: Field Trials													
E1c: Warm and Cold Mixes													UWM
E1c-1: Warm Mixes													
E1c-1-i. Effects of Warm Mix Additives on Rheological Properties of Binders													
E1c-1-ii. Effects of Warm Mix Additives on Mixture Workability and Stability					JP								
E1c-1-iii. Mixture Performance Testing											P	DP	
E1c-1-iv. Develop Revised Mix Design Procedures													
E1c-1-v. Field Evaluation of Mix Design Procedures and Performance Recommendations													
E1c-2: Improvement of Emulsions' Characterization and Mixture Design for Cold Bitumen Applications													UWM/UNR
E1c-2-i. Review of Literature and Standards		D1					D3						
E1c-2-ii. Creation of Advisory Group													
E1c-2-iii. Identify Tests and Develop Experimental Plan		D1								D5			
E1c-2-iv. Develop Material Library and Collect Materials													
E1c-2-v. Conduct Testing Plan					JP			D4			P		
E1c-2-vi. Develop Performance Selection Guidelines													
E1c-2-vii. Validate Performance Guidelines					D2								
E1c-2-viii. Develop CMA Mix Design Guidelines													
E1c-2-ix. Develop CMA Performance Guidelines													

**Deliverable codes**  
D: Draft Report  
F: Final Report  
M&A: Model and algorithm  
SW: Software  
JP: Journal paper  
P: Presentation  
DP: Decision Point

**Deliverable Description**  
Report delivered to FHWA for 3 week review period.  
Final report delivered in compliance with FHWA publication standards  
Mathematical model and sample code  
Executable software, code and user manual  
Paper submitted to conference or journal  
Presentation for symposium, conference or other  
Time to make a decision on two parallel paths as to which is most promising to follow through

 Work planned  
 Work completed  
 Parallel topic

Engineered Materials Year 2 - 5	Year 2 (4/08-3/09)				Year 3 (4/09-3/10)				Year 4 (04/10-03/11)				Year 5 (04/11-03/12)				Team
	Q1	Q2	Q3	Q4	Q1	Q2	Q3	Q4	Q1	Q2	Q3	Q4	Q1	Q2	Q3	Q4	
<b>(1) High Performance Asphalt Materials</b>																	
E1a: Analytical and Micro-mechanics Models for Mechanical behavior of mixtures																	
E1a-1: Analytical Micromechanical Models of Binder Properties				P, JP	JP	P	P		M&A	D	F, SW						TAMU
E1a-2: Analytical Micromechanical Models of Modified Mastic Systems				P, JP	JP	P	P		M&A	JP	D	F, SW					
E1a-3: Analytical Models of Mechanical Properties of Asphalt Mixtures	P	P, JP		P, JP	JP	P	P	P, M&A			D	SW, JP	F				
E1a-4: Analytical Model of Asphalt Mixture Response and Damage				P, JP	JP	P	P	P	M&A	D	F, JP	SW					
E1b: Binder Damage Resistance Characterization																	
E1b-1: Rutting of Asphalt Binders																	
E1b-1-1: Literature review																	
E1b-1-2: Select Materials & Develop Work Plan	DP, P		P														
E1b-1-3: Conduct Testing			P			JP		P									
E1b-1-4: Analysis & Interpretation		JP	P	JP		JP		P			JP						
E1b-1-5: Standard Testing Procedure and Recommendation for Specifications										P		DP	P	D	JP	F	
E1b-2: Feasibility of Determining rheological and fracture properties of asphalt binders and mastics using simple indentation tests (modified title)																	
E1b-2i: Literature Review																	
E1b-2ii: Proposed SuperPave testing modifications or new testing devices						P											
E1b-2iii: Preliminary testing and correlation of results								D									
E1b-2iv: Feasibility of using indentation tests for fracture and rheological properties								D, P, JP		F							
E2a: Comparison of Modification Techniques																	
E2a-1: Identify modification targets and material suppliers				DP		DP											UWM
E2a-2: Test material properties								P									
E2a-3: Develop model to estimate level of modification needed and cost index																	
E2a-4: Write asphalt modification guideline/report on modifier impact over binder properties																	
E2c: Critically Designed HMA Mixtures																	
E2c-1: Identify the Critical Conditions		JP		D, F		JP	D	F									UNR
E2c-2: Conduct Mixtures Evaluations								D	D, F	JP				D, F	JP		
E2c-3: Develop a Simple Test																	
E2c-4: Develop Standard Test Procedure														D, F			
E2c-5: Evaluate the Impact of Mix Characteristics																D, F	
E2d: Thermal Cracking Resistant Mixes for Intermountain States																	
E2d-1: Identify Field Sections			D, F	D, F			D										UWM/UNR
E2d-2: Identify the Causes of the Thermal Cracking						D			D, F	JP							
E2d-3: Identify an Evaluation and Testing System					DP	JP	DP, D						D, F	JP			
E2d-4: Modeling and Validation of the Developed System																D, F	
E2d-5: Develop a Standard																D, F	
E2e: Design Guidance for Fatigue and Rut Resistance Mixtures																	
E2e-1: Identify Model Improvements																	
E2e-2: Design and Execute Laboratory Testing Program								P									AAT
E2e-3: Perform Engineering and Statistical Analysis to Refine Models										JP		P, D, F					
E2e-4: Validate Refined Models														JP			
E2e-5: Prepare Design Guidance															M&A	P, D, F	
<b>(2) Green Asphalt Materials</b>																	
E2b: Design System for HMA Containing a High Percentage of RAP Material																	
E2b-1: Develop a System to Evaluate the Properties of RAP Materials		JP		P	D	JP	F	P									UNR
E2b-2: Compatibility of RAP and Virgin Binders														D, F	JP		
E2b-3: Develop a Mix Design Procedure								D						D, F	JP		
E2b-4: Impact of RAP Materials on Performance of Mixtures																D, F	
E2b-5: Field Trials																D, F	
E2c: Warm and Cold Mixes																	
E1c-1: Warm Mixes																	
E1c-1i: Effects of Warm Mix Additives on Rheological Properties of Binders.																	UWM
E1c-1iii: Effects of Warm Mix Additives on Mixture Workability and Stability	P		D	F, DP		JP											UWM
E1c-1iii: Mixture Performance Testing								P, DP									UW/UNR
E1c-1iv: Develop Revised Mix Design Procedures									JP	P							UW/UNR
E1c-1v: Field Evaluation of Mix Design Procedures and Performance Recommendations														JP	D	P, F	UW/UNR
E1c-2: Improvement of Emulsions' Characterization and Mixture Design for Cold Bitumen Applications																	UWM
E1c-2i: Review of Literature and Standards		JP, P, D	F		D1	D3											
E1c-2ii: Creation of Advisory Group																	
E1c-2iii: Identify Tests and Develop Experimental Plan				P, DP	D1		D5										
E1c-2iv: Develop Material Library and Collect Materials.																	
E1c-2v: Conduct Testing Plan						JP	D4	P									
E1c-2vi: Develop Performance Selection Guidelines									JP	D	P, F						
E1c-2vii: Validate Guidelines							D2							JP	P		
E1c-2viii: Develop CMA Mix Design Procedure											P						
E1c-2ix: Develop CMA Performance Guidelines														JP	D	F	

**Deliverable codes**  
D: Draft Report  
F: Final Report  
M&A: Model and algorithm  
SW: Software  
JP: Journal paper  
P: Presentation  
DP: Decision Point

**Deliverable Description**  
Report delivered to FHWA for 3 week review period.  
Final report delivered in compliance with FHWA publication standards  
Mathematical model and sample code  
Executable software, code and user manual  
Paper submitted to conference or journal  
Presentation for symposium, conference or other  
Time to make a decision on two parallel paths as to which is most promising to follow through



## **PROGRAM AREA: VEHICLE-PAVEMENT INTERACTION**

### **CATEGORY VP1: WORKSHOP**

#### **Work element VP1a: Workshop on Super-Single Tires**

This work element is complete.

### **CATEGORY VP2: DESIGN GUIDANCE**

#### **Work element VP2a: Mixture Design to Enhance Safety and Reduce Noise of HMA (UWM)**

##### Work Done This Quarter

Work focused on evaluating the laser profilometer device. Surface profile measurements (distance and elevation) on gyratory samples were collected as part of an experimental plan to compare profiles from gyratory-compacted samples to field cores. The work included comparative measurements for the sake of calibration with researchers at the University of Pisa, Italy. Split samples were shipped for measurements and results are in the process of being compared. The research team also finalized modifying the Excel spreadsheet provided by the University of Pisa to analyze data from the laser device. Noise absorption measurements on gyratory samples were conducted at the University of Pisa as part of the collaboration between the University of Wisconsin–Madison and the asphalt research group at the University of Pisa.

The UW–Madison research team held a meeting in Madison, Wis., with Dr. Losa from the University of Pisa. Several issues were discussed, including laser measurements, the noise absorption device, and polishing and friction measurements of gyratory samples. The research teams will continue the collaboration in the coming year of the project, and the potential for implementing the friction measurements and analysis protocol developed by University of Pisa researchers in the project will be assessed.

##### Significant Results

The Excel analysis spreadsheet was finalized to accommodate the raw data produced by the laser profilometer and produce the texture spectrum levels and mean texture depth following the ISO 13473-1 procedure. The original spreadsheet was designed to analyze profiles of 1500 mm in length. The research team modified the spreadsheet to allow measuring the texture spectrum for profiles of different lengths, such 150-mm, 600-mm, 750-mm and 1500-mm profiles. This will allow for analyzing profiles obtained from gyratory samples as well as slab-compacted samples. Figures VP2a.1 and VP2a.2 show an example of the output from the Excel analysis spreadsheet for a 150-mm gyratory profile.

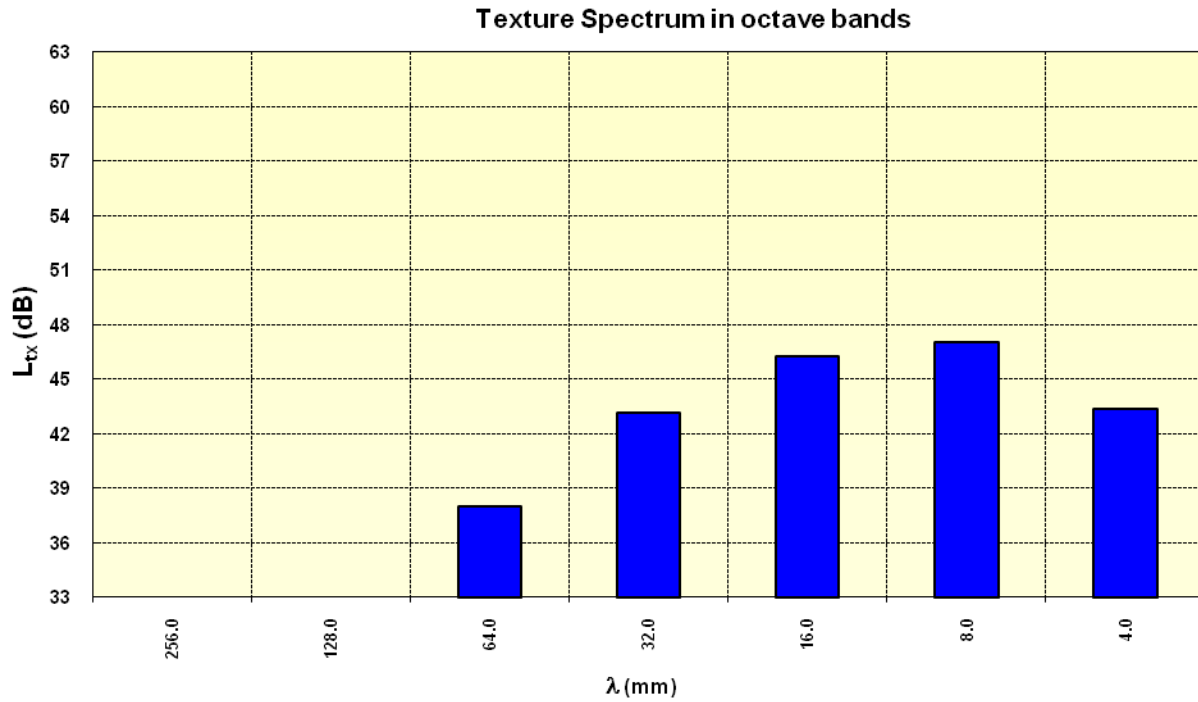


Figure VP2a.1. Chart. Texture spectrum in octave bands for 150-mm gyratory profile.

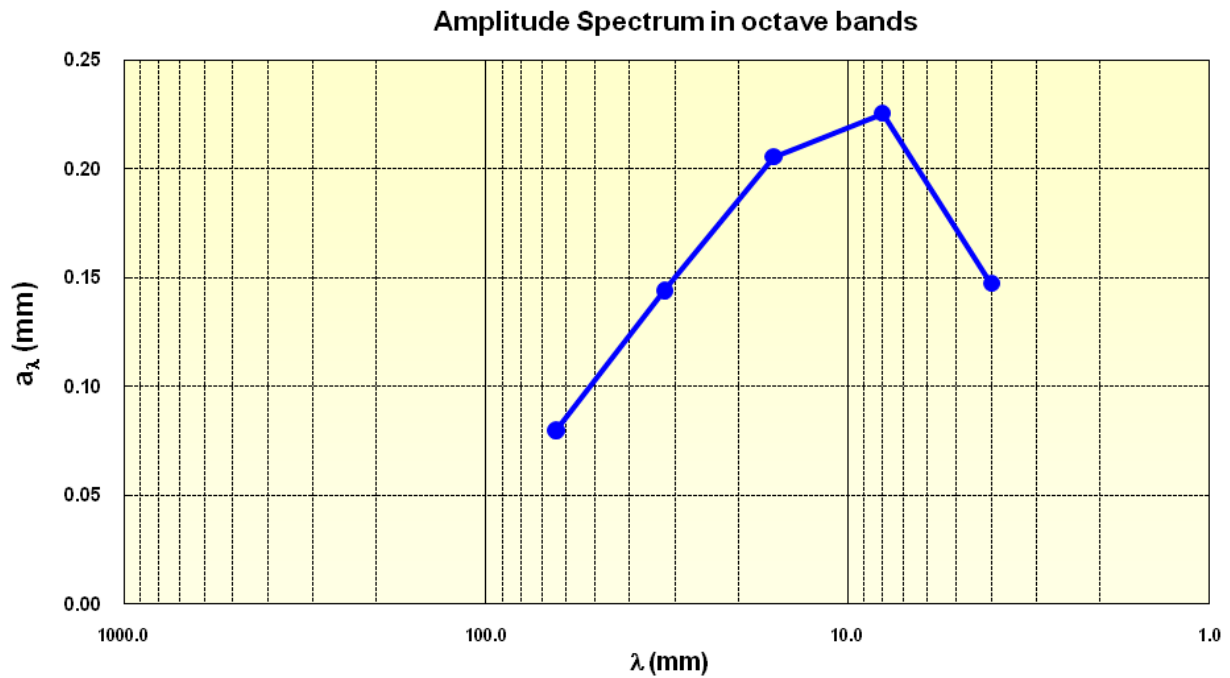


Figure VP2a.2. Graph. Amplitude spectrum in octave bands for 150-mm gyratory profile.

In order to cover more area of the gyratory sample surface, and to meet the minimum length requirement (600 mm) for the full texture spectrum analysis, the research team developed a protocol to measure four different profiles on each gyratory sample. Figure VP2a.3 illustrates the location of the different profiles. The first profile starting point is selected randomly. After collecting the profile data using the laser profilometer, the sample is rotated 45 degrees to scan the second profile. The same rotation angle is used to obtain the third and fourth profiles.

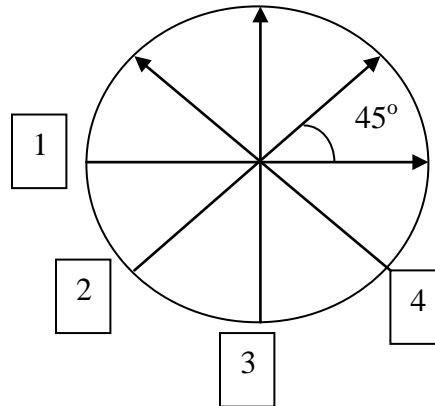


Figure VP2a.3. Illustration. Profile locations for gyratory sample.

The texture spectrum is shown in figure VP2a.4 for the four different directions for one sample.

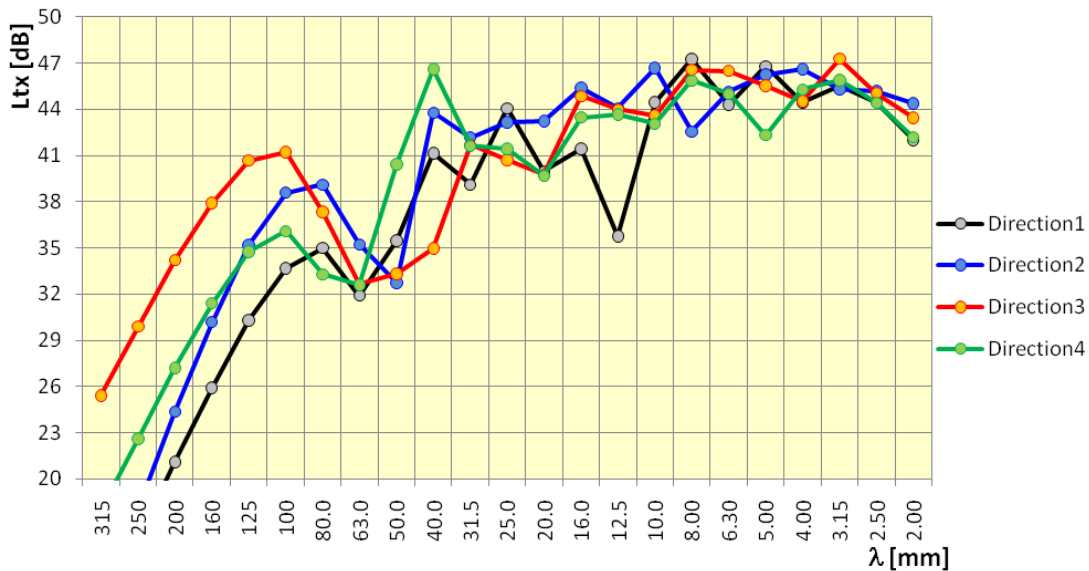


Figure VP2a.4. Graph. Texture spectrum for single profiles.

The next step was to combine the profiles into one profile. After combining the four profiles, the data was analyzed as one profile (600 mm). However, the data was analyzed before and after applying a filter to smooth the connection points between the four profiles. A simple moving average was applied. Figure VP2a.5 shows the raw data for the combined profiles before and after applying the filter.

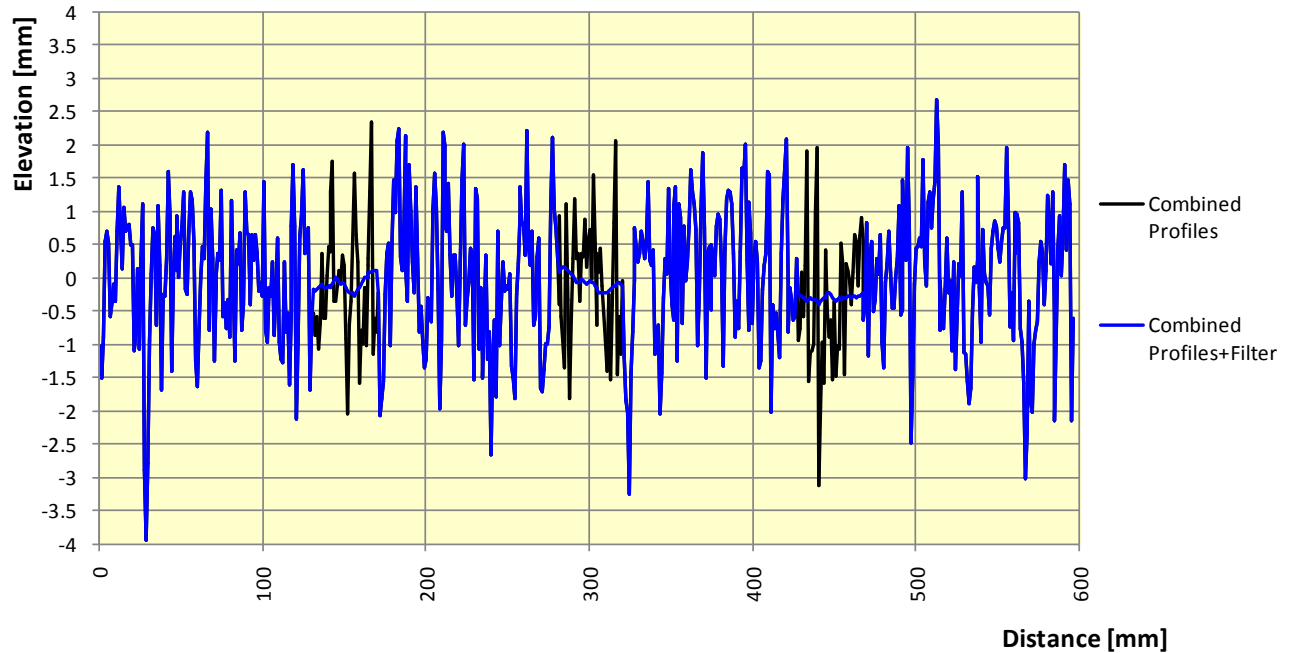


Figure VP2a.5. Graph. Combined elevation profile with and without filtering.

Finally, figure VP2a.6 shows the texture spectrum results for the combined profiles. The results illustrated in this figure indicate that the filtering for the combined profiles might not be a necessity. However, the research team will continue evaluating the need for this filter on more samples.

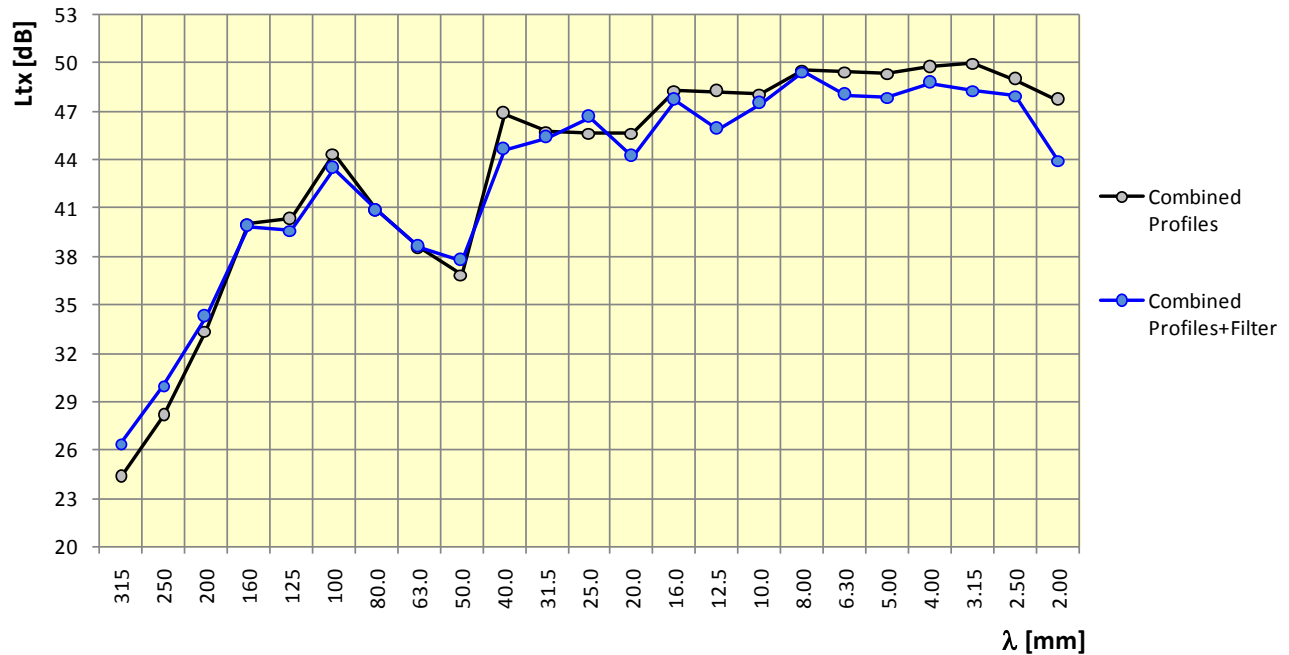


Figure VP2a.6. Graph. Texture spectrum for combined profile with and without filtering.

Table VP2a.1 summarizes the progress in measuring profile data for gyratory samples. One to three field cores are available for measurements for each road section.

Table VP2a.1. Progress in profile data measurements for the laboratory samples.

Road #	Lab Compaction Temperature/Pressure					
	60/300	60/600	90/300	90/600	120/300	120/600
I-39	Tested	"N/A"	Tested	"N/A"	Tested	Tested
I-39 M	"N/A"	Tested	Tested	Tested	"N/A"	"N/A"
STH 59	Tested	Tested	Tested	Tested	Tested	Tested
STH 60	Tested	Tested	Tested	Tested	Tested	Tested
STH 153 Mix 1	Tested	Tested	"N/A"	Tested	Tested	Tested
STH 153 Mix 2	Tested	Tested	Tested	Tested	Tested	Tested
STH 96	"N/A"	"N/A"	Tested	Tested	"N/A"	"N/A"
STH 181	"N/A"	"N/A"	Tested	Tested	"N/A"	"N/A"
US 8	"N/A"	"N/A"	Tested	Tested	"N/A"	"N/A"
US 41	Tested	Tested	Tested	Tested	Tested	Tested
US 45	Tested	Tested	Tested	Tested	Tested	Tested
US 53 Mix 1	Tested	Tested	Tested	Tested	Tested	Tested
US 53 Mix 2	"N/A"	"N/A"	Tested	Tested	"N/A"	"N/A"
STH 3	"N/A"	"N/A"	Tested	"N/A"	"N/A"	"N/A"
US 53	Tested	Tested	Tested	Tested	Tested	Tested

The research team at the University of Pisa performed noise absorption coefficient measurements on two gyratory samples—one open-graded mix and one dense mix. Details of the samples can be found in the ARC Q4 2009 report. Figure VP2a.7 summarizes the absorption coefficient results. The results clearly show that the typical Superpave dense mix has a low absorption compared to the open-graded mix. More gradations will be tested to identify dense gradations with higher absorption coefficient.

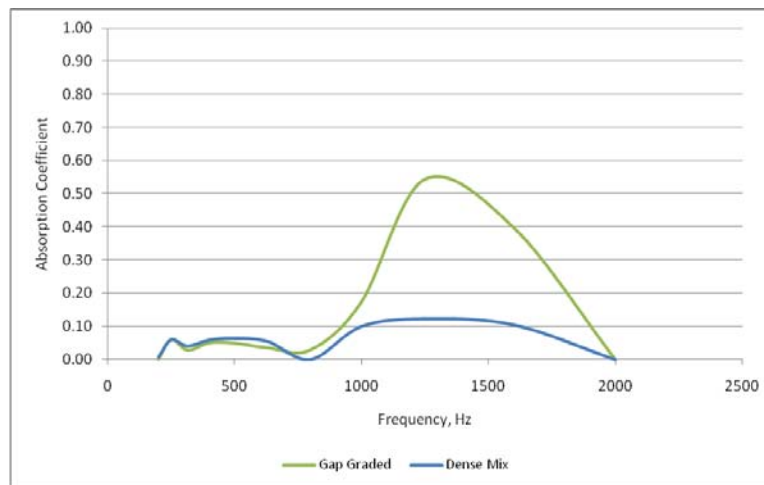


Figure VP2a.7. Graph. Absorption coefficient (gap- and dense-graded mixes).

A meeting with the research group of the New Zealand consulting firm Opus regarding friction and noise research was held during the first week of March 2010. The Opus group has done significant work in estimating friction and rolling resistance of tires on pavements using the surface roughness spectrum. The research team is reviewing a series of published and unpublished reports provided by the Opus group to explore the possibility of conducting joint work with Opus.

#### Significant Problems, Issues and Potential Impact on Progress

The progress in noise measurements was delayed. In order to collect noise absorption measurements, the acoustic tubes should be calibrated with reference material—material with known absorption-frequency curve. The research team contacted the manufacturer of the tube, and a reference material is being shipped to UW–Madison.

#### Work Planned Next Quarter

Next quarter, the research team will finalize the calibration of the noise absorption tube. The team will continue in collaboration with the researchers at the University of Pisa to finalize the calibration of the laser profilometer. The profile of cores from the field will be measured using the laser profilometer. Analysis will be conducted to compare the texture data between laboratory-compacted samples and field cores. The research team will also review the literature

and consult with the research group at the University of Pisa to decide on the testing matrix for the noise absorption part of this study. A review of reports received from the consulting firm Opus will also be conducted to explore possible methods of estimating friction characteristics from surface texture measurements.

## **CATEGORY VP3: MODELING**

### ***Work element VP3a: Pavement Response Model to Dynamic Loads (UNR)***

#### Work Done This Quarter

Continued the work on the 3D-Move model to make it a menu-driven software to integrate the post-processing forms. Continued the testing of the alpha-version of the 3D-Move model.

#### Significant Results

The tire load which gives rise to the pavement contact stress distribution is a moving load that varies with time about its mean value as the tire traverses the pavement. A number of past studies have focused on quantifying the load variation (or perturbation) measured in field tests and analytically-computed from vehicle-road interaction models. Many used Dynamic Load Coefficient (DLC), which was defined as the coefficient of variation (std. deviation/mean load). The variation in the tire load (or contact stress distribution) strongly depends on road roughness, vehicle speed and truck suspension system. In 3D-Move, the variability of the pavement response can be investigated by using DLC and it is included under “Vehicle Suspension and Road Roughness” option that is available in the 3D-Move’s main start-up window.

The window “Vehicle Suspension and Road Roughness” shown in Figure VP3a.1 facilitates the calculation of DLC value. In 3D-Move, DLC is calculated by two different options. First option (Option 1) “DLC from Database,” estimates DLC as a function of vehicle suspension system, road roughness (smooth, average or rough) and vehicle speed. In this case, the DLC value is obtained from a database compiled from many different sources (Woodrooffe and LeBlanc 1986; LeBlanc and Woodrooffe 1995; and Sweatman 1983). The second option (Option 2) in 3D-Move for the DLC uses regression equations developed by Sweatman (1983). In this case, DLC is also a function of axle type and the road roughness specified in terms of counts/km. If the role of the tire load variability is not be included, the “Default (DLC = 0.0)” option shown near the top of the window should be selected.

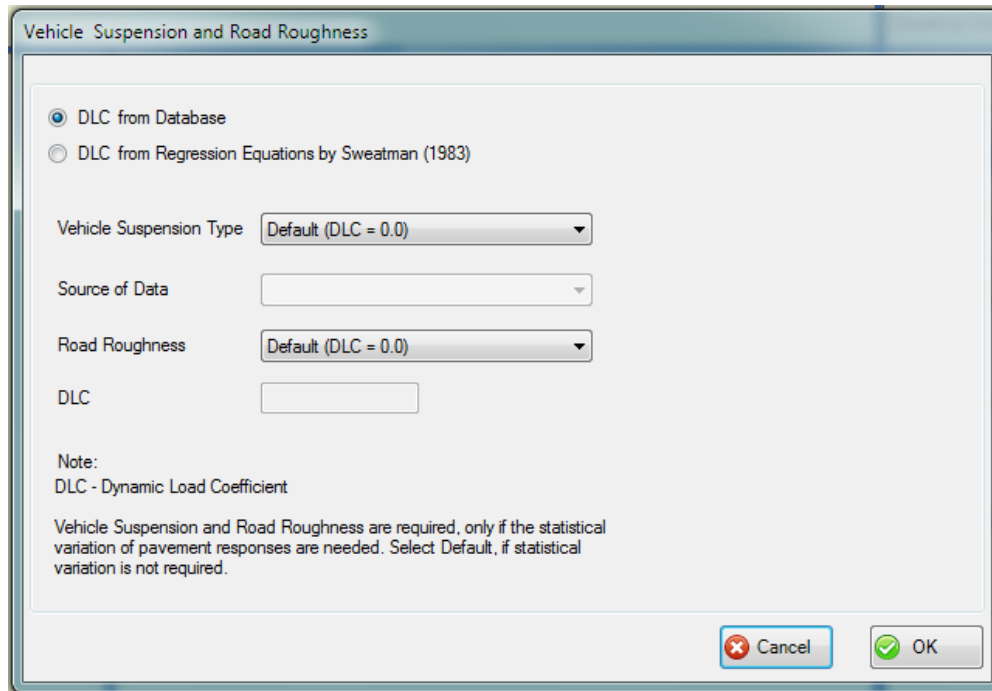


Figure VP3a.1. Main window for vehicle suspension and road roughness.

Figure VP3a.2 shows the available options in the database (Option 1) for the Vehicle Suspension system. There are altogether four types of suspension systems. A selection for Suspension Type along with Source of Data and Road Roughness can be subsequently made from this window. The DLC value from the database will be displayed in the text box on the screen as shown. On the other hand, if the option of “DLC from Regression Equations” (Option 2) is chosen, a new window (figure VP3a.3) is displayed and data required for the regression equations (Axle Type, Vehicle Suspension Type, Road Roughness) need to be input. It may be noted that under this option, as many as five options are available for Vehicle Suspension Type, which in turn depends on the selection of Axle Type (tandem or tridem). Only those that are available for the selected Axle Type will be displayed and the appropriate selection for Suspension Type can be subsequently made (figure VP3a.4).

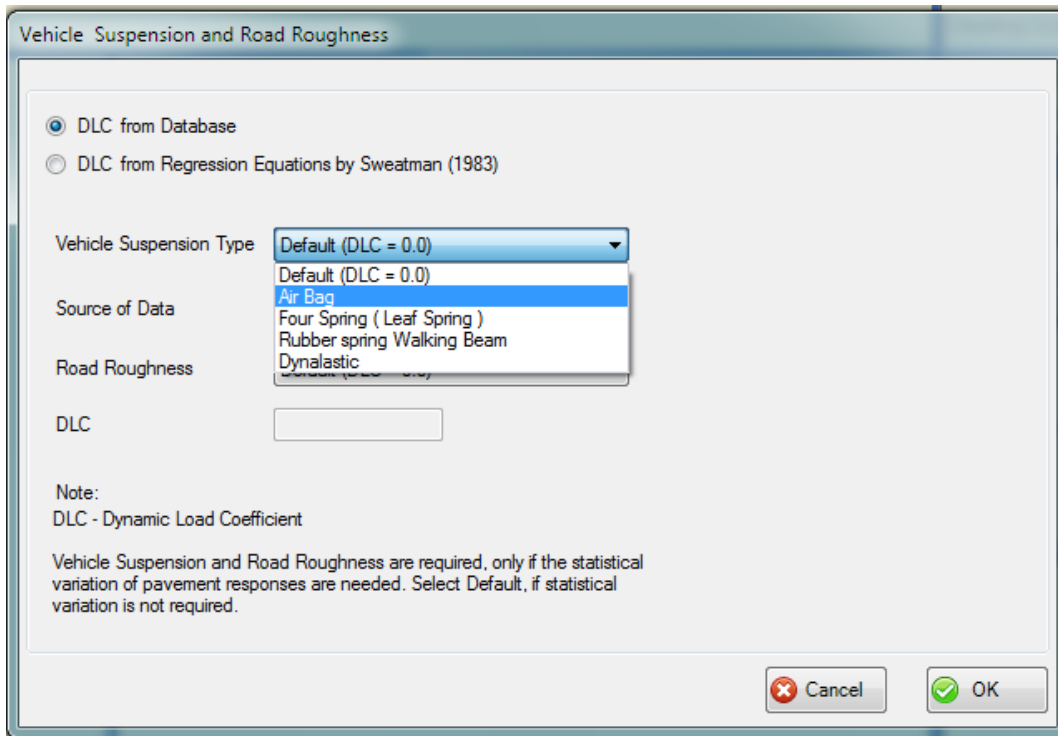


Figure VP3a.2. Available options for vehicle suspension under “DLC from Database.”

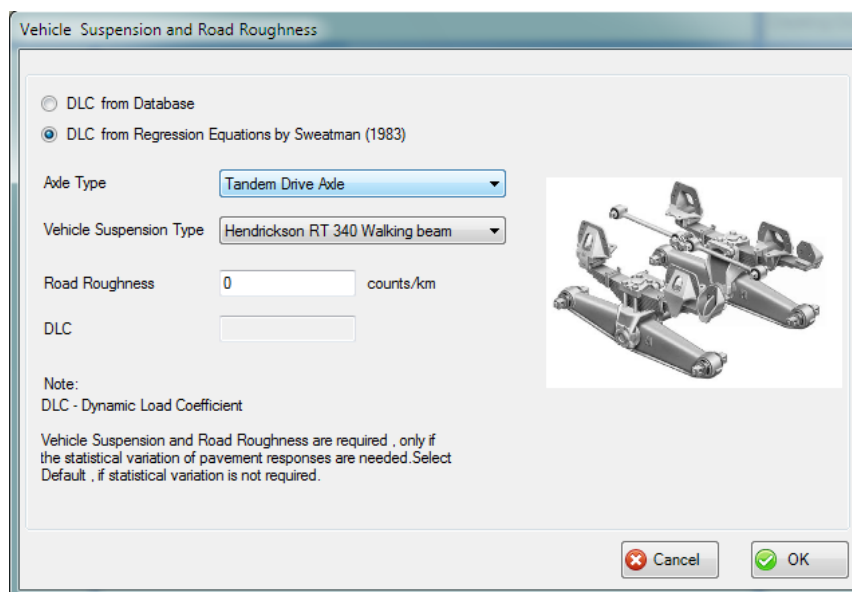


Figure VP3a.3. Option of DLC estimation from regression equations (Sweatman 1983).

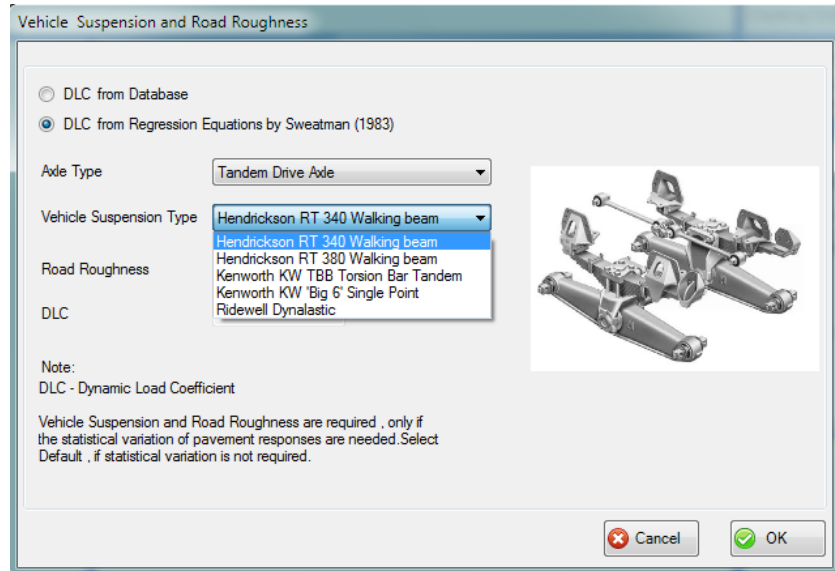


Figure VP3a.4. Available suspension types for the tandem axles when using regression equations.

The 3D-Move run that evaluates the pavement response time histories is originally carried out for the constant mean tire load (i.e., no tire load variability) traversing the pavement. Subsequently a procedure developed by Siddharthan et al. (1998) is used to estimate the variation of those response histories that accounts for the tire load variability. This procedure is based on the assemblage of a population of responses at each instant of time with a normal distribution about those 3D-Move responses computed with the mean tire loads. The variability can be superimposed on the original responses as shown in figures VP3a.5 and VP3a.6. These figures show two sets of longitudinal axial strain time histories at base of the HMA layer for two cases of road roughness conditions (smooth,  $DLC = 0.07$ ; and rough,  $DLC = 0.25$ ). As expected, the variability of the strain response with higher DLC value is significant.

This beta-version of the program is to be released in the coming quarter and once it is released we expect to receive many valuable feedbacks and comments from users. We intent to address the concerns and suggestions made by the users and release modified versions in a periodic manner. In the mean time, incorporating special vehicles used in port and other industry (e.g., loaders), busses and off-road agricultural vehicles (e.g., terragators) under the existing Non-Highway and Special Vehicle option that is available in 3D-Move is our immediate priority.

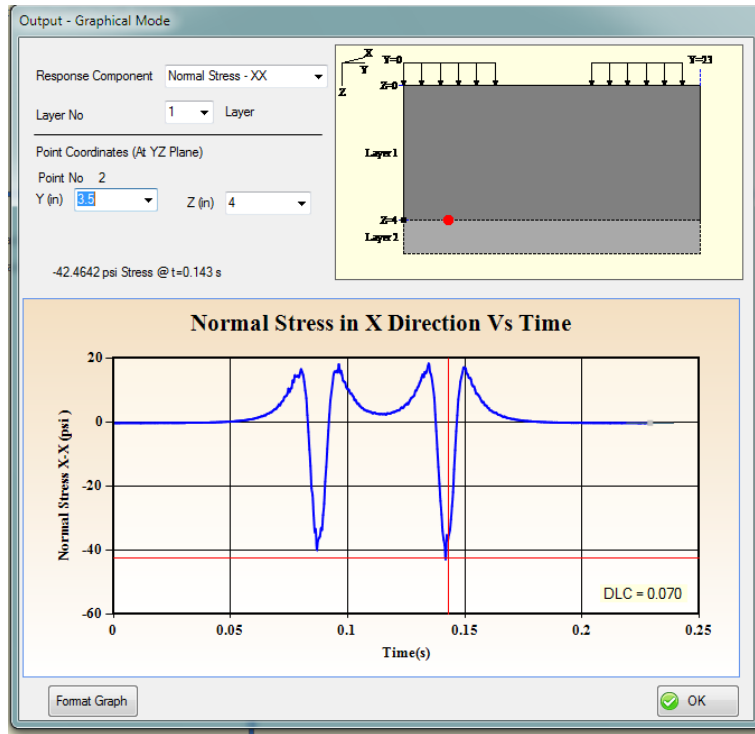


Figure VP3a.5. Variability of longitudinal axial strain for smooth pavement (DLC = 0.07).

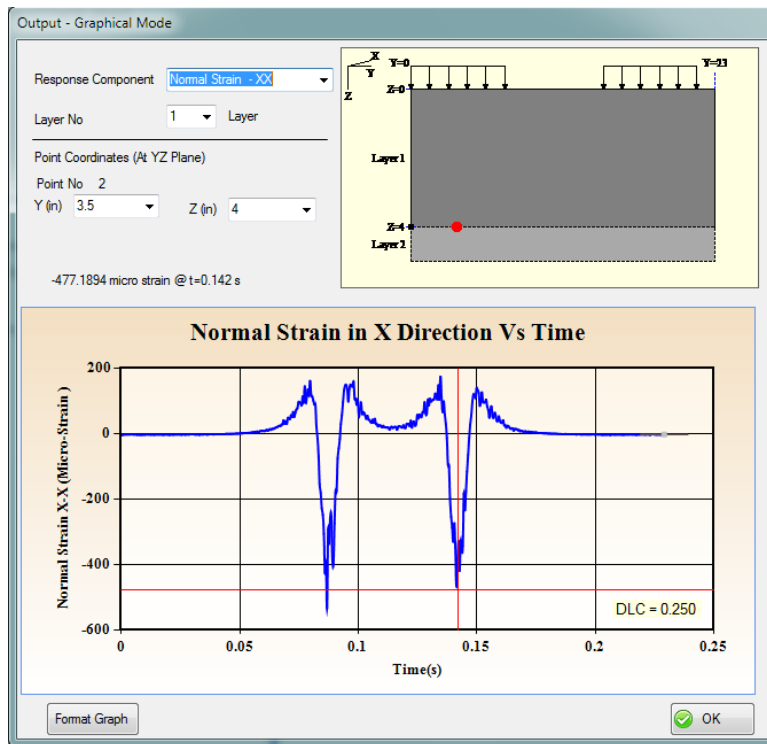


Figure VP3a.6. Variability of longitudinal axial strain for rough pavement (DLC = 0.25).

### Significant Problems, Issues and Potential Impact on Progress

None

### Work Planned Next Quarter

Continue working on the 3D-Move model to make it a menu-driven software. Evaluate the beta version for 3D-Move.

### Cited References

LeBlanc, P.A., and J. Woodrooffe, 1995, Spatial correlation of dynamic wheel loads, *Proc.*, 4<sup>th</sup> Int. Symp. in Heavy Vehicle Weights and Dimensions, 4, 281-290.

Siddharthan, R., J. Yao, and P. Sebaaly, 1998, Pavement Strain from Moving Dynamic 3D Load Distribution. *Journal of Transportation Engineering*, 134 (6), November 1998.

Sweatman, P. F., 1983, "A Study of dynamic wheel forces in axle group suspensions of heavy vehicles", Australian Road Research Board, Special Report SR No. 27,

Woodrooffe, J.H.F., and P.A. LeBlanc, 1986, The influence of suspension variations on dynamic wheel loads of heavy vehicles. *Proc.*, SAE Truck and Bus Meeting and Exposition, Soc. of Automotive Engrs. Inc., Warrendale, Pa.

Vehicle-Pavement Interaction Year 3	Year 3 (4/2009-3/2010)												Team	
	4	5	6	7	8	9	10	11	12	1	2	3		
<b>(1) Workshop</b>														
VP1a: Workshop on Super-Single Tires														UNR
<b>(2) Design Guidance</b>														
VP2a: Mixture Design to Enhance Safety and Reduce Noise of HMA														UWM
VP2a-1: Evaluate common physical and mechanical properties of asphalt mixtures with enhanced frictional skid characteristics														
VP2a-2: Evaluate pavement macro- and micro-textures and their relation to tire and pavement noise-generation mechanisms														
VP2a-3: Develop a laboratory testing protocol for the rapid evaluation of the macro and micro-texture of pavements														
VP2a-4: Run parametric studies on tire-pavement noise and skid response					JP									
VP2a-5: Establish collaboration with established national and international laboratories specialized in transportation noise measurements. Gather expertise on measurements and analysis														
VP2a-6: Model and correlate acoustic response of tested tire-pavement systems														
VP2a-7: Proposed optimal guideline for design to include noise reduction, durability, safety and costs														
<b>(3) Pavement Response Model Based on Dynamic Analyses</b>														
VP3a: Pavement Response Model to Dynamic Loads														UNR
VP3a-1: Dynamic Loads														
VP3a-2: Stress Distribution at the Tire-Pavement Interface														
VP3a-3: Pavement Response Model											SW, v.β			
VP3a-4: Overall Model														

**Deliverable codes**

- D: Draft Report
- F: Final Report
- M&A: Model and algorithm
- SW: Software
- JP: Journal paper
- P: Presentation
- DP: Decision Point

**Deliverable Description**

- Report delivered to FHWA for 3 week review period.
- Final report delivered in compliance with FHWA publication standards
- Mathematical model and sample code
- Executable software, code and user manual
- Paper submitted to conference or journal
- Presentation for symposium, conference or other
- Time to make a decision on two parallel paths as to which is most promising to follow through

 Work planned  
 Work completed  
 Parallel topic

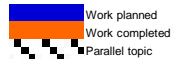
Vehicle-Pavement Interaction Years 2 - 5	Year 2 (4/08-3/09)				Year 3 (4/09-3/10)				Year 4 (04/10-03/11)				Year 5 (04/11-03/12)				Team
	Q1	Q2	Q3	Q4	Q1	Q2	Q3	Q4	Q1	Q2	Q3	Q4	Q1	Q2	Q3	Q4	
<b>(1) Workshop</b>																	
VP1a: Workshop on Super-Single Tires																	UNR
<b>(2) Design Guidance</b>																	
VP2a: Mixture Design to Enhance Safety and Reduce Noise of HMA																	UWM
VP2a-1: Evaluate common physical and mechanical properties of asphalt mixtures with enhanced frictional skid characteristics				DP													
VP2a-2: Evaluate pavement macro- and micro-textures and their relation to tire and pavement noise-generation mechanisms				DP													
VP2a-3: Develop a laboratory testing protocol for the rapid evaluation of the macro and micro-texture of pavements		M&A															
VP2a-4: Run parametric studies on tire-pavement noise and skid response						JP		D	JP								
VP2a-5: Establish collaboration with established national laboratories specialized in transportation noise measurements. Gather expertise on measurements and analysis																	
VP2a-6: Model and correlate acoustic response of tested tire-pavement systems									JP,P								
VP2a-7: Proposed optimal guideline for design to include noise reduction, durability, safety and costs														P			
<b>(3) Pavement Response Model Based on Dynamic Analyses</b>																	
VP3a: Pavement Response Model to Dynamic Loads																	UNR
VP3a-1: Dynamic Loads			JP														
VP3a-2: Stress Distribution at the Tire-Pavement Interface																	
VP3a-3: Pavement Response Model								SW, v. β			JP			SW, JP			
VP3a-4: Overall Model										SW			D	F			

**Deliverable codes**

- D: Draft Report
- F: Final Report
- M&A: Model and algorithm
- SW: Software
- JP: Journal paper
- P: Presentation
- DP: Decision Point

**Deliverable Description**

- Report delivered to FHWA for 3 week review period.
- Final report delivered in compliance with FHWA publication standards
- Mathematical model and sample code
- Executable software, code and user manual
- Paper submitted to conference or journal
- Presentation for symposium, conference or other
- Time to make a decision on two parallel paths as to which is most promising to follow through



## **PROGRAM AREA: VALIDATION**

### **CATEGORY V1: FIELD VALIDATION**

#### **Work element V1a: Use and Monitoring of Warm Mix Asphalt Sections (Year 1 start)**

##### Work Done This Quarter

The small samples obtained from the Yellowstone sections using a masonry drill bit are being stored until this method is further validated. The goal of the small sampling method is to be able to obtain pavement aging properties that compare well with traditional core samples. In the case of the Yellowstone samples, there are no traditional core samples for comparison so effort is being directed at sites where comparison of the small sample technique can be compared with core extraction. A key element of using small samples is the use of the 4-mm DSR method. The validation of the 4-mm DSR method has been further advanced at WRI and other organizations. Comparison of the 4-mm plate rheological data and torsion bar rheological data has found good agreement. The comparison of the 4-mm plate DSR method with the torsion bar rheology at WRI and other organizations is validating the 4-mm method. The results have been reported in the “Fundamental Properties of Asphalts and Modified Asphalts III” quarterly reports and also at the ETG meetings in Irvine, California in February 2010.

##### Significant Results

None.

##### Significant Problems, Issues and Potential Impact on Progress

None.

##### Work Planned Next Quarter

Work will continue to assess the small sampling method.

#### **Work element V1b: Construction and Monitoring of Additional Comparative Pavement Validation sites (Year 1 start)**

##### Work Done This Quarter

Laboratory work on samples from the Manitoba RAP sections is continuing. The samples are being used (along with others) in the RAP compatibility study being done in Work Element E2b-2. This work is also investigating the blending of RAP and virgin binder as well as the composition of the blended components. Progress on the Manitoba work was presented to Manitoba personnel in March.

Communication with Manitoba personnel regarding the resumption date of construction of the Manitoba warm-mix project is continuing. It is still planned to collect samples during construction of the warm-mix sections.

#### Significant Results

A new comparative pavement performance site using high RAP content, moderate RAP content, and conventional hot-mix was constructed in Manitoba, Canada. This site should provide valuable performance data, especially on the effect of RAP on low temperature properties.

#### Significant Problems, Issues and Potential Impact on Progress

Partial construction of the warm-mix site in Manitoba Canada was not as planned. The effect of the comparison of materials is to be determined.

#### Work Planned Next Quarter

It is planned to continue to analyze the Manitoba samples. Resumption of the construction of the Manitoba warm-mix sections may occur during the next quarter.

### **CATEGORY V2: ACCELERATED PAVEMENT TESTING**

#### **Work element V2a: Accelerated Pavement Testing including Scale Model Load Simulation on Small Test Track (Later start)**

#### Work Done This Quarter

No activity this quarter. This work element was included in order to accommodate any accelerated testing that may occur during the project.

#### Significant Results

None.

#### Significant Problems, Issues and Potential Impact on Progress

None.

#### Work Planned Next Quarter

No accelerated (field) testing is planned.

## **Work element V2b: Construction of Validation Sections at the Pecos Research & Testing Center (Later start)**

This work element is included to indicate that this may be a possibility for accelerated pavement testing for ARC research because it is a facility in the TAMU system.

## **CATEGORY V3: R&D VALIDATION**

### **Work element V3a: Continual Assessment of Specifications (UWM)**

#### Work Done This Quarter

Work this quarter focused on improving the data collection system used in the monthly round-robin binder testing coordinated by the Western Cooperative Test Group (WCTG), connecting each WCTG binder tested since July 2009 to specific DOT projects, and continuing University of Wisconsin–Madison research group involvement in performing the round-robin tests. A draft AASHTO standard of the linear amplitude sweep test (LAS) for binder fatigue characterization was written and submitted to the ETG for review. Further implementation tests were conducted for the Single-Edge Notched Bending (SENB) test and the Asphalt Binder Cracking Device (ABCD). A new geometry for the SENB testing was proposed to avoid adhesion problems between binder and metal inserts previously observed. The new geometry is in the process of being implemented based on both experimental results and finite element (FE) simulations using Abaqus.

The transition to an online reporting system for the WCTG round-robin test results managed by UW–Madison is nearly complete. The main hurdle remaining is to encourage and accomplish the full participation in the new system from the member labs. An abundance of useful feedback from the member labs identified the following concerns:

- Consistency of significant figures.
- Privacy of an online reporting form template provided by Google.
- Multiple Stress Creep and Recovery (MSCR) testing using ASTM or AASHTO formulas.

These issues were addressed at the annual Rocky Mountain Asphalt User/Producer Group (RMAUPG) and WCTG joint meeting. Due to the relatively high coefficient of variation of the test results, having inconsistent significant figures being reported is not an important issue. The spreadsheet used with the Google template is encrypted and password-protected, so it is realistically as safe as it would be on any other server.

The confusion of whether to use the ASTM or AASHTO standard for the MSCR tests is an important problem. The differences in nonrecoverable creep compliance (Jnr) results were very inconsistent. The AASHTO method uses the Jnr at a stress level of 100 Pa. On the other hand, the ASTM method uses the Jnr at 3.2 kPa. To help solve this problem, labs are now asked to

report the Jnr at 100 Pa. Manual reporting of the percent difference in Jnr may be dropped in the future and instead calculated from the Jnr values to eliminate any confusion and resulting error.

### Significant Results

Three of the WCTG binders tested have been connected to DOT projects in the Rocky Mountain region. Mix design and mixture testing data were provided on two of the binders. One binder was only used in a ½-inch chip seal; therefore, no mixture data was available.

The MSCR test results have very high variability, especially at the 10 kPa stress level, where the coefficient of variation was above 100% for almost every binder. The usefulness of testing at this high stress level may need to be reevaluated.

A new Dynamic Shear Rheometer (DSR) test procedure for fatigue has been developed, and a draft AASHTO standard titled “Estimating Fatigue Resistance of Asphalt Binders Using the Linear Amplitude Sweep” has been submitted. The test has shown very good correlation with actual fatigue cracking of LTPP sections. Discussion and results of the test are included in the quarterly report for work element F2e.

The SENB testing geometry was changed from using a specimen with a cross-section of 1-inch by 0.5-inch with metal inserts to a specimen with the same cross-section as a Bending Beam Rheometer (BBR) specimen—0.5-inch by 0.25-inch—but including a notch at the center. This also eliminated the need for the sample preparation for the old geometry, which was very time-consuming. Moreover, specimens prepared with the current geometry had premature failure at the metal-binder interface. The new geometry has much simpler sample preparation using common BBR molds, and there are no longer problems with adhesion. FE model simulations also show that the new geometry has no discontinuity in the stress distribution, as in the case of the previous geometry. Sample results of the modified test geometry are shown in the quarterly reports for work element E2d.

### Significant Problems, Issues and Potential Impact on Progress

None.

### Work Planned Next Quarter

WCTG round-robin binder testing will continue. The remaining binders from the 2009/2010 academic year will be connected to DOT projects.

Development and validation of the LAS and the SENB test procedures will continue.

**Work element V3b: Validation of the MEPDG Asphalt Materials Models Using New MEPDG Sites and Selected LTPP Sites (UNR, UWM)**

***Subtask V3b-1: Design and Build Sections (Start Year 1, Year 2, and Year 3)***

Work Done This Quarter

None

Significant Results

The ARC researchers faced serious hesitation from the DOTs to built MEPDG test sections. Therefore, no new MEPDG test sections were constructed in Year 3. Since no test sections were constructed, no additional testing (subtask V3b-2) was needed to help the DOT's. The UNR team shifted the year 4 and 5 budgets allocated for the appropriate subtasks into the subtasks for warm mixes (E1c-1) and cold mixes (E1c-2). Without MEPDG test sections to compare lab data with field data, it is not possible to review and/or revise the material models and assess the impact of moisture and aging. Therefore, this affects subtasks V3b-5 and V3b-6 also and no further effort is planned in these subtasks.

Significant Problems, Issues and Potential Impact on Progress

Only two agencies have committed to the construction of MEPDG sites: the Washoe RTC in northern Nevada in 2008, The South Dakota DOT in 2009/2010. The researchers are facing significant hesitation from the DOTs to use the MEPDG to design and construct HMA pavements. The level of this work element has been reduced.

Work Planned Next Quarter

Continue discussions with the states to select field sections for the MEPDG validations sites.

***Subtask V3b-2: Additional Testing (Start Year 2, Year 3, and Year 4)***

The reader is referred to subtask V3b-1.

***Subtask V3b-3: Select LTPP Sections (Start Year 1 thru Year 5)***

Work Done This Quarter

In this quarter, the research group completed the frequency sweep tests to determine the  $\alpha$  values for the LTPP binders. In the previous report, the research team assumed an  $\alpha$  value of 2.5 for all LTPP binders. The analysis of the linear amplitude sweep (LAS) test results using viscoelastic continuum damage theory (VECD) and the measured  $\alpha$  values are presented in table V3b-3.1.

Table V3b-3.1. Results for LTPP binder evaluation using the LAS.

Binder	Testing Temp [°C]	Climate Type	Cracked Area [m <sup>2</sup> ]	A	B
PG 76-10 (04-B901)	37	DN	328	3.978E+06	-3.804
PG 76-28 (34-0961)	28	WF	178.8	5.483E+06	-4.296
PG 76-22 (37-0962)	31	WN	0.01*	1.180E+08	-4.592
PG 58-34 (09-0961)	16	WN	2.1	1.436E+07	-4.679
PG 64-22 (34-0901)	25	WN	49.5	7.936E+06	-4.265
PG 52-40 (89-A902)	10	WF	6.7	7.278E+06	-4.495
PG 64-22 (35-0902)	25	DN	32	9.880E+06	-4.338

DN = dry-nonfreeze. WF = wet-freeze. WN = wet-nonfreeze.

The  $\alpha$  values have a significant impact on the estimation of the fatigue performance of binders. As noted in a previous quarterly report, the correlation between field performance and LAS results was statistically insignificant when the  $\alpha$  values were assumed to be the same for all LTPP binders. However, the correlation between fatigue cracking of the LTPP sections and the A parameter from LAS tests becomes significant when different  $\alpha$  values measured from frequency tests are used in the VECD analysis, as shown in figure V3b-3.1.

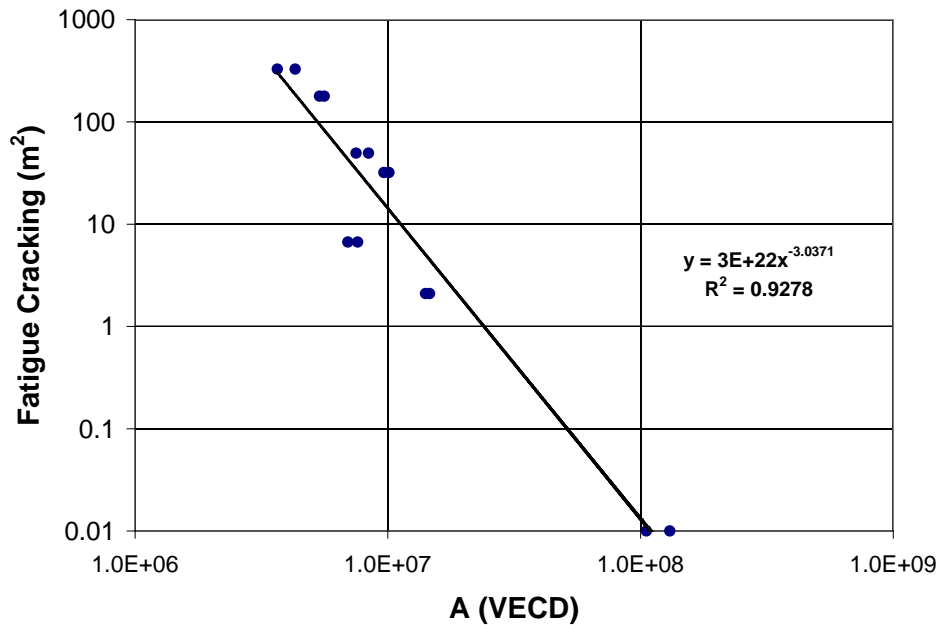


Figure V3b-3.1. Graph. Fatigue cracking in m<sup>2</sup>/ Km from LTPP measurements compared to the LAS VECD A parameter.

### Significant Results

A good correlation using a power law relationship was observed between the VECD fatigue model parameter A and the reported fatigue cracking area from LTPP sections, as shown in figure V3b-3.1. An increase in the parameter A generally indicates an increase in fatigue resistance. The relationship shown in figure V3b-3.1 is thus reasonable since it shows that fatigue cracking decreases as the A parameter increases. As more test results for binders from different sections become available, the relationship can be useful in determining appropriate specification limits for the LAS testing.

### Significant Problems, Issues and Potential Impact on Progress

None.

### Work Planned Next Quarter

Seven LTPP binders have been tested; the research team plans to expand this number to approximately 30 binders to determine specification limits. The research group also plans to send a set of binders to Turner-Fairbank Highway Research Center (TFHRC) for Double-Edge Notched Tension (DENT) tests.

The research team will continue data collection of LTPP sections for which low-temperature cracking and moisture damage performance is available.

### ***Subtask V3b-4: Testing of Extracted Binders from LTPP Sections (Start Year 1)***

#### Work Done This Quarter

None.

#### Work Planned Next Quarter

No work planned.

### ***Subtask V3b-5: Review and Revisions of Materials Models (Start Year 2, Year 3, Year 4, and Year 5)***

The reader is referred to subtask V3b-1.

### ***Subtask V3b-6: Evaluate the Impact of Moisture and Aging (Start Year 3, Year 4, and Year 5)***

The reader is referred to subtask V3b-1.

Validation Year 3	Year 3 (4/2009-3/2010)											Team	
	4	5	6	7	8	9	10	11	12	1	2		3
<b>(1) Field Validation</b>													
V1a: Use and Monitoring of Warm Mix Asphalt Sections													WRI
V1b: Construction and Monitoring of additional Comparative Pavement Validation sites													WRI
<b>(2) Accelerated Pavement Testing</b>													
V2a: Accelerated Pavement Testing including Scale Model Load Simulation on small test track (This work element will include all accelerated pavement testing)													WRI
V2b: Construction of validation sections at the Pecos Research & Testing Center													WRI
<b>(3) R&amp;D Validation</b>													
V3a: Continual Assessment of Specification													UWM
V3a-1: Evaluation of the PG-Plus practices and the motivations for selecting the "plus" tests.													
V3a-2: Detailed analysis of all PG-Plus tests being proposed or in use today, documentation of benefits and costs of these tests, and comparison with new tests			D										
V3a-3: Development of protocols for new binder tests and database for properties measured					JP								
V3a-4: Development of specification criteria for new tests based on field evaluation of construction and performance						D					P		
V3a-5: Interviews and surveys for soliciting feedback on binder tests and specifications													
V3b: Validation of the MEPDG Asphalt Materials Models and Early Verification of Technologies Developed by ARC using new MEPDG Sites and Selected LTPP sites													UNR/UWM/ WRI
V3b-1: Design and Build Sections													UNR
V3b-2: Additional Testing (if needed)													
V3b-3: Select LTPP Sites to Validate New Binder Testing Procedures													UWM
V3b-4: Testing of Extracted Binders from LTPP Sections													
V3b-5: Review and Revisions of Materials Models													
V3b-6: Evaluate the Impact of Moisture and Aging													

**Deliverable codes**

- D: Draft Report
- F: Final Report
- M&A: Model and algorithm
- SW: Software
- JP: Journal paper
- P: Presentation
- DP: Decision Point

**Deliverable Description**

- Report delivered to FHWA for 3 week review period.
- Final report delivered in compliance with FHWA publication standards
- Mathematical model and sample code
- Executable software, code and user manual
- Paper submitted to conference or journal
- Presentation for symposium, conference or other
- Time to make a decision on two parallel paths as to which is most promising to follow through

-  Work planned
-  Work completed
-  Parallel topic

Validation Years 2 - 5	Year 2 (4/08-3/09)				Year 3 (4/09-3/10)				Year 4 (04/10-03/11)				Year 5 (04/11-03/12)				Team	
	Q1	Q2	Q3	Q4	Q1	Q2	Q3	Q4	Q1	Q2	Q3	Q4	Q1	Q2	Q3	Q4		
<b>(1) Field Validation</b>																		
V1a: Use and Monitoring of Warm Mix Asphalt Sections																	WRI	
V1b: Construction and Monitoring of additional Comparative Pavement Validation sites																	WRI	
<b>(2) Accelerated Pavement Testing</b>																		
V2a: Accelerated Pavement Testing including Scale Model Load Simulation on small test track																	WRI	
V2b: Construction of validation sections at the Pecos Research & Testing Center																	WRI	
<b>(3) R&amp;D Validation</b>																		
V3a: Continual Assessment of Specification																	UWM	
V3a-1: Evaluation of the PG-Plus practices and the motivations for selecting the "plus" tests.		P	D,F															
V3a-2: Detailed analysis of all PG-Plus tests being proposed or in use today, documentation of benefits and costs of these tests, and comparison with new tests				P	D													
V3a-3: Development of protocols for new binder tests and database for properties measured						JP				P								
V3a-4: Development of specification criteria for new tests based on field evaluation of construction and performance						D		P		P			JP	P		JP	F	
V3a-5: Interviews and surveys for soliciting feedback on binder tests and specifications										P			JP	P		D	F	
V3b: Validation of the MEPDG Asphalt Materials Models and Early Verification of Technologies Developed by ARC using new MEPDG Sites and Selected LTPP sites																	UNR/UWM	
V3b-1: Design and Build Sections																		
V3b-2: Additional Testing (if needed)																		
V3b-3: Select LTPP Sites to Validate New Binder Testing Procedures							DP		P				JP,DP		P		D	F
V3b-4: Testing of Extracted Binders from LTPP Sections																		
V3b-5: Review and Revisions of Materials Models																		
V3b-6: Evaluate the Impact of Moisture and Aging																		

**Deliverable codes**

- D: Draft Report
- F: Final Report
- M&A: Model and algorithm
- SW: Software
- JP: Journal paper
- P: Presentation
- DP: Decision Point

**Deliverable Description**

- Report delivered to FHWA for 3 week review period.
- Final report delivered in compliance with FHWA publication standards
- Mathematical model and sample code
- Executable software, code and user manual
- Paper submitted to conference or journal
- Presentation for symposium, conference or other
- Time to make a decision on two parallel paths as to which is most promising to follow through

 Work planned  
 Work completed  
 Parallel topic



## **PROGRAM AREA: TECHNOLOGY DEVELOPMENT**

### **Work element TD1: Prioritize and Select Products for Early Development (Year 1)**

#### Work Done This Quarter

None. This work element has been completed.

#### Significant Results

Six early technology development projects have been identified and all have received favorable ratings from the ETGs.

#### Significant Problems, Issues and Potential Impact on Progress

None

#### Work Planned Next Quarter

None

### **Work element TD2: Develop Early Products (Year 3)**

#### Work Done This Quarter

No additional work on the continuum damage fatigue system was completed this quarter pending the outcome of the extended uniaxial fatigue study described in Work element E2e.

#### Significant Results

A complete continuum damage fatigue system has been assembled for the Interlaken AMPT owned by the NCHRP. An Excel spreadsheet to perform the reduced cycles analysis has been developed. A draft standard test method for performing fatigue testing and analyzing the data using the reduced cycles analysis has been prepared. These will likely be modified based on the results of the extended uniaxial fatigue study described in Work element E2e.

#### Significant Problems, Issues and Potential Impact on Progress

None.

#### Work Planned Next Quarter

The test method and equipment will be applied to fatigue data from several mixtures. A ruggedness testing plan for the simplified continuum damage fatigue test will be developed.

### **Work element TD3: Identify Products for Mid-Term and Long-Term Development (Years 2, 3, and 4)**

#### Work Done This Quarter

The research team continued to review interim research products to identify potential mid-term and long-term development projects.

Dr. Bonaquist prepared a work plan for an experiment to evaluate the various flow number approaches that have been proposed for evaluating mixture rutting resistance. The work plan was developed for and presented to the FHWA Mixtures and Construction Expert Task Group (ETG) at its meeting in February, 2010 in Irvine, California. The work plan will evaluate six different flow number approaches. Testing will be performed at the AASHTO Materials Reference Laboratory and the University of Nevada, Reno.

The ETG recommended that the proposed work proceed. Dr. Bonaquist assisted the Mixtures and Construction ETG chairman, Mr. Frank Fee, with recruiting mixtures for the study.

#### Significant Results

A work plan for an experiment to evaluate six different flow number approaches has been developed and materials for the experiment have been located.

#### Work Planned Next Quarter

Dr. Bonaquist will assist the Mixtures and Construction ETG with the planned experiment, providing analysis of the data and reporting of the results.

The research team will continue to review interim research products to identify potential mid-term and long-term development projects.

### **Work Element TD4: Develop Mid-Term and Long-Term Products (Years 3, 4, and 5)**

This activity is planned for later in the project.

## **PROGRAM AREA: TECHNOLOGY TRANSFER**

### **CATEGORY TT1: OUTREACH AND DATABASES**

#### **Work element TT1a: Development and Maintenance of Consortium Website (Duration: Year 1 through Year 5)**

##### Work Done This Quarter

The ARC website was maintained and updated. The ARC quarterly technical progress report, Oct 1- Dec 31, was uploaded to the ARC website. Useful and asphalt related links were added to the ARC website under the “Links” webpage.

##### Significant Results

None

##### Significant Problems, Issues and Potential Impact on Progress

None

##### Work Planned Next Quarter

Continue maintaining and updating the ARC website.

#### **Work element TT1b: Communications (Duration: Year 1 through Year 5)**

##### Work Done This Quarter

The sixth ARC Newsletter was published in March 2010.

##### Significant Results

None

##### Significant Problems, Issues and Potential Impact on Progress

None

##### Work Planned Next Quarter

None

## **Work element TT1c: Prepare Presentations and Publications**

### Presentations

Daranga, C., C. Clopotel, and H. Bahia, “Replacing the Elastic Recovery Test of Asphalt Binders with a DSR Test: Development of Protocol and Relationship to Binder Fatigue.” Poster presentation at the 89th Transportation Research Board Annual Meeting, Washington, D.C., January 12, 2010.

Faheem, A., R. Velasquez, and H. Bahia, “Partnership between Rocky Mountain Asphalt User/Producer Group, WCTG and Asphalt Research Consortium.” Rocky Mountain Asphalt User/Producer Group Spring Meeting, Albuquerque, NM, March 24, 2010.

Hajj, E. Y., Ulloa, A., and P. Sebaaly. “UNR Approach for Flow Number Test.” FHWA Asphalt Mixture and Construction Expert Task Group, Irvine, California, February 23, 2010.

Hajj, E. Y., Siddharthan, R., Rasanayagam, N., and P. Sebaaly. “Overview of the 3D-Move Pavement Response Model.” FHWA Fundamental Properties and Advanced Modeling of Asphalt Expert Task Group, Irvine, California, February 26, 2010.

Hanz, A., and H. U. Bahia, “Effects of Warm Mix Additives on Binder Rheology and Mixture Workability – Manitoba Field Project.” Presented at the Asphalt Research Consortium/Manitoba Infrastructure and Transportation Workshop, Winnipeg, Manitoba, Canada, March 3, 2010.

Hanz, A., T. Miller, and H. Bahia, "Research Update - Improvement of Emulsions' Characterization and Mixture Design for Cold Bitumen Applications." Panel discussion at the 37th Annual Meeting of the Asphalt Emulsion Manufacturers Association, Sunny Isles Beach, FL, March 5, 2010.

Hanz, Andrew, Zelalem Arega, and Hussain Bahia, “Rheological Behavior of Emulsion Residues Produced by Evaporative Recovery Method.” Poster presentation at the 89th Transportation Research Board Annual Meeting, Washington, D.C., January 12, 2010.

Hanz, Andrew, Ahmed Fatin Faheem, Enad Mahmoud, and Hussain Bahia, “Measuring the Effects of Warm-Mix Additives Using a Newly Developed Asphalt Binder Lubricity Test for the DSR.” Oral presentation at the 89th Transportation Research Board Annual Meeting, Washington, D.C., January 13, 2010.

Johnson, Carl, Raul Velasquez, and Hussain U. Bahia, “ARC Update on Binder Fatigue: BYET and Linear Amplitude Sweep (LAS) Test.” Asphalt Binder Expert Task Group, Irvine, CA, February 22, 2010.

Kuzay, B., and H. Bahia, “WCTG Round-robin Test Results: Transition to Online Reporting.” Rocky Mountain Asphalt User/Producer Group Spring Meeting, Albuquerque, NM, March 24, 2010.

Ma, T., H. Bahia, E. Mahmoud, and E. Hajj, “Estimating Allowable RAP in Asphalt Mixes to Meet Target Low Temperature PG Requirements.” Presented at the 2010 Annual Meeting of the Association of Asphalt Pavement Technologists, Sacramento, CA, March 10, 2010.

Ma, T., E. Mahmoud, and H. Bahia, “Development of Testing Procedure for the Estimation of RAP Binder Low-Temperature Properties without Extraction.” Oral presentation at the 89th Transportation Research Board Annual Meeting, Washington, D.C., January 11, 2010.

Mahmoud, E., and H. U. Bahia, “Methods for Measuring Surface Characteristics of Gyratory Compacted Asphalt Mixes and Relationships to Volumetric Design.” Poster presentation at the 89th Transportation Research Board Annual Meeting, Washington, D.C., January 12, 2010.

Miller, Timothy, Zelalem Arega, and Hussain Bahia, “Correlating Rheological Properties of Emulsion Residue to Early Chip Seal Performance.” Poster presentation at 89th Transportation Research Board Annual Meeting, Washington, D.C., January 12, 2010.

Sebaaly, P.E., Hajj, E. Y., Loria, L., Kasozi, A. and M. Barton. “Update on the Laboratory Evaluation of Mixes from the PTH8 and PTH14 Sections in Manitoba.” Winnipeg, Manitoba, March 3, 2010

Texas A&M University, “Viscoelastic Characterization of Aged Field Asphalt Mixtures Using Direct Tension Test” presented at the “DAWG” Forum on Pavement Performance Data Analysis sponsored by the Transportation Research Board Data Analysis Working Group (the “DAWG”) in Washington, D.C., January 2010.

Texas A&M University, “Anisotropic Viscoelastic Properties of Undamaged Asphalt Mixtures” presented at the “DAWG” Forum on Pavement Performance Data Analysis sponsored by the Transportation Research Board Data Analysis Working Group (the “DAWG”) in Washington, D.C., January 2010.

Texas A&M University, “Viscoelastic Characterization of Aged Asphalt Field Cores” presented at the International Society for Asphalt Pavements (ISAP) Technical Committee on Constitutive Modeling of Asphaltic Materials Annual Meeting held in Washington, D.C., January 2010.

Texas A&M University, “Viscoelastic and Fatigue Characterization of Asphalt Mixtures” presented at the Transportation Research Board (TRB) 89<sup>th</sup> Annual Meeting in Washington, D.C., January 2010.

Texas A&M University, “Characterization of Damage in Asphalt Mixtures Using Dissipated Pseudo Strain Energy” presented at the Transportation Research Board (TRB) 89<sup>th</sup> Annual Meeting in Washington, D.C., January 2010.

Texas A&M University, “Characterization of the Tensile Viscoelastic Properties of an Undamaged Asphalt Mixture” presented at the Transportation Research Board (TRB) 89<sup>th</sup> Annual Meeting in Washington, D.C., January 2010.

Texas A&M University, “Characterization of Fatigue Properties of Asphalt Mixtures” presented at the Fundamental Properties and Advanced Models Expert Task Group of the Federal Highway Administration (FHWA) in Irvine, California, February 2010.

Texas A&M University, “Characterization of Engineered Properties of Asphalt Mixtures” presented at the Fundamental Properties and Advanced Models Expert Task Group of the Federal Highway Administration (FHWA) in Irvine, California, February 2010.

### Publications

Bahia, H., A. Meruva, and R. Velasquez, 2010, “Modification of the Penetration Test to Measure Rheological Properties of Bitumen.” *4th Technical Week of Asphalt*, accepted.

Bahia, H. and R. Velasquez, 2010, “Understanding the Cause of Low Temperature Physical Hardening of Asphalt Binders.” *55<sup>th</sup> Canadian Technical Asphalt Association Conference*, accepted.

Bahia, H. U., R. Moraes, and R. Velasquez, 2010, “Measuring the Asphalt-Aggregate Bond Strength under Different Conditions.” *ICTI2010 – 2nd International Conference on Transport Infrastructures*, accepted.

Hajj, E. Y., Ullao, A., Siddharthan, R., and P. E. Sebaaly. “Characteristics of the Loading Pulse for the Flow Number Performance Test,” *Association of Asphalt Paving Technologists 85th Annual Meeting*, to appear in AAPT Journal Volume 79, 2010.

Hajj, E. Y., Ullao, A., Siddharthan, R., and P. E. Sebaaly. “Estimation of Stress Conditions for the Flow Number Simple Performance Test,” *Transportation Research Board 89th Annual Meeting, 2010*, Accepted for publication.

Rongbin Han, Xin Jin, Charles J. Glover. “Modeling Pavement Temperature for Use in Binder Oxidation Models and Pavement Performance Prediction,” submitted July 2009 to *Journal of Materials in Civil Engineering* (resubmitted, under review as of 1/15/10).

Hanz, A., Z. Arega, and H. Bahia, 2010, “Rheological Behavior of Emulsion Residues Produced by Evaporative Recovery Method.” *Transportation Research Record*, in press.

Hanz, A., A. Faheem, E. Mahmoud, and H. U. Bahia, 2010, “Measuring the Effects of Warm Mix Additives Using a Newly Developed Asphalt Binder Lubricity Test for the DSR.” *Transportation Research Record*, accepted.

Hanz, A., E. Mahmoud, and H. U. Bahia, March 2010, “Evaluation of Conventional Warm Mix Asphalt Design Procedures Using a Laboratory Foaming Device.” Submitted to *Advanced Asphalt Technologies* as documentation related to UW–Madison support of NCHRP 9-43: Mix Design Procedures for Warm Mix Asphalt.

Kvasnak, A., West, R., Michael, J., Loria, L., Hajj, E. Y., and N. Tram. "Evaluation of the Effect of Reclaimed Asphalt Pavement Aggregate Bulk Specific Gravity on Voids in Mineral Aggregate," *Transportation Research Board 89th Annual Meeting, 2010*, Accepted for publication.

Ma, T., Bahia, H., Mahmoud, E., and E. Y., Hajj. "Estimating Allowable RAP in Asphalt Mixes to Meet Target Low Temperature PG Requirements," *Association of Asphalt Paving Technologists 85th Annual Meeting*, to appear in *AAPT Journal Volume 79*, 2010.

Miller, T., Z. Arega, and H. Bahia, 2010, "Correlating Rheological Properties of Emulsion Residue to Early Chip Seal Performance." *Transportation Research Record*, in press.

Miller, T., and H. Bahia, 2010, "Establishing a Framework for Analyzing Asphalt Pavement Sustainability." *International Journal of Pavement Research and Technology*, accepted.

Pauli, A.T., R.W. Grimes, A.G. Beemer, J.J. Miller, J.D. Beiswenger, J.E. MacNaughton, T.F. Turner, and J.F. Branthaver. "Morphology of asphalts, asphalt chromatographic fractions and model wax-doped asphalts studied in thin-films by atomic force microscopy" was submitted to the *International Journal of Pavement Engineering*.

## **Work element TT1d: Development of Materials Database (Duration: Year 2 through Year 5)**

### Work Done This Quarter

Significant testing of the ARC materials database occurred this quarter providing the opportunity to improve usability and to locate and fix bugs. Significant content was created for the Help system along with improvements to the Help system's user interface. A workshop was held for ARC members where feedback was gathered for future work items.

The discussion of significant results this quarter is broken down into three sections as follows:

- User Interface and Application Development
- Help System
- Workshop

### Significant Results

#### *User Interface and Application Development*

Two new forms were created allowing users to create and edit material suppliers and to create and edit standard procedures. Figures TT1d.1 shows the Suppliers form. The Standard Procedures form has a similar user interface and is not shown for brevity.

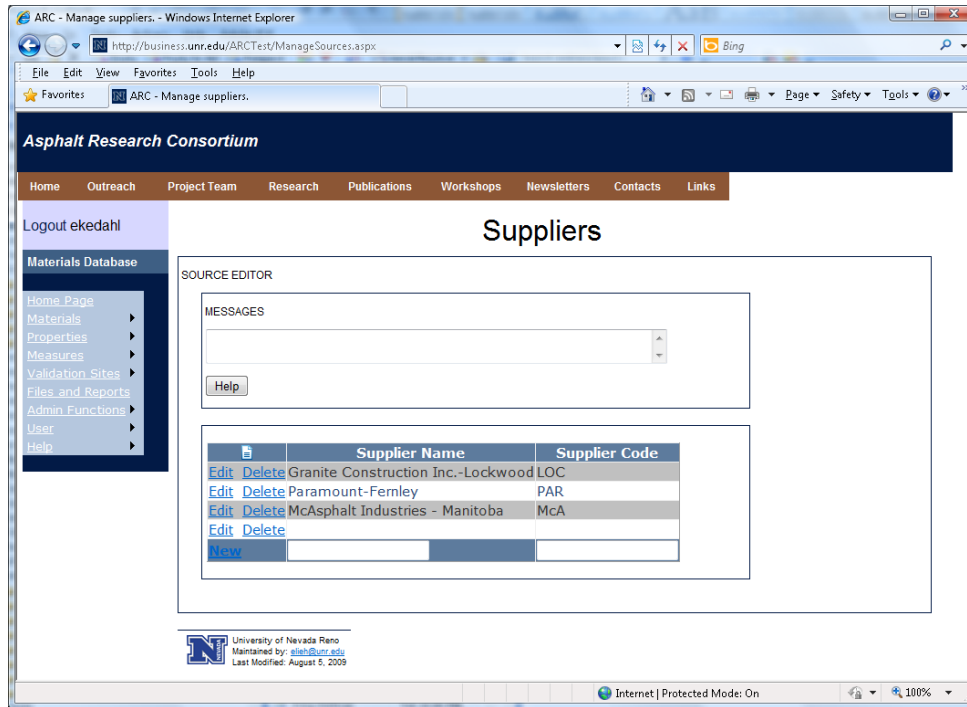


Figure TT1d.1. Suppliers form.

A prototype has been added for subtask editing and filtering functions for Files and Reports. This feature allows reports to be linked with specific materials or specific work tasks. This feature uses the same Work Task Editor used throughout the application. Note that from information gathered at the workshop, enhancements will need to be made to better link reports and data items, and to upload multiple files and supporting documents concurrently.

Several “cosmetic” changes have been made to the user interface along with some bug fixes as follows:

- The Validation Site form has been restructured and reorganized.
- The menu system is now hierarchical so as to better organize tasks along functional boundaries.
- The date selection control has been modified making it easier to select long date spans.
- Error alert icons with mouse-over tool tips have been added to selected grids that alert users to problems with data entry.
- Soft limit validation errors have been fixed for quantitative measures. Added the ability to input value “0” in quantitative measures.
- A “Number Format” selector box on the Measures form was added, which allows user to choose how quantitative values are displayed (e.g., scientific notation.)
- The editor for Location Units is now embedded in Validation Section grid.
- The ability to delete property groups was added.

- Fixed the data refresh issues on selected pages.
- Page titles were added to forms.
- Formatting was enhanced to provide a similar look-and-feel to all grid controls.

### Help System

Work continues on the application's Help system. Two new features were added. To better communicate database usage structure, a data flow diagram was added as an entry point into the Help system. Hotspots will be created in the diagram that will link to other Help components. Figure TT1d.2 shows the data flow diagram.

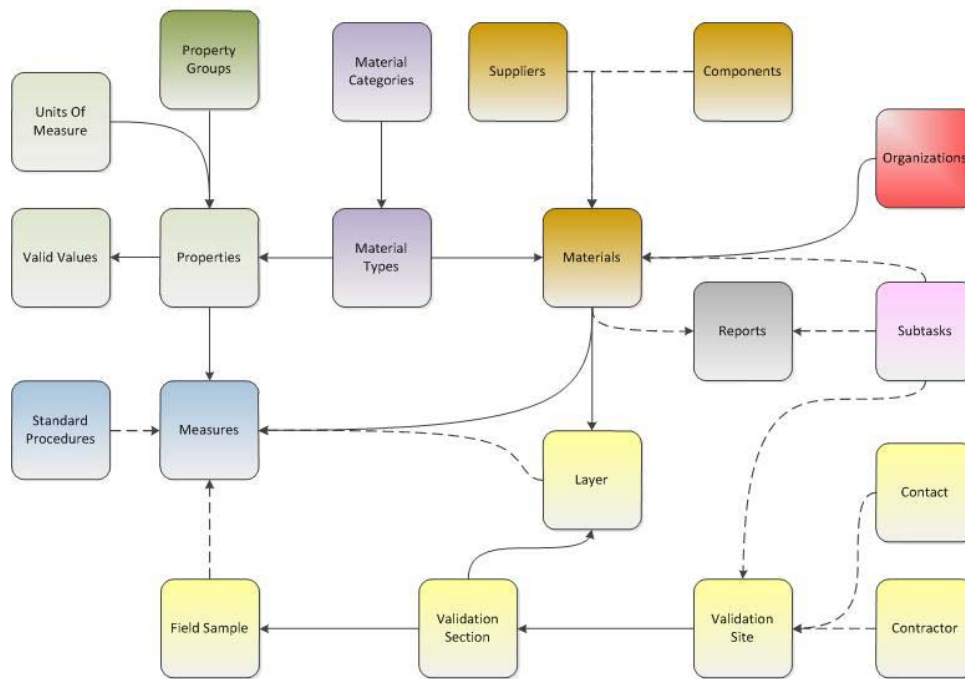


Figure TT1d.2. Data flow diagram.

Within the user interface, users commonly enter grid-based data. Data definitions that correspond to these grids have been incorporated into the Help system. Furthermore, each grid now has an icon that links to the corresponding data definition. Figure TT1d.3 shows the data definition for a Material.

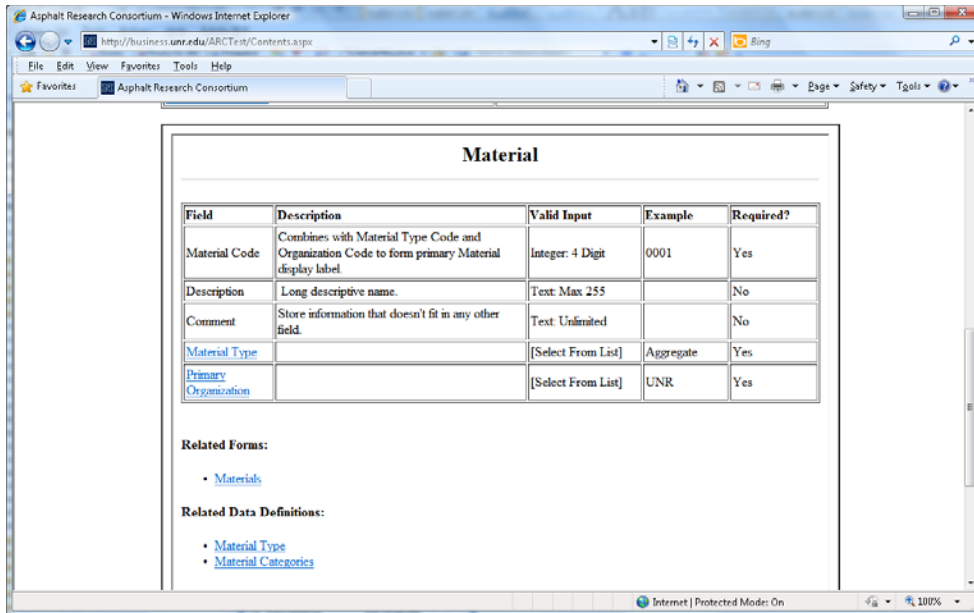


Figure TT1d.3. Material data definition.

As shown in figure TT1d.3, a data definition describes each field, describes the valid input parameters, and denotes whether the field is required or optional. Note that a data definition also has links to related data definitions.

A table of contents was also created to provide an entry point into the application's forms and data definitions as shown in figure TT1d.4.

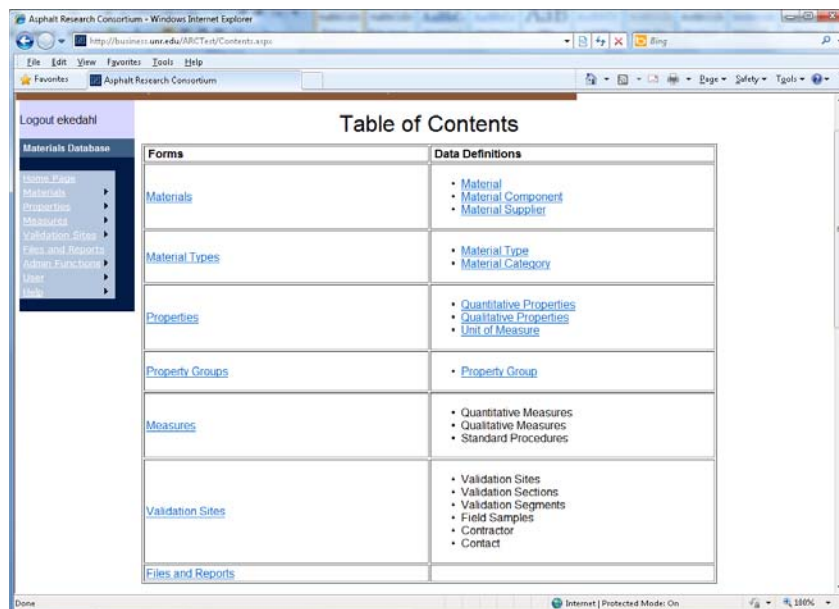


Figure TT1d.4. Help Table of Contents.

## *Workshop*

A training workshop was provided to ARC constituents on March 11, 2010. The workshop activities are summarized in the following list.

- Provided a summary of the software and technologies used to create the database. Provided a high-level overview of the database structure and the user interface.
- The second part of the workshop contained a detailed demonstration of the user interface for the software and best practices for its use.
- Hands-on labs were distributed to the participants so that they could perform their own structured walkthroughs.

From the Q and A session, the following work-items were identified:

- Presently, users can upload only one report at a time. Consortium members need to upload different file types and supporting documents related to a report. The report management component will need to be expanded to support these features. In addition, other application elements (material, measures, etc... will need to be linked to those reports.)
- The infrastructure for the role management system is in place that grants or revokes permission to create and edit different data items. However, administrative decisions had not been made to define those business processes. The role management system will be revised so that a data item can only be modified by the user that created it. Each organization will have a “super user” that can modify the data created by the constituents of that organization. Finally, there is a “global super user” who will have permission to modify any and all data.
- Changes need to be made to handle and denote lab and field mixes using lab or field compaction. Links will need to be created from field samples to this data.

## Significant Problems, Issues and Potential Impact on Progress

None

## Work Planned Next Quarter

- Completion of the user interface forms for Contractors and Contacts.
- Expansion of user role system to define and control the data access levels of each user.
- Enhancements to user upload file system, including a directory structure, and the ability to link files and directories to other data.
- “Bulk editing” features for measures, allowing faster data entry by editing multiple records at once.
- Ability to copy properties, individually or by group, from one material type to another.
- Ability to filter materials by their components.

- Additional data fields for validation sections.
- Continued development of Help system, including data definition files for all data types.
- Complete transactional logging system.

**Work element TT1e: Development of Research Database (Duration: Year 2 through Year 5)**

Work Done This Quarter

Uploaded the quarterly technical progress report to the ARC website.

Significant Results

None

Significant Problems, Issues and Potential Impact on Progress

None

Work Planned Next Quarter

Upload the ARC quarterly technical progress report to the ARC website.

**Work Element TT1f: Workshops and Training**

Work Done This Quarter

A training workshop for the Materials Database was provided for the ARC members on March 11, 2010 at UNR campus. At the workshop a summary of the database structure and the software and technologies used to create the database was provided. Additionally a detailed demonstration of the user interface for the software was provided. Feedback was gathered for future work items on the Materials Database.

Significant Results

The following work-items were identified:

- Presently, users can upload only one report at a time. Consortium members need to upload different file types and supporting documents related to a report. The report management component will need to be expanded to support these features. In addition, other application elements (material, measures, etc., will need to be linked to those reports.)

- The infrastructure for the role management system is in place that grants or revokes permission to create and edit different data items. However, administrative decisions had not been made to define those business processes. The role management system will be revised so that a data item can only be modified by the user that created it. Each organization will have a “super user” that can modify the data created by the constituents of that organization. Finally, there is a “global super user” who will have permission to modify any and all data.
- Changes need to be made to handle and denote lab and field mixes using lab or field compaction. Links will need to be created from field samples to this data.

Significant Problems, Issues and Potential Impact on Progress

None

Work Planned Next Quarter

None

Technology Transfer Year 3	Year 3 (4/2009-3/2010)											Team	
	4	5	6	7	8	9	10	11	12	1	2		3
<b>(1) Outreach and Databases</b>													
TT1a: Development and Maintenance of Consortium Website													UNR
TT1b: Communications													UNR
TT1c: Prepare presentations and publications													UNR
TT1d: Development of Materials Database													UNR
TT1d-1: Identify the overall Features of the Web Application													
TT1d-2: Identify Materials Properties to Include in the Materials Database													
TT1d-3: Define the Structure of the Database													
TT1d-4: Create and Populate the Database									SW, v. β			SW	
TT1e: Development of Research Database													UNR
TT1e-1: Identify the Information to Include in the Research Database													
TT1e-2: Define the Structure of the Database													
TT1e-3: Create and Populate the Database													
TT1f: Workshops and Training													UNR

**Deliverable codes**

- D: Draft Report
- F: Final Report
- M&A: Model and algorithm
- SW: Software
- JP: Journal paper
- P: Presentation
- DP: Decision Point

**Deliverable Description**

- Report delivered to FHWA for 3 week review period.
- Final report delivered in compliance with FHWA publication standards
- Mathematical model and sample code
- Executable software, code and user manual
- Paper submitted to conference or journal
- Presentation for symposium, conference or other
- Time to make a decision on two parallel paths as to which is most promising to follow through

 Work planned  
 Work completed  
 Parallel topic

Technology Transfer Years 2 - 5	Year 2 (4/08-3/09)				Year 3 (4/09-3/10)				Year 4 (04/10-03/11)				Year 5 (04/11-03/12)				Team
	Q1	Q2	Q3	Q4	Q1	Q2	Q3	Q4	Q1	Q2	Q3	Q4	Q1	Q2	Q3	Q4	
<b>(1) Outreach and Databases</b>																	
TT1a: Development and Maintenance of Consortium Website																	
TT1b: Communications																	
TT1c: Prepare presentations and publications																	
TT1d: Development of Materials Database																	
TT1d-1: Identify the overall Features of the Web Application																	
TT1d-2: Identify Materials Properties to Include in the Materials Database																	
TT1d-3: Define the Structure of the Database																	
TT1d-4: Create and Populate the Database								SW, v, β	SW								
TT1e: Development of Research Database																	
TT1e-1: Identify the Information to Include in the Research Database																	
TT1e-2: Define the Structure of the Database																	
TT1e-3: Create and Populate the Database																	
TT1f: Workshops and Training																	

**Deliverable codes**  
D: Draft Report  
F: Final Report  
M&A: Model and algorithm  
SW: Software  
JP: Journal paper  
P: Presentation  
DP: Decision Point

**Deliverable Description**  
Report delivered to FHWA for 3 week review period.  
Final report delivered in compliance with FHWA publication standards  
Mathematical model and sample code  
Executable software, code and user manual  
Paper submitted to conference or journal  
Presentation for symposium, conference or other  
Time to make a decision on two parallel paths as to which is most promising to follow through

 Work planned  
 Work completed  
 Parallel topic